

Alma Mater Studiorum – Università di Bologna

**DOTTORATO DI RICERCA IN
Ingegneria Civile, Chimica, Ambientale e dei Materiali**

Ciclo XXIX

Settore Concorsuale di afferenza: 09/D3 – Impianti e processi industriali chimici

Settore Scientifico disciplinare: ING-IND/25 – Impianti Chimici

**ANALYSIS OF SUSTAINABLE
TECHNOLOGIES
FOR ACID GAS REMOVAL**

Presentata da: Alessandro DAL POZZO

Coordinatore Dottorato

Prof. Ing. Luca VITTUARI

Relatore

Prof. Ing. Valerio COZZANI

Correlatori

Prof. Ing. Alessandro TUGNOLI

Ing. Giacomo ANTONIONI

Esame finale anno 2017

Index

Abstract	5
----------------	---

General Introduction	6
----------------------------	---

PART I - Acid gas removal by dry processes

1 Acid gases	10
1.1 Typical acid pollutants in flue gases from combustion processes.....	10
1.2 Sulfur dioxide and acid rains.....	10
1.3 Hydrogen halides and airborne toxicity	11
1.4 Carbon dioxide and the climate change challenge	13
1.5 Acid neutralisation	14
2 Acid gas abatement in Waste-to-Energy plants: state of the art	16
2.1 Overview of air pollution control in the waste incineration sector.....	16
2.2 Solid sorbents for acid gas removal: Ca-based sorbents	17
2.3 Solid sorbents for acid gas removal: Na-based sorbents	19
2.4 Review of the latest developments in dry sorbent injection technologies.....	21
3 Carbon capture with solid sorbents: state of the art.....	26
3.1 The concept of carbon capture and storage.....	26
3.2 Approaches to CO ₂ capture	26
3.3 Perspective of carbonate looping in pre- and post-combustion CO ₂ capture	29
4 Research needs and motivation of the study.....	31
4.1 Challenges in the use of sorbents for acid gas removal	31
4.2 Overcoming the limitations of gas-solid reactions by process optimisation.....	32
4.3 Overcoming the limitations of gas-solid reactions by synthesis approaches.....	32
References (Part I).....	34

PART II - Application to HCl and SO₂ removal in Waste-to-Energy plants

5 Experimental study of acid gas removal processes: the reaction between Ca(OH) ₂ and HCl.	41
5.1 The reaction.....	41
5.2 Set-up of a dedicated laboratory apparatus	42
5.3 Materials and experimental procedure	44
5.4 HCl removal monitored by infrared spectroscopy	46
5.5 Identification of the solid reaction product	50
6 Phenomenological model for acid gas removal processes	53
6.1 Literature overview	53

6.2	The issue of incomplete conversion	54
6.3	Phenomenological model: the grain model framework	56
6.4	Phenomenological model: the crystallisation and fracture submodel.....	63
6.5	Model input and output parameters.....	66
6.6	Model validation against literature data	69
6.7	Model validation against experimental data	76
7	Operational model for process optimisation of acid gas removal systems.....	80
7.1	Formulation of the operational model.....	80
7.2	Calibration of the model with operational data from Waste-to-Energy plants.....	82
7.3	Case study: optimisation and benchmarking of a two-stage treatment system.....	84
7.4	Methodology	86
7.5	Benchmarking data.....	87
7.6	Cost estimate.....	90
7.7	Optimal configuration of the two-stage system and benchmarking results	95
7.8	Influence of uncertain parameters and Monte Carlo sensitivity analysis.....	97
8	Sustainability analysis of acid gas removal systems	103
8.1	A holistic approach to environmental protection	103
8.2	Definition of the case study	104
8.3	Data inventories and associated uncertainties	108
8.4	Characterisation approach and adopted indicators	111
8.5	Two-stage system: environmental and economic optima	113
8.6	Comparison of the alternative acid gas removal systems.....	116
8.7	Closing remarks on single stage vs. multistage dry treatment systems.....	123
	References (Part II).....	124

Part III - Application to CO₂ capture by MgO-based sorbents

9	Development of MgO-based sorbents.....	135
9.1	Alternatives to limestone in carbonate looping technologies	135
9.2	Use of residues from dry acid gas removal as CO ₂ sorbents	136
9.3	Potentiality of MgO as a CO ₂ sorbent.....	140
9.4	Enhancement of MgO reactivity with molten salt promotion	141
9.5	Synthesis protocol for alkali metal nitrate-coated MgO-based CO ₂ sorbents.....	142
10	Analysis of the carbonation of MgO-based sorbents.....	146
10.1	CO ₂ uptake	146
10.2	In situ analysis of carbonation: DRIFTS spectroscopy	153
10.3	In situ analysis of carbonation: synchrotron-based XRD/PDF analysis	155
10.4	Performance of MgO-based sorbents over repeated carbonation/calcination cycles....	158
10.5	Indications for further research in MgO-based sorbents.....	159

References (Part III).....	161
Conclusions	167
List of publications	169
Ringraziamenti / Acknowledgments	170

Abstract

Acid gases, such as sulphur dioxide and hydrogen halides and – in a broad sense – carbon dioxide, are typical pollutants generated by combustion processes. Their removal by means of solid sorbents represent an efficient and cost-effective approach in dry acid gas treatment systems for waste incineration flue gas, while for CO₂ capture the process is exploratively studied as a promising alternative to amine scrubbing. The present study addressed both aspects.

In waste incineration flue gas cleaning, acid gas removal by sorbent injection is a well-established process. Nonetheless, a thorough understanding of the gas-solid reactions involved in the process has not been reached yet and, thus, the operation of dry treatment systems is still highly empirical. In the present study, the process was analysed using different levels of detail: from the microscopic level of a lab-scale experimental campaign and phenomenological description of the kinetic and mass transfer phenomena governing the gas-solid reaction to the macroscopic level of techno-economic and environmental assessment of alternative full-scale dry treatment systems.

With respect to CO₂ capture technologies, the process is still in the development stage and research is focused on the identification of highly-efficient sorbents. The present study analysed the enhancement of CO₂ uptake potential of magnesium oxide, a promising sorbent for intermediate-temperature carbon capture, by means of coating with alkali metal molten salts.

The joint analysis of gas-solid reaction for flue gas cleaning in two diverse contexts allowed the identification of common issues and of possible shared solutions.

General Introduction

“A clever person solves a problem. A wise person avoids it.” This quote attributed to physicist Albert Einstein is frequently used when referring to environmental issues to state an important concept: prevention is better than cure.

Historically, environmental problems have been faced by introducing “cures”, i.e. pollution mitigation measures. Air pollution has been fought by implementing so-called end-of-pipe technologies, like dedusting equipment in energy plants or catalytic converters in cars, to treat emissions and reduce the load of pollutants. Likewise, waste accumulation has been faced by operating treatment and incineration plants aimed at reducing and sanitising the refuses generated by society.

In the last decades, a novel approach to environmental protection has been increasingly put into practice: pollution prevention. Instead of managing a pollutant only after its emission, thus focusing on the reduction of its impact on the environment, pollution prevention aims to eliminate pollution at its source. Typical examples of prevention measures are the modification of a production process in order to generate less waste, the substitution of toxic chemicals with non-toxic alternatives, the implementation of water and energy conservation strategies, the recycling and reusing of materials. Intertwining concepts proper of engineering and management, of design and sociology, pollution prevention has been truly a Copernican revolution in the field of environmental protection.

Yet, pollution prevention cannot be an all-healing panacea. Although prevention strategies can significantly curb our environmental impact, human activity still needs inherently polluting activities. Industries such as ceramics, glass manufacturing or steelmaking, which basically relies on thermal processes, unavoidably emit airborne pollutants. The sorted fractions of municipal and industrial waste can be recycled and reused to greater extent, but the management of residual unrecyclable waste fractions still requires incineration, in order to avoid landfilling. Even in the power sector, despite the remarkable progresses of renewable sources, the consumption of fossil fuels is expected to steadily increase in the upcoming years, as the thirst for cheap energy of emerging economies keeps growing and the political support for CO₂ emission targets worldwide remains lukewarm.

In this framework, the “clever person” of Einstein’s quote is still needed. Since we are not going to get rid of certain polluting activities any time soon, the optimisation of current pollution mitigation technologies and the implementation of new ones will still be relevant points in the environmental protection agenda. Problems typical of the process and chemical engineering await solution in order to further improve current end-of-pipe approaches and to start up new technologies to tackle new target pollutants such as CO₂.

The present PhD work aimed at offering a contribution towards a better understanding of theoretical and operational aspects in acid gas removal processes of either current industrial relevance (HCl and SO₂ removal in waste incinerators) or perspective interest (pre- or post-combustion CO₂ capture). The manuscript is organised as follows.

Part I of the thesis provides the general framework in which the present PhD project finds its motivation. Targets of the study are acid gases: HCl, SO₂, HF and, in a broad sense, CO₂. Their characteristics and the environmental problems associated with their emission in industrial

processes are illustrated in chapter 1. Chapters 2 and 3 provide the state of the art of acid gas removal in Waste-to-Energy plant and CO₂ capture technologies, respectively. Chapter 4 outlines the pressing research needs which motivates the present study.

Part II is focused on the analysis of acid gas removal by solid sorbents in the Waste-to-Energy context. The process is explored at different levels. Chapter 5 shows an experimental investigation of the gas-solid reaction between Ca(OH)₂ and HCl (the most relevant target acid pollutant for WtE plants), testing the influence of different operating parameters and clarifying doubts regarding the actual solid product of chloridisation. Chapter 6 presents a phenomenological model for dry acid gas removal, based on the description of kinetics and mass transfer phenomena. The model is validated against both relevant literature data and experimental data illustrated in the previous chapter. Chapter 7 shifts the attention to a simplified approach to acid gas removal modelling: an empirical model, calibrated on operational plant data, is presented as a useful tool for process optimisation of full-scale dry treatment systems. This modelling approach is applied to an economic comparison between two-stage and benchmark single stage dry acid gas removal configurations. Chapter 8 expands the economic process optimisation shown in chapter 7 to a broader sustainability analysis, taking into account the indirect environmental impacts generated by the supply and disposal chains of solid reactants and residues. Final considerations about the overall optimisation of acid gas removal systems are drawn.

Part III reports the investigation of CO₂ capture by MgO-based sorbents. Chapter 9 introduces the research of new CO₂ sorbents (also briefly discussing the possibility of re-use of acid gas removal solid residues for CO₂ capture) and illustrates potentialities and limitations of MgO as CO₂ sorbent, identifies molten salt promotion as a viable route for the enhancement of reactivity and presents a facile and reproducible synthesis protocol for alkali metal nitrate-coated MgO sorbents. Chapter 10 reports the CO₂ uptake performances of the synthesised materials and delves into a spectroscopic investigation of the actual mechanisms governing MgO carbonation, eventually providing indications for further research in the area.

The general conclusions highlight the cross problems identified between the two gas-solid removal processes respectively shown in Part II and Part III and the common strategies carried out to overcome them.

Alessandro Dal Pozzo

Part I

Acid gas removal by dry processes

1 Acid gases

1.1 Typical acid pollutants in flue gases from combustion processes

Acid gases are a class of atmospheric pollutants emitted by combustion processes, whose main components are sulphur dioxide and hydrogen halides. They are grouped on the basis of their acid behaviour, which determines their hazardous profile as corrosive substances, toxic compounds and precursors of environmental acidification, but also defines the chemical principle allowing their abatement in flue gas cleaning systems (see section 1.5).

Figure 1.1 summarises the expected concentration range of acid pollutants in raw exhaust gas for different industrial processes. The present thesis will make specific reference to the waste incineration sector, since waste-to-energy (WtE) facilities – especially in Europe – are the most challenging proving ground for acid gas removal processes, because of the combined effect of stricter emission limit values at stack and higher loads of pollutants in the untreated gas. Nonetheless, findings and indications obtained for WtE plants are exportable to other relevant industrial contexts where acid gas control is a concern and more demanding emission regulations have been recently issued (BREF GLS, 2012). Furthermore, the present thesis identifies an interesting parallelism between concepts and issues proper of dry acid gas treatment and the challenges faced by the carbonate looping technology in the novel field of CO₂ pre- and post-combustion capture (see chapter 3).

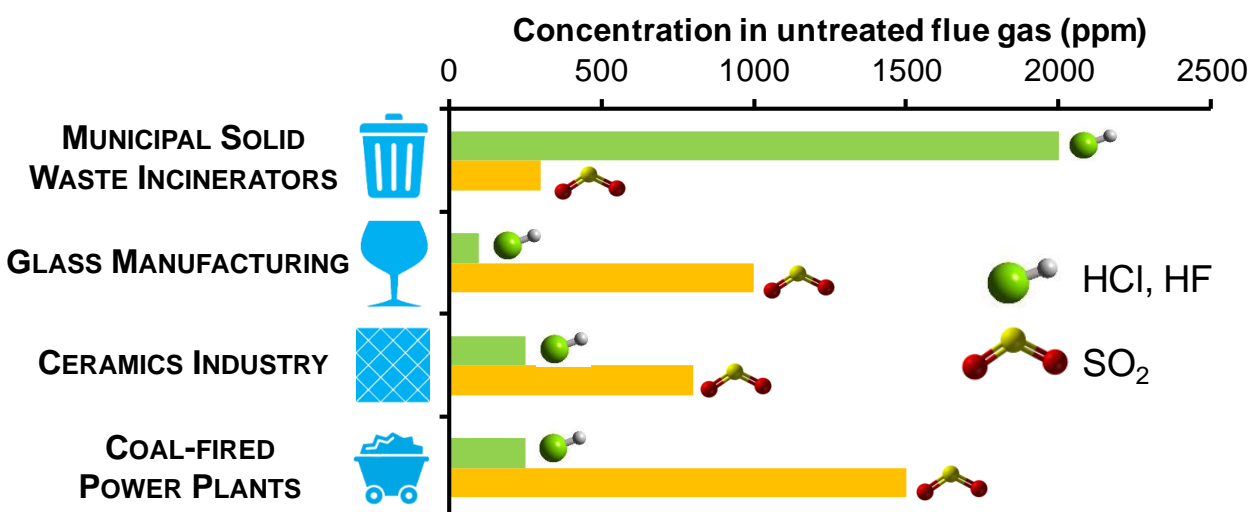


Figure 1.1. Typical concentration range of acid contaminants in the flue gas of some industrial processes.

1.2 Sulfur dioxide and acid rains

Sulphur dioxide (SO₂) is a typical fuel-related contaminant of combustion off-gas. In waste incineration, its presence in the flue gas is related to the combustion of organic substances, due to the elementary oxidation reactions of S and H₂S (Niessen, 2002). It is a major air pollutant, carrying significant impacts upon human health and integrity of habitats (EPA, 1999).

In particular, sulfur dioxide emissions have been a historical precursor to *acid rain*. The collective term covers a variety of phenomena connected to the atmospheric precipitation of acid substances (acid rainfall, snowfall and fog). In addition to moist deposition, acid gases can also precipitate due to dry deposition on particulate matter, fumes and aerosol. Acid precipitations, having a pH lower

than 5 (Baird and Cann, 2008), cause soil acidification, suppress microbial fauna, wash nutrients out of terrains, dissolve and mobilise other toxic substances like aluminium. All these effects contribute to the weakening of vegetation. Thin soils, poor in organic matter, like the alpine soils, are particularly vulnerable (Krug and Frink, 1983). Likewise, effects on aquatic ecosystems are severe, since rivers and lakes – being the final receptors of meteoric waters – suffer the accumulation of the precipitated acid substances.

Sulfur dioxide, along with other precursors like nitric oxide (NO), is the primary pollutant responsible for acid rain. During the transport of the air masses containing SO₂, the primary pollutant is transformed in the actual strong acid provoking acid rain, i.e. sulphuric acid (H₂SO₄):

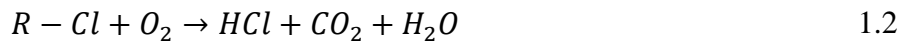


Then, acid rain containing H₂SO₄ can precipitate far downwind from the original source of SO₂ emissions. For instance, acid rain was first scientifically characterised in Norway and Sweden in the 1960s (Revelle and Revelle, 1992) and the Swedish scientist Svante Odén found enough evidences linking the acidification of Swedish lakes to pollutants emitted abroad (Odén, 1968) to allow Sweden drawing international attention on the issue of transboundary pollution at the 1972 United Nations Conference on the human environment (Schreurs, 2007). Nowadays, a similar pattern of long-range transport of pollutants is observed in China, where the South-eastern regions suffer the main effects of acid precipitations although coal burning and SO₂ emissions are mainly concentrated in North-eastern regions (Tang and Wu, 2012).

1.3 Hydrogen halides and airborne toxicity

Hydrogen halides are diatomic inorganic compounds formed by a hydrogen atom and a halogen.

Hydrogen chloride is the most abundant acid gas in flue gases generated in municipal solid waste incinerators. The main reaction responsible for the emission of HCl during waste combustion is the dechlorination of Cl-containing plastics (Matsukata et al., 1996):



Cl-containing plastics include polyvinyl chloride (PVC, 59.0 wt. % of Cl), polyvinylidene chloride (PVDC, 73.2 wt. % of Cl) and polychloroprene (Neoprene, 39.5 wt. % of Cl). Conversely, inorganic chlorine (e.g., table salt) cannot release HCl at the typical temperatures attained in the combustion chamber (Wey et al., 2001).

Hydrogen fluoride is the second most relevant halide released by waste combustion, although its concentration in the exhaust gas is usually 2-3 order of magnitudes lower than that of HCl (Dal Pozzo et al., 2017). Specific industrial waste fractions can be particularly rich in fluorine, like automotive shredder residues, which show F mass fractions up to 0.5-0.75% in dry waste, generally coupled with a high Cl content (Viganò et al., 2010).

Similarly, halogens with higher atomic number are transformed during combustion in the respective halides. For example, the combustion of electronic boards containing brominated flame retardants gives rise to the emission of hydrogen bromide (Barontini et al., 2005). Likewise, exceptionally high loadings of pharmaceutical waste containing iodine can provoke a spike in hydrogen iodide concentration in flue gas (Zemba et al., 2013), generating a purple-tinted plume (Figure 1.2) and an understandable alarm in the nearby population.



Figure 1.2. Purple-coloured plume emanating from the exhaust stack of the WtE plant in Pisa (Italy) due to hydrogen iodide emission (March 2007).

The emission of hydrogen halides can cause harm to both human health and ecosystem integrity. Concerning damages to human health, the halides are classified as toxic compounds. An evaluation of the dangerousness of acid gases is given by toxicological threshold values such as the ones presented in Table 1.1. The IDLH (Immediately Dangerous to Life or Health) is the minimum concentration of an airborne contaminant for which a 30 min exposure is “*likely to cause death, or immediate or delayed permanent adverse health effects, or prevent escape from such an environment*”. The AEGL (Acute Exposure Guideline Levels) values are the respective concentrations of an airborne pollutant which cause irritation and reversible effects (AEGL-1), permanent or long-term damages (AEGL-2), death risk (AEGL-3).

Hydrogen chloride is irritating for eyes and skin. It forms corrosive hydrochloric acid on contact with water found in body tissue. Acute exposure can cause eye burns, inflammation and ulcer in the respiratory tracts and, in severe cases, pulmonary edema (EPA, 1999). Concerning chronic effects, long-term exposure to HCl is linked to gastritis, chronic bronchitis, dermatitis and photosensitisation (Hazardous Substances Data Bank, 1993; CalEPA, 1999).

Hydrogen fluoride is extremely corrosive and toxic. The affinity of the F⁻ anion towards the ubiquitous biologically important Ca²⁺ and Mg²⁺ cations can cause severe interference with blood, bone and tissue calcium levels (Hoffman et al., 2007). For instance, the CML-IA methodology for life cycle assessment attributes to HF a human toxicity potential three orders of magnitude higher than those of HCl and SO₂ (Huibregts et al., 2000),

Table 1.1. AEGL (60 min) and IDLH threshold limit values for the main acid gaseous species. Source: CAMEO Database, U.S. EPA.

Composto	AEGL-1 (ppm)	AEGL-2 (ppm)	AEGL-3 (ppm)	IDLH (ppm)
SO ₂	0.2	0.75	30	100
HCl	1.8	22	100	50
HF	1	24	44	30

1.4 Carbon dioxide and the climate change challenge

Although not usually included in the acid gas category, carbon dioxide (CO_2), the product of complete combustion of carbon, is slightly acidic in nature. Its concentration in a typical flue gas exiting from a combustion chamber ranges from 8 vol. % for waste-to-energy plants (BREF WI, 2006) to 15 vol. % for coal-burning power plants (Dieter et al., 2014).

Carbon dioxide is not a pollutant *stricto sensu*, being non-toxic and non-harmful, unlike the acid gases presented so far. However, worldwide concern has grown in the last decade on the causality between CO_2 emissions and global warming. CO_2 is a so-called *greenhouse gas*, i.e. it absorbs and emits thermal radiation in the infrared range, thus producing an effect which is actually essential in keeping Earth surface at an average temperature compatible with life. Yet, the atmospheric concentration of CO_2 has increased by more than 45% since 1750 (see Figure 1.3), as a consequence of human industrial activity and fossil fuel utilization, and this unprecedented trend has strengthened the radiative forcing of the greenhouse effect, leading to a steady increase in average global surface temperature (Figure 1.4). Since the scientific community has reached an overwhelming consensus regarding the anthropogenic cause of climate change (Cook et al., 2016) and world governments have decided to take action (Paris Agreement, United Nations, 2015), technological solutions for the mitigation of CO_2 emissions are under widespread study and deployment.

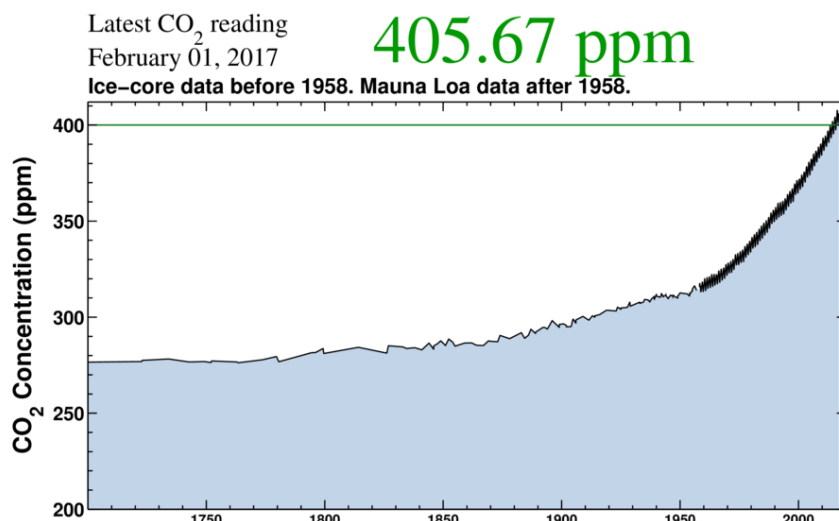


Figure 1.3. The Keeling curve of CO_2 atmospheric concentration in the last 300 years (Scripps Institution of Oceanography, 2016).

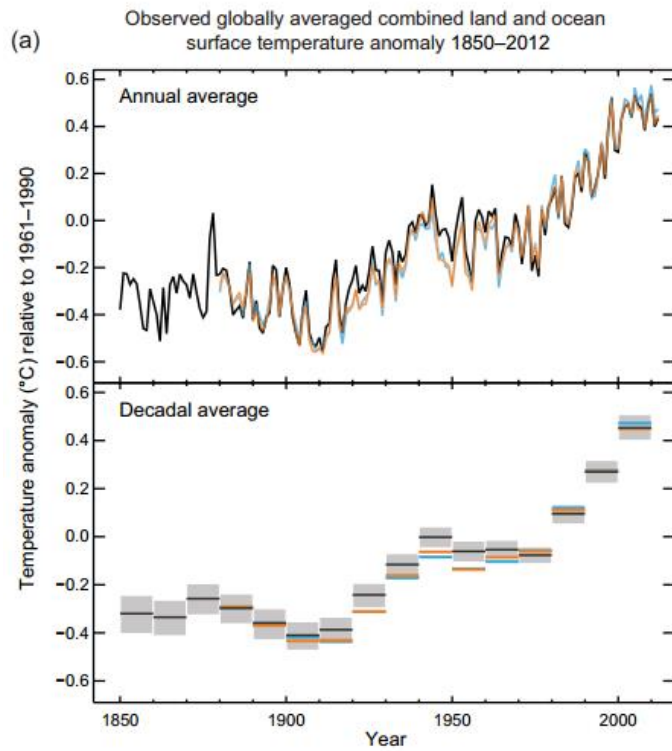


Figure 1.4. Global temperature anomaly in the last 150 years (IPCC, 2015).

1.5 Acid neutralisation

Tackling acid gas emissions has been one of the first challenges in the history of environmental protection and several environmental milestones have been put with reference to acid gases (Figure 1.5). Actually, HCl has been the first major pollutant to be object of a pollution control legislation. The Leblanc process, the earliest industrial process for the production of soda ash – a crucial chemical in the glass, textile, soap and paper manufacturing –, generated significant amounts of HCl, which were simply vented into the atmosphere. In order to target these noxious emissions, in 1863 the British Parliament passed the so-called Alkali Act, a law imposing that no more than 5% of the hydrochloric acid produced by soda plants could be vented to the atmosphere (Radojevic and Bashkin, 2006).



Figure 1.5. Some key events in the history of acid gas emission control.

Later, with the exponential growth of industrial production in the late XIX and early XX century, the soaring energy demand of the Western world was satisfied with increasing coal burning (Tertzakian, 2007), resulting in spiking SO₂ emissions and consequent acid raining. As mentioned in section 1.2, the first scientific observations about acid rain damages in Scandinavia in the 1960s

raised global awareness on the issue, evidencing that pollution does not respect regional or national boundaries and atmospheric contaminants can undergo long-range transport. This led to the ratification of the international Convention on Long-Range Transboundary Air Pollution (1979) in Helsinki, which obligated the signatory countries to curb SO₂ emissions. A decade after, the U.S. EPA Acid Rain Program (1990) introduced the first *emissions trading* scheme in history, a market-based initiative aimed at promoting efforts in reducing SO₂ emissions. Thanks to a combination of worldwide political will and efficient technological solutions, the global emissions of sulfur dioxide have been steadily declining since the 1980s (Smith et al., 2011).

Flue gas cleaning systems currently implemented in power plants generate emissions that are 4-5 orders of magnitude lower than before environmental legislation against acid gases was conceived (Damgaard et al., 2010). The chemical principle behind the vast majority of technologies for the abatement of SO₂, HCl and HF is the acid-base neutralisation:



Putting the acid gaseous pollutants in contact with a basic reactant generates a salt, either in liquid or solid form, thus removing the acid compounds from the flue gas. Neutralisation can be performed by injecting in the flue gas a basic solution (wet scrubbing) or a powdered basic solid sorbent (dry scrubbing), as detailed in chapter 2. In spite of the apparent simplicity of equation 1.3, acid gas neutralisation is a complex process, encompassing a stunning richness of chemical reaction engineering principles, and research is still needed to grasp a fundamental understanding of the involved phenomena and perform a fully aware process optimisation (see the research needs listed in chapter 4).

2 Acid gas abatement in Waste-to-Energy plants: state of the art

2.1 Overview of air pollution control in the waste incineration sector

The thermal treatment of waste plays a relevant role even in the current paradigm of circular economy (European Commission, 2015), by contributing to landfill diversion (Nizami et al., 2016) and by guaranteeing energy recovery from those wastes for which recycling would be technically and economically unfeasible (Arena, 2015). The emission of pollutants typically related to the combustion of wastes is the main environmental drawback of a waste-to-energy (WtE) process (Ouda et al., 2016). However, properly operated plants can greatly reduce the load of pollutants emitted to atmosphere (Wojdyga et al., 2014).

As mentioned in section 1.1, acid gases are typical pollutants in the flue gas emitted by waste combustion processes. Historically, acid gas treatment has been implemented by means of wet scrubbers, i.e. washing flue gas with basic solutions, taking advantage of both the high water solubility and acid/base reactivity of acid pollutants (Damgaard et al., 2010). In the last decades, the traditional wet processes have been increasingly replaced by the cheaper dry treatments, based on the injection of solid reactants in the flue gas. Surveying data from national environmental agencies, utility companies and industry consortiums (see Dal Pozzo et al., 2016), the market shares of wet, dry and semi-dry acid gas treatment systems over time in Europe were reconstructed in Figure 2.1, showing the unambiguous positive trend for the dry and semi-dry processes.

The basic scheme for dry acid gas removal is the so-called dry sorbent injection (DSI). It consists in the direct injection of a powdered basic sorbent (typically, calcium hydroxide or sodium bicarbonate, as detailed in section 2.2 and 2.3 respectively) in the flue gas ductwork, downstream of the air preheater and upstream of a dedusting equipment, such as an electrostatic precipitator (ESP) or a fabric filter, which collects the solid residues generated by acid gas neutralisation. When a fabric filter is used as dedusting equipment, the injected sorbent powders get captured by the filter bags, forming a filter cake which acts as a fixed bed reactor towards the flowing acid gases, actually incrementing the performance of the system.

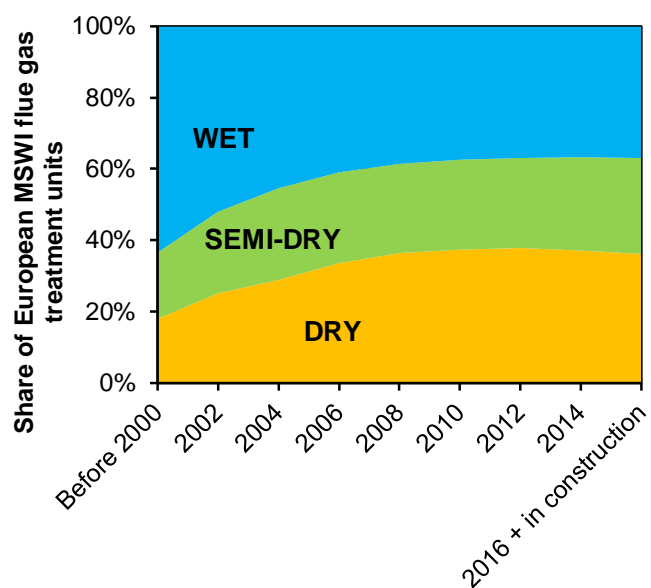


Figure 2.1. Market shares of wet, semi-dry and dry acid gas treatment units in European WtE plants.

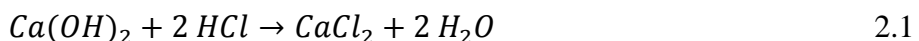
The advantages attracting the interest of plant operators and technology suppliers towards dry methods are, mainly, i) lower capital and maintenance costs due to lower equipment complexity; ii) easier and cheaper handling of solid residues compared to the wastewater generated by wet methods; iii) avoidance of “rain-out” issues at stack due to the condensation of wet flue gas.

The downside of dry methods is the intrinsic lower removal efficiency of gas-solid reactions when compared to gas-liquid reactions (Vehlow, 2015). This generally leads to the feed of solid reactant in relevant stoichiometric excess. Therefore, improving the removal efficiency to sorbent consumption ratio is a paramount target, pursued by the novel design choices illustrated in section 2.4 and by renewed efforts in enhanced process modelling (see section 4.2).

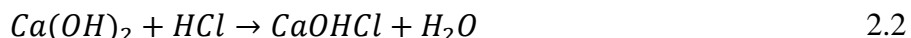
2.2 Solid sorbents for acid gas removal: Ca-based sorbents

Calcium-based sorbents have been the first powders to be considered for dry acid gas removal. Earlier approaches focused on the use of raw limestone (chemically, calcium carbonate, CaCO_3) to tackle HCl and SO_2 emissions at high temperature, directly in the combustion chambers of coal-fired or WtE plants (Petrini et al., 1979). Then, industrial interest quickly shifted towards calcium hydroxide, $\text{Ca}(\text{OH})_2$, the product of the calcination and subsequent hydration of limestone. Commonly known also as hydrated lime or slaked lime, $\text{Ca}(\text{OH})_2$ is more reactive than calcium carbonate, mainly because of the increased basic strength (Foo et al., 2016) and the higher porosity (Weinell et al., 1992).

Calcium hydroxide is generally assumed to react with HCl according to the following reaction:

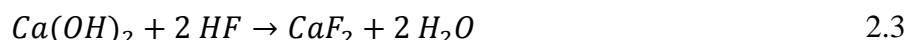


although relevant studies (Allal et al., 1997; Bodénan and Deniard, 2003; Bogush et al., 2015) point out that the actual stable solid product of HCl removal by $\text{Ca}(\text{OH})_2$ is calcium hydroxychloride (CaOHCl), formed via partial chloridisation:



This topic will be explored in chapter 5.

Towards other acid gases, $\text{Ca}(\text{OH})_2$ reacts as follows:



At the typical operating temperatures for acid gas removal, calcium sulphite (CaSO_3) further oxidises to calcium sulphate (anhydrite):



Conversion to sulphate is generally incomplete and both sulphite and sulphate can be found in the reaction products (Bodénan and Deniard, 2003).

In addition, the undesired interaction between $\text{Ca}(\text{OH})_2$ and the carbon dioxide in flue gas cannot be neglected:



Although carbon dioxide shows only limited acidic behaviour, its concentration in combustion flue gases is 3-4 orders of magnitude higher than HCl or SO_2 , hence up to 30% of the injected hydrated

lime can be subtracted to useful acid gas removal by competing carbonation (Antonioni et al., 2014).

When in-duct injection of hydrated lime takes place at high temperatures (> 400 °C, Gullett et al., 1992), calcium hydroxide is dehydrated to quicklime (calcium oxide, CaO):



Calcium oxide presents higher porosity and specific surface area than calcium hydroxide, but its prolonged exposure to heat can trigger severe sintering (see paragraph X).

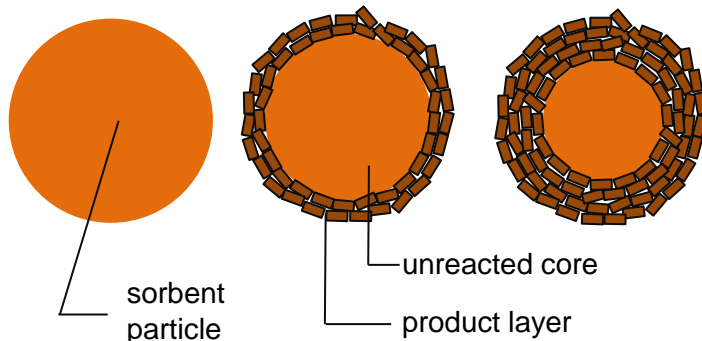


Figure 2.2. Gas-solid reaction according to the shrinking core model.

Kinetics and mass transfer phenomena involved in the dry sorption of acid pollutants by $Ca(OH)_2$ will be thoroughly discussed in chapter 6. Here, in order to understand the conceptual framework behind the design of dry acid gas treatment systems (paragraph 2.4), the mechanisms governing the gas-solid reaction between $Ca(OH)_2$ and acid gases can be simplified according to the so-called *shrinking core model* (Levenspiel, 1998). Chemical reaction takes place at the interface between gas and sorbent particles, where a shell of solid products (*product layer*) start accumulating. As reaction proceeds, the reacting particle gets consumed and shrinks, while product layer thickness increases (Figure 2.2). Consequently, acid gas sorption is mainly controlled by kinetics in the first seconds and by diffusional limitations afterwards.

The ideal range of temperatures for $Ca(OH)_2$ injection lays between 120 and 160 °C (Dal Pozzo et al., 2016), with improved efficiency as temperature decreases, because – while the water content in the flue gas remains constant – relative humidity (RH) increases (Harriott, 1990). The promoting effect of RH on the reactivity of Ca-based sorbents can be explained with reference to the shrinking core model: as sketched in Figure 2.3, adsorbed water can induce a rearrangement of the crystalline structure of the product layer, liberating new surface for reaction. Fonseca et al. (1998) advanced this hypothesis by comparing SEM images of lime reacted with HCl in dry or wet environment and Bausach et al. (2006) provided AFM imaging proving water-induced rearrangement of sulfate-based product layers.

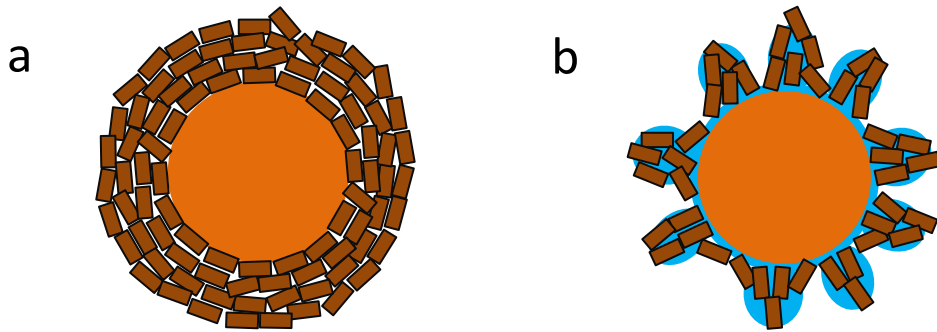


Figure 2.3. Product layer formed a) in dry gas conditions, b) in wet gas conditions.

The solid residues of acid gas abatement by $\text{Ca}(\text{OH})_2$ are generally known as calcium-based waste (CBW) or residual calcium chemicals (RCC). RCC are a mixture of the products of reactions 2.2, 2.3, 2.4, 2.5 plus unreacted calcium hydroxide. In addition, since they are usually collected by the first dedusting equipment in the flue gas cleaning line of a WtE plant, RCC are mixed with fly ash coming from the combustion chamber and activated charcoal injected for dioxine and furans adsorption.

Although several research projects have recently been started up with the aim of exploring recycling routes for RCC (Margallo et al., 2015), the actual fate of RCC across Europe is the disposal in landfills for hazardous materials or in underground storage sites (ISWA, 2008).

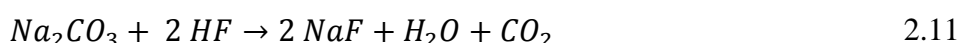
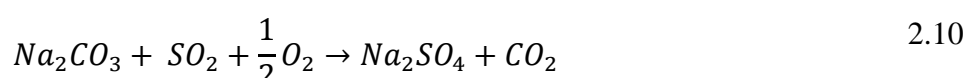
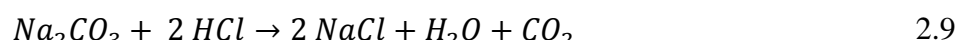
2.3 Solid sorbents for acid gas removal: Na-based sorbents

The use of sodium carbonate (Na_2CO_3) as acid gas removal agent was first explored in the 1980s (Mocek et al., 1983; Kimura and Smith, 1987) and became a widespread approach in WtE plants in the mid-1990s (Vehlow, 2015), when Solvay S.A. marketed the so-called NEUTREC process consisting in the injection of NaHCO_3 in flue gas and its subsequent collection by means of a fabric filter or electrostatic precipitator.

When dry NaHCO_3 is injected into the hot flue gas duct, it quickly decomposes to Na_2CO_3 via the reaction:



The thermal decomposition is an almost instantaneous and complete process at temperature higher than 130 °C (Hartman et al., 2013). Nonporous bicarbonate particles release water vapour and carbon dioxide, turning into porous sodium carbonate (see Figure 2.4). Then, sodium carbonate reacts with the acid gases according to the following schemes:



Thermal decomposition, sometimes referred as *thermal activation* (Brivio, 2007) in order to highlight its role in triggering reactivity towards acid gases, is a crucial step in generating a highly porous material.

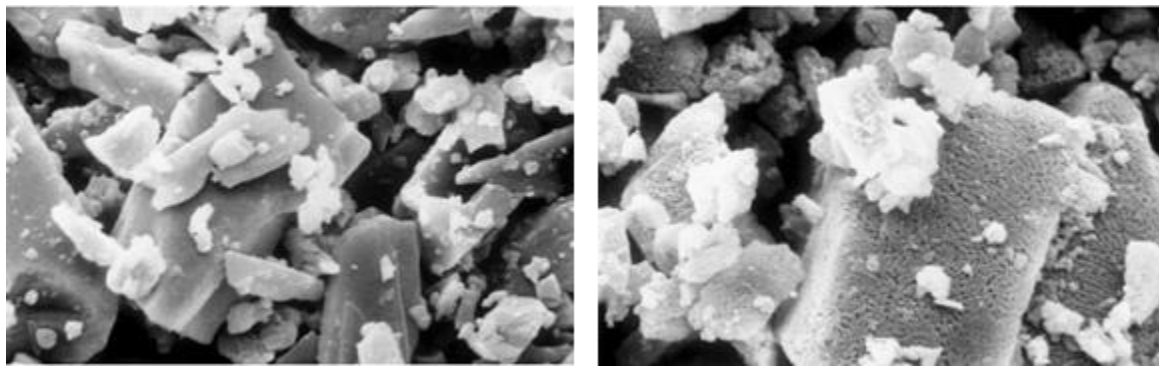


Figure 2.4. SEM images of: a) raw sodium bicarbonate, b) sodium carbonate obtained via reaction 2.8 (source: Kong and Davidson, 2010).

The kinetics of acid gas sorption by Na_2CO_3 is knowingly higher than that of Ca-based sorbents (Duo et al., 1996; Antonioni et al., 2014; Vehlow, 2015). Although scholarly literature regarding gas-solid reactions between Na_2CO_3 and acid pollutants is limited (mainly due to the fact that Na-based acid gas sorption is patented), the higher performance of Na_2CO_3 when compared to $\text{Ca}(\text{OH})_2$ might be ascribed to an higher intrinsic chemical reaction rate and a lower volume expansion associated with acid gas neutralisation.

In particular, volume expansion of the solid phase during sorption is a critical factor limiting the total molar conversion of sorbent particles. For example, with reference to reaction 2.1, the molar volume of CaCl_2 is larger than that of $\text{Ca}(\text{OH})_2$ and, thus, the reaction causes an expansion in the pores of the solid, eventually filling the voids within sorbent particles before 100% conversion is reached. The theoretical final conversion due to the complete filling of intraparticle voids (Simons and Garman, 1986) can be expressed through eq. 2.12:

$$X_{s,max} = \frac{\varepsilon_p}{(1 - \varepsilon_p)(\alpha - 1)} \quad 2.12$$

where ε_p is the initial void fraction of the sorbent and α the volumetric expansion factor, defined as the ratio of the molar volume of the solid product to the molar volume of the solid reactant.

Figure 2.5 shows the maximum theoretical conversion of sorbent exposed to HCl as a function of its initial void fraction and the volumetric expansion factor associated with chloridisation. The conversion of $\text{Ca}(\text{OH})_2$ to anhydrous CaCl_2 entails an $\alpha = 1.54$, while, if the CaCl_2 product is assumed to be in dihydrate form, $\alpha = 2.39$. Significantly less volume expansion ($\alpha = 1.29$) is associated with Na_2CO_3 chloridisation. This means that, while a particle of Na_2CO_3 with a porosity $\varepsilon_p = 0.3$ can be in theory entirely converted to NaCl , a particle of $\text{Ca}(\text{OH})_2$ with the same starting porosity can only reach a maximum theoretical conversion of 80% if the product is anhydrous CaCl_2 and 30% if the product is CaCl_2 dihydrate. Further details about the importance of the issue of incomplete conversion in formulating a phenomenological model for $\text{Ca}(\text{OH})_2$ -based acid gas removal will be given in chapter 6. As for the moment, it is sufficient to state that the absence of theoretical limitations to complete conversion is one of the main advantages of Na-based sorbents over Ca-based ones.

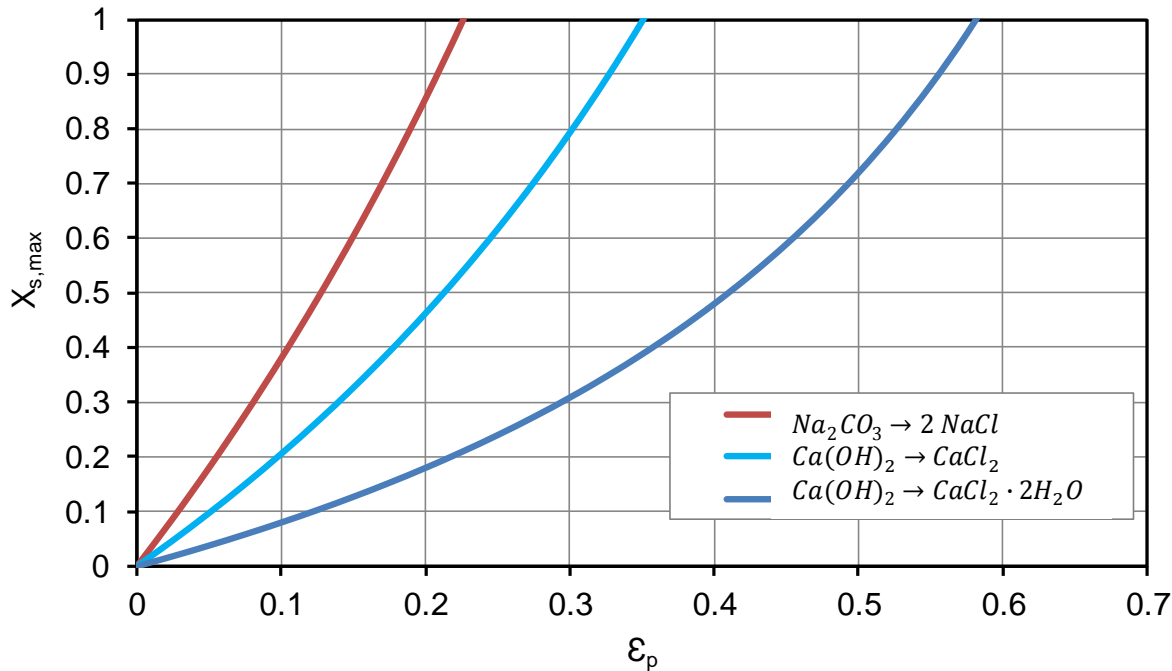


Figure 2.5. Maximum theoretical conversion for sorbent chloridisation as a function of its initial void fraction and the volumetric expansion associated with the specific reaction (eq. 2.12).

The typical range of temperatures for $NaHCO_3$ injection in the flue gas is 140-300 °C (Dal Pozzo et al., 2016), with slight improvement of performance as temperature increases due to kinetic effects. The residues of acid gas neutralisation by $NaHCO_3$ are known as sodium-based waste (SBW) or residual sodium chemicals (RSC) and contain the products of reactions 2.9, 2.10 and 2.11. Unlike RCC, RSC benefits from a market-ready solution for their recycling, the brine recovery process performed by Solvay S.A. in two dedicated plants, in France and Italy (Brivio, 2005). The precondition is the separate collection of RSC and fly ash, which can be achieved by installing a dedusting equipment upstream of the $NaHCO_3$ injection point. The process for recycling RSC is described by several sources (Brivio, 2005; Ninané et al., 1995; ISWA, 2008; Solvay, 2014). The RSC are mixed with water in order to obtain a saturated brine of the soluble salts ($NaCl$, Na_2SO_4 , Na_2CO_3), while the heavy metals and impurities precipitate. Additives such as sodium sulphide, sodium silicate and iron chloride are usually added in this phase. The brine is then filtered in a filter press, and further purified by activated charcoal and ion exchange resins. The depurated brine is suitable for use as a raw material in the sodium carbonate production (BREF LVIC-S, 2007).

2.4 Review of the latest developments in dry sorbent injection technologies

As shown in section 2.1, dry treatment systems are increasingly valued as reliable and cost-efficient solutions for acid gas control in the waste incineration sector. However, European recommendation on best available techniques (BAT) for flue gas cleaning in WtE plants, collected in a dedicated BAT reference document, was released more than 10 years ago (BREF WI, 2006). Therefore, the document mentions only the simple DSI as state-of-the-art dry treatment technique, providing a narrow and incomplete representation of the wide gamma of dry acid gas removal solutions currently available on the market. The following overview, based on the technical Italian paper by Dal Pozzo et al. (2016), aims at filling the gap by concisely sketching the main innovations introduced to couple the compliance to stricter emission limit values (Directive 2010/75/EU) with cost optimisation. Some of the systems described hereunder are sketched in Figure 2.6.

DSI with pre-conditioning. At the typical operating temperatures of DSI systems (120-180 °C), even flue gases with relatively high water content (10-15 vol. %) such as the ones deriving from waste combustion present values of relative humidity only at 1-5%. Therefore, considering the link between RH and the acid gas sorption performance of Ca-based sorbents, further flue gas humidification is required if a European WtE plant has to rely only on a single stage injection of Ca(OH)₂ in order to remove acid gases down to the emission limit values. Pre-conditioning is performed by installing a quenching tower upstream of the lime injection point: spraying pulverised water in the ductwork simultaneously increases the water content of the flue gas and decreases its temperature, rising its relative humidity. DSI units with pre-conditioning, fed with Ca(OH)₂, are actually able to comply with the limits set by Directive 2010/75/EU and, for instance, have been the adopted solution in the recently-built MSWIs in Bialystok and Bydgoszcz (Poland). In order to reduce the consumption of fresh lime, a common approach is to recirculate part of the RCC collected by the fabric filter.

Furnace sorbent injection (FSI). Another alternative to simple DSI is the sorbent injection directly performed in the combustion chamber, in order to take advantage of the higher chemical reaction rate achievable at high temperatures (850-1000 °C). The drawback is that high temperatures also trigger sorbent sintering, drastically reducing the active surface area of reactant particles.

While historically FSI was the first approach at acid gas removal by limestone, as mentioned in paragraph 0, it has been recently reevaluated after the successful testing of a dolomitic sorbent – commercially known as Depurcal – in three WtE plants in Northern Italy since 2011 (Biganzoli et al., 2015). The adopted sorbent is a mixture of calcium hydroxide and magnesium oxide (Ca(OH)₂·MgO, Ca/Mg ratio > 1.4) resulting from the calcination of dolomite. Upon furnace injection, Depurcal undergoes a thermal decomposition similar to the one of NaHCO₃ in DSI, releasing hydration water and developing a microporous structure. Unlike regular Ca-based sorbents, Depurcal does not suffer significant sintering. Indeed, while acid gas sorption is mainly performed by the calcium fraction of Depurcal, the almost inert MgO acts as a structural agent, preventing the collapse of the pores thanks to its high resistance to sintering (the concept will be expanded in section 3.3 with reference to solid sorbents for CO₂ capture).

Biganzoli et al. (2015) observed that FSI with Depurcal allowed an average reduction of the loadings of SO₂ and HCl to the flue gas cleaning line of 25 and 70%, respectively, and resulted particularly helpful in attenuating short-time spikes of acid gas emissions.

Spray dryer absorption (SDA). SDA equipments are used to further enhance the reactivity of Ca-based sorbents thanks to the promoting effect of water. In these systems, Ca(OH)₂ is first suspended in water to produce a milk of lime with a 20-25 wt. % concentration (Gambarè, 2013) and then the obtained basic slurry is sprayed in a scrubber vessel. The contact between the flue gas and the pulverised slurry promotes the sequestration of acid pollutants via mass transfer from the gas phase to the liquid phase and subsequent chemical reaction. At the same time, the water content in the slurry evaporates, leading to the formation of solid residues.

The main parameter governing the process is the so-called *approach to saturation temperature* (AST), defined as the difference between the temperature of the inlet flue gas and its adiabatic saturation temperature (Harriott et al., 1991). SDA performance increases when AST decreases (i.e., when RH increases), but at the same time a low AST implies problems in terms of acid condensation in the vessel and agglomeration of the filter cake on the bags of the fabric filter downstream. Optimal values of AST lie between 10 and 15 °C (Srivastava and Jozewicz, 2001).

The semi-dry approach of SDA systems shares the advantages of a typical wet process (*viz.* low consumption of reactants and high removal efficiency), without the drawback of generating liquid residues. Nonetheless, in order to avoid costs and complications related to slurry preparation, the most recent design practices tend to separate the injections of water and lime, thus resorting to the aforementioned DSi with pre-conditioning or to the so-called CDS systems.

Circulating dry scrubbing (CDS). CDS are semi-dry solutions based on $\text{Ca}(\text{OH})_2$ injection which are aimed at achieving high acid gas removal efficiency with the lowest sorbent consumption, by increasing the residence time of solid reactants in the system. They can be sorted in two categories: circulating bed scrubbers and systems with humidified solids recirculation.

In the former, water and lime are separately introduced inside a vertical reactor, designed to create a fluidised bed. The reactor is aimed at guaranteeing both high relative humidity and high solid residence time. Downstream, part of the solid residues of the process, collected by a fabric filter, are recirculated back to the reactor, in order to increase the sorbent-to-acid gas ratio.

Conversely, systems based on the recirculation of humidified solids recall the essential design of DSi (for example, the reactor is often a simple vertical conduit), but focus on an optimised recirculation section as the key factor to enhance performance.

As a matter of fact, the bare recirculation of RCC “as is”, adopted in several DSi units, has a strong, intrinsic limitation: partially reacted lime particles exhibit a noticeably lower reactivity than fresh $\text{Ca}(\text{OH})_2$, because the shell of solid product covering the unreacted core of sorbent particles remarkably hinders the diffusion of acid pollutants towards reaction interface.

In order to promote the reactivity of recirculated lime, several technology suppliers propose patented recirculation systems aimed at “reactivating” the partially reacted sorbent in two ways:

- mechanical reactivation – the action of a mixing cochlea induces the fracture of product layers on sorbent particles via attrition and grinding between particles.
- rehydration – pulverised water is sprayed in order to wet the partially reacted lime, triggering a rearrangement in the product layer (the effect already shown in Figure 2.3). Lime is a hygroscopic material and adsorbs water, which in turn interacts with the product layer, exposing fresh lime surface. A similar effect can be obtained without spraying water, but employing a stream of steam, generated e.g. by using the heat of flue gas exiting the combustion chamber.

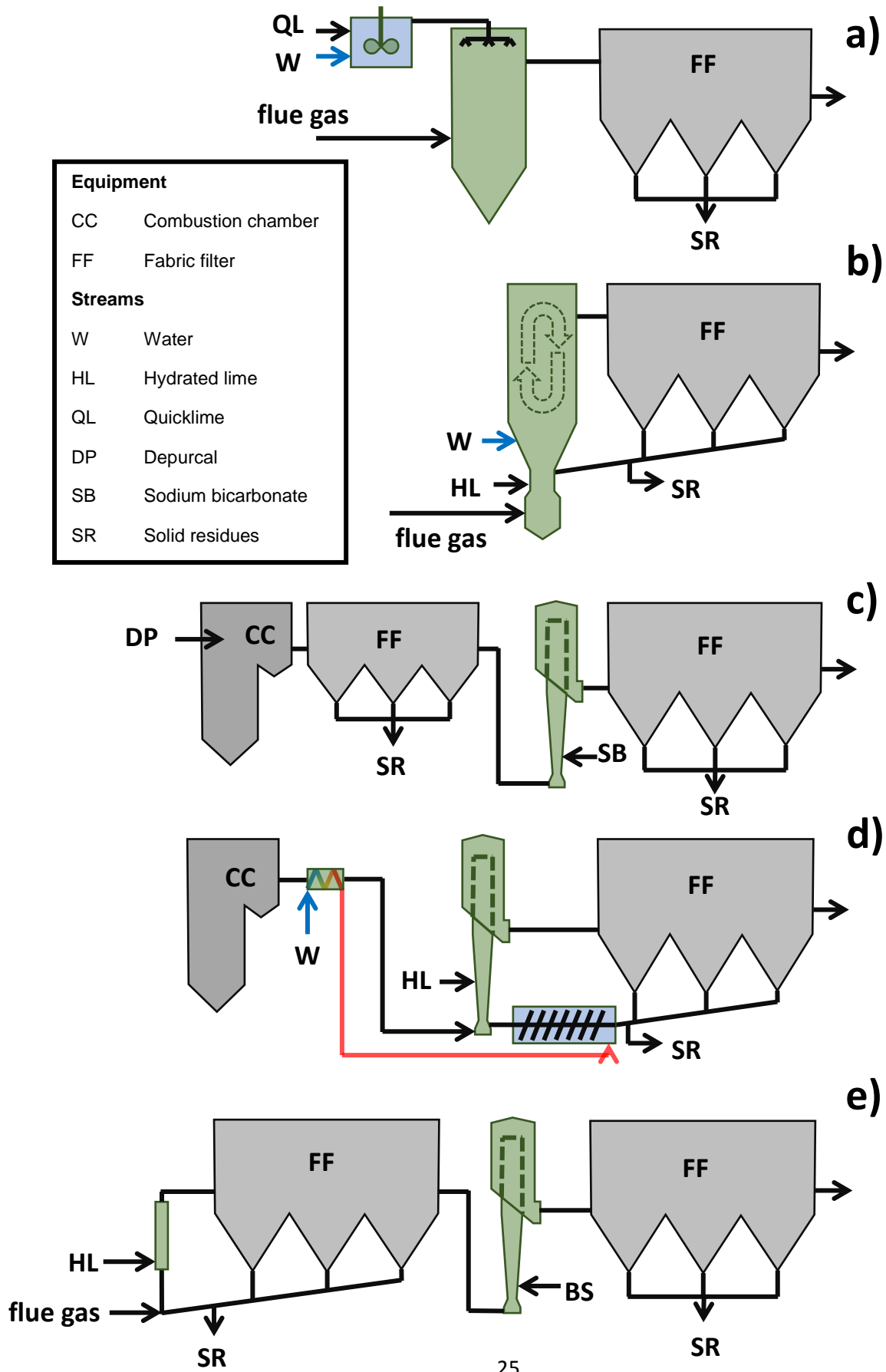
Two-stage dry treatment systems. Lastly, among the most novel solutions for dry acid gas removal, the double reaction/double filtration dry treatment system (Acquistapace, 2014) – adopted since 2006 in some Italian WtE plants – consists in two consecutive stages of sorbent injection and dedusting with a fabric filter. This configuration, which is essentially the connection in series of two DSi units, has the twofold target of increasing the overall removal efficiency and significantly lowering operating costs in comparison with usual single stage approaches. A detailed economic analysis of the savings achievable with a two-stage acid gas removal system is presented in chapter 7.

In the typical two-stage system, the first stage is fed with the cheaper sorbent (i.e., hydrated lime) and has the role to remove most of the acid gas loading, while the more reactive sodium bicarbonate is injected in the second stage, in order to abate the residual acid pollutants down to the set-point for their concentrations at stack. Furthermore, by acting downstream of a fabric filter, the second stage generates RSC which are not contaminated with fly ash and thus recyclable.

Anyway, the two-stage configuration, besides offering a useful redundancy, allows operating versatility in terms of choice of sorbents. It is also possible to operate with two Ca-based stages,

like in the Runcorn WtE facility and in the hazardous waste incinerator in Grundon, both in the United Kingdom (de Greef et al., 2013), or with two Na-based stages, in a set-up potentially able to further reduce operating costs (Guglielmi et al., 2014). In contrast, the high space requirements and the design focused on the removal of high loads of acid pollutants make the two-stage system a viable solution mainly for mid-to-large WtE plants (> 400 t/day of treated waste).

Figure 2.6. Some dry acid gas removal configurations: a) spray dryer absorption; b) circulating dry scrubber; c) furnace sorbent injection + dry sorbent injection w/ pre-dusting; d) system with rehydrated sorbent recirculation; e) two-stage dry treatment system.



3 Carbon capture with solid sorbents: state of the art

3.1 The concept of carbon capture and storage

Despite the scientific and political awareness of the threats of climate change mentioned in section 1.4, meaningful actions to limit CO₂ emissions worldwide collide with the tight bond between CO₂ generation and energy production. Even if renewable energies are making remarkable progress, fossil fuel consumption worldwide is still increasing year-by-year (IEA, 2016). Coal, oil and natural gas are still expected to play a major role in the world energy mix in the near- to mid-term future (McKinsey & Company, 2008).

Large stationary sources like coal-fired power plants are the main contributors to CO₂ emissions (Choi et al., 2009) and, therefore, the deployment of industrial CO₂ capture and storage (CCS) technologies could be a promising approach to achieve a meaningful reduction of CO₂ emissions in the near term (MacDowell et al., 2010). The CCS process consists in capturing waste CO₂ from large point sources and disposing of it in safe storage sites, like underground geological formations. Therefore, CCS has to be seen as an interim solution, a direct emissions mitigation option to buy time for a 50-year transition away from fossil fuels (Stuart Haszeldine, 2009).

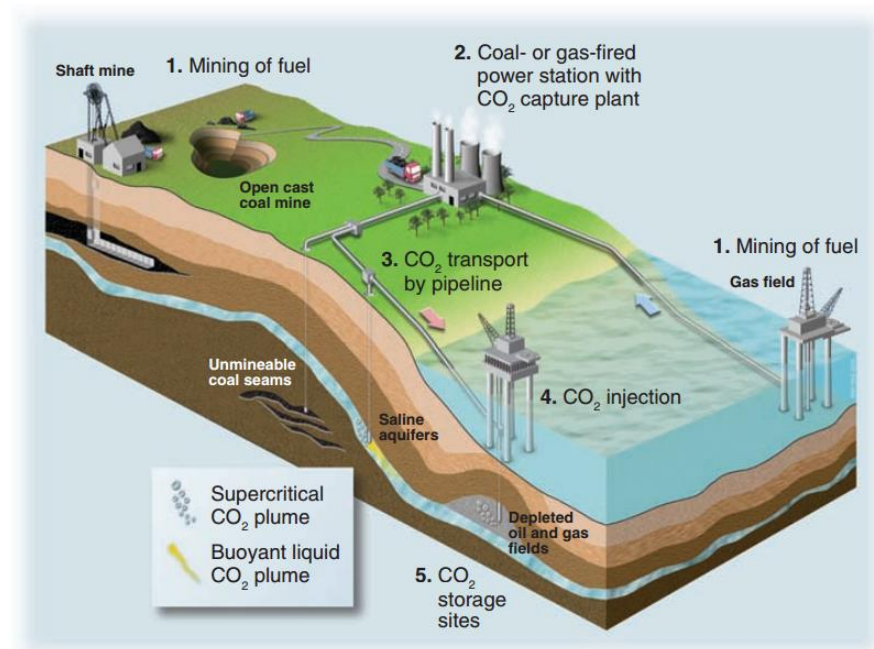


Figure 3.1. The life-cycle chain of fossil fuel use with CCS employment. CO₂ is separated and captured at power plants and stored in porous rocks deep below ground. Source: Stuart Haszeldine, 2009.

3.2 Approaches to CO₂ capture

Three methods of CO₂ capture are currently under study:

- **Post-combustion capture.** CO₂ is removed from the flue gas of the combustion process with an end-of-pipe approach, like for the acid gases (chapter 2). Post-combustion schemes are attractive for retrofitting existing power plants. Here, the major challenge for separation technologies is obtaining a pure (> 95 vol. %), concentrated stream of CO₂ from the typically dilute (< 15 vol. %) flue gas, without excessive energy penalty (Leung et al., 2014).

- **Pre-combustion capture.** In this approach, the fuel (e.g., coal or natural gas) is pre-treated before combustion. For example, coal might be gasified to produce a syngas consisting of CO and H₂. Then, the syngas undergoes water gas shift reaction with steam in order to form more H₂ while CO is converted to CO₂ (Rahman et al., 2017). The CO₂ concentration in the gas stream is generally rather high (20-30%, Boon et al., 2016), facilitating the separation needed to obtain a hydrogen-rich fuel gas.
- **Oxyfuel combustion.** In oxyfuel combustion, the fuel is combusted in nearly pure O₂, instead of air. Therefore, the amount of nitrogen present in the flue gas is drastically reduced and the main exhaust gases are CO₂ and H₂O. The water content is easily removed by condensation, leaving a pure CO₂ stream which is suitable for compression, transport and storage (MacDowell et al., 2010).

Several technological solutions have been explored to realise pre- or post-combustion CO₂ capture processes, as an emanation of the diverse research programmes financed by public institutions and private companies in the last years.

Absorption, i.e. the use of a liquid sorbent to remove CO₂ from the flue gas, has been the first separation process to be studied, with the first patent regarding amine scrubbing dating back to 1930 (Rochelle, 2009). Currently, monoethanolamine (MEA) is the reference solvent used in CO₂ absorption pilot plants, showing CO₂ separation efficiencies > 90% (Aaron and Tsouris, 2005), while other solvents such as piperazine (Zhang et al., 2016) and anion-functionalised ionic liquids (Macfarlane et al., 2014) are catalysing novel research efforts.

Membranes constitute another viable option for selective CO₂ separation. Current ceramic or polymeric membrane can achieve CO₂ separation efficiencies in the range 80-85% (Leung et al., 2014), but performances are strongly affected by CO₂ concentration. Breakthrough developments in enhancing CO₂ performance and solving fouling issues are needed to harness the full potential of this technology (Brunetti et al., 2010).

Chemical looping combustion (CLC) is based on the use of a metal oxide as oxygen carrier in order to obtain a CO₂-rich flue gas. During CLC, the metal oxide is reduced to metal while the fuel is being oxidised to CO₂ and water. Hence, like in oxyfuel combustion, a pure CO₂ stream can be easily produced via condensation. The metal is reconverted to metal oxide in a dedicated oxidation stage and recirculated back in the process. Several low-cost metal oxides, such as CuO (Imtiaz et al., 2012), Fe₂O₃ (Yüzbasi et al., 2016) and Mn₂O₃ (Hosseini et al., 2015), have been demonstrated suitable for CLC applications, but operating experience at pilot scale is still lacking.

Adsorption processes, in contrast to absorption, make use of solid sorbents to physically or chemically bind CO₂. Sorbent as diverse as activated carbon (Xing et al., 2012), zeolites (Bae et al., 2013), metal-organic frameworks (Bae and Snurr, 2011), hydrotalcites (Coenen et al., 2016) and metal oxides (Wang et al., 2014) have been tested extensively. Adsorbed CO₂ can be recovered via desorptive regeneration of the sorbent, by swinging pressure or temperature of the system (Leung et al., 2014). A particularly promising scheme is represented by the *carbonate looping technology* described in the following section.

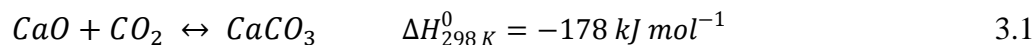
Table 3.1. Summary of advantages and disadvantages of main CO₂ separation technologies.

Separation technology	Advantages	Disadvantages	References
Absorption	<ul style="list-style-type: none"> - Most mature technology (the basic principle of the process was patented in 1930) - Regeneration by heating and/or depressurisation - MEA-based absorption mature process for CO₂ separation - Important industrial players actively engaged in research and deployment of this technology - New promising schemes based on piperazine as highly reactive CO₂ solvent are under study 	<ul style="list-style-type: none"> - Significant energy penalty associated with solvent regeneration - High solvent flow rates required to achieve high rate of CO₂ capture, given the low CO₂ partial pressure in the flue gas - Generation of wastewater (exhaust solvent) - Fugitive solvent emissions rise environmental concerns 	Aaron and Tsouris (2005) Rochelle (2009) MacDowell et al. (2010)
Adsorption	<ul style="list-style-type: none"> - Use of abundant and inexpensive natural sorbents (e.g. limestone, dolomite) - Potential higher cost-efficiency compared to amine scrubbing - Important synergy with the cement industry - Process successfully tested at demonstration scale in Spain and Germany - Alternatives to Ca-based sorbents for CO₂ capture at low, intermediate and high temperature currently under study (e.g. Na₂CO₃, MgO, Li₄SiO₄, etc.) 	<ul style="list-style-type: none"> - High energy penalty for CO₂ desorption - Ca-based sorbents are vulnerable to decay in capture capacity over repeated cycling - Competitive reactions with acid gases (HCl, SO₂) may consume relevant amounts of the sorbent, if separate desulfurisation is not employed 	Blamey et al. (2010) Dean et al. (2011) Boot-Handford et al. (2014)
Membrane separation	<ul style="list-style-type: none"> - Several membrane classes currently researched (inorganic membranes, polymeric membranes, facilitated liquid membranes) - Successful operational experience in the separation of other gases 	<ul style="list-style-type: none"> - At least a 10-fold higher CO₂ permeance than current commercial membranes is required to provide enough driving force to the process - Reliability concerns due to several operational problems (e.g. low fluxes, fouling, etc.) 	Brunetti et al. (2010) D'Alessandro et al. (2010) Merkel et al. (2010)
Chemical looping combustion	<ul style="list-style-type: none"> - Like for the oxyfuel approach, CO₂ is the main combustion process, thus avoiding energy intensive separation from N₂ - Wide portfolio of oxygen-carriers tested in literature for different combustion conditions 	<ul style="list-style-type: none"> - No large scale operational experience to-date - Lack of information on CLC performances in pressure 	Adanez et al. (2012)

3.3 Perspective of carbonate looping in pre- and post-combustion CO₂ capture

The carbonate looping concept for CO₂ capture, first proposed by Shimizu et al. (1999), is based on the reversible reaction between certain metal oxides and carbon dioxide to form metal carbonate. The most studied solid sorbent candidate is calcium oxide (CaO), which can be derived from natural limestone. Hence, the process is frequently referred to as *Calcium Looping* (Blamey et al., 2010).

The reaction of interest is the following:



The carbonation reaction is exothermic and the reverse reaction, known as calcination, is endothermic. Carbonation is characterised by a rapid initial rate followed by an abrupt transition to a sluggish regime, whereas calcination typically proceeds rapidly to completion in minutes over a wide range of conditions (Silaban and Harrison, 1995).

Calcium looping has been first conceived for post-combustion CO₂ capture. The simplified post-combustion process flow diagram is shown in Figure 3.2. In one vessel, the carbonator, the carbonation reaction removes CO₂ from a flue gas (e.g., the exhaust gas from coal combustion), forming solid CaCO₃. CaCO₃ is then transferred to a second reaction vessel, the calciner, where it is heated to trigger the reverse calcination reaction, releasing CO₂ and regenerating the CaO sorbent, which is recycled back into the carbonator. A circulating fluidised bed reactor (CFB), which is a mature technology at the large scale, is the typical configuration proposed for both carbonator and calciner (MacDowell et al., 2010).

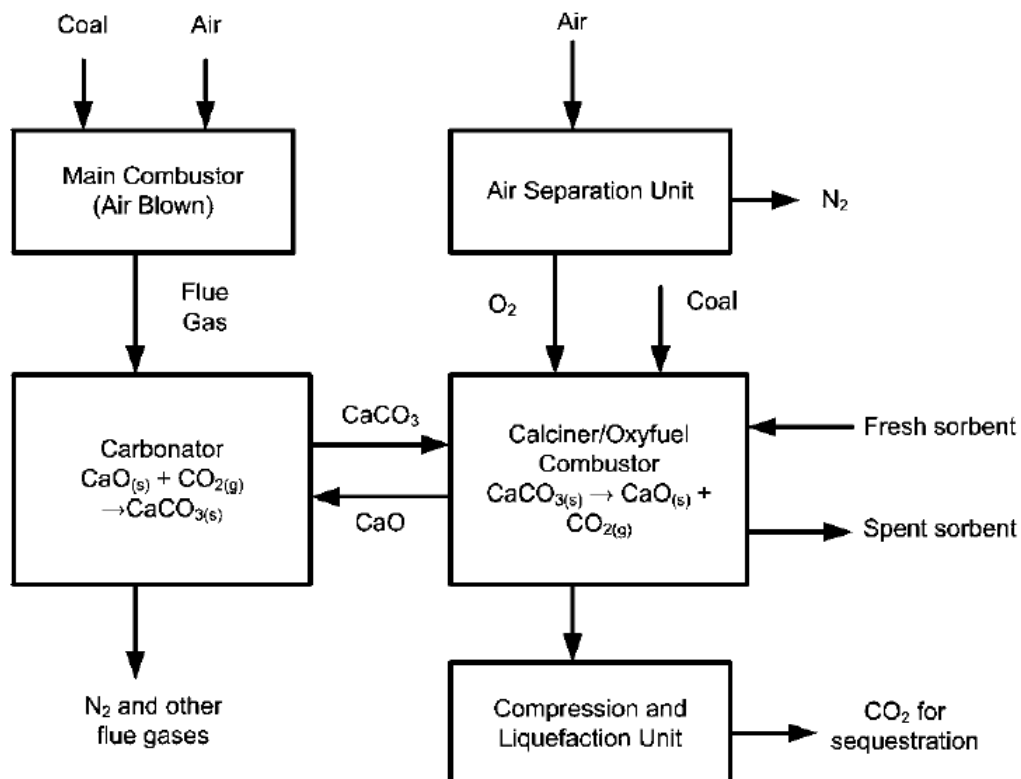
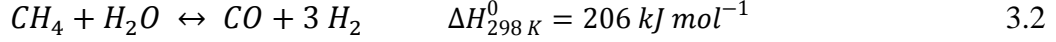


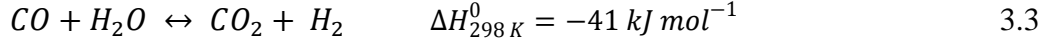
Figure 3.2. Post-combustion carbonate looping. Source: MacKenzie et al. (2007).

Whilst originally introduced for post-combustion capture applications, carbonate looping is also suitable in pre-combustion capture schemes aimed at the selective production of hydrogen from hydrocarbons (coal and biomass gasification, methane reforming, etc.). These approaches,

commonly referred to as sorbent-enhanced reforming (SER; MacDowell et al., 2010), take advantage of the carbonation of sorbent for the twofold goal of separating CO₂ and promoting H₂ generation. An explicative application is the sorbent-enhanced methane steam reforming (Broda et al., 2012). In a dedicated hydrogen production plant, the methane steam reforming reaction, performed over a Ni catalyst, proceeds as follows:



and the effluent gas is further enriched in H₂ thanks to the water gas shift reaction (over Fe or Cu catalyst, depending on operating temperature; Newsome, 1980):



By coupling CO₂ sorption by CaO (reaction 3.1) with reactions 3.2 and 3.3, the equilibrium of the overall process:



is shifted on the product side, thus producing high-purity hydrogen.

As summarised in Table 3.1, the carbonate looping scheme boasts the potential to provide cost-effective CO₂ capture. Sorbents derived from natural limestone are inexpensive and the process economics appears particularly favourable when the exhausted reactants are considered as a feedstock for cement manufacturing (Dean et al., 2011). In addition, several researchers pointed out that the carbonate looping process might significantly reduce the efficiency penalty (i.e. the net decrease in the power efficiency of a thermoelectric plant caused by the CO₂ capture and compression process) when compared to the more mature amine scrubbing technology: the energy penalty associated with Calcium Looping have been estimated in the range 3-8% (Goto et al., 2013; Hanak et al., 2015), an extremely competitive figure compared to the 10-12% drop in efficiency estimated for MEA-based scrubbing (Xu et al., 2010; Hanak et al., 2014). These are the main reasons which have been driving a rapid evolution of post-combustion carbonate looping from the lab- and pilot- to demonstration-scale (Arias et al., 2013; Dieter et al., 2014). Furthermore, whereas calcium oxide is clearly the most studied carbonate looping sorbent, thriving research efforts are currently dedicated worldwide to the study of alternative sorbents, capable of operating at different temperature ranges or overcoming the intrinsic shortcomings of CaO (see sections 4.1 and 9.1), and the work presented in Part III of the thesis goes into that direction.

4 Research needs and motivation of the study

4.1 Challenges in the use of sorbents for acid gas removal

In the light of the state-of-the-art described in the above chapters, the perspectives for a strengthened role of solid sorbents in the energy sector appear promising. In the waste incineration sector, the market outlook is favourable for acid gas treatment systems based on dry sorbent injection over traditional wet approaches. In the CCS field, the development of the carbonate looping concept is making steady progress towards the deployment of marketable CO₂ capture solutions based on the cycling of solid sorbents.

Nonetheless, several aspects still need to be addressed.

- **Lack of fundamental understanding.** Its heterogeneous nature makes gas-solid reaction a complex process, which results from the superimposition of different effects, such as flow through a porous fixed or fluidised bed of particles, diffusion in the particle pores and in the shell of solid products, and chemical reaction with the sorbent, where also equilibrium thermodynamics plays an important role (Antonioni et al., 2016). A detailed description of the kinetic and mass transfer phenomena involved in acid gas sorption will be given in chapter 6. Although the dry acid gas removal process has been serving as a reliable commercial technology for more than 30 years, some fundamental aspects are still obscure. For instance, even well-established gas-solid reaction models struggle to grasp the complex dependence of sorbent reactivity on several conditions (temperature, humidity, sorbent morphology, acid gas concentration) without resorting to empirical, adjustable parameters. At the same time, modelling efforts have been regularly focused to the description of laboratory data and to-date only a handful of studies approached the modelling of full-scale treatment systems (see chapter 7). Casting light on these open issues is the key step in enabling a fully-aware process optimisation, which can result in a reduced consumption of sorbents and, consequently, in lower operating costs and lower generation of residues to be disposed of.
- **Incomplete conversion.** One of the main problems affecting acid gas removal by Ca-based sorbents is the incomplete utilisation of the solid reactant: the sorption of acid gases stops before the sorbent particles are completely converted to the solid product of reaction. The same behaviour has been observed for CaO reacting with CO₂ in the carbonate looping process: after a fast, initial chemically-controlled reaction stage, reactivity declines abruptly and tends asymptotically to a “*maximum conversion*” value. The decay appears to be related to the total available reacting surface of the sorbent, since the maximum conversion decreases over cycling due to sintering, but even the increased resistance to CO₂ diffusion generated by product layer growth plays a major role. According to a widely accepted explanation (Alvarez and Abanades, 2005), the maximum conversion should be related to a critical thickness of the carbonate layer, which stems from the same thermodynamic considerations which will be addressed in chapter 6 with reference to HCl removal. Analogous issue affects the conversion of MgO, the sorbent for CO₂ capture at intermediate temperature investigated in Part III of the thesis.
- **Sintering.** Shrinkage and loss of porosity upon exposure to heat affects materials prone to sintering such as the solid reactants for acid gas removal. In the industrial practice of dry injection systems, this issue prevents the use of Ca-based and Na-based sorbents at high

temperature, because the loss of reactivity due to sintering outweighs the gains in terms of reaction kinetics. Sintering is even more problematic for the CO₂ capture technologies based on carbonate looping, which rely on the prolonged cycling of sorbents in loops of carbonation and calcination at high temperature. In both contexts, proper material choice and synthesis approaches are the routes currently investigated to tackle sintering: the introduction of commercial dolomitic sorbents has recently enabled efficient furnace sorbent injection for acid gas removal (Dal Pozzo et al., 2016), as mentioned in section 2.4, while the incorporation of sintering-resistant matrices in Ca-based CO₂ sorbents has been explored by several investigators as a promising way to increase cyclic stability of CO₂ capture (Kierzkowska et al., 2013).

- **Fate of the solid residues.** Although one of the main advantages that have made dry sorption competitive towards wet treatment methods is the avoided generation of wastewater, even the solid waste associated to dry operation can constitute a problem in a holistic approach to environmental protection as the one underlying the European circular economy strategy (European Commission, 2014). Currently, disposal is the main management solution for dry sorption residues (Margallo et al., 2015) and the introduction of valorisation routes is sought after in order to divert waste fluxes from landfills and increase the overall sustainability of flue gas cleaning technologies. If the carbonate looping process for CO₂ capture eventually breaks into market, management of carbonated residues will be a likewise issue and some studies are already exploring the possibility of integration with other industrial sectors, such as cement manufacturing (Hills et al., 2016).

4.2 Overcoming the limitations of gas-solid reactions by process optimisation

In the industrial practice of dry injection systems, the lack of detailed knowledge about gas-solid reactions is offset by over-stoichiometric feed rates of reactants and proper automated control systems, which ensure a safe compliance to emission limit values of acid pollutants.

However, when multi-stage acid gas treatment systems or recirculating equipment are employed, the degrees of freedom increase and just setting the automated control in order to guarantee the bare emission compliance does not ensure that the treatment system is operated at its optimum (de Greef et al., 2013). Given the overall acid gas removal performance required, what is the most efficient repartition of reactants between the multiple treatment stages of the system? What is the best recirculation ratio for systems allowing recycling of residues? How does the optimal configuration change as a function of operating conditions (e.g., type of waste or acid gas concentration required at stack)?

The answer to these questions, which translates in significant savings in operating costs and indirect environmental gains related to the lower consumption of sorbents, relies on process modelling. Models can derive from a fundamental approach, taking into account the actual physical and chemical phenomena involved in the gas-solid reaction and extending this microscopic description to geometries of increasing complexity (from the single sorbent particle to the filter cake growing on the bags of a fabric filter), or from an empirical “black box” approach, finding a relationship between sorbent feed rate and removal efficiency and calibrating a model fit thanks to operational plant data. **Part II in the thesis shows the implementation of both these strategies.**

4.3 Overcoming the limitations of gas-solid reactions by synthesis approaches

If careful process modelling allows harnessing the full potential of natural and commercial solid sorbents, the development of new, synthetic materials is needed when the required performances are

out of the reach of conventional materials. This is particularly urgent in the carbonate looping context, where substantial research efforts are dedicated to the modification of natural sorbents in order to obtain i) a high CO₂ uptake capacity and ii) an appreciable stability of performance over repeated carbonation and calcination cycles (Kierzkowska et al., 2013).

This is the main aim of Part III in the thesis. Magnesium oxide, a promising sorbent for intermediate temperature CO₂ capture, boasts a very high theoretical CO₂ uptake capacity (1.09 g CO₂/ g MgO), but its reactivity is severely hindered by diffusional limitations which restrict the actual solid conversion after hours of exposure to CO₂ to values lower than 2-3%. The problem of MgO incomplete conversion is akin to what observed for Ca-based acid gas removal at low temperature (section 6.2), but the effect is magnified by the superior diffusional resistance constituted by carbonate layer than that of chlorinated layer.

References (Part I)

- Adanez, J., Abad, A., Garcia-Labiano, F., Gayan, P., de Diego, L.F., 2012. *Progress in Chemical-Looping Combustion and Reforming technologies*. Progress in Energy and Combustion Science 38, 215-282.
- Alvarez, D., Abanades, J.C., 2005. *Determination of the Critical Product Layer Thickness in the Reaction of CaO with CO₂*. Industrial & Engineering Chemistry Research 44 (15), 5608-5615.
- Antonioni, G., Guglielmi, D., Cozzani, V., Stramigioli, C., Corrente, D., 2014. *Modelling and simulation of an existing MSWI flue gas two-stage dry treatment*. Process Safety and Environmental Protection 92, 242-250.
- Antonioni, G., Dal Pozzo, A., Guglielmi, D., Tugnoli, A., Cozzani, V. (2016). *Enhanced modelling of heterogeneous gas-solid reactions in acid gas removal dry processes*. Chemical Engineering Science 148, 140-154.
- Arias, B., Diego, M.E., Abanades, J.C., Lorenzo, M., Diaz, L., Martinez, D., Alvarez, J., Sanchez-Biezma, A., 2013. *Demonstration of steady state CO₂ capture in a 1.7 MW_{th} calcium looping pilot*. International Journal of Greenhouse Gas Control 18, 237-245.
- Bae, T.-H., Hudson, M.R., Mason, J.A., Queen, W.L., Dutton, J.J., Sumida, K., Micklash, K.J., Kaye, S.S., Brown, C.M., Long, J.R., 2013. *Evaluation of cation-exchanged zeolite adsorbents for post-combustion carbon dioxide capture*. Energy and Environmental Science 6, 128-138.
- Bae, Y.-S., Snurr, R.Q., 2011. *Development and evaluation of porous materials for carbon dioxide separation and capture*. Angewandte Chemie 50 (49), 11586-11596.
- Baird, C., Cann, M., 2008. *Environmental Chemistry*. 4th edition, W. H. Freeman, New York, NY (USA).
- Barontini, F., Marsanich, K., Petarca, L., Cozzani, V., 2005. *Thermal degradation and decomposition products of electronic boards containing BFRs*. Industrial & Engineering Chemistry Research 44 (12), 4186-4199.
- Bausach, M., Pera-Titus, M., Fite, C., Cunill, F., Izquierdo, J.F., Tejero, J., Iborra, M., 2006. *Water-induced rearrangement of Ca(OH)₂ (001) surfaces reacted with SO₂*. AIChE Journal 52, 2876-2886.
- Biganzoli, L., Racanella, G., Rigamonti, L., Marras, R., Grosso, M., 2015. *High temperature abatement of acid gases from waste incineration. Part I: experimental tests in full scale plants*. Waste Management 36, 98-105.
- Blamey, J., Anthony, E.J., Wang, J., Fennell, P.S., 2010. *The calcium looping cycle for large-scale CO₂ capture*. Progress in Energy and Combustion Science 36 (2), 260-279.
- Bodénan, F., Deniard, P., 2003. *Characterization of flue gas cleaning residues from European solid waste incinerators: assessment of various Ca-based sorbent processes*. Chemosphere 51, 335-347.
- Bogush, A., Stegemann, J.A., Wood, I., Roy, A., 2015. *Element composition and mineralogical characterisation of air pollution control residue from UK energy-from-waste facilities*. Waste Management 36, 119-129.
- Boon, J., Spallina, V., van Delft, Y., van Sint Annaland, M., 2016. *Comparison of the efficiency of carbon dioxide capture by sorption-enhanced water-gas shift and palladium-based membranes for power and hydrogen production*. International Journal of Greenhouse Gas Control 50, 121-134.
- Boot-Handford, M.E., Abanades, J.C., Anthony, E.J., Blunt, M.J. et al., 2014. *Carbon capture and storage update*. Energy and Environmental Science 7, 130-189.

BREF GLS, 2012. *Reference Document on the Best Available Techniques for the Manufacture of Glass (GLS)*. European Commission. Available at: eippcb.jrc.ec.europa.eu/reference/BREF/GLS_Adopted_03_2012.pdf (last accessed: 14/03/2016)

BREF LVIC-S, 2007. *Reference Document on the Best Available Techniques on Large Volume Inorganic Chemicals - Solids and Others industry (LVIC-S)*. European Commission. Available at: eippcb.jrc.ec.europa.eu/reference/BREF/lvic-s_bref_0907.pdf (last accessed: 14/03/2016)

BREF WI, 2006. *Reference Document on the Best Available Techniques for Waste Incineration*.

Brivio, S., 2005. *The SOLVAL platform: a sodium sludges valorization, an industrial reality for the environment* (in Italian). L'Ambiente 3, 48-49. Available at: www.ranierieditore.it/pdf/solval.pdf (last accessed: 14/03/2016)

Brivio, S., 2007. *Depurazione dei fumi e valorizzazione dei prodotti* (in Italian). Power Technology 4, 42–44.

Broda, M., Kierzkowska, A.M., Baudouin, D., Imtiaz, Q., Copéret, C., Müller, C.R., 2012. *Sorbent-Enhanced Methane Reforming over a Ni–Ca-Based, Bifunctional Catalyst Sorbent*. ACS Catalysis 2, 1635-1646.

Brunetti, A., Scura, F., Barbieri, G., Drioli, E., 2010. *Membrane technologies for CO₂ separation*. Journal of Membrane Science 359, 115–25.

Coenen, K., Gallucci, F., Cobden, P., van Dijk, E., Hensen, E., van Sint Annaland, M., 2016. *Chemisorption working capacity and kinetics of CO₂ and H₂O of hydrotalcite-based adsorbents for sorption-enhanced water-gas-shift applications*. Chemical Engineering Journal 293, 9-23.

Cook, J., Oreskes, N., Doran, P.T., Anderegg, W.R., Verheggen, B., Maibach, E.W., Carlton, J.S., Lewandowsky, S., Skuce, A.G., Green, S.A., Nuccitelli, D., Jacobs, P., Richardson, M., Winkler, B., Painting, R., Rice, K., 2016. *Consensus on consensus: a synthesis of consensus estimates on human-caused global warming*. Environmental Research Letters 11 (4), 1-7.

D'Alessandro, D.M., Smit, B., Long, J.R., 2010. *Carbon Dioxide Capture: Prospects for New Materials*. Angewandte Chemie 49, 6058-6082.

Dal Pozzo, A., Guglielmi, D., Antonioni, G., Cozzani, V., Calvani, S., Bonanini, G. (2016). *Trattamento a secco dei fumi di combustione prodotti nella termovalorizzazione di RSU* (in Italian). La Termotecnica 70 (3), 53-57.

Dal Pozzo, A., Guglielmi, D., Antonioni, G., Tugnoli, A., Cozzani, V. (2017). *Environmental assessment of combined acid gas emission control with alternative dry sorbent injection systems*. Submitted for ICheaP-13, 28-31 May 2017, Milano.

de Greef, J., Villani, K., Goethals, J., Van Belle, H., Van Caneghem, J., Vandecasteele, C., 2013. *Optimising energy recovery and use of chemicals, resources and materials in modern waste-to-energy plants*. Waste Management 33, 2416–2424.

Dean, C.C., Blamey, J., Florin, N.H., Al-Jeboori, M.J., Fennell, P.S., 2011. *The calcium looping cycle for CO₂ capture from power generation, cement manufacture and hydrogen production*. Chemical Engineering Research and Design 89, 836-855.

Dieter, H., Bidwe, A.R., Varela-Duelli, G., Charitos, A., Hawthorne, C., Scheffknecht, G., 2014. *Development of the calcium looping CO₂ capture technology from lab to pilot scale at IFK, University of Stuttgart*. Fuel 127, 23-37.

Duo, W., Kirkby, N., Seville, J.P.K., Kiel, J.H.A., Bos, A., den Uil, H., 1996. *Kinetics of HCl reactions with calcium and sodium sorbents for IGCC fuel gas cleaning*. Chemical Engineering Science 51 (11), 2541-2546.

- European Commission, 2014. *Towards a circular economy: A zero waste programme for Europe*. Communication. <eur-lex.europa.eu/legal-content/EN/TXT/?uri=CELEX:52014DC0398R%2801%29>
- Fonseca, A.M., Orfao, J.J., Salcedo, R.L., 1998. *Kinetic modeling of the reaction of HCl and solid lime at low temperatures*. Industrial & Engineering Chemistry Research 37, 4570-4576
- Foo, R., Berger, R., Heiszwolf, J.J., 2016. *Reaction Kinetic Modeling of DSI for MATS Compliance*. Power Plant Pollutant Control and Carbon Management “MEGA” Symposium (16-19 August 2016), Baltimore, MD (USA).
- Gambaré, A., Palini, E., Spadoni, L., Gnatta, A., 2013. *Il sistema di desolforazione a semi-secco della Centrale Lamarmora di Brescia* (in Italian). La Termotecnica 67 (10), 63-66.
- Goto, K., Yogo, K., Higashii, T., 2013. *A review of efficiency penalty in a coal-fired power plant with post-combustion CO₂ capture*. Applied Energy 111, 710–720.
- Guglielmi, D., Antonioni, G., Stramigioli, C., Cozzani, V., 2014. *Investigation of performance of different sorbents in a two-stage flue gas dry treatment of a MSWI*. Chemical Engineering Transactions 43, 1921-1926.
- Gullett, B.K., Jozewicz, W., Stefanski, L.A., 1992. *Reaction Kinetics of Ca-Based Sorbents with HCl*. Industrial & Engineering Chemistry Research 31, 2437-2446.
- Hanak, D.P., Biliyok, C., Yeung, H., Bialecki, R., 2014. *Heat integration and exergy analysis for a high ash supercritical coal-fired power plant integrated with a post-combustion carbon capture process*. Fuel 134, 126–139.
- Hanak, D.P., Anthony, E.J., Manovic, V., 2015. *A review of developments in pilot-plant testing and modelling of calcium looping process for CO₂ capture from power generation systems*. Energy and Environmental Science 8, 2199-2249.
- Harriott, P., 1990. *A Simple Model for SO₂ Removal in the Duct Injection Process*. Journal of the Air & Waste Management Association 40 (7), 998-1003.
- Harriott, P., Ruether, J., Sudhoff, F., 1991. *Prediction of SO₂ Removal for Power Plants Using Duct Injection of Lime Slurry*. Energy & Fuels 5, 254-258.
- Hartman, M., Svoboda, K., Pohorely, M., Syc, M., 2013. *Thermal Decomposition of Sodium Hydrogen Carbonate and Textural Features of Its Calcines*. Industrial & Engineering Chemistry Research 52, 10619-10626.
- Hills, T., Leeson, D., Florin, N., Fennell, P., 2016. *Carbon Capture in the Cement Industry: Technologies, Progress, and Retrofitting*. Environmental Science and Technology 50 (1), 368-377.
- Hoffman, R.S., Nelson, L.S., Howland, M.A., Lewin, N.A., Flomenbaum, N.E., Goldfrank, L.R., 2007. *Goldfrank's Manual of Toxicologic Emergencies*. 1st edition, McGraw-Hill, New York, NY (USA).
- Hosseini, D., Imtiaz, Q., Abdala, P.M., Yoon, S., Kierzkowska, A.M., Weidenkaff, A., Müller, C.R., 2015. *CuO promoted Mn₂O₃-based materials for solid fuel combustion with inherent CO₂ capture*. Journal of Materials Chemistry A 3 (19), 10545-10550.
- Kimura, S., Smith, J. M., 1987. *Kinetics of the Sodium Carbonate-Sulfur Dioxide Reaction*. AIChE Journal 33, 1522–1532.
- Kong, Y., Davidson, H., 2010. *Dry sorbent injection of sodium sorbents for SO₂, HCl and mercury mitigation*. 18th Annual North American Waste-to-Energy Conference (11-13 May 2010), Orlando, FL (USA).
- Krug, E.C., Frink, C.R., 1983. *Acid Rain on Acid Soil: A New Perspective*. Science 221, 520-525.

Imtiaz, Q., Kierzkowska, A.M., Müller, C.R., 2012. *Coprecipitated, copper-based, alumina-stabilized materials for carbon dioxide capture by chemical looping combustion*. ChemSusChem 5 (8), 1610-1618.

ISWA, 2008. *Management of APC residues from WtE plants – an overview of management options and treatment methods*. International Solid Waste Association. Available at: www.iswa.org/uploads/ttx_iswaknowledgebase/Management_of_APC_residues_from_WtE_Plants_2008_01.pdf (last accessed: 14/03/2016)

Leung, D.Y.C., Caramanna, G., Mercedes Maroto-Valer, M., 2014. *An overview of current status of carbon dioxide capture and storage technologies*. Renewable and Sustainable Energy Reviews 39, 426-443.

Levenspiel, O., 1998. *Chemical Reaction Engineering*. 3rd edition, John Wiley & Sons, New York, NY (USA).

MacDowell, N., Florin, N., Buchard, A., Hallett, J., Galindo, A., Jackson, G., Adjiman, C.S., Williams, C.K., Shah, N., Fennell, P., 2010. *An overview of CO₂ capture technologies*. Energy and Environmental Science 3, 1645-1669.

Macfarlane, D.R., Tachikawa, N., Forsyth, M., Pringle, J.M., Howlett, P.C., Elliott, G.D., Davis, J.H., Watanabe, M., Simon, P., Angell, C.A., 2014. *Energy applications of ionic liquids*. Energy and Environmental Science 7 (1), 232-250.

MacKenzie, A., Granatstein, D.L., Anthony, E.J., Abanades, J.C., 2007. *Economics of CO₂ capture using the calcium cycle with a pressurized fluidized bed combustor*. Energy & Fuels 21(2), 920–926.

Margallo, M., Taddei, M.B.M., Hernández-Pellón, A., Aldaco, R., Irabien, A., 2015. *Environmental sustainability assessment of the management of municipal solid waste incineration residues: A review of the current situation*. Clean Technologies and Environmental Policy 17, 1333-1353.

Matsukata, M., Takeda, K., Miyatani, T., Ueyama, K., 1996. *Simultaneous chlorination and sulphation of calcined limestone*. Chemical Engineering Science 51 (11), 2529-2534.

Merkel, T.C., Lin, H., Wei, X., Baker, R., 2010. *Power plant post-combustion carbon dioxide capture: An opportunity for membranes*. Journal of Membrane Science 359, 126-139.

Mocek, K., Lippert, E., Erdös, E., 1983. *Reactivity of the Solid Sodium Carbonate towards the Gaseous Hydrogen Chloride and the Sulfur Dioxide*. Collection Czechoslovak Chemistry Communications 48, 3500–3507.

Newsome, D.S., 1980. *The Water-Gas Shift Reaction*. Catalysis Reviews: Science and Engineering 21 (2), 275-318.

Niessen, W.R., 2002. *Combustion and Incineration Processes: Applications in Environmental Engineering*. 3rd edition, CRC Press, Oxford (UK).

Ninané, L., Adam, J.F., Humblot, C., 1995. *Method for producing an aqueous industrial sodium chloride solution*. U.S. Patent 5478447A.

Odén, S., 1968. *The acidification of air and precipitation and its consequences on the natural environment*. Ecology Committee Bulletin 1, Swedish National Science Research Council.

United Nations, 2015. *Adoption of the Paris Agreement*. Framework Convention on Climate Change, 21st Conference of the Parties, Paris (France).

Petrini, S., Eklund, H., Bjerle, I., 1979. *HCl-Absorption durch Kalkstein* (in German). Aufbereitungstechnik 6, 309–311.

Radojevic, M., Bashkin, V. N., 2006. *Practical Environmental Analysis*. RSC Publishing, Oxford (UK).

- Rahman, F.A., Aziz, M.M.A., Saidur, R., Abu Bakar, W.A.W., Hainin, M.R., Putrajaya, R., Abdul Hassan, N., 2017. *Pollution to solution: Capture and sequestration of carbon dioxide (CO₂) and its utilization as a renewable energy source for a sustainable future*. Renewable and Sustainable Energy Reviews 71, 112-126.
- Revelle, P., Revelle, C., 1992. *Global Environment: Securing a Sustainable Future*. Jones & Bartlett Publishing, Burlington, MS (USA).
- Rochelle, G.T., 2009. *Amine Scrubbing for CO₂ Capture*. Science 325, 1652-1654.
- Schreurs, M. A., 2007. *The Politics of Acid Rain in Europe*. In: Visgilio, G.R., Whitelaw, D.M., 2007. *Acid in the Environment: Lesson Learned and Future Prospects*. Springer, Berlin (Germany).
- Scripps Institution of Oceanography, 2016. *The Keeling Curve*. <<http://scripps.ucsd.edu/programs/keelingcurve/>> (accessed: 12/12/2016)
- Shimizu, T., Hirama, T., Hosoda, H., Kitano, K., Inagaki, M., Tejima, K., 1999. *A Twin Fluid-Bed Reactor for Removal of CO₂ from Combustion Processes*. Chemical Engineering Research and Design 77, 62-68.
- Silaban, A., Harrison, D.P., 1995. *High temperature capture of carbon dioxide: characteristics of the reversible reaction between CaO(s) and CO₂(g)*. Chemical Engineering Communications 137, 177–190.
- Simons, G.A., Garman, A.R., 1986. *Small pore closure and the deactivation of the limestone sulfation reaction*. AIChE Journal 32, 1491–1499.
- Smith, S.J., van Aardenne, J., Klimont, Z., Andres, R.J., Volke, A., Delgado Arias, S., 2011. *Anthropogenic sulfur dioxide emissions: 1850–2005*. Atmospheric Chemistry and Physics 11, 1101-1116.
- Srivastava, R.K., Jozewicz, W., 2001. *Flue Gas Desulfurization: The State of the Art*. Journal of the Air & Waste Management Association 51 (12), 1676-1688.
- Stuart Haszeldine, R., 2009. *Carbon Capture and Storage: How Green Can Black Be?* Science 325, 1647-1652.
- Tang, J., Wu, K., 2012. *Trend of acid rain over China since the 1990s*. 2013 NOAA ESRL Global Monitoring Annual Conference (21 March 2013), Boulder, CO (USA).
- Tertzakian, P., 2007. *A Thousand Barrels a Second: The Coming Oil Break Point and the Challenges Facing an Energy Dependent World*. McGraw-Hill, New York, NY (USA).
- Vehlow, J., 2015. *Air pollution control systems in WtE units: an overview*. Waste Management 37, 58–74.
- Viganò, F., Consonni, S., Grossi, M., Rigamonti, L., 2010. *Material and energy recovery from Automotive Shredded Residues (ASR) via sequential gasification and combustion*. Waste Management 30 (1), 145-153.
- Wang, J., Huang, L., Yang, R., Zhang, Z., Wu, J., Gao, Y., Wang, Q., O'Hare, D., Zhong, Z., 2014. *Recent advances in solid sorbents for CO₂ capture and new development trends*. Energy and Environmental Science 7, 3478-3518.
- Weinell, C.E., Jensen, P.I., Dam-Johansen, K., Livbjerg, H., 1992. *Hydrogen Chloride Reaction with Lime and Limestone: Kinetics and Sorption Capacity*. Industrial & Engineering Chemistry Research 31, 164-171.
- Wey, M.-Y., Ou, W.-Y., Liu, Z.-S., Tseng, H.-H., Yang, W.-Y., Chiang, B.-C., 2001. *Pollutants in incineration flue gas*. Journal of Hazardous Materials B82, 247-262.
- Xing, W., Liu, C., Zhou, Z., Zhang, L., Zhou, J., Zhuo, S., Yan, L., Gao, H., Wang, G., Qiao, S.Z., 2012. *Superior CO₂ uptake of N-doped activated carbon through hydrogen-bonding interaction*. Energy and Environmental Science 5, 7323-7327.

Xu, G., Jin, H.G., Yang, Y.P., Xu, Y.J., Lin, H., Duan, L., 2010. *A comprehensive techno-economic analysis method for power generation systems with CO₂ capture*. International Journal of Energy Research 34 (4), 321-332.

Yüzbasi, N.S., Kierzkowska, A.M., Imtiaz, Q., Abdala, P.M., Kurlov, A., Rupp, J.L.M., Müller, C.R., 2016. *ZrO₂-Supported Fe₂O₃ for Chemical-Looping-Based Hydrogen Production: Effect of pH on Its Structure and Performance As Probed by X-ray Absorption Spectroscopy and Electrical Conductivity Measurements*. Journal of Physical Chemistry C 120 (34), 18977-18985.

Zemba, S.G., Crouch, E.A.C., Miller, M.E., Green, L.C., 2013. *Pink Sky in the Morning, Should There Be a Warning?* 21st Annual North American Waste-to-Energy Conference (21-25 April 2013), Ft. Myers, FL (USA).

Zhang, Y., Freeman, B., Hao, P., Rochelle, G.T., 2016. *Absorber modeling for NGCC carbon capture with aqueous piperazine*. Faraday Discussions 192, 459-477.

Part II

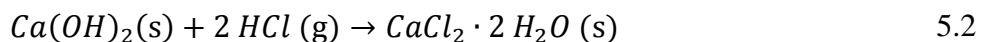
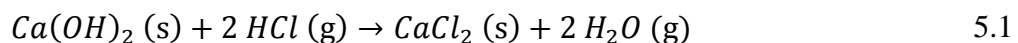
Application to HCl and SO₂ removal in Waste-to-Energy plants

5 Experimental study of acid gas removal processes: the reaction between Ca(OH)₂ and HCl

5.1 The reaction

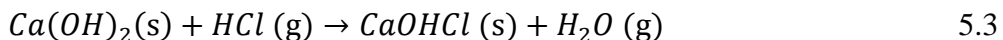
As outlined in the motivation of the study (chapter 4), goal and scope of Part II in the thesis is to explore acid gas removal from the basics of gas-solid reaction mechanisms up to the economic and environmental considerations on full-scale process implementation. Firstly, in order to lay the foundations for the formulation of a fundamental model for acid gas removal, described in chapter 6, an experimental campaign was carried out to study the reaction between calcium hydroxide, the most inexpensive and abundant natural sorbent (see section 2.2), and hydrogen chloride, the most relevant acid pollutant in flue gas deriving from waste combustion (see section 1.3).

The overall reaction between Ca(OH)₂ and HCl, also referred to as *chloridisation*, leads to the formation of calcium chloride (CaCl₂), in anhydrous (5.1) or dihydrate form (5.2):

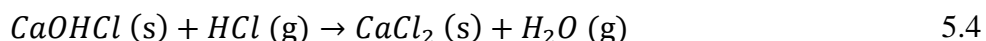


The formation of dihydrate calcium chloride besides that of anhydrous calcium chloride was evidenced by X-ray diffraction tests carried on by Gullett et al (1992) and by Jozewicz and Gullett (1995). However, Partanen et al. (2005) observed that, given the highly hygroscopic nature of calcium chloride, it is possible that the actual reaction product is anhydrous CaCl₂, that is then rapidly hydrated when the sample is extracted from the reactor and cooled at room temperature for XRD analysis.

Several authors also reported the formation of calcium hydroxychloride (CaOHCl) as solid product at the typical temperatures of industrial acid gas removal treatments (150-200 °C):



Weinell et al.(1992) and Gullett et al. (1992) stated that CaOHCl is an intermediate product that can further react with HCl to form CaCl₂:



Conversely, some studies (e.g., Bausach et al., 2006; Chin et al., 2005b) suggest that CaOHCl is the final product of the reaction between Ca(OH)₂ and HCl. Allal et al. (1998), confirming the study of Jozewicz et al. (1995), evidenced that Ca(OH)₂ and CaCl₂ can react to form CaOHCl:



Bodénan and Deniard (2003) analysed air pollution control (APC) residues of the flue gas treatment systems of 12 European MSWIs and found CaOHCl as the only product of the chlorination process. However, it is still unclear if the formation CaOHCl from CaCl₂ takes places during flue gas treatment or after the APC residues are removed from the process and stored at ambient conditions. Table 5.1 summarises the findings of studies aimed at specifying the products of Ca-based HCl sorption. Indeed, there is still a lack of knowledge about the yield of the HCl removal process by reaction with Ca(OH)₂ and, as a consequence, of the entire flue gas treatment section (Yassin et al., 2007), since the true utilisation of the sorbent depends on the actual reaction stoichiometry.

Table 5.1. Studies addressing identification of the solid product of the reaction between $\text{Ca}(\text{OH})_2$ and HCl.

Source	Identified product	Experimental conditions			Method of identification	Notes
		T (°C)	RH (%)	C _{HCl,in} (ppm)		
Gullett et al. (1992)	57% $\text{CaCl}_2 \cdot 2\text{H}_2\text{O}$ 28% unreacted CaO 10% CaOHCl 5% $\text{Ca}(\text{ClO})_2$	500	-	5000	XRD	<i>The hydrated form of CaCl_2 may be due to reaction with ambient air humidity of the highly deliquescent sample during interlaboratory transfer</i>
Jozewicz and Gullett (1995)	$\text{CaCl}_2 \cdot 2\text{H}_2\text{O}/\text{CaOHCl}$	500	-	1000	DSC, XRD	
	CaOHCl	200	-	1000	DSC, XRD	
Allal et al. (1998)	CaOHCl	250	-	1000	XRD	
Bodénan and Deniard (2003)	CaOHCl	140-170	0-10	?	XRD	<i>Samples of APC residues from 12 MSWIs across Europe</i>
Bausach et al. (2004)	CaOHCl	120	18	240	XRD	<i>Conversion to CaCl_2 can only take place if $\text{Ca}(\text{OH})_2$ is lacking, at least locally</i>
Chin et al. (2005a)	CaOHCl	200	-	500	XRD	
Partanen et al. (2005)	Final product: CaCl_2 Intermediate: CaOHCl	650/850	-	2000	XRD	<i>Hydrous CaCl_2 detected by XRD, but attributed to hydration after the sample was taken out of the reactor</i>
Bogush et al. (2015)	CaOHCl	150-200	0-10	?	XRD, FTIR, EDX	<i>Samples of APC residues from 6 British MSWIs</i>

5.2 Set-up of a dedicated laboratory apparatus

Aim of the experimental investigation of chloridisation was to collect data on the reaction at different temperature and HCl concentration, in order to provide a dataset for the validation of the fundamental model proposed in chapter 6. Previous studies on the reaction (Weinell et al., 1992; Duo et al., 1996; Yan et al., 2003; Partanen et al., 2005) only provided data about solid conversion, whereas data on the gas phase could give additional information. Therefore, an experimental apparatus designed for monitoring the HCl abatement by means of a fixed bed reactor was set up and Fourier transform infrared technology was chosen as monitoring media for its capacity to follow through cascading IR spectra acquisition the time-scale evolution of reaction with accurate definition. Furthermore, the analysis of reacted solid samples via TGA and XRD methods allowed advancing new evidences about product identification.

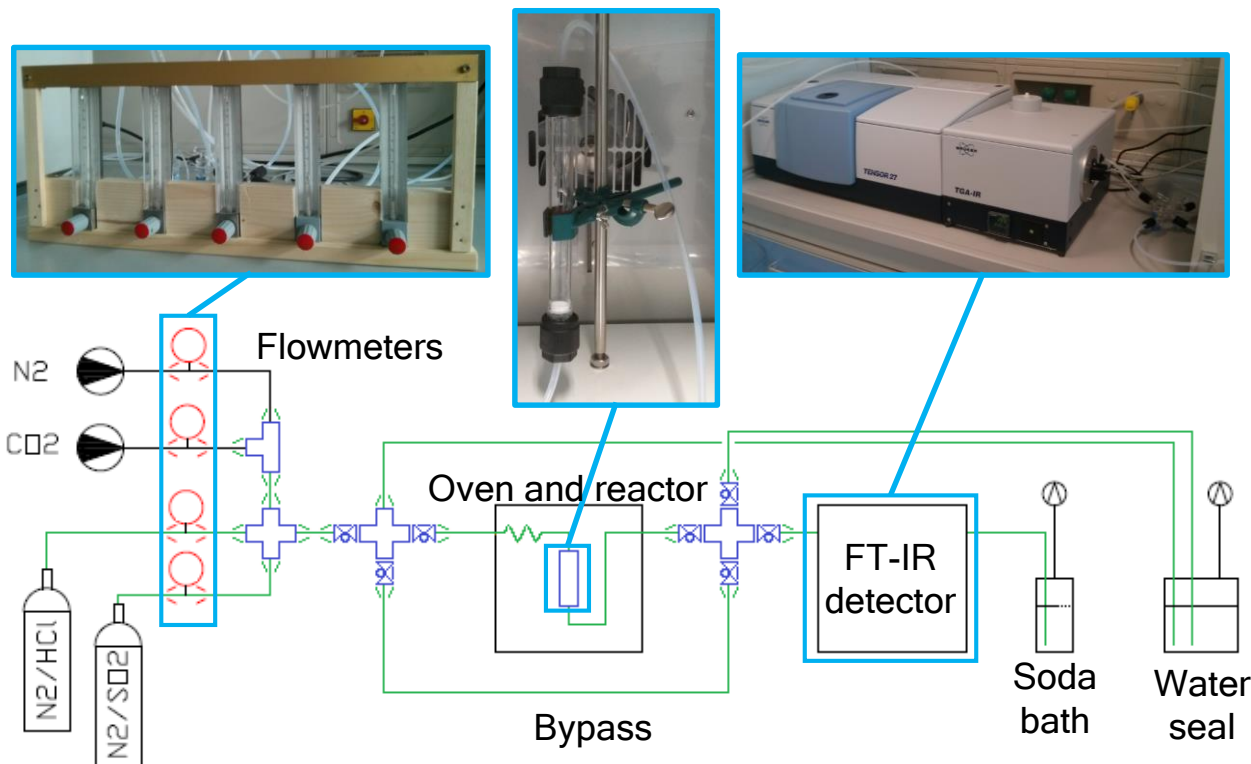


Figure 5.1. Layout of the experimental apparatus.

The experimental setup is laid out in Figure 5.1. The designed apparatus consists in a tubular reactor filled with a solid sorbent, where a synthetic flue gas was fluxed (a fixed bed reactor, FBR, configuration). The gas mixture was synthesised by diluting the stream coming from a cylinder containing HCl at 3% in nitrogen with a stream of dry nitrogen coming from a laboratory supply line. The output of the N₂/HCl cylinder was regulated by a mass flow controller (Bronkhorst, EL-FLOW) operating in the range 0.4-20 NmL/min, while the dry N₂ stream was controlled with a rotameter (Rota-Yokogawa, RAGK) of flow scale 1-14 NL/h.

Before entering the reactor, the simulated flue gas flowed in a section of tube placed inside the oven that is aimed to bring the gas to the design temperature. When the gas reached the reactor, it flowed through a fixed bed of sorbent particles, where neutralization reactions of acid gases took place.

The reactor was a cylinder 150 mm long by 15 mm of inner diameter, as shown in Figure 5.2. The tubular reactor housed a fixed bed of sorbent, deposited on a sintered glass frit disk settled at 20 mm from the outlet section. The body of the reactor was made of borosilicate glass, while screw joints and tubing were made of PTFE. In order to operate at a constant temperature, the reactor was placed in an oven (Binder, FD-53) and kept in contact with a K-type thermocouple. The reactor was designed to simulate the conditions of the cake of particles deposited on the filter bags of a fabric filter: in particular, inner diameter was chosen in order to obtain a superficial velocity of the flue gas of 0.9 m/min at 180 °C, which corresponds to a typical design value for baghouse (Green and Perry, 2007).

A Fourier transform infrared (FTIR) spectrometer was used to characterise quantitatively the gaseous products of the neutralization process. The FTIR spectrometer was a Bruker TENSOR 27 equipped with a low volume external gas cell (8.7 mL), which allowed an online measurement of the flue gas composition by recording infrared energy absorbance spectra over time. The reactor was connected to the FTIR spectrometer using a transfer line with a 2 mm internal diameter PTFE

tube. A bypass line permitted to flux the reagent gas directly to the FTIR, both before starting and at the end of the neutralisation process in order to verify the actual composition of the reagent gas. Finally, the outgoing gas from the FTIR cell flowed through a soda bath, which operated as absorption system, while a cylinder filled with water was used as water seal.

Given the highly corrosive nature of HCl, the section of the apparatus exposed to the acid gas exhibited tubing and tube fittings made of PTFE and 3-way stopcocks and cross connectors made of glass. The rest of the system was composed of polyamide-11 tubing.

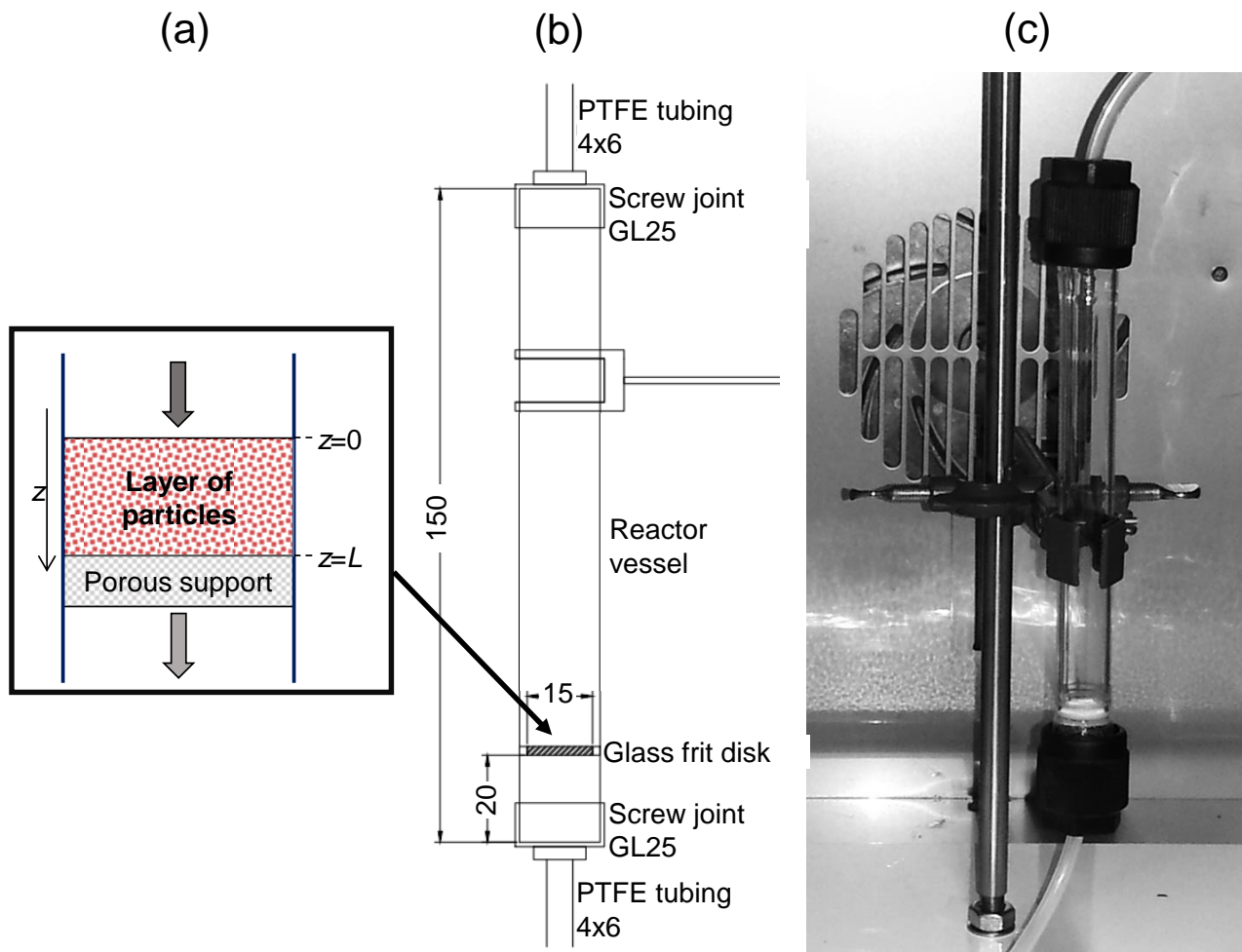


Figure 5.2. Tubular reactor: a) sketch of the reacting system, b) drawing and c) picture of the reactor.

5.3 Materials and experimental procedure

The solid reactant was calcium hydroxide, ACS reagent grade, supplied by Sigma Aldrich. A thermogravimetric analysis (TA Instruments, Q300) determined that the material was composed of 96% calcium hydroxide, $\text{Ca}(\text{OH})_2$, with the balance being calcium carbonate, CaCO_3 , as stated by the supplier. To prevent further carbonation of the samples due to contact with ambient air, the material was kept in HDPE sealed containers, placed in a ventilated cabinet. In order to restrict the natural variability of the material, the hydrated lime was sieved and only the fraction composed by particles between 45 and 123 μm of diameter was used in the experimental runs. The specific surface area of the sieved samples, as determined by nitrogen porosimetry (Micromeritics, Flow Sorb II 2300), was $15.1 \text{ m}^2/\text{g}$. Porosity and pore size distribution (see porosigram in Figure 5.3) were determined by mercury intrusion porosimetry (Carlo Erba Strumentazione, Porosimeter 2000).

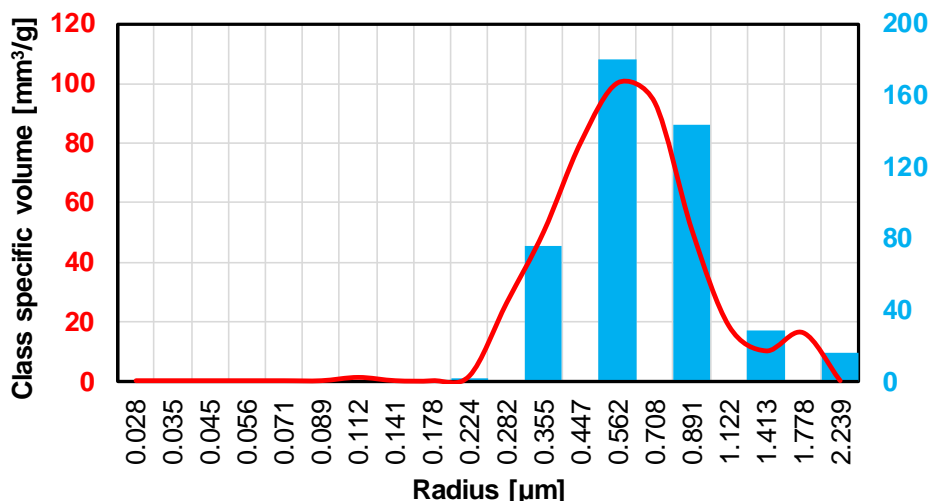


Figure 5.3. Mercury porosigram of the calcium hydroxide adopted in the study and division of the pore volume in 8 pore classes (see section 6.7).

Quartz sand was used as inert filling material in the sorbent bed, in order to reduce the tendency of calcium hydroxide to form agglomerates and to minimise gas channelling (Chisholm and Rochelle, 1999). A fraction of the same range of diameters as calcium hydroxide (45–123 µm) was used and preliminary runs performed by flowing the gas mixture through the reactor with and without a bed of only quartz sand showed no HCl sorption, thus confirming the material as inert.

The experimental FBR runs, listed in Table 5.2. were conducted as follows. For a typical experiment, the reactor was charged with sorbent and inert material, taking care of forming an even layer of particles, and put in oven in order to reach the temperature set for the run. Meanwhile, a mixture of nitrogen and HCl at the desired concentration was prepared by means of the mass flow controllers and sent through the bypass line to the FTIR in order to double-check the composition of the simulated flue gas and verify the attainment of a steady state.

Table 5.2. Performed runs and experimental conditions.

Type of run	HCl conc. (ppm)	Temperature (°C)	Mass of sorbent (mg)	Inert-to-sorbent mass ratio
1	2500	120	100	3:1
2		150		
3		180		
4	2500	120	50	6:1
5		150		
6		180		
7	1250	120	50	6:1
8		150		
9		180		

The FTIR scans from 8000 to 400 cm⁻¹, at a resolution of 4 cm⁻¹. Every spectrum recorded is obtained as average of 16 consecutive scans, giving an absorbance versus wavelength plot every 3.7 seconds. The FTIR spectra were recorded and elaborated using the Bruker OPUS/IR software. The profile of HCl and of H₂O in the outlet gas and the total amount reacted were obtained assessing the integrated absorbance as a function of time on the characteristic wavenumber intervals: for HCl, the absorption band between 3150 and 2500 cm⁻¹, corresponding to roto-vibrational transitions of HCl in the gas phase (Tipler and Llewellyn, 2012), and for water vapour, the interval between 4000 and

3500 cm^{-1} . Integrated absorbance values were correlated to the concentration in the gas by the Lambert-Beer law, which can be expressed over a characteristic wavenumber interval as follows:

$$I = \int_{\nu_1}^{\nu_2} A(\nu) \cdot d\nu = \int_{\nu_1}^{\nu_2} \varepsilon(\nu) \cdot l \cdot C \cdot d\nu = K \cdot C \quad 5.6$$

where I is the integral absorbance value, A the measured spectral absorbance, ε the extinction coefficient of the gaseous compound, l the optical length used in the measurement, C the concentration, and (ν_1, ν_2) the wavenumber interval selected for the measurement. The calibration constant, K , may be considered independent of the concentration if deviations from the Lambert-Beer linear correlation can be neglected. The value of K for HCl was obtained from experimental calibration using gas mixtures of known composition, following the procedure described by Bak et al. (1995). No quantitative calibration was applied to water integrated absorbance.

At a registered time, the flow of the simulated flue gas was switched from the bypass line to the reactor line and the subsequent measurement by the FTIR recorded the drop in the HCl infrared signal. The abatement of HCl took place according to a typical breakthrough curve, as shown in section 5.4. The run was stopped when the breakthrough curve of HCl showed a derivative close to zero. In order to verify that any further reaction happening is negligible, the gas flow was diverted to the bypass line. If the differences between traces of HCl coming from reactor or bypass were within the natural fluctuation of the signal, the N_2/HCl cylinder was closed and the system purged with dry nitrogen.

The conversion of the solid reactant X_s was calculated cumulatively from the registered data on HCl removal as follows:

$$\chi_s = \frac{b}{n_s} \int_0^{t_{fin}} Q \cdot C_{in} \left(1 - \frac{C_{out}}{C_{in}} \right) dt \quad 5.7$$

where b is the stoichiometric coefficient of the sorbent (1 if the product is CaOHCl , 0.5 if the product is CaCl_2), n_s the moles of sorbent initially charged in the reactor, Q the flow rate of the gas mixture, C_{in} and C_{out} respectively the inlet and outlet molar concentration of HCl in the gas.

Part of the reacted solid samples was analysed to check the agreement of final solid conversion with the conversion calculated from HCl removal and to identify the actual product compound generated by the reaction (CaCl_2 or CaOHCl). A first screening of the solid samples was conducted by thermogravimetric analysis (TG), abiding by the following procedure. Samples used in TG runs were previously dried at $105\text{ }^\circ\text{C}$ under a dry nitrogen flux of 60 mL/min for 10 min. Then, the constant heating rate runs were carried out on the dried samples using the same nitrogen purge gas flow rate of 60 mL/min and a heating ramp of $10\text{ }^\circ\text{C}/\text{min}$. Other fractions of the reacted solid samples were subjected to phase identification via X-ray diffractometry. The powder XRD patterns were collected using a Philips PW 1840 diffractometer (40 kV/20 mA, $\text{Cu K}\alpha$ radiation), step-scanning over a 2θ range of $5\text{--}80^\circ$.

5.4 HCl removal monitored by infrared spectroscopy

By following the procedure in section 5.3, the acquisition of cascading IR spectra allowed to follow the time evolution of the gas-solid reaction, as exemplified in Figure 5.4 for a reference run. The figure shows the integrated absorbance of HCl and H_2O during the time of an experiment, along with three illustrative IR spectra. As described in section 5.3, the gas flow was first sent to the spectrometer bypassing the reactor, in order to verify the attainment of a steady, given concentration of HCl in the gas mixture. At time 0, the activation of the switching valve diverted the flow to the

reactor. The permanence time of the gas in the system was estimated to be of 20 s and the time scale in the subsequent plots was corrected accordingly.

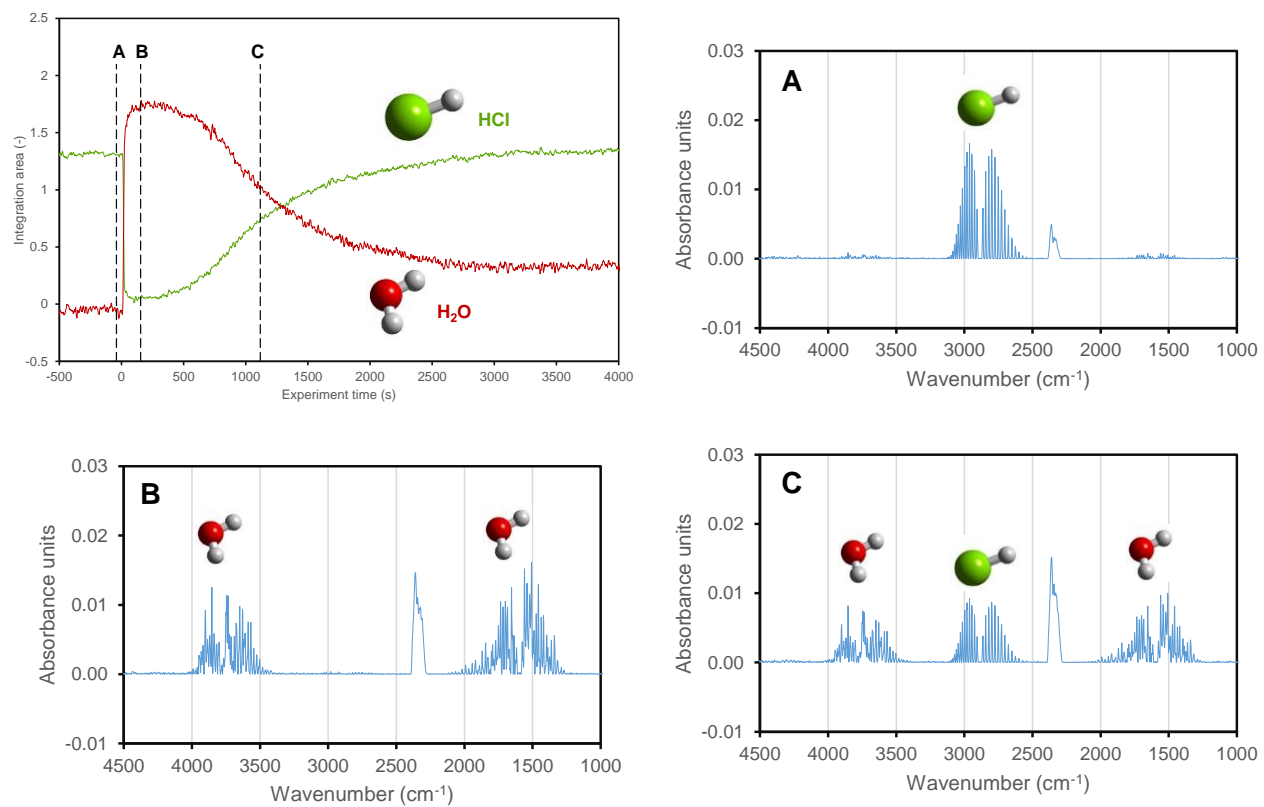


Figure 5.4. Integrated absorbance of HCl and H₂O for a reference FBR run (reactant gas sent to the reactor at experiment time = 0). Conditions: temperature = 180 °C, HCl inlet concentration = 2500 ppm, mass of sorbent = 100 mg. For selected characteristic instants, panels A-C show full IR spectra: A) before reaction starts, B) immediately after reaction starts, C) after 18 min of reaction.

At first, HCl molecules encountered a bed of fresh Ca(OH)₂ and almost complete removal of HCl in the outlet gas was detected, with the simultaneous release of water vapour, according to the reaction stoichiometry. The phenomenon is well illustrated by the comparison between spectrum A and spectrum B, respectively taken shortly before and after the reaction start, showing the disappearance of the HCl absorption peaks and the appearance of water-related absorption bands in the 4000-3500 cm⁻¹ and in the 2000-1200 cm⁻¹ areas. The absorption peak around 2350 cm⁻¹ is associated with the CO₂ generation due to the reaction between HCl and the small fraction of CaCO₃ included in the samples of hydrated lime. With the continuation of the reaction, the solid product accumulated at the surface of the calcium hydroxide particles, generating a growing diffusional resistance to the sorption of the gaseous reactant, which slowed down the reaction and led to an increasing HCl penetration through the bed (see spectrum C).

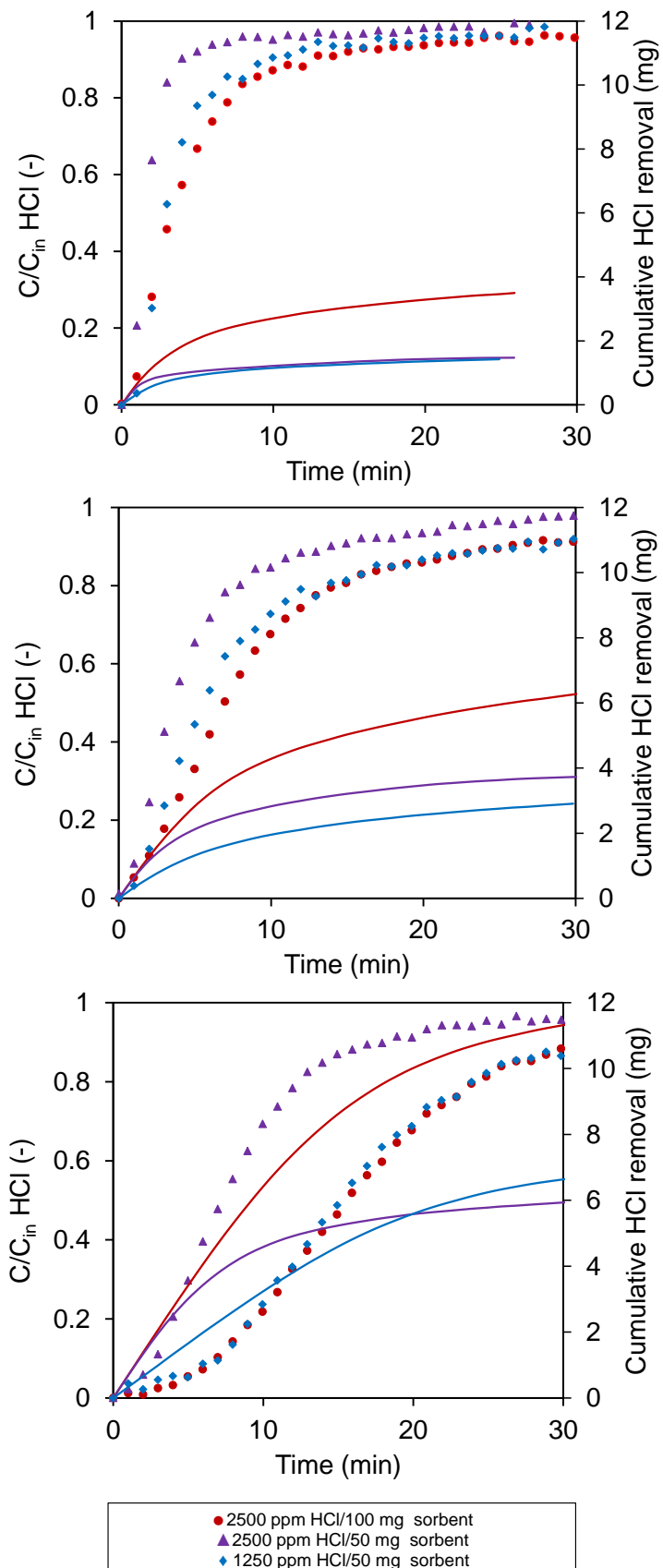
The run was stopped when the curve of HCl integrated absorbance showed a derivative close to zero. By applying eq. 5.6, the curves of integrated absorbance of HCl obtained for the different experimental conditions listed in Table 5.2 were converted to curves of normalised HCl concentration exiting the reactor (breakthrough curves), shown in Figure 5.5 along with the associated curves of cumulative HCl removal for the first 30 min of reaction¹. The time at which

¹ HCl breakthrough curves classified for reaction temperatures for all the experimental runs are reported in section 6.7, alongside model simulations.

50% of the inlet HCl concentration penetrated through the bed (t_{50}) and the amount of HCl cumulatively removed at the end of each FBR run are reported in Table 5.3. The main parameter governing HCl sorption in dry gas conditions is temperature, with delayed breakthrough and higher cumulative HCl removal at higher temperatures. Clearly enough, for the same HCl inlet concentration of 2500 ppm, runs with 50 mg Ca(OH)₂ show approximately halved t_{50} and cumulative HCl removal than runs with 100 mg Ca(OH)₂. More interestingly, the runs at HCl = 1250 ppm, Ca(OH)₂ = 50 mg share the same Ca-to-HCl ratio of the runs at HCl = 2500 ppm, Ca(OH)₂ = 100 mg, but their breakthrough time is consistently shorter, thus evidencing a slight positive effect of HCl concentration on bed reactivity. This is also noticeable from the curves of cumulative HCl sorption, which exhibit faster initial accumulation for runs at HCl inlet concentration of 2500 ppm.

Table 5.3. t_{50} and total HCl removed at the end of experiment for the different FBR runs.

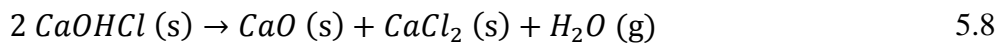
Temperature (°C)	HCl concentration (ppm)	Mass of sorbent (mg)	t_{50} (min)	Total HCl removed (mg)
120	2500	100	3.3±0.2	3.8±0.1
	2500	50	1.6±0.0	1.5±0.1
	1250	50	3.0±0.5	1.5±0.2
150	2500	100	7.2±1.1	6.9±1.1
	2500	50	3.5±0.3	3.7±0.1
	1250	50	5.6±1.1	3.0±0.2
180	2500	100	15.8±0.9	12.8±0.9
	2500	50	7.3±0.4	6.3±0.2
	1250	50	14.3±0.8	6.7±0.4



5.5 Identification of the solid reaction product

The correct identification of the solid product generated by the gas-solid reaction is needed to correctly quantify the solid conversion on a molar basis. TGA and XRD analyses were employed to cast light on the issue regarding CaCl_2 or CaOHCl formation (see section 5.1).

In Figure 5.6 the TG runs of two samples, reacted respectively at 120 °C and 180 °C with the same inlet concentration of HCl (4000 ppm), are compared with the TG scan of unreacted calcium hydroxide. The unreacted material shows two separate weight losses approximately in the intervals 350-400 °C and 500-600 °C, the former due to the release of chemically-bound water (dehydration of $\text{Ca}(\text{OH})_2$ to CaO) and the latter due to the release of CO_2 (calcination of the CaCO_3 impurities to CaO). The reacted samples display an additional, well distinguishable weight loss in the range 450-500 °C, which is higher for higher reaction temperature. This positive relationship with reaction temperature reflects the positive effect of temperature on sorbent conversion. Therefore, the weight loss can be attributed to the thermal degradation of the solid product of the gas-solid reaction. The various hydrated forms of CaCl_2 lose their water content at $T < 200$ °C (Patek et al., 2008; N'Tsoukoe et al., 2015), while CaCl_2 itself does not exhibit thermal weight loss at temperatures lower than its melting point, 772 °C (Wang et al., 2014). By process of elimination, TG evidence leads to the identification of the solid product as calcium hydroxychloride, which might undergo thermal decomposition by dehydroxilation:



as suggested by Allal et al. (1998) and observed by Prigobbe et al. (2009). The occurrence of reaction 5.8 might also explain why previous investigators found the product of the $\text{Ca}(\text{OH})_2/\text{HCl}$ reaction to be CaOHCl at temperatures of 150-200 °C and CaCl_2 at temperatures above 500 °C (see Table 5.1).

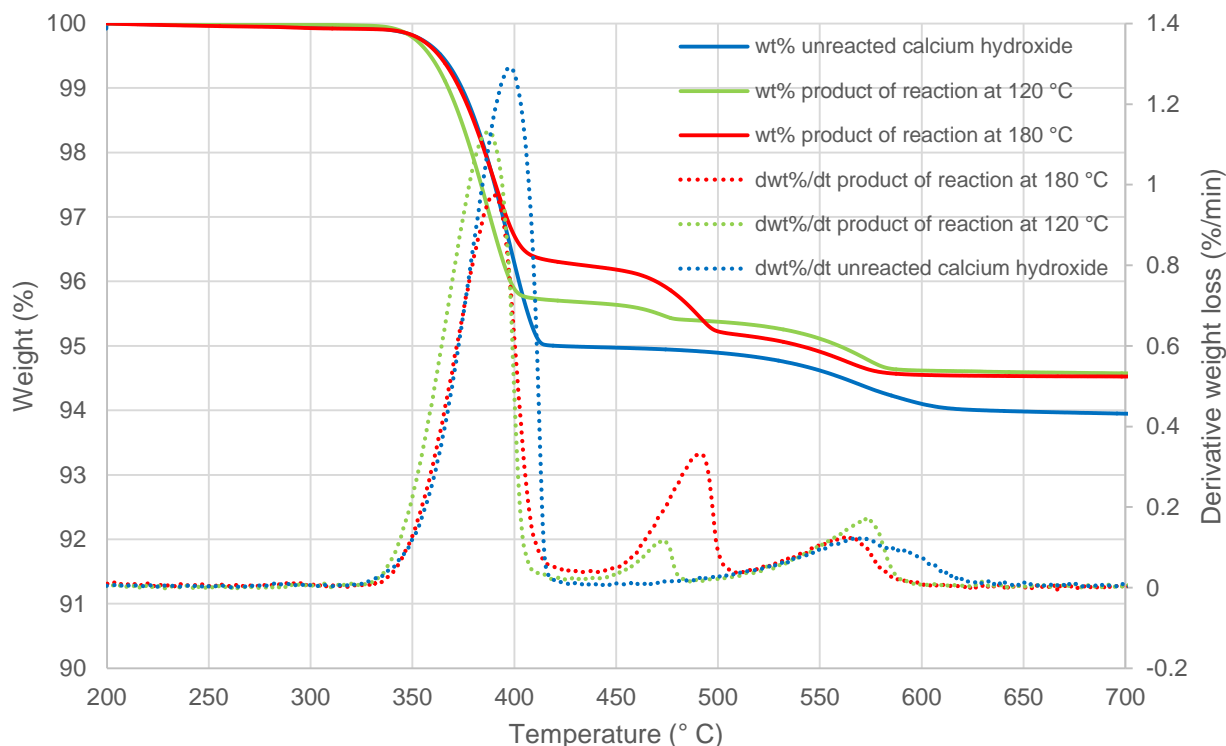


Figure 5.6. TG and dTG curves for unreacted $\text{Ca}(\text{OH})_2$ and $\text{Ca}(\text{OH})_2$ reacted with HCl (2500 ppm) at 120 and 180 °C.

In order to confirm the TG observations, other fractions of the reacted samples were analysed via X-ray diffractometry. The PDF cards and the main peaks of the species of interest are reported in Table 5.4 for reference, while the XRD spectra of a sample reacted with 2500 ppm of HCl at 180 °C is shown in Figure 5.7. The strongest signals are related to quartz, as it was the dilution material used in the preparation of the sorbent bed. Regarding the Ca-based compounds, both unreacted calcium hydroxide and calcium carbonate can be seen and the only chlorinated phase identified is CaOHCl, in agreement with previous XRD investigations on products of Ca(OH)₂/HCl reaction in laboratory apparatuses (Bausach et al., 2004; Chin et al., 2005a).

Table 5.4. PDF card and 2-theta positions of the main peaks of the compounds of interest for XRD phase identification.

Compound	PDF no.	2-theta locations (°)
Ca(OH) ₂ , portlandite	04-0733i	18.1, 28.7, 34.1 , 47.1, 50.8, 54.3
CaOHCl, calcium hydroxide chloride	36-0883i	28.1, 32.3, 38.3 , 47.0
CaCl ₂ , calcium chloride	24-0233	19.8 , 29.3 , 31.2, 38.6
CaCO ₃ , calcite	05-0586	23.0, 29.4 , 36.0, 40.0, 47.5, 48.5

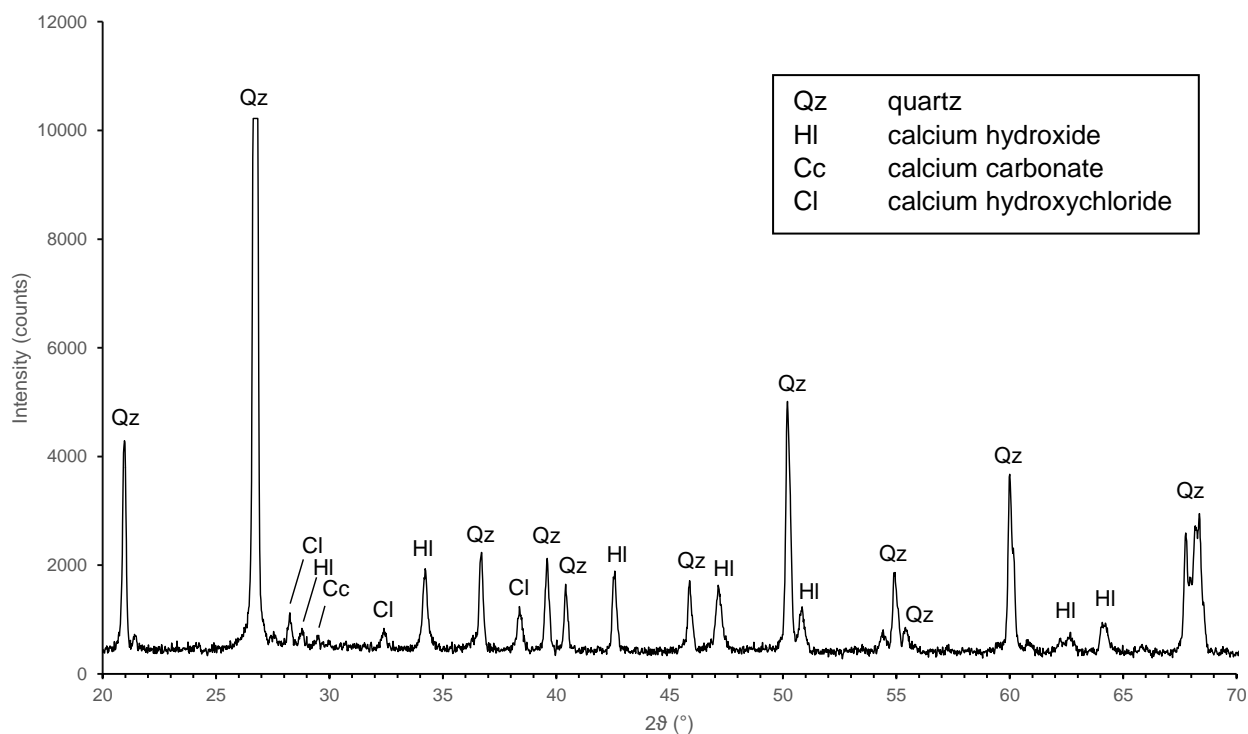


Figure 5.7. XRD spectrum of Ca(OH)₂ reacted with HCl (2500 ppm) at 180 °C.

Therefore, the reaction product was assumed to be CaOHCl and the conversion of the solid reactant was calculated accordingly (eq. 5.7). Curves of solid conversion will be shown in section 6.7 alongside model simulations, while final values of conversion obtained in the various FBR runs are listed in Table 5.5.

Table 5.5. Final conversion of the sorbent for the set of FBR runs.

Temperature (°C)	HCl concentration (ppm)	Mass of sorbent (mg)	Final conversion (%)
120	2500	100	7.0
	2500	50	5.7
	1250	50	6.2
150	2500	100	14.0
	2500	50	14.3
	1250	50	13.5
180	2500	100	24.2
	2500	50	24.8
	1250	50	23.3

The asymptotic value of final conversion in dry gas conditions appears to be mainly dependent on temperature. For this reason, the values in Table 5.5 are in agreement with results obtained in previous studies on the dry Ca(OH)₂/HCl system, even if other experimental conditions (mainly, sorbent-to-HCl ratio) are different. Weinell et al. (1992) showed final sorbent conversion values in the temperature range 100-200 °C varying between 5.2 and 21.9%. Chisholm et al. (1999) reported a total Ca(OH)₂ utilisation at 120 °C of 5.1%. Yan et al. (2003) obtained an ultimate Ca(OH)₂ conversion of 20.1% at 170 °C and of 31.0% at 200 °C. For a full understanding of the interplay of kinetic and mass transfer phenomena determining the reaction outcome, the FBR runs were interpreted by modelling.

6 Phenomenological model for acid gas removal processes

6.1 Literature overview

As outlined in the introductory chapters 1 and 2, acid gas removal is a key step in the flue gas cleaning lines of Waste-to-Energy plants and dry sorbent injection (DSI) is a cost-effective and reliable treatment technique capable of reducing outlet concentrations of acid gases far below current legislative requirements (BREF WI, 2006). Nonetheless, industrial practice is still mostly empirical and DSI systems are often not operated at their optimum (de Greef et al., 2013). Detailed process modelling would allow a full-aware process optimisation, reducing sorbent consumption, waste production and operating costs. However, to date only few studies attempted the modelling of DSI performance. Chisholm and Rochelle (1999) adopted a semi-empirical approach to determine kinetic parameters and to simulate the performance of a dry treatment system using data from laboratory-scale experiments on hydrogen chloride removal by calcium hydroxide. Other authors modelled in-duct desulphurisation by applying empirical kinetic equations (Kaiser et al., 2000; Gutiérrez Ortiz and Ollero, 2008). Recently, an attempt was done to study such systems by computational fluid dynamics, yet applying a simplified model to the chemical reaction process (Marocco and Mora, 2013). The adoption of a more fundamental modelling approach, based on the description of the actual chemical and physical phenomena involved in the acid gas removal process, is an indispensable step in order to gain a deeper understanding of the process and interpret both laboratory-scale experimental results such as the ones of chapter 5 and full-scale applications.

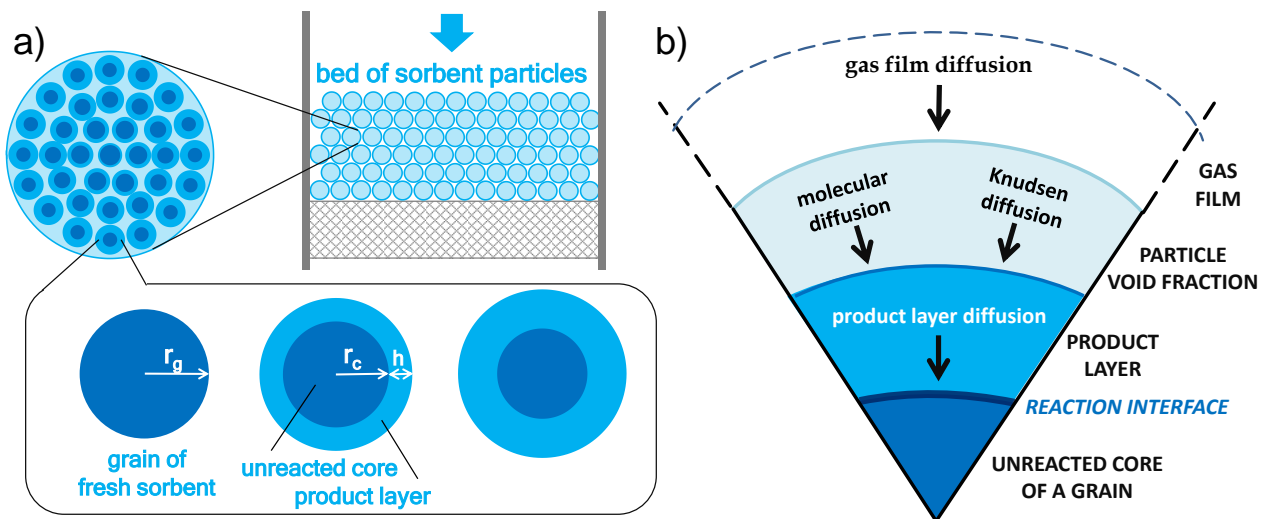


Figure 6.1. a) grain model schematisation: a bed of sorbent particles is represented as an assembly of spheres formed by non-porous grain immersed in the sorbent porosity. The grains react according to the shrinking core model (Levenspiel, 1998). b) Diffusional mechanisms involved in the gas-solid reaction according to the grain model schematisation.

Acid gas neutralisation with sorbent particles is a complex process, which results from the superimposition of different effects, such as flow through a porous fixed bed of particles, diffusion in the particle pores and reaction with the sorbent, where also equilibrium thermodynamics plays an important role. The gas-solid reaction is controlled by several kinetic and mass transfer phenomena: Figure 6.1, adopting the schematisation of the grain model (which will be detailed in section 6.3), shows that a molecule of acid gas has to penetrate the gas film covering sorbent particles, diffuse inside the particle pores according to different diffusion mechanisms depending on the size of the pores and flow through the growing shell of solid reaction products before reaching the interface with the unreacted core surface where chemical reaction takes place.

Several studies addressed single aspects of the process. Thermodynamic calculations to identify the theoretical limit for HCl removal by calcium- and sodium-based sorbents were undertaken by different authors (Shemwell et al., 2001; Verdone and De Filippis, 2004; Chin et al., 2005a). Weinell et al. (1992) carried out a comprehensive investigation of the reactivity of $\text{Ca}(\text{OH})_2/\text{CaO}$ towards HCl considering a wide range of operating conditions (temperature, moisture, surface area of the solid reactant). Daoudi and Walters (1991) and Yan et al. (2003) focused on the determination of the chemical reaction rate respectively for the CaO/HCl and the $\text{Ca}(\text{OH})_2/\text{HCl}$ systems, while Duo et al. (1995) and Fonseca et al. (1998) studied the role of the solid-state diffusion of the gaseous reactant in controlling the process over longer reaction times.

In spite of the relevant work carried out in the field, to date no detailed model is available to describe the gas-solid heterogeneous reaction process and the associated transport phenomena taking place in acid gas removal processes with calcium-based sorbents. Actually, an unreacted shrinking core model (Levenspiel, 1998) for gas-solid reactions is not able to correctly predict the incomplete conversion of the solid sorbent observed in several experimental studies (Weinell et al., 1992; Fonseca et al., 1998; Chisholm and Rochelle, 1999; Yan et al., 2003). Coupling the shrinking core model to a grain model (Szekely et al., 1976) to describe particle behaviour improved the quality of results, but still such approach is not able to reproduce experimental findings, and in particular the limited temperature-dependent final conversion of the solid sorbent (Duo et al., 1994). Presently, available models use empirical parameters derived from data fitting to introduce an arbitrary maximum conversion or an ultimate conversion value based on experimental data fitting (Chisholm and Rochelle, 1999). Alternatively, the diffusivity of the gaseous reactants through the layer of solid product is decreased introducing an empirical dependency on sorbent conversion as reaction proceeds (Wang and Teng, 2009). Such empirical approach allows the model to reproduce the abrupt decrease in the reactivity of the solid reactant observed experimentally (Stendardo and Foscolo, 2010).

6.2 The issue of incomplete conversion

As discussed above, the main open problem in the modelling of the reactions between Ca-based sorbents and acid gases (HCl , SO_2 , CO_2) is the experimental evidence that shows unambiguously the presence of a limit in the conversion of solid particles (Weinell et al., 1992; Chisholm and Rochelle, 1999; Yan et al., 2003). This was found to be far lower than the almost complete conversion of the solid reactant that would be expected from equilibrium thermodynamics.

The main parameters affecting the value of the experimental final conversion were reported to be: temperature (Weinell et al., 1992; Yan et al., 2003), relative humidity (Weinell et al., 1992; Fonseca et al., 1998; Chisholm and Rochelle, 1999), as well as the concentration of the gaseous reactant (Chisholm and Rochelle, 1999).

Focusing on the reaction between HCl and $\text{Ca}(\text{OH})_2$ in dry gas conditions, available experimental evidence shows that the extent of final conversion is mainly dependent on temperature (Yan et al., 2003). In the range between 150 and 300 °C, an Arrhenius dependence of the final conversion from temperature was observed (Figure 6.2). At lower temperatures (50-130°C) the data reported by Fonseca et al. (1998) do not show an influence of temperature on ultimate conversion. This could be due to the short duration of experimental runs (20 min), that may have been stopped before the ultimate conversion value was reached. Alternatively, due to the low temperatures, an effect of the interaction of the liquid water generated by reaction with the solid sorbents can also be supposed. It should be remarked that CaCl_2 is a highly hygroscopic (deliquescent) salt.

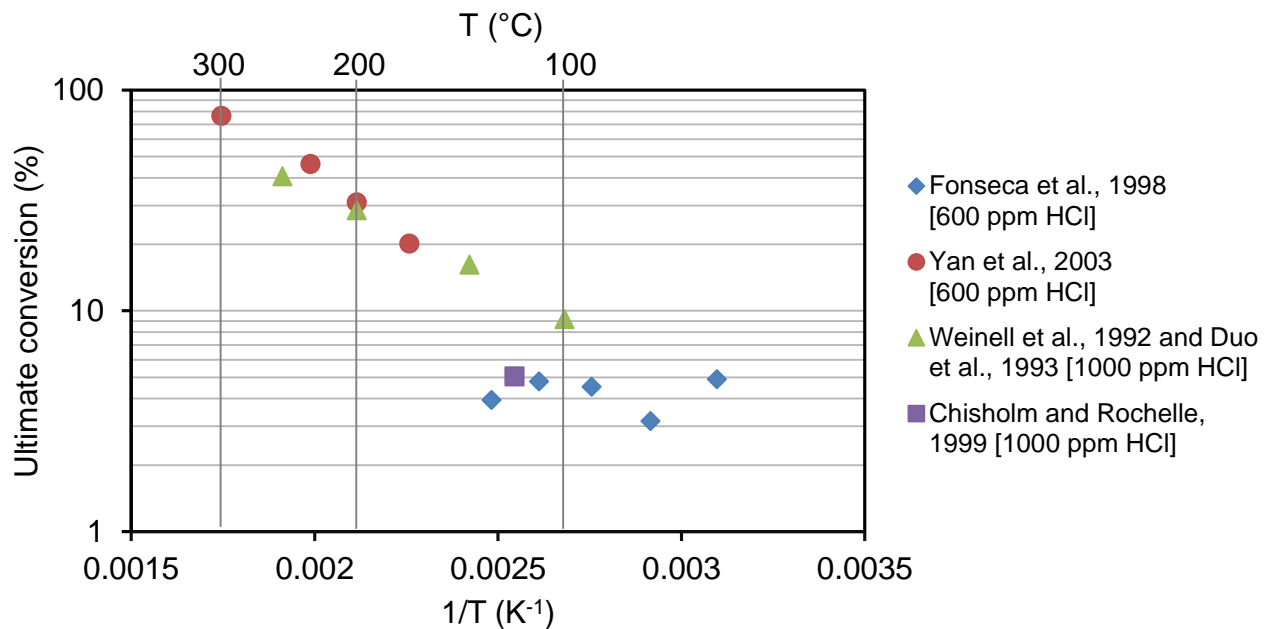


Figure 6.2. Literature values obtained for the ultimate sorbent conversion in dry conditions reported with respect to the reciprocal of temperature.

Even if widespread evidence of incomplete conversion of the solid sorbent is available in the literature, a widely accepted theoretical explanation of this phenomenon has not been provided yet. Some authors (Simons and Garman, 1986; Yan et al., 2003) attributed the incomplete conversion to the plugging of the porous structure of the sorbent: since the molar volume of CaCl_2 is larger than that of $\text{Ca}(\text{OH})_2$, the reaction causes an expansion of the solid fraction of the sorbent particles, eventually filling the available void fraction before 100% conversion is reached. The theoretical final conversion due to the complete filling of intraparticle voids (Simons and Garman, 1986) can be expressed through eq. 6.1:

$$X_{s,max} = \frac{\varepsilon_p}{(1 - \varepsilon_p)(\alpha - 1)} \quad 6.1$$

where ε_p is the initial void fraction of the sorbent and α the volumetric expansion factor. However, eq. 6.1 depends solely on the properties of the sorbent and of the reaction solid product, thus it cannot explain why the ultimate conversion value is affected by operating conditions and in particular by temperature.

An alternative mechanism suggested by Yan et al. (2003) is the blockage of pore mouth (in other words, the occlusion of the external pores of the sorbent particles), which would exclude the inner part of a sorbent particle from further reacting. However, this does not agree with the findings reported by Weinell and coworkers (Weinell et al., 1992) concerning calcium hydroxide particles having the typical size range used in flue gas treatment systems ($d < 50 \mu\text{m}$). Experimental results evidenced an almost uniform conversion of solid particles along their radial coordinate.

A modelling approach aimed at overcoming the limits in accounting the low values of the ultimate conversion is the comprehensive Crystallisation and Fracture (CF) model proposed by Duo et al. (1994; 1995). The model was based on free energy-work analysis in order to thermodynamically explain the presence of an ultimate conversion of the sorbent. The conventional models proposed for gas-solid reactions (namely, the shrinking core model and the grain model) represent the solid

product as a uniform shell (product layer) which is formed around the spherical core of the solid reactant. However, it is still uncertain how the product layer is formed and how the formation mechanism influences product layer diffusion. The approach of Duo et al. (1994), supported by the results of Scanning Electron Microscopy (SEM) observations (Duo et al., 2000; Li and Bie, 2006), is based on the assumption that the products, rather than forming an initial layer as thin as the size of a molecule, form clusters of molecules following a crystallisation process. Four main steps were assumed for the process, as sketched in Figure 6.3: i) nuclei of product are formed at the reaction interface (nucleation); ii) stable nuclei grow to larger crystals (a product layer composed by crystals is formed and gets thicker as the reaction progresses); iii) for reactions involving volume expansion, the growth phase requires mechanical work in order to displace the product layer and create a free volume at the interface for the newly generated solid; and iv) the reaction stops when the energy required for further crystallisation and fracture (surface energy and mechanical work) is higher than the chemical potential available (free energy change of the reaction). In the present implementation, the CF approach was modified and integrated in a conventional grain model framework to simulate the overall reaction process and the transport phenomena involved.

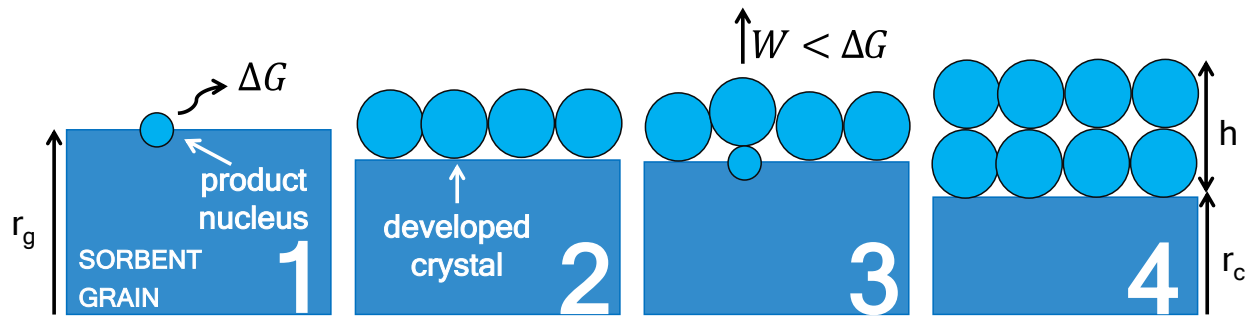


Figure 6.3. Product layer growth as described in the crystallisation and fracture model: 1) nuclei of product are formed at the reaction interface (nucleation); 2) stable nuclei grow to crystals: a product layer composed by crystals is formed and gets thicker as the reaction proceeds; 3) for reactions involving volume expansion, further nucleation needs mechanical work $W(h)$ to displace the product layer and make room at the interface for the increased volume; 4) the reaction stops when the energy required for further nucleation is greater than the chemical potential available ($W(h) > \Delta G$). Further details in section 6.4.

6.3 Phenomenological model: the grain model framework

Acid gas removal in full-scale flue-gas treatment systems mostly takes place on a thin layer of sorbent particles formed on the filtering surface of filter bags (Chisholm and Rochelle, 1999; Kavouras et al., 2002). Laboratory experiments aimed at the study of the reactivity of solid sorbents used for acid gas removal are usually based on feeding gaseous streams containing acid gases to fixed beds of solid reactants. Bed thickness is usually of few millimetres only (Weinell et al., 1992).

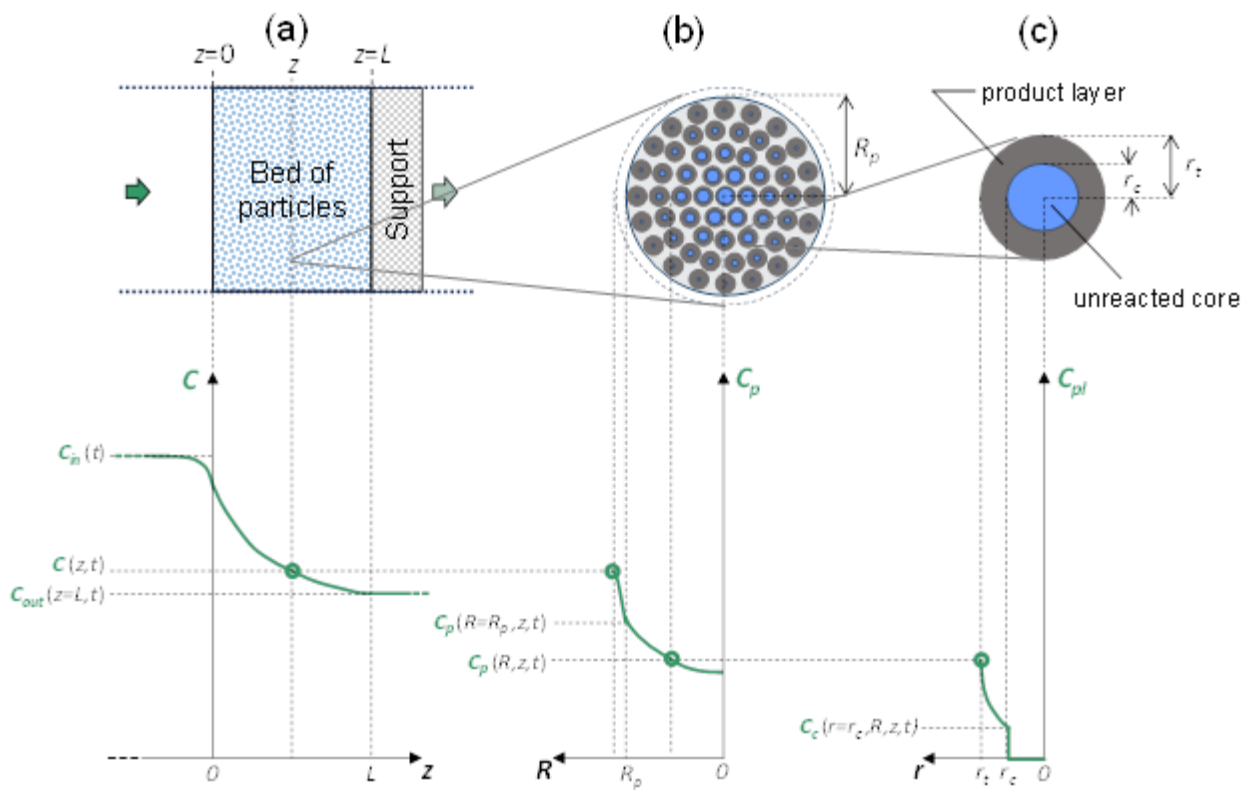


Figure 6.4. Geometrical references for the model: bed (a), sorbent particle (b) and grain (c). Dimensions: thickness of the fixed bed (L), radius of a sorbent particle (R_p), total radius of a grain (r_t) and radius of its unreacted core (r_c). Concentration profile of the gaseous reactant within bed (C), particle pores (C_p) and product layer of a grain (C_{pl}).

The geometry of the system suggests adopting a dispersed plug flow model for describing the continuity equation of the gas phase through the bed (Carberry, 1976; Levenspiel, 1998). The direction of the reference axis of the model is assumed parallel to the main flow direction across the bed, as shown in Figure 6.4a. The apparent reaction rate in the bed is described using a grain model (Szekely et al., 1976), which assumes that each porous particle of the bed is spherical and made up of individual non-porous spherical grains. Each grain reacts individually according to the unreacted shrinking core model described by Levenspiel (Levenspiel, 1998). This implies coupling a diffusion resistance model for the particle (i.e. gas film and pore diffusion of the acid gases from the bulk gas phase to the inner grain surface, Figure 6.4b) with an unreacted shrinking core model for the grain (i.e. diffusion through the product layer of the grain and reaction at the surface of the fresh reactant core, Figure 6.4c). Since the heat generation rate of the reaction is practically negligible due to the low concentrations of the acid-gas in the stream, isothermal conditions are assumed in the model set-up (Gullett et al., 1992; Verdone and De Filippis, 2006).

This assumption was checked by calculating the significant non-dimensional parameters and overall heat balance for the experimental dataset provided by Yan et al. (2003), whose temperature and HCl concentration represent a worst-case scenario for most real applications. The grain and the particle Biot numbers (Ruthven, 1984) resulted respectively equal to $8 \cdot 10^{-3}$ and $2 \cdot 10^{-2}$, suggesting a uniform temperature profile within the grains and the particles. The Damköhler's fourth dimensionless number (Land, 1972) resulted equal to $8 \cdot 10^{-7}$, suggesting heat generation in reaction to be slower than the heat removal rate. Finally an overall heat balance assuming complete conversion of HCl

predicts a maximum temperature increase in the bed of $2.6 \cdot 10^{-3}$ °C, thus confirming that isothermal conditions could reasonably be assumed².

The overall structure of the proposed model is sketched in Figure 6.5. The acid gas removal performed by a bed of solid reactant is described by a mass balance equation that considers an overall apparent reaction rate, r_{vb} . This term takes into account inter- and intra-particle transport phenomena and the actual reaction kinetics. The value of r_{vb} is determined by the mass balance of the gaseous reactant through the void fraction of the sorbent particles and the layer of solid product. This is carried out by applying a grain model approach, corrected by a reduction factor RF. RF is the output of the CF submodel and describes the reduction of the actual reactive area due to the mechanical inhibition of product nucleation exerted by the growing product layer.

² The value calculated for the Biot number for heat transfer from grain to particle resulted:

$$Bi_g = \frac{\text{heat transfer grain to particle}}{\text{heat transfer within grain}} = \frac{d_g \lambda_p}{\lambda_s d_p} = 8 \cdot 10^{-3}$$

Nomenclature is explained in the table at the end of this note.

The above reported value of the Biot number suggests that the temperature profile within a grain is essentially uniform. The value of the Biot number for particle-to-fluid heat transfer is:

$$Bi = \frac{\text{heat transfer particle to fluid}}{\text{heat transfer within particle}} = \frac{h \cdot d_p}{\lambda_p} = 2 \cdot 10^{-2}$$

This confirms that the external temperature gradient, whatever its value, is in general much higher than the temperature gradient within the particle and grain. Therefore, the heat-transfer resistance can be represented by the packed-bed-to-fluid coefficient h , which controls the overall heat removal from the reactive system. The heat generated was compared to the heat removed by means of the Damköhler's fourth dimensionless number (Land, 1972):

$$Da^{IV} = \frac{\text{Heat generated}}{\text{Heat conducted}} = \frac{-\Delta \tilde{H}_r \cdot k_s \cdot A_r''' \cdot C_{HCl,in} \cdot d_p^2}{h \cdot d_p \cdot T_{in}} = 8 \cdot 10^{-7}$$

where A_r''' is the surface area per unit volume. The value obtained for Da^{IV} confirms, that the heat generation is much slower than the heat transfer, suggesting practically isothermal conditions between bed and fluid.

Finally, the temperature increase can be calculated from a global heat balance. Under the assumption of a pseudo-steady state approximation, this can be expressed as follows:

$$\dot{n}_f \cdot \tilde{c}_{p,f} \cdot (T_{in} - T_{out}) + \dot{Q}_r = 0$$

Calculating the heat of reaction \dot{Q}_r assuming a complete reaction ($C_{HCl,out}=0$), the temperature increase results of only $2.6 \cdot 10^{-3}$ °C.

Thus, since isothermal conditions may be assumed for the problem of interest, the introduction of free energy distribution seems an unnecessary complication of the model, with no real benefit for the results.

Variables	Definitions	References
d_g	Grain diameter	Yan et al., 2003
d_p	Particle diameter	Yan et al., 2003
λ_s	Thermal conductivity of the sorbent	Schaube et al., 2011
λ_p	Thermal conductivity of the porous particle	Kantorovich and Bar-Ziv, 1999
ΔH_r	Enthalpy of reaction R1	Chemistry WebBook (NIST)
k_s	Chemical reaction rate constant	Yan et al., 2003
h	Packed-bed-to-fluid heat-transfer coefficient	Green and Perry, 2007

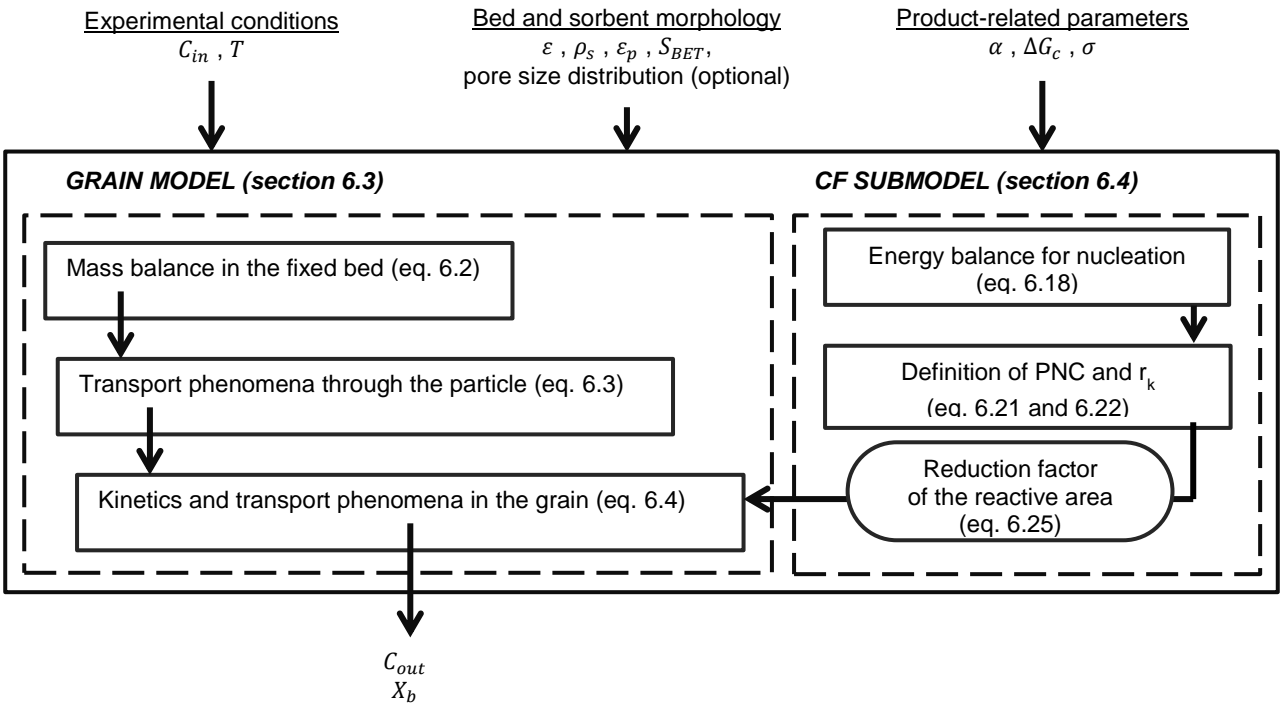


Figure 6.5. Flow chart of the modelling procedure. Acronyms: crystallisation and fracture (CF), population of nuclei of critical size (PNC). C_{in} : inlet concentration of the gaseous reactant, T : temperature, ε : void fraction of the bed, ρ_s : true (particle) density of the sorbent, ε_{pl} : intra-particle void fraction of the sorbent, r_k : radius of a critical nucleus, S_{BET} : specific surface area, α : volumetric expansion factor, ΔG_c : free energy change associated to the chemical reaction, σ : surface energy per unit area of the solid product, C_{out} : outlet concentration of the gaseous reactant, X_p : average sorbent conversion in the bed.

Porous sorbent particles (Figure 6.4b) were described using the grain model (Szekely et al., 1976). The profile of hydrogen chloride concentration within particle pores and grains is schematically shown in Figure 6.4b and Figure 6.4c respectively. Hydrogen chloride diffuses through the gas boundary layer surrounding the external surface of the sorbent particle, then it enters the particle and diffuses inside the particle porosity. Different types of diffusion mechanisms are involved in intra-particle diffusion (i.e. molecular, Knudsen and surface diffusions). Once the acid gas molecules reach the grain surface, mass transfer becomes governed by solid-state diffusion through the product layer. Finally, the reaction takes place on the unreacted core surface.

The equations governing the flow of the gaseous reactant through bed, particle and product layer, according to the processes described above, were discussed by several authors (e.g. see Hartman and Coughlin, 1976; Duo et al., 1993; Verdone and De Filippis, 2006) and are reported in Table 1. In the following, expressions for the reaction rates per unit volume of fixed bed, r_{vb} , and of sorbents particle, r_{vp} , are derived.

Table 6.1. Equations of the grain model in the fixed bed geometry assumed (see the nomenclature section for symbols in equations).

Type	Equation and boundary conditions
Mass balance in the fixed bed	$\varepsilon \cdot \frac{\partial C}{\partial t} = -u_0 \cdot \frac{\partial C}{\partial z} + \varepsilon \cdot D_z \cdot \frac{\partial^2 C}{\partial z^2} - r_{vb} \quad 6.2$ $C(z, t = 0) = 0, \text{ for } 0 < z < L \quad (6.2a)$ $u_0 \cdot [C_{in} - C(z = 0, t)] = -\varepsilon \cdot D_z \cdot \frac{\partial C}{\partial z} \Big _{z=0} \quad (6.2b)$ $\frac{\partial C}{\partial z} \Big _{z=L} = 0 \quad (6.2c)$
Mass balance in the particle	$\varepsilon_p \cdot \frac{\partial C_p}{\partial t} - \frac{1}{R^2} \frac{\partial}{\partial R} \left(R^2 \cdot D_{ef} \cdot \frac{\partial C_p}{\partial R} \right) = -r_{vp} \quad 6.3$ $C_p(R, z, t = 0) = 0 \quad (6.3a)$ $C_p(R = R_p, z, t) = C_g(z, t) \quad (6.3b)$ $\frac{\partial C_p}{\partial R} \Big _{R=0} = 0 \quad (6.3c)$ $D_{ef} \frac{\partial C_p}{\partial R} \Big _{R=R_p} = k_g \cdot [C(z, t) - C_g(z, t)] \quad (6.3d)$
Mass balance in the product layer (grain i)	$\varepsilon_{pl} \cdot \frac{\partial C_{pl,i}}{\partial t} - \frac{1}{r_i^2} \frac{\partial}{\partial r_i} \left(r_i^2 \cdot D_s \cdot \frac{\partial C_{pl,i}}{\partial r_i} \right) = 0 \quad 6.4$ $C_{pl,i}(r_i, R, z, t = 0) = 0 \quad (6.4a)$ $C_{pl,i}(r_i = r_{t,i}, R, z, t) = C_p(R, z, t) \quad (6.4b)$ $D_s \frac{\partial C_{pl,i}}{\partial r_i} \Big _{r_i=r_{c,i}} = k_s \cdot [C_{c,i}(R, z, t) - C_{eq}] \quad (6.4c)$
Shrinking rate of the unreacted core (grain i)	$\frac{dr_{c,i}}{dt} = -\frac{bM_s}{\rho_s} \cdot k_s \cdot (C_{c,i} - C_{eq}) \quad 6.5$ $r_{c,i}(R, z, t = 0) = r_{g,i} \quad (6.5a)$

The core of the model is the behaviour of sorbent grains. In the classical grain model approach, it is assumed that all the grains have the same initial radius, r_g (Weinell et al., 1992). The initial grain radius can be calculated assuming that the sum of the surface of the grains in a single, unreacted particle corresponds to the specific surface area S_{BET} of the solid reactant:

$$r_g = \frac{3}{\rho_s \cdot S_{BET}} \quad 6.6$$

where ρ_s is the solid density. More generally, the distribution of pore sizes occurring in the particle can be taken into account by specifying a set of grain sizes (Maya and Chejne, 2014). Heesink et al.

(1993) proposed a method to correlate a set of size distribution of grains to the size distribution of pores, as determined by mercury porosimetry measurements. If the pores are divided into a set of size classes and the initial grain radius for each class is determined by:

$$r_{g,i} = F \cdot r_{pore,i} \quad 6.7$$

where $r_{g,i}$ is the initial radius of the grains belonging to the size class i and $r_{pore,i}$ is the pore radius associated to the related pore class. The pore-to-sphere factor F , which is the proportionality factor between corresponding pore and grain radius introduced by Heesink et al. (1993), is given by:

$$F = \frac{3}{\rho_s \cdot S_{BET}} \sum_i \frac{v_i}{r_{pore,i}} \quad 6.8$$

where v_i is the fraction of grains belonging to size class i and is equal to the ratio of the volume of the corresponding pore class to the total pore volume of the sorbent.

Sintering phenomena could reasonably be excluded for the process of interest. In fact, proper sintering phenomena (the compacting and loss of surface area caused by heat or pressure) can be discarded for the typical operating temperatures of dry sorbent injection (DSI) processes (150-200 °C), based both on experimental evidence (Borgwardt, 1989) and on the much higher value of the Tamman temperature for Ca-based compounds (Kierzkowska et al., 2013; Valverde, 2013). Loss of surface area due to pore blockage/occlusion, resulting in the coalescence of grains, could be excluded based on the results of Maya and Chejne Janna (2016) for the sulfation of lime.

During the reaction process, the initially homogeneous grain undergoes partial conversion and the radius of the core of fresh sorbent, $r_{c,i}$, has to be distinguished from the total radius of the grain, $r_{t,i}$, comprising both the core and the external shell of solid product. When the reaction process starts, $r_{c,i}(t=0) = r_{t,i}(t=0) = r_{g,i}$. Then, $r_{t,i}$ changes due to the formation of the solid product (e.g. CaCl_2), which in general will have a different molar density. If α is defined as the ratio between the molar volume of the solid reactant and that of the solid product, the overall radius of the grain at a generic time t , $r_{t,i}$, can be expressed as a function of the initial grain radius, $r_{g,i}$, and of the unreacted core radius, $r_{c,i}$, through a volume balance:

$$r_{t,i} = [r_{c,i}^3 + \alpha \cdot (r_{g,i}^3 - r_{c,i}^3)]^{1/3} \quad 6.9$$

As reported in Table 6.1, the variation with time of the radius of the unreacted core of the grains, $r_{c,i}$, can be expressed by the mass balance of the solid reactant at the core surface where the reaction takes place (eq. 6.5 in Table 6.1).

The concentration of the gaseous reactant at the surface of the unreacted core of each class of grains, $C_{c,i}$, is dependent, through diffusive mass transfer in the ash layer of the solid product, on the concentration at the grain surface, which is equal to the concentration in the pores, C_p , at that position in the particle (see the concentration profile in Figure 6.4b). The relationship between $C_{c,i}$ and C_p can be obtained from the integration of the mass balance for the diffusing gas in the layer formed by the solid product around the unreacted core (eq. 6.4), with the inner boundary condition including surface reaction (eq. 6.4c). Under the assumption of a pseudo-steady state approximation (Duo et al., 1993) the following solution is obtained:

$$C_{c,i} - C_{eq} = \frac{D_s}{D_s + k_s \cdot r_{c,i} \cdot (1 - r_{c,i}/r_{t,i})} \cdot (C_p - C_{eq}) \quad 6.10$$

where D_s is the solid-state diffusion coefficient of the gaseous reactant in the product layer and C_{eq} is the equilibrium concentration of the gaseous reactant, determined as in Shemwell et al. (2001).

The difference $C_{c,i} - C_{eq}$ may be considered the driving force of the reaction. The reaction rate per unit volume of a particle, r_{vp} , in eq. 6.3, can be calculated as a function of the concentration of the gaseous reactant at the surface of the grains, $C_{c,i}$, by the following expression:

$$r_{vp} = \sum_i [A_{vp,i} \cdot k_s \cdot (C_{c,i} - C_{eq})] \quad 6.11$$

where $A_{vp,i}$, the reaction interfacial area associated to the grain class i per unit volume of sorbent particles, is given by:

$$A_{vp,i} = v_i \cdot \frac{3 \cdot (1 - \varepsilon_p) \cdot r_{c,i}^2}{r_{g,i}^3} \quad 6.12$$

where ε_p is the void fraction of a sorbent particle and v_i is the volumetric fraction of pores represented by the grain class i (see eq. 6.8), assumed to be the same at any radius of the particle (homogenous distribution of pores through the particle). Therefore, substituting eq. 6.12 into eq. 6.11, the following expression may be obtained for the reaction rate per unit volume:

$$r_{vp} = \sum_i [v_i \cdot \frac{3 \cdot (1 - \varepsilon_p) \cdot r_{c,i}^2}{r_{g,i}^3} \cdot \frac{D_s \cdot k_s}{D_s + k_s \cdot r_{c,i} \cdot (1 - r_{c,i}/r_{t,i})}] \cdot (C_p - C_{eq}) \quad 6.13$$

Eq. 6.13 implies a first order overall rate for the process in the description of the reaction rate, which has indeed been observed by several investigators for the CaO/HCl system (Daoudi and Walters, 1991; Gullett et al., 1992; Li et al., 2000) and for the Ca(OH)₂/HCl system (Yan et al., 2003). Assuming a constant value for the particle radius, R_p , the overall reaction rate per unit volume of the fixed bed, r_{vb} , in eq. 6.2, can be obtained by integrating eq. 6.13 over the volume of each particle, and multiplying the result by the average number of particles per unit volume in the fixed bed:

$$r_{vb} = \frac{3 \cdot (1 - \varepsilon)}{R_p^3} \cdot \int_0^{R_p} r_{vp} \cdot R^2 dR \quad 6.14$$

where R is the radial coordinate inside a particle and ε is the void fraction of the bed packed with sorbent particles. Equation 6.14 can be easily extended to beds with a distribution of particles of different radius as described by Gbor and Jia (2004); this generalisation is not reported here for sake of simplicity in the discussion.

Substituting eqs. 6.13 and 6.14 respectively in eqs. 6.3 and 6.2, the system in Table 6.1 is completely defined. Its solution provides the concentration of the gaseous reactant (C , C_p , $C_{pl,i}$) and the radius of the unreacted core $r_{c,i}$ as a function of time and position within the bed and the sorbent particles. The local conversion of the sorbent is then related to the unreacted core radius as follows:

$$X_{sl} = \sum_i \left[v_i \left(1 - \frac{r_{c,i}^3}{r_{g,i}^3} \right) \right] \quad 6.15$$

From the local conversion the average solid conversion in the particle, X_p , and in the bed, X_b , can be calculated as follows:

$$X_p = \frac{3}{R_p^3} \int_0^{R_p} X_{sl}(R) \cdot R^2 dR \quad 6.16$$

$$X_b = \frac{1}{L} \int_0^L X_p(z) \cdot dz \quad 6.17$$

As mentioned in literature review, the grain model described in this section, although effectively accounting for transport phenomena and geometry changes due to reaction, does not address the issue of incomplete conversion. To overcome this limitation, in the following the model is coupled with a specific crystallisation and fracture submodel.

6.4 Phenomenological model: the crystallisation and fracture submodel

In order to address the issue of incomplete conversion of the sorbent, an active area reduction factor, RF, is introduced. The factor is obtained from a crystallisation and fracture (CF) model. The theoretical basis and the comprehensive mathematical derivation of CF models are discussed in Duo et al. (1994). In the following, the features of the specific model applied and the modifications introduced with respect to the model of Duo et al. (1994) are discussed.

The trigger of the crystallisation process is nucleation. In the initial stage of the reaction, when a product layer has yet to be formed, the overall free energy change ΔG associated with the formation of a spherical nucleus of radius r of the new product phase is given by the sum of a volume term and a surface term (Duo et al., 1994). After the first layer of product is formed, if the molar volume of the solid product is greater than that of the solid reactant ($\alpha > 1$), in order that a new nucleus is formed, the mechanical work required to displace the product layer in order to accommodate the increased volume at the boundary between the unreacted core of solid reactant and the product layer itself should be overcome. This new energy barrier to nucleation, W , adds to the other energy terms required for the nucleation process:

$$\Delta G = \Delta G_{surface} + \Delta G_{volume} + W = 4\pi r^2 \sigma + \frac{4}{3}\pi r^3 \rho_m \Delta G_c + W \quad 6.18$$

where σ is the surface energy per unit area, ρ_m the molar density of product and ΔG_c the molar free energy change due to chemical reaction, which can be expressed by means of eq. 6.19, if the reference reaction 5.1 is considered:

$$\Delta G_c = \Delta G^0 + RT \cdot \ln \left(\frac{P_{H_2O}^2}{P_{HCl}^2} \right) \quad 6.19$$

On the basis of the mechanism of adhesive fracture, derived from the work of Kendall et al. (1987) on the mechanical strength of assemblies of small particles, Duo et al. (1995) proposed a relationship in order to express W as a function of the thickness of the product layer h (the difference between r_t and r_c). The relationship can be expressed as follows:

$$W = \frac{K 4\pi r \sigma (1 - 1/\alpha)^{\frac{1}{3}} (1 - \varepsilon_{pl})^4 h^{\frac{3}{2}}}{d^{\frac{1}{2}}} = M_W 4\pi r \sigma h^{\frac{3}{2}} \quad 6.20$$

where K is a non-dimensional numerical coefficient accounting for the mechanical properties of the product layer, d the diameter of the developed crystallites that constitute the product layer and ε_{pl} the porosity of the product layer. In the following, these quantities will be represented by the parameter M_W as shown in eq. 6.20.

With reference to the classical nucleation theory (Abraham, 1974), the key step of the nucleation and crystallisation process is the formation of nuclei of product having a critical radius r_k (i.e. the nuclei for which the associated energy change expressed by eq. 6.18 reaches its maximum value). The nuclei of critical size are the primers for the crystallisation process, since only nuclei with radius greater than r_k tend to grow in order to reduce their total free energy, thus producing stable nuclei (Fletcher, 1958; Duo et al., 1994). In particular, a nucleus becomes stable when it reaches a radius r_s , larger than the critical radius, such that the associated ΔG equals zero (Duo et al., 1995). Thus, the critical radius is obtained deriving eq. 6.18 with respect to r and imposing that the derivative is equal to zero:

$$r_k = -\frac{\sigma}{\rho_m \Delta G_c} \left(1 + \sqrt{1 - \frac{\rho_m \Delta G_c}{\sigma} M_W h^{\frac{3}{2}}} \right) \quad 6.21$$

When a product layer has not yet developed ($h = 0$) or the formation of a nucleus does not imply any deformation of the product layer ($\alpha = 1$), the term into brackets in eq. 6.21 equals 1, and the value of the critical radius is the same obtained by conventional nucleation theory. However, if the product layer grows, the size of the critical nuclei increases (note that ΔG_c is negative for spontaneous reaction). Conversely, the population of nuclei of critical size (PNC, i.e. the number of nuclei of critical size on the surface of a grain) tends to decrease during the reaction, owing to the increased mechanical work required to displace the increasingly thicker product layer. This phenomenon is that eventually stopping the reaction.

The relationship between the PNC and the thickness of the product layer may be expressed as follows:

$$PNC = N_s \cdot \exp\left(-\frac{\Delta G_k}{k_b T}\right) \quad 6.22$$

where N_s is the number of potential nucleation sites and ΔG_k the maximum free energy change associated with the formation of a nucleus of critical size. It is assumed that each molecule of the solid reactant can act as a nucleation site, therefore N_s is equal to the total number of sorbent molecules at the reaction interface:

$$N_s = 4\pi r_c^2 \zeta \quad 6.23$$

where ζ is the number of sorbent molecules per unit area at the reaction interface.

In the implementation of the model, a geometrical constraint was set for the PNC in order to take into account the maximum space available on the surface of one grain. Considering that the nuclei were described as spheres, the overall cross section of active nuclei lying on the surface of one grain cannot exceed the maximum surface area that can be covered by packed spheres of equal diameter:

$$PNC r_k^2 \leq \frac{2\pi}{\sqrt{3}} r_g^2 \quad 6.24$$

The term ΔG_k in eq. 6.22 incorporates the dependence of PNC on the thickness of the product layer. In Duo et al. (1994), ΔG_k was calculated with reference to a single molecule. In the present approach, since the entire critical nucleus has to obtain its space at the interface, it was considered more adequate to evaluate the mechanical work required for the growth of a nucleus of critical radius r_k , in order to take into account the contribution of all the molecules that coalesce to form a nucleus.

The parameters involved in the determination of the mechanical work, which takes into account the mechanical properties of the product layer that is formed during the reaction, can be estimated introducing some assumptions. The porosity of the product layer ε_{pl} can be assumed as the void fraction of a close-packing of equal, non-overlapping spheres. Therefore, physically consistent values lie in the range between $(1 - \frac{\pi}{3\sqrt{2}})$ and $(1 - \frac{\pi}{6})$, corresponding to the void fractions of hexagonal and cubic packing respectively. The lower value was selected in the present study, since product layers formed in dry gas conditions generally show limited porosity (Fonseca et al., 2001). The parameter d , according to the CF model, is the average diameter of spherical crystallites assembled together to form the product layer. Its value can float, at most, between the average diameter of the stable nuclei formed so far ($2 \cdot r_s$) and the thickness of the product layer (h): $2 \cdot r_s \leq d \leq h$. Dennis et al. (2009), who applied the CF approach to model the overall uptake of CO₂ by a Ca-based sorbent, used a constant value of d , that was used as an adjustable parameter. In the present application, in order to take into account the evolution of d during reaction, it was assumed that the increase in the size of the developed crystallites depends on the increase of the size of stable nuclei. Therefore, the growth of the crystallites was assimilated to the growth of the stable radius and it was thus imposed for d to be equal to $2 \cdot r_s$.

In order to introduce the CF model in the kinetic framework previously described, the decrease of the population of active nuclei was related to the decrease of the surface area available for the reaction, which, for any grain of sorbent, is given by the number of nuclei of critical size multiplied by the cross section of a nucleus. The integration of the CF model in the grain model was realised defining a reduction factor for the active surface (RF), expressed as:

$$RF = \frac{PNC(C_c, h) \cdot r_k(C_c, h)^2}{PNC(C_c, h = 0) \cdot r_k(C_c, h = 0)^2} \quad 6.25$$

The overall active area is proportional to the number of nuclei of critical size (PNC) multiplied by their cross section ($\pi \cdot r_k^2$). The reduction factor is calculated as the ratio among the actual active area and the maximum potential active area. The maximum potential active area is obtained considering no product layer. The actual active area takes into account the inhibition of reactivity due to the accumulation of the product layer around the reacting grains, proportional to the layer thickness. Both terms are function of the thickness of the product layer, h . RF is equal to 1 at the beginning of the reaction, when the product layer is not formed yet, and decreases monotonically as h increases.

Since product layer thickening for a given conversion degree is a function of grain radius, different RF_i have to be defined for the classes i of grain size. RF_i is applied to the reaction rate per unit volume of particle reported in eq. 6.13 independently for each grain class i :

$$r_{vp} = \sum_i [v_i \cdot RF_i \cdot \frac{3 \cdot (1 - \varepsilon_p) \cdot r_{c,i}^2}{r_{g,i}^3} \cdot \frac{D_s \cdot k_s}{D_s + k_s \cdot r_{c,i} \cdot (1 - r_{c,i}/r_{t,i})}] \cdot (C_p - C_{eq}) \quad 6.26$$

The reaction rate per unit volume of bed (eq. 6.14) is corrected accordingly. The introduction of RF_i allows the grain model to incorporate the CF model in the evaluation of the overall reaction rate. Accordingly, RF_i is also introduced as a multiplying factor in the equation for the time evolution of the grain radius (eq. 6.5):

$$\frac{dr_{c,i}}{dt} = -RF_i \cdot \frac{M_s}{2 \rho_s} \cdot k_s \cdot (C_{c,i} - C_{eq}) \quad 6.27$$

Actually, the velocity at which the reaction interface moves towards the centre of the grain has to be calculated taking into account the actual reactive area, as expressed by RF_i.

It is worth remarking that the coupling of the CF with the grain model allows the model to include the quantitative dependence on the two factors that cause the decrease of the reaction rate due to the growth of the product layer: i) the grain model considers the increase of the characteristic length for solid-state diffusion, ($r_{t,i} - r_{c,i}$); ii) the CF model considers the increase in the mechanical work, W , needed for further product nucleation at the reaction interface.

6.5 Model input and output parameters

The input data and the model parameters that need to be defined in order to apply the model are summarised in Table 6.2. The table also reports the range of values or the correlations available to estimate the parameters for the $\text{Ca(OH)}_2/\text{HCl}$ system.

As shown in Table 6.2, all the model parameters can be estimated from literature data, calculated a priori or obtained from the experimental characterisation of the solid reactant, except k_s , D_s and K . These parameters are inherently dependent on the morphology of solid particles, which may show important differences even when the same reactant is used (Borgwardt et al., 1987; Koch et al., 2005), and also on the experimental techniques used in their assessment (Koch et al., 2005).

As further discussed in section 6.6, in the model validation a single value for k_s was assumed, based on literature analysis with reference to the $\text{Ca(OH)}_2/\text{HCl}$ system. Generally speaking, the value of k_s can be assessed in specifically designed experiments aimed at identifying the initial reaction rate in conditions where mass transfer limitations are negligible (Yan et al., 2003). However, the technical hindrances in performing the measurement as well as the limited influence of the chemical reaction rate on the overall rate of gas-solid reactions, typically dominated by diffusive control (Weinell et al., 1992) led to its use as a fitting parameter in previous studies (Duo et al., 1993; Wang and Teng, 2009). With reference to the $\text{Ca(OH)}_2/\text{HCl}$ system, values estimated using different modelling approaches are in the range between 10^{-5} and 10^{-4} m/s (Karlsson et al., 1981; Duo et al., 1993).

Similarly, the assessment of the diffusion coefficient in the product layer is affected by uncertainties. Actually, direct measurement of diffusivity in the product layer is hardly possible, and the different modelling approaches used to-date to extrapolate such parameter from experimental data have an important influence on the values obtained, as shown in Figure 6.6. The values of Mura and Lallai (1994) were derived for the reaction between calcium carbonate and hydrogen chloride using a grain model and considering both chemical reaction and product layer diffusion. The data of Koch et al. (2005) were obtained from single-particle experiments for the $\text{Ca(OH)}_2/\text{HCl}$ system analysed taking into account pore diffusion, product layer diffusion and an interface reaction step. The data of Weinell et al. (1992) were obtained by the authors using the experimental data which are shown in section 6.6 and a grain model assuming only product layer diffusion control. The data of Duo et al. (1993) were obtained from the same experimental data but considering also pore diffusion and chemical reaction in the grain model, hence demonstrating how the estimated value of D_s is widely dependent on the modelling assumption introduced for experimental data analysis.

Table 6.2. Summary of input parameters required for the coupled grain and CF models (CALC: parameter calculated according to reported references or to equations in the text; FIT: fitting parameter as discussed in the text)

Type	Item	Description / Definition	Value	Units	Reference
Geometrical parameters	ε	Inter-particle void fraction of the fixed bed	0.4-0.6	-	Weinell et al. (1992) Duo et al. (1993) Verdone and De Filippis (2006)
	ε_p	Intra-particle void fraction (porosity)	0.5 [†]	-	Duo et al. (1993)
	ρ_b	Bulk (apparent) density of sorbent	500-650 [†]	kg/m ³	Weinell et al. (1992)
	ρ_s	True (particle) density of sorbent: $\rho_s = (1-\varepsilon_p) \cdot \rho_b$	CALC	kg/m ³	
	S_{BET}	Specific surface area (usually measured with the Brunauer-Emmett-Teller method)	10-20 [†]	m ² /g	Weinell et al. (1992) Gullett et al. (1992) Yan et al. (2003)
	$V_{m,s}$	Molar volume of sorbent	51.6 [†]	m ³ /mol	Chemistry WebBook (NIST)
	$V_{m,p}$	Molar volume of solid product	33.1 [†]	m ³ /mol	Chemistry WebBook (NIST)
	α	Volumetric expansion factor, i.e. ratio of the molar volume of the solid product to that of the solid reactant: $\alpha = V_{m,p} / V_{m,s}$	CALC	-	
	τ	Tortuosity of the sorbent porous structure (used for D_{ef} estimation)	CALC	-	Correlations: Mackie-Meares, Wakao-Suzuki, Suzuki-Smith (Green and Perry, 2007)

<i>Thermodynamic parameters (dependent on the actual reaction equation assumed)</i>	C_{eq}	Equilibrium concentration of the gaseous reactant	CALC	mol/m ³	JANAF Thermochemical Tables (NIST)
	ΔG_c	Free energy change associated to reaction (eq. 8.18)	CALC	J/mol	JANAF Thermochemical Tables (NIST)
	k_b	Boltzmann constant	$1.38 \cdot 10^{-23}$	m ² kg s ⁻² K ⁻¹	
	σ	Surface energy per unit area of the solid product	0.1-0.5	J/m ²	Duo et al. (1994)
	ε_{pl}	Void fraction of the product layer	0.26-0.48	-	Geometrical boundaries
	d	Diameter of a crystallite of solid product, corresponding to the stable radius of a nucleus: $d = 2 \cdot r_s$	CALC	-	
	K	Mechanical work-related numerical coefficient (eq. 8.27)	FIT	-	Least squares method (Wolberg, 2006)
<i>Kinetic and transport parameters</i>	k_s	Chemical reaction rate constant	$3.2 \cdot 10^{-4}^{\dagger}$	m/s	Yan et al. (2003)
	k_g	Exterior gas film mass transfer coefficient	CALC	m/s	Ranz-Marshall correlation (Levenspiel, 1998)
	D_s	Product layer diffusivity of the gaseous reactant (eq. 8.26)	FIT	m ² /s	Least squares method (Wolberg, 2006)
	D_m	Molecular diffusivity of the gaseous reactant	CALC	m ² /s	Fuller-Schettler-Giddings correlation (Fogler, 2005)
	D_z	Axial dispersion coefficient	$0.7 \cdot D_m$	m ² /s	Harker et al. (2002)
	D_k	Knudsen diffusivity	CALC	m ² /s	Dusty gas model (Duo et al., 1993)
	D_{ef}	Effective gas diffusivity in the pores: $D_{ef} = \frac{\varepsilon_p}{\tau} \left(\frac{1}{D_m} + \frac{1}{D_k} \right)^{-1}$	CALC	m ² /s	Smith (1981)

[†]with reference to Ca(OH)₂ and the Ca(OH)₂/HCl system

Lastly, the non-dimensional coefficient K, taking into account the mechanical properties of the product layer in the expression of the mechanical work W (eq. 6.20), is a specific feature of the present model. The parameter was introduced by Duo et al. (1994) in deriving the original CF model, but no numerical values were proposed.

In the light of the above discussion, D_s and K were used as fitting parameters in the following, although their variation with temperature was bound to physical considerations. As shown in Figure 6.6, available data suggest the exponential dependency of D_s on temperature, which is typical of an activated process such as solid-state diffusion (Bhatia and Perlmutter, 1982). Thus, an Arrhenius-type behaviour was assumed:

$$D_s = A_D \cdot \exp\left(-\frac{E_{a,D}}{RT}\right) \quad 6.28$$

where A_D (m^2/s) is the pre-exponential factor and $E_{a,D}$ the activation energy (kJ/mol).

Also for the coefficient K an exponential dependency on temperature was supposed. Assuming that K is the term in the expression of the mechanical work W which takes into account the mechanical resistance of the product layer, its log-linear decrease with temperature recalls the typical behaviour of the elastic modulus of several materials (Wachtman et al., 1961). Thus, by analogy with D_s , the following expression was used to calculate K:

$$K = A_K \cdot \exp\left(\frac{E_{a,K}}{RT}\right) \quad 6.29$$

where A_K (dimensionless) and $E_{a,K}$ (kJ/mol) are an apparent pre-exponential factor and an apparent activation energy, respectively, which were estimated from data fitting.

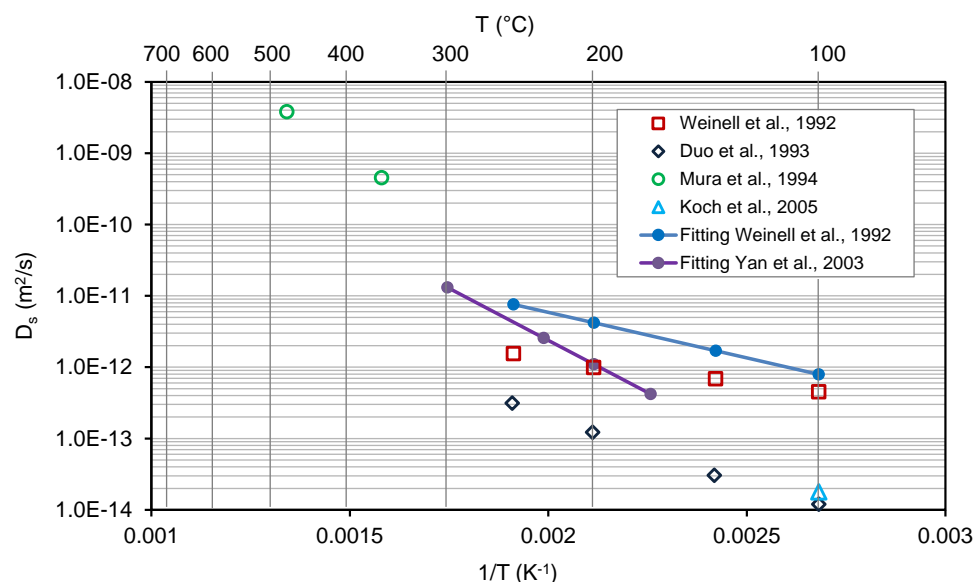


Figure 6.6. Product layer diffusivity for the reaction between Ca-based sorbents and HCl obtained from different literature sources.

6.6 Model validation against literature data

The model described in sections 6.3 and 6.4 was applied to the analysis of different sets of experimental data, reported in two different literature studies concerning the $\text{Ca(OH)}_2/\text{HCl}$ system (Weinell et al., 1992; Yan et al., 2003).

The set of data reported by Weinell et al. (1992) concerns the reaction of gaseous HCl with a thin particle layer of calcium hydroxide or calcium oxide in a tubular reactor at different temperatures. The data obtained for HCl reaction with calcium hydroxide at 100, 140, 200 and 250 °C were used in the present validation. Further details on the experimental runs are reported in Duo et al. (1993). The second validation data set was obtained from the study of Yan et al. (2003). The data concerned the reaction between gaseous HCl and calcium hydroxide in the range 170-300 °C in a thermogravimetric analyser. Further details on experimental conditions are reported in the original paper. Table 6.3 reports the specific values of the main parameters and operating conditions considered for the application of the model to the simulation of the two sets of experimental data considered.

Table 6.3. Experimental parameters reported in the studies considered for model validation.

Parameter	Weinell et al. (1992)	Yan et al. (2003)
Total flow rate [L/min]	1	0.15
Gas velocity [m/s]	$5 \cdot 10^{-2}$	$3 \cdot 10^{-2}$ *
HCl inlet concentration [ppm]	1000	562
Mass of sorbent [mg]	25	10
BET surface area of sorbent [m^2/g]	12.1	17.1
True density of sorbent [kg/m^3]	2240	Bulk density of sorbent: 530 kg/m^3
Void fraction of the bed [-]	0.6	
Porosity of sorbent [-]	0.519	
Bed thickness [mm]	0.10 †	0.24 *

* Superficial gas velocity and bed thickness were estimated on the basis of a standard 10 mm diameter platinum pan.

† The thickness of the particle layer of calcium hydroxide was estimated from the axial Peclet number of 0.2 reported by the authors using the reported gas velocity and the molecular diffusivity of HCl.

No porosimetry measurements providing the pore size distribution of the sorbent are reported in the two papers. Even if, in general, the model can take into account a distribution of the grains, at this stage a uniform radius of the grains, calculated according to eq. 6.6, was adopted in modelling the two datasets. Maya and Chejne Janna (2016) showed the possibility to reconstruct a reference pore size distributions from BET surface area and the porosity data by applying the method illustrated by John et al. (2007). This is however deemed to introduce arbitrary assumptions concerning unknown pore size distributions, and is therefore avoided in this validation step.

Due to the specific geometrical features of the experimental systems, few simplifying assumptions were introduced. In particular, since the fixed reactant bed is formed by an extremely thin layer of solid particles (as confirmed by the value of the Peclet number reported by Weinell et al., 1992), a uniform concentration of HCl all through the bed, $C(t)$, was assumed, neglecting position in the z axis. Accordingly, the reaction rate and the sorbent consumption are uniform within the bed. Furthermore, the accumulation term of eq. 6.2 can be neglected because the mean flow time through the bed is negligible with respect to the characteristic time of the reaction (Hartman and Coughlin, 1976; Verdone and De Filippis, 2006). Therefore, the hydrogen chloride concentration in the bed at the initial condition ($t = 0$) is driven by the HCl removal at the initial reaction rate, when the inlet of the experimental system shows an abrupt step change from 0 to C_{in} . Thus, a pseudo steady-state perfect-mixing approximation was applied. Eq. 6.2 was accordingly changed to eq. 6.30 in Table 6.4.

In the simplified set-up assumed for experimental data simulation, the concentration of HCl in the bed depends only on the variation of the reaction term. Indeed, r_{vb} decreases due to the formation of

the product layer and the consumption of the fresh sorbent, with velocity given by eq. 6.32 (Table 6.4). With specific reference to the chemical system of interest, a further assumption introduced is that the HCl concentration within the pores (i.e. within the particle) can be considered as uniform. This was based on experimental results obtained by Weinell et al. (1992), that evidence that the conversion of the sorbent within a particle can be assumed as homogeneous. These results were confirmed by Guglielmi (2014), which solved the governing mass transport equations within particle porosity finding an almost uniform profile of HCl concentration inside the particles. Therefore, the intra-particle concentration of the gaseous reactant was assumed equal to the bulk gas concentration at any radial coordinate within the sorbent particles: $C_p(R,t) = C(t)$. Accordingly, eq. 6.3 is no more necessary for the description of the simplified geometrical system considered.

As a consequence of the simplifications discussed above, only the HCl concentration gradient within the product layer was considered in the model validation stage. Thus, governing phenomena result the chemical reaction and solid-state diffusion. This is in agreement with the findings of several investigators, specifically addressing the HCl/Ca(OH)₂ system (Gullett et al., 1992; Weinell et al., 1992; Fonseca et al., 1998), as well as general acid gas removal processes (Stendardo and Foscolo, 2010). The overall reaction rate per unit volume of the fixed bed (eq. 6.15) may be modified as in eq. 6.31 (Table 6.4).

The model results in the system of Table 6.4, where the main unknowns are the HCl concentration within the bed, $C(t)$, and the radius of the unreacted core of the grains, $r_c(t)$. According to the assumption of a uniform HCl concentration profile within the bed and in the particle porosity, from the application of eqs. 6.16 and 6.17, the average conversion of the sorbent bed, X_b , results equal to the local conversion, X_{sl} .

Table 6.4. Model equations associated with initial conditions under the assumptions introduced for model validation.

Type	Model equation	
Mass balance in fixed bed	$u_0(C_{in} - C(t)) = L \cdot r_{vb}$	6.30
Reaction term in fixed bed	$r_{vb} = RF \cdot \frac{3 \cdot (1 - \varepsilon) \cdot (1 - \varepsilon_p) \cdot D_s \cdot k_s}{r_g^3} \cdot \frac{r_c^2}{D_s + k_s \cdot r_c \cdot (1 - r_c/r_t)} \cdot (C - C_{eq})$	6.31
Shrinking rate of unreacted core	$\frac{dr_c}{dt} = -RF \cdot \frac{b \cdot M_s}{\rho_s} \cdot \frac{D_s \cdot k_s}{D_s + k_s \cdot r_c \cdot (1 - r_c/r_t)} \cdot (C - C_{eq})$	6.32
	$r_c(t = 0) = r_g$	6.32a

For both experimental datasets considered, the stoichiometry of reaction 7.1 was assumed, since the sorbent conversion was reported accordingly in the original studies. The model parameters dependent on the reaction product formed were thus selected as follows: i) the molar free energy due to chemical reaction ΔG_c was calculated from the energies of formation of the compounds involved in reaction 7.1 (NIST-JANAF Thermochemical Tables); ii) the volumetric expansion factor α was set to 1.58 (i.e. the ratio of the molar volumes of CaCl₂ to that of Ca(OH)₂); iii) the value of 0.25 J/m² was assumed for the surface energy of the product, σ , since typical values for inorganic salts vary in the range between 0.1 and 0.5 (Duo et al., 1994), while for liquid CaCl₂ Ferguson (1928) assessed a value of 0.15 J/m² and for CaCO₃ estimated values between 0.23 and 0.38 J/m² are reported by Gilman (1960).

Limited data are available in literature for the surface reaction rate constant k_s , since only experiments designed to minimise mass transfer limitations and aimed at evaluating only the initial stage of reaction (i.e. before the formation of a continuous product layer) could provide a reliable measure of the chemical reaction rate of a gas-solid reaction. For the $\text{Ca}(\text{OH})_2/\text{HCl}$ system at the temperatures of interest for DSI application, Yan et al. (2003) estimated chemical reaction rates of $2.1 \cdot 10^{-4}$ m/s and $3.2 \cdot 10^{-4}$ m/s for two lime samples of lower and higher surface area, respectively. No data are reported by Weinell et al. (1992). Thus, the value of $3.2 \cdot 10^{-4}$ m/s proposed by Yan et al. (2003) for the experimental conditions detailed in Table 6.3 was also used for the fitting of the data from Weinell et al. (1992). The adoption of the same value of k_s is supported by the nature of the parameter, which should not be dependent on the morphology of the sorbent. Regarding the temperature dependence of k_s , this was neglected by Yan et al. (2003), and Duo et al. (1993) found k_s to be constant in the interval 100–250 °C. Actually, it will be shown that the value assumed for k_s has a limited influence on model results.

Eqs. 6.28 and 6.29 were used to determine D_s and K for the experimental data available. A least squares best-fit procedure was used to calculate the parameters in the equations. The values obtained are reported in Table 6.6.

Figure 6.7 reports the results of model simulations for the overall conversion of $\text{Ca}(\text{OH})_2$ as a function of time compared to the experimental data by Weinell et al. (1992). Figure 6.8 reports the model results compared to experimental data by Yan et al. (2003).

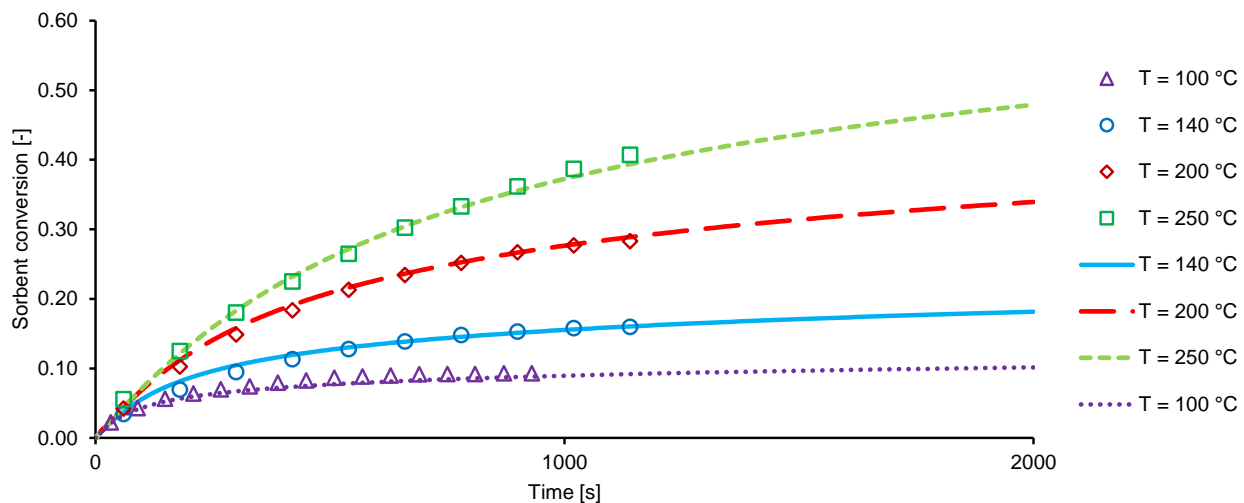


Figure 6.7. Sorbent conversion at different temperatures. Points: experimental data by Weinell et al. (1992); curves: model results.

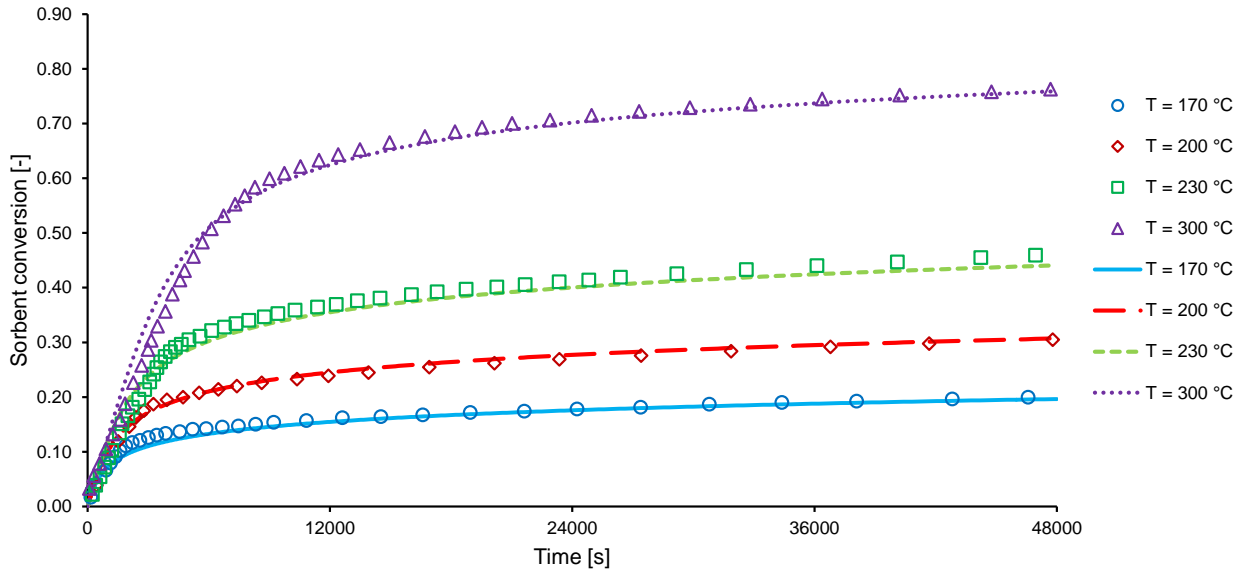


Figure 6.8. Sorbent conversion at different temperatures. Points: experimental data by Yan et al. (2003); Curves: model results.

Experimental data from Weinell et al. (1992) were available only for 20 minutes, hence the decrease of reactivity over time given by the increase of the diffusional resistance and the energy barrier to nucleation is captured only in its earlier stage. Nonetheless, the model is capable to fit the data with sufficient precision and, by extending the time scale to 30 minutes, to show the decline in reactivity leading to increasingly slower overall reaction rates.

Differently, Yan et al. (2003) ran the reaction over a longer time scale (more than 13 hours). Figure 6.8 clearly shows the good reproduction of the asymptotic tendency to a different ultimate conversion value at different temperature and in general a good agreement with experimental data, especially for larger time intervals, which are of main concern in conditions of practical interest.

Even if a uniform size of the sorbent grains was assumed, a satisfactory fitting of the data was obtained. Thus, it was confirmed unnecessary to add further hypotheses about grain size distribution in the current model validation by available data.

A direct comparison of the two datasets is difficult both because of the different time scale and of the different reactant ratios used. Although the mass of sorbent and the HCl inlet concentration set in the two experiments are similar (see Table 6.3), the gas flow rate in Yan et al. (2003) is an order of magnitude higher than in Weinell et al. (1992), resulting in a different sorbent to HCl ratio. A normalisation was thus introduced to compare the two datasets and the model results at a temperature of 200 °C, at which both studies provide experimental data. Figure 7 shows the sorbent conversion with respect to a normalised time variable t/τ , obtained dividing actual time of experimental runs, t , by the time τ needed to approach the stoichiometric saturation of the bed (i.e. the time at which the cumulated molar flowrate of HCl through the bed equals the moles of HCl which the sorbent bed could adsorb according to the stoichiometry of reaction 7.1). The time τ is calculated as follows:

$$\tau = \frac{2 \cdot n_{Ca(OH)_2}}{\dot{n}_{HCl}} \quad 6.33$$

where $n_{Ca(OH)_2}$ is the number of moles of calcium hydroxide in the bed and \dot{n}_{HCl} is the molar flowrate of hydrogen chloride in the gas stream.

Figure 7 shows that the two samples of calcium hydroxide initially have a similar reactivity. However, for longer time periods, the reaction slows down and the two datasets become different, possibly due to the dissimilar structure of the product layer, resulting in different diffusion and work-related coefficients D_s and K , reported respectively in Figure 6.6 and in Table 6.5.

Table 6.5. Values of K at different temperatures for the two datasets.

Dataset	T (°C)	K (-)
Weinell et al. (1992)	100	$1.22 \cdot 10^{-2}$
	140	$4.30 \cdot 10^{-3}$
	200	$1.25 \cdot 10^{-3}$
	250	$5.54 \cdot 10^{-4}$
Yan et al. (2003)	170	$9.80 \cdot 10^{-3}$
	200	$5.55 \cdot 10^{-3}$
	230	$3.36 \cdot 10^{-3}$
	300	$1.28 \cdot 10^{-3}$

Table 6.6. Parameters of solid-state diffusivity and mechanical work-related coefficient K (eqs. 6.28 and 6.29) calculated from the data of Weinell et al. (1992) and Yan et al. (2003).

Parameter	Weinell et al. (1992)	Yan et al. (2003)
A_D [m ² /s]	$2.12 \cdot 10^{-9}$	$1.64 \cdot 10^{-6}$
$E_{a,D}$ [J/mol]	24.5	55.9
K_D [-]	$2.53 \cdot 10^{-7}$	$1.25 \cdot 10^{-6}$
$E_{a,K}$ [J/mol]	33.4	33.0

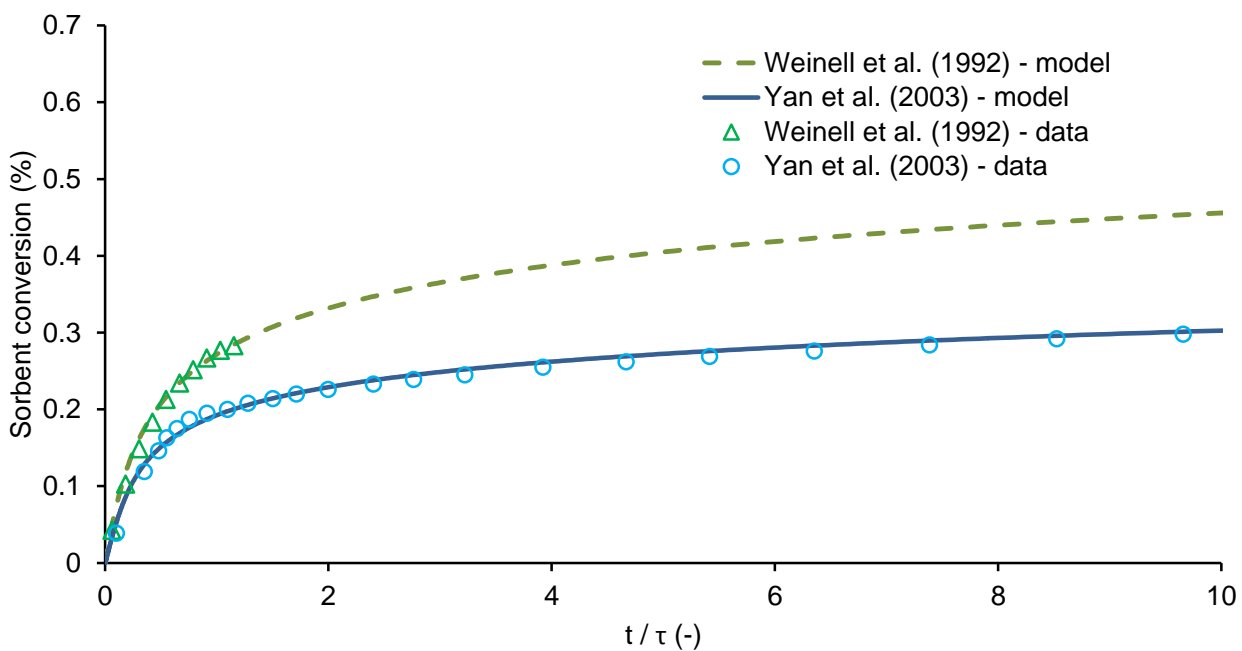


Figure 6.9. Plot of the sorbent conversion at $T = 200$ °C versus normalised time according to eq. 6.33. Points: experimental data; curves: present model.

In Figure 6.6 the values obtained for the diffusivity of HCl in the product layer are shown along with the values of D_s proposed in literature. The values of D_s obtained here cannot be directly compared to the literature values, since the effect of energy barrier to nucleation exerted by the product layer has been extracted from D_s through the definition of the reduction factor RF. Nonetheless, estimated solid layer diffusivities are still within the typical range of these reaction

systems. In addition, the activation energies calculated for the solid state diffusion process (Table 6.6) are comparable with the broad range of values estimated by previous authors (10-15 kJ/mol (Weinell et al., 1992); 19 kJ/mol (Fonseca et al., 1998); 36.5 kJ/mol (Duo et al., 1993); 40 kJ/mol (Mura and Lallai, 1994).

Furthermore, the difference in the values of D_s calculated in the present study for the two data sets considered is hardly surprising, even if the same modelling approach is adopted. Although for the sample of Yan et. al (2003) a higher BET surface was reported, the calculated diffusivity is almost one order of magnitude lower than that calculated for the data by Weinell et. al (1992). Actually SEM photographs of particles of calcium hydroxide after exposure to HCl show highly inhomogeneous solid textures and significant particle-to-particle variations (Koch et al., 2005). Hu et al. (2008), who performed direct sulfation experiments on limestone, observed oriented nucleation and growth of the solid product along fractures on the surface of sorbent particles. Duo et al. (2000) observed product crystals developing in “plate-like” structures in sulfation experiments, while Bausach et al. (2006) reported “needle-like” features. Due to the complexity of nucleation promoted by defect sites and due to the wide variation in morphology of the reactants, the crystalline structure of product layers might be highly sample-dependent. Hence, the cohesion and the diffusivity through product layers formed on different samples might differ. Nonetheless, the model developed proved to be suitable for the reproduction of experimental data from different datasets incorporating such conformational variations in the variation of D_s within a reasonable range of values, well in agreement with previous literature data and comprised between $10^{-12} \div 10^{-14}$ m²/s for temperatures between 150 and 250 °C.

With respect to the non-dimensional parameter K, the assumption of an Arrhenius-type behaviour allowed a satisfactory reproduction of experimental data. Almost identical values of the activation energy were found in the fitting of the two datasets, as shown in Table 6.6. This highlights that the variation of K with temperature is not a mere adjustable feature of the model, but is bound to physical considerations (i.e. mechanical properties and cohesion of the product layer, probably function of sample-dependent nucleation mode), although a further investigation of this issue falls out of the scope of the present study.

It is also interesting to verify the influence of the value assumed for the kinetic constant, k_s , on the overall reaction rate. An estimate of the influence of k_s in determining the value of the sorbent conversion is given by the ratio of the % variation of the conversion to that of k_s . The average solid conversion value at a quarter of the total experiment time ($\frac{1}{4} t_{fin}$) and at the end of the experiment (t_{fin}) were chosen for this calculation, as shown in Table 6.7.

Table 6.7. Results of the sensitivity analysis carried out for k_s values (experiments at $T = 200$ °C).

Dataset	k_s (m/s)	X_{sl} ($t = \frac{1}{4} t_{fin}$)	$\left \frac{\% \Delta X_{sl}}{\% \Delta k_s} \right $	X_s ($t = t_{fin}$)	$\left \frac{\% \Delta X_{sl}}{\% \Delta k_s} \right $
Weinell et al. (1992)	$1.0 \cdot 10^{-4}$	0.176	0.227	0.319	0.087
	$3.2 \cdot 10^{-4}$	0.209	-	0.339	-
	$5.0 \cdot 10^{-4}$	0.209	0.002	0.333	0.033
Yan et al. (2003)	$1.0 \cdot 10^{-4}$	0.257	0.069	0.319	0.056
	$3.2 \cdot 10^{-4}$	0.245	-	0.307	-
	$5.0 \cdot 10^{-4}$	0.235	0.076	0.297	0.056

The influence of k_s is generally low and decreases as reaction proceeds. Varying the values within the order of magnitude of 10^{-4} m/s does not significantly affect the conversion of the sorbent over

long reaction times, which are of interest in flue gas treatment systems. In fact, k_s exerts two opposite effects on solid conversion: a higher chemical reaction rate means faster conversion but also faster appearance of a thicker, reaction-inhibiting product layer. Therefore, with the exclusion of the very first instants, the reaction progress is mainly controlled by reactant diffusion in the product layer, in agreement with previous findings (Duo et al., 1993; Fonseca et al., 1998). This can be confirmed calculating a Thiele-like modulus (Stendardo et al., 2011) which evaluates the relative magnitude of the diffusion through the chloride layer and the reaction at the surface of Ca(OH)_2 grains:

$$\varphi = r_g \sqrt{\frac{k_s \cdot \rho_s \cdot S_{BET}}{D_s}} \quad 6.34$$

According to eq. 6.6 and to data reported in Table 6.3, the values of 5.0 and 8.3 can be calculated for φ for the experiments at 200 °C of Weinell et al. (1992) and Yan et al. (2003) respectively, thus confirming diffusive control.

6.7 Model validation against experimental data

Once tested against relevant literature data, the phenomenological model was validated against the data collected in the experimental campaign described in chapter 5. In the adopted experimental configuration (section 5.2), acid gas removal takes place in a fixed bed of porous particles of thickness L , through which the gaseous phase flows at a constant velocity u_0 , mixing axially according to a dispersion coefficient D_z . Thus, the governing one-dimensional mass balance differential equation with convection, axial diffusion and reaction through a porous medium can be applied:

$$\varepsilon \cdot \frac{\partial C}{\partial t} = -u_0 \cdot \frac{\partial C}{\partial z} + \varepsilon \cdot D_z \cdot \frac{\partial^2 C}{\partial z^2} - r_{vb} \quad 6.35$$

with the following initial and boundary conditions:

$$C(z, t = 0) = 0$$

$$C(z = 0, t) = C_0$$

$$\left. \frac{\partial C}{\partial z} \right|_{z=L} = 0$$

where C is the bulk concentration of reactant gas, ε is the interparticle void fraction of the packed bed, r_{vb} is the reaction rate for a unit volume of bed and C_0 is the concentration of the reactant gas at the entrance of the bed ($z = 0$).

The reaction term r_{vb} can be expressed through eq. (3), where k_o is an overall reaction rate constant (expressed in s^{-1}) and C_{eq} is the minimum theoretical concentration that would be reached at thermodynamic equilibrium:

$$r_{vb} = k_o \cdot (C - C_{eq}) \quad 6.36$$

The expression for k_o is derived following the steps of section 6.3 and 6.4, resulting in:

$$k_o = \sum_i [v_i \cdot RF_i \cdot \frac{3 \cdot (1 - \varepsilon) \cdot (1 - \omega_{in}) \cdot (1 - \varepsilon_p) \cdot r_{c,i}^2}{r_{g,i}^3} \cdot \frac{D_s \cdot k_s}{D_s + k_s \cdot r_{c,i} \cdot (1 - r_{c,i}/r_{t,i})}] \quad 6.37$$

Accordingly, the conversion of the sorbent is a weighted summation of the conversion of the grain classes i , which is a function of the shrinking of the unreacted grain core (equation 6.15).

The parameters required by the model, as well as their related values in the present application, are reported in Table 8.7. In addition, pore size distribution of the sorbent sample, shown in Figure 5.3 is used to determine the initial size of sorbent grains, following the method introduced by Heesink et al. (1993) as described in section 6.3. For the present case, the value of F was found to be 0.164. Computed grain radius for the 8 class subdivision of Figure 5.3 are reported in Table 6.8.

Table 6.8. Division of the pore size distribution in Figure S1 in pore classes and related grain sizes.

Pore class	Average class radius μm	Cumulative pore volume mm ³ /g	Class specific volume		r _{g,i}
-			mm ³ /g	%	m
1	2.239	16.1	16.1	3.6%	3.67E-07
2	1.413	44.4	28.3	6.3%	2.32E-07
3	0.891	188.3	143.9	32.2%	1.46E-07
4	0.562	368.3	180.0	40.2%	9.23E-08
5	0.355	444.4	76.1	17.0%	5.82E-08
6	0.224	446.1	1.7	0.4%	3.67E-08
7	0.141	447.2	1.1	0.2%	2.32E-08
8	0.089	447.2	0.0	0.0%	1.46E-08

In the light of the analyses on the reacted samples (section 5.5), the solid product was assumed to be CaOHCl and the parameters of the nucleation submodel were calculated accordingly. Three parameters (k_s , D_s and K) were determined by experimental data fitting. It is assumed that their variation with temperature follows an Arrhenius-type law: in particular, k_s and D_s increase exponentially with temperature, being chemical reaction and product layer diffusivity activated processes (Bhatia and Perlmutter, 1982), while K follows the log-linear decrease with temperature of the resistance to deformation of the product layer, as already detailed in section 6.5.

Model training. In order to determine the temperature dependence of the fitting parameters, the set of experiments performed at HCl inlet concentration of 2500 ppm and 100 mg of sorbent in the bed (runs 1-3 in Table 5.2) was used as training case.

The model fitting of HCl removal and Ca(OH)₂ conversion is shown in Figure 6.10. The adherence to experimental data is satisfactory and the model succeeds in reproducing the decline in reactivity over time. The associated values of k_s , D_s and K are listed in Table 6.9. Their trend with temperature is in line with the previous application of the model to literature data: values of D_s are within the range of relevant values reported in previous modelling studies of the chloridisation reaction in similar conditions (Figure 7), while the apparent activation energy for K , 38 kJ/mol, is comparable to the 33 kJ/mol found for the fitting of Weinell's and Yan's data in section 6.6.

Table 6.9. Temperature-dependent parameters for the model fitting of Figure 6.10.

Parameter	120 °C	150 °C	180 °C
k _s (m/s)	3.0 · 10 ⁻⁵	3.9 · 10 ⁻⁵	5.0 · 10 ⁻⁵
D _s (m ² /s)	0.38 · 10 ⁻¹³	1.87 · 10 ⁻¹³	7.51 · 10 ⁻¹³
K (-)	2.55 · 10 ⁻²	1.10 · 10 ⁻²	0.53 · 10 ⁻²

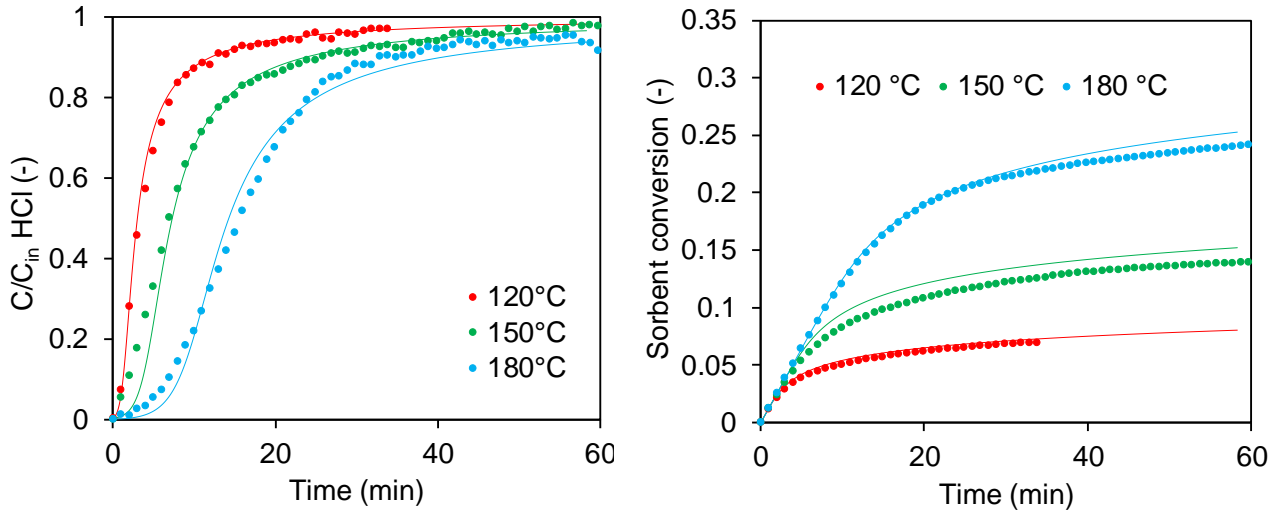


Figure 6.10. Training case. Model fitting of breakthrough curves of HCl removal (left) and corresponding Ca(OH)_2 conversion (right). Mass of sorbent: 100 mg, HCl inlet concentration: 2500 ppm. Model in continuous lines, experimental data (average of 3 runs) in dotted lines.

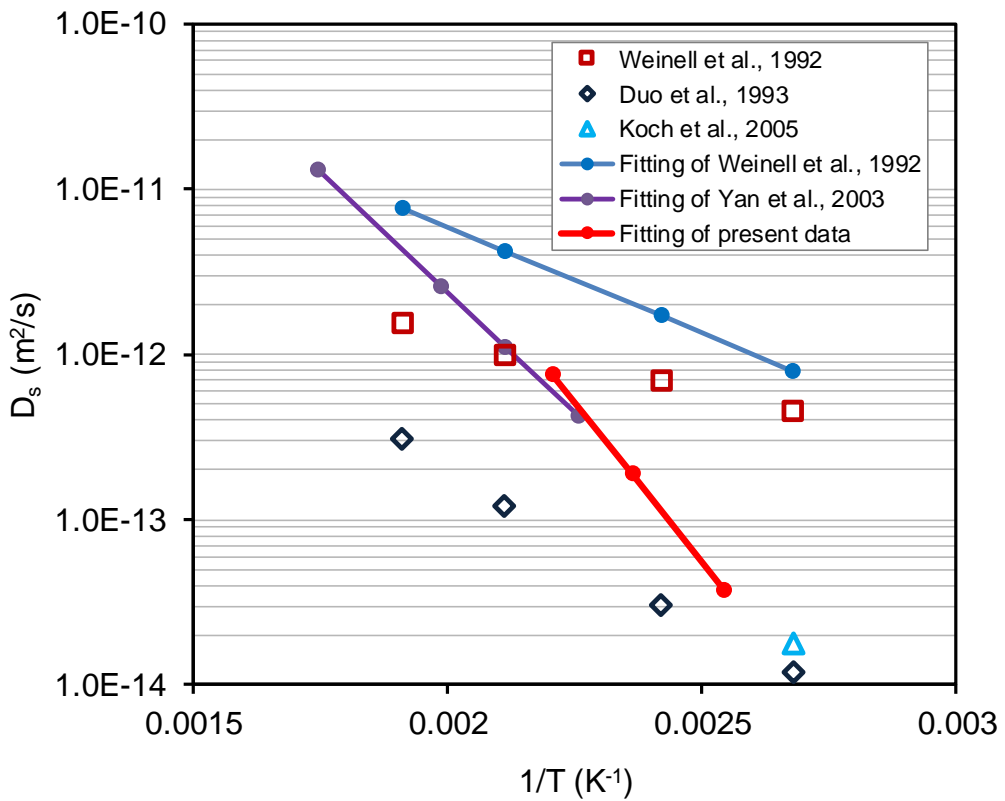


Figure 6.11. Product layer diffusivity for the reaction between Ca(OH)_2 and HCl estimated in different studies. Continuous lines are specifically related to the applications of the phenomenological model.

Model validation. In order to evaluate the capability of the model calibrated on the training case to predict the HCl removal behaviour in different conditions, the set of runs 4-6 and the set of runs 7-9 (see Table 5.2) were used as validation cases. The former presents half the mass of calcium hydroxide in the bed, while in the latter also the HCl inlet concentration is halved. In both cases the model shows a satisfactorily match with experimental data. In particular, for runs 7-9 the Ca-to-HCl ratio is equal to the training case, but breakthrough time is slightly anticipated, since reaction

kinetics is slower due to the halved inlet concentration of gaseous reactant, and the model calibrated on the training case is capable to reproduce this phenomenon. This result is significant since previous modelling studies devoted to the $\text{Ca}(\text{OH})_2/\text{HCl}$ system (Chisholm and Rochelle, 1999; Duo et al., 1993; Fonseca et al., 1998; Weinell et al., 1992) rarely explored the validity of model parameters over different concentrations of HCl and generally required the adoption of concentration-dependent coefficients (Duo et al., 2004).

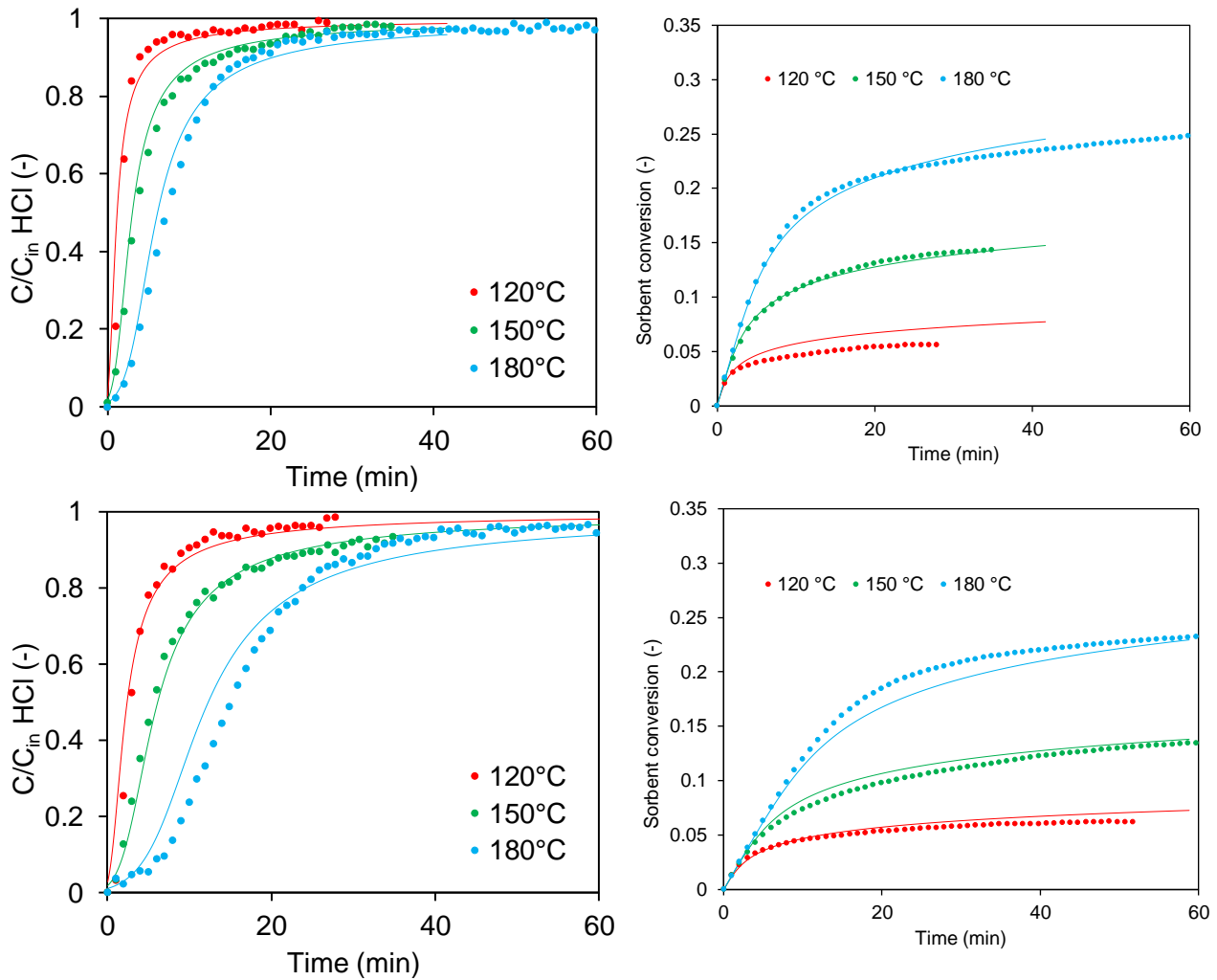


Figure 6.12. Validation cases. Breakthrough curves (left) and sorbent conversion (right) for the case with 2500 ppm HCl and 50 mg of calcium hydroxide (up) and the case with 1250 ppm HCl and 50 mg of calcium hydroxide (down).

7 Operational model for process optimisation of acid gas removal systems

7.1 Formulation of the operational model

The approach followed in chapter 6 derives a description of the acid gas removal process by modelling the mass transfer and kinetic phenomena governing the gas-solid reaction. This sort of “bottom-up” route allows to define a comprehensive, physically-based model for the process, but requires due consideration of all the parameters possibly influencing the reaction, a thorough experimental campaign and carefulness in adapting laboratory results to process conditions.

An alternative, operational approach consists in proposing a simplified description of the flue gas cleaning process, tailored on design data (mass flow rates, waste composition and plant components) of a specific WtE facility (Jannelli and Minutillo, 2007). This was the purpose of the operational “conversion model” formulated by Antonioni et al. (2012) for the process optimisation of acid gas control lines in WtE plants, successfully applied in the last years in joint collaboration with private plant operators and technology suppliers³.

The conversion of the acid gas i (i.e. HCl, SO₂ or HF) is defined as:

$$\chi_{i,j} = \frac{\dot{n}_{i,IN} - \dot{n}_{i,OUT}}{\dot{n}_{i,IN}} \quad 7.1$$

where $\dot{n}_{i,IN}$ and $\dot{n}_{i,OUT}$ are the molar flow rates of i respectively entering and exiting the stage where the sorbent j (i.e. calcium hydroxide or sodium bicarbonate) is injected.

The operational model is based on a simplified Langmuir-type correlation linking the acid gas conversion to the feed rate of the solid reactant:

$$\chi_{i,j} = \frac{rs_j^{n_{i,j}} - rs_j}{rs_j^{n_{i,j}} - 1} \quad 7.2$$

where $\chi_{i,j}$ is the removal efficiency expressed as the conversion of the acid pollutant i when reacting with j , rs_j is the ratio between the actual feed rate of solid reactant j and the stoichiometric rate of reactant j required for the total conversion of all the acid compounds present in the flue gas, and $n_{i,j}$ are fitting parameters to be determined for each neutralisation reaction. For a given value of rs_j , the higher is the value of $n_{i,j}$, the higher is the removal efficiency, as shown in Figure 7.1.

Thus, the conversion of each reaction is a function only of a single fitting parameter that will take into account all the physical phenomena and operating conditions actually involved in the heterogeneous reactions taking place in the reference stage (e.g. temperature, contact time, sorbent properties, etc.). Therefore, the model needs to be tuned with specific plant data in order to properly predict the process operating performance.

Besides the need of plant-specific tuning (which is discussed in section 7.2), the model is general and can be applied to the injection of different sorbents. However, while for sodium bicarbonate equation 7.2 is enough to correctly describe the acid gas removal process, the application to calcium hydroxide requires the due consideration of two additional aspects: the undesired reaction with CO₂

³ Formulation and first application of the operational model took place before the present PhD project and are reported in the doctoral thesis by Daniele Guglielmi (2014). Here, the operational model constitute the foundation for the comprehensive economic evaluation (chapter 7) and environmental assessment (chapter 8) of alternative acid gas removal systems, which are the original contributions in the present thesis.

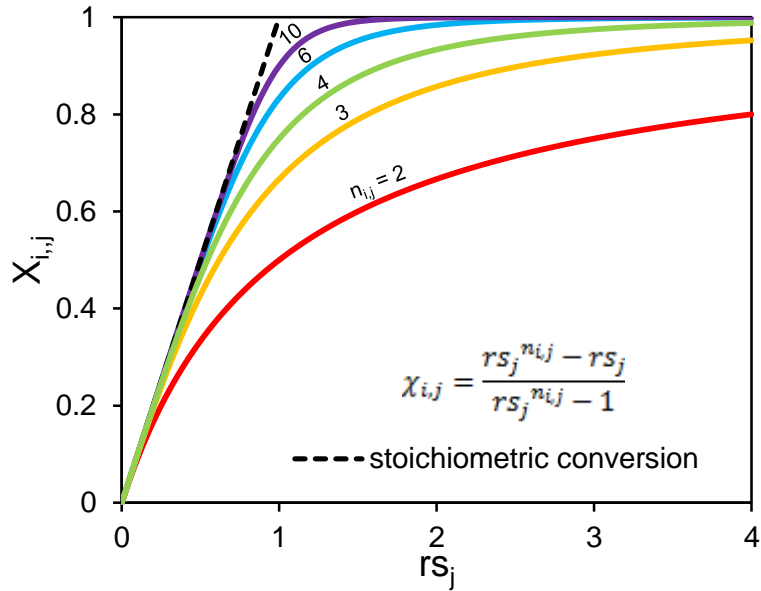


Figure 7.1. Acid gas conversion as a function of the rs_j ratio according to the operational model, for different values of the empirical parameter $n_{i,j}$.

in the flue gas (see section 2.2) and the already discussed incomplete conversion issue (see section 6.2). The carbonation reaction has to be taken into account because CO_2 concentration is orders of magnitude higher than the concentration of the other acid gases produced during waste combustion. Therefore, even if the reaction with Ca(OH)_2 does not affect significantly the carbon dioxide concentration, it consumes a considerable amount of calcium hydroxide, which is then not directly available for the neutralisation of acid gases. The conversion of CO_2 was assumed to be proportional to the feed rate of sorbent: indeed, the injected Ca(OH)_2 is much lower than the stoichiometric amount theoretically needed to adsorb all the CO_2 in the flue gas, thus (with respect to CO_2) the model function of eq. 7.2 is on the very left part of the plot in Figure 7.1, where conversion and sorbent feed rate are proportional. Hence, in the model the CO_2 conversion can be calculated by a pseudo-first order relationship:

$$\chi_{\text{CO}_2} = k \cdot \frac{\dot{m}_{\text{Ca(OH)}_2}}{\dot{m}_{\text{Ca(OH)}_2, \text{design}}} \quad 7.3$$

where $\dot{m}_{\text{Ca(OH)}_2, \text{design}}$ is the design value of the mass flow rate of lime in the analysed WtE plant and $\dot{m}_{\text{Ca(OH)}_2}$ the actual mass flow rate entering the system. The proportionality factor k is determined from design data.

The other adjustment to the model for Ca(OH)_2 is required to take into account the limitation to the maximum sorbent conversion. To include this phenomenon, rs_j is replaced in eq. 7.2 by an effective rs_j^* :

$$rs_j^* = rs_j \cdot \chi_{j,\max} \quad 7.4$$

With this correction, when the solid reactant is in defect (i.e. for $rs_j < 1$), the maximum acid gas conversion expressed by eq. 7.2 is limited to the corresponding sorbent conversion. As broadly discussed in section 6.2, $\chi_{j,\max}$ strongly depends on process conditions (e.g. relative humidity, temperature, acid gas concentrations, initial void fraction of the Ca(OH)_2 particles). In the empirical framework of the operational model, the actual value of $\chi_{j,\max}$ is set on the basis of site-specific considerations.

7.2 Calibration of the model with operational data from Waste-to-Energy plants

The empirical nature of the operational model requires tailored calibration. Two approaches can be followed in order to obtain plant-specific data for model tuning: fitting of historical operational data or planning of dedicated test runs.

Historical operational data. This approach takes advantage of data already available at plant. WtE plants generally archive hourly averages of operational data which are relevant for model calibration: total volumetric flow rate, temperature, pressure, humidity, concentration of macropollutants like the acid gases, flow rate of solid reactants for DSI (calcium hydroxide and sodium bicarbonate). The parameters $n_{i,j}$ can be determined from the calculated hourly averaged values of $X_{i,j}$ and rs_j through non-linear regression techniques.

Test runs. Test runs have the objective to systematically monitor the response of the flue gas treatment system for different, given input conditions. The advantage over the use of already available historical data is the possibility to explore a broader range of operating conditions. Indeed, even if the variability of the burnt waste generates a rather variable flue gas composition at the inlet of multi-stage acid gas removal system, the automated control tends to favour a balanced operation of stages. In contrast, dedicated test run for a multi-stage treatment system can force situations in which acid gas abatement is maximised in one stage and the other one has to fulfil very low conversion requirements: although these extreme configurations are usually far from the operational optimum of the system, their observation allows to obtain calibration data over a wide range of $X_{i,j}$ and rs_j . Therefore, the resulting model tuning is more accurate and, when applied to process optimisation, it is ensured that it won't work in extrapolation mode.

An example of test run procedure can be outlined with reference to the process monitoring scheme shown in Figure 7.2. Other than the measurement of acid gas concentration at stack, WtE plants operating a two-stage treatment system (see section 7.3 for process description) generally collect intermediate measurements before the injection of the first reactant, $\text{Ca}(\text{OH})_2$, and of the second reactant, NaHCO_3 (respectively, SMP1 and SMP2 points in the figure). Therefore, a test run for the 1st reaction stage can be simply devised as follows: the flow rate of $\text{Ca}(\text{OH})_2$ is changed stepwise at regular intervals (e.g. 1 h) and the corresponding acid gas removal efficiency is calculated on the basis of the concentration of pollutants at SMP1 and SMP2. In contrast, in the 2nd reaction stage the outlet concentration of acid gases has to remain fixed (being the actual value emitted at stack). Consequently, the test run can be conducted by inducing a stepwise variation in the concentration of inlet acid gases at SMP2 (as a consequence of a stepwise variation of $\text{Ca}(\text{OH})_2$ flow rate in the 1st stage) and measuring the varying flow rate of NaHCO_3 commanded by the automated control system in order to ensure a constant emission value at stack. Clearly enough, the broad variability of process conditions due to temporal variations in waste composition and, thus, in the acid gas concentration entering the treatment system (point SMP1) requires redundancy in test runs.

Being covered by nondisclosure agreements with WtE operators and technology suppliers participating to the present research, test run results and related data treatment are not reported here. Table 7.1 summarises the model parameters obtained for a reference plant and applied in the following applications of the model (both chapters 7 and 8).

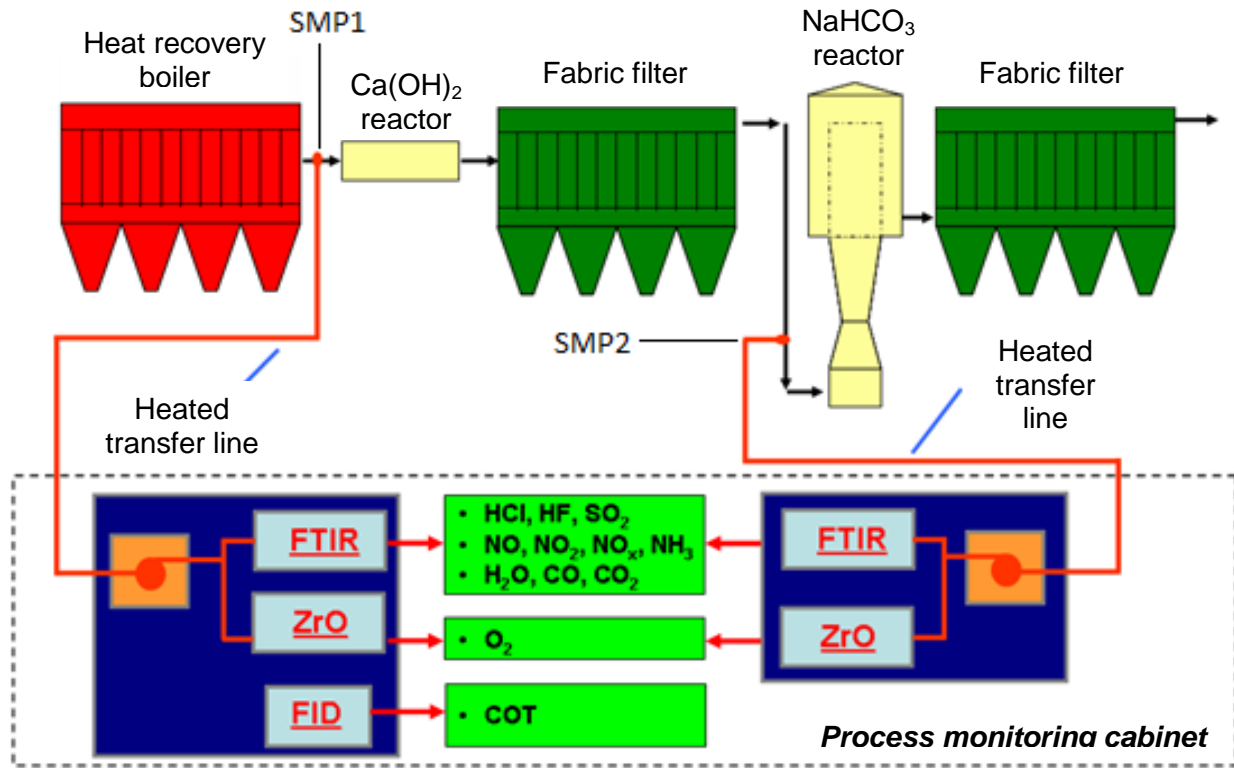


Figure 7.2. Process monitoring scheme in a typical two-stage acid gas removal system (see section 2.4 and section 7.3 for process description).

Table 7.1. Relations and empirical parameters used in the operational model to express the acid gas conversion X as a function of the actual-to-stoichiometric ratio of the sorbent rs .

Correlation for the conversion of the acid gas i by means of solid reactant j	$X_{i,j} = \frac{rs_j^{n_{i,j}} - rs_j}{rs_j^{n_{i,j}} - 1}$		
Parameters of the model $n_{i,j}$		Ca(OH) ₂	NaHCO ₃
	HCl	2.29	11.6
	SO ₂	1.27	12.3
Competitive effect due to carbonation	$X_{CO_2} = 0.004 \cdot \frac{\dot{m}_{Ca(OH)_2}}{\dot{m}_{Ca(OH)_2,design}}$		
Correction to take into account the maximum conversion of solid reactant	$rs_j^* = rs_j \cdot X_{j,max}$		

7.3 Case study: optimisation and benchmarking of a two-stage treatment system

The overview of the state-of-the-art in acid gas control outlined in chapter 2 showed that treatment methods based on dry sorbent injection have been increasingly applied in WtE plants worldwide in the last 20 years. In particular, since their introduction in the mid-1990s, dry treatment systems based on sodium bicarbonate (NaHCO_3) injection have demonstrated cost-effectiveness and ease of operation and maintenance (Quicker et al., 2014). About 29% of municipal solid waste incinerators (MSWI) built in Europe after 2000 adopt NaHCO_3 injection. In France and Italy sodium-based dry treatment systems are implemented respectively in 33% and 59% of the WtE plants that started operation after 2005 (ISWA, 2012).

Recently, as described in section 2.4, the need to combine the compliance to increasingly lower emission limit values with cost optimisation requirements has led to the development of novel solutions. In particular, dry treatment systems based on double reaction and filtration stages are an emerging technology, which has been adopted by several WtE plants in Northern Italy since 2006 (ISPRA, 2013). These two-stage systems carry out the removal of acid pollutants by two consecutive steps of neutralisation with alkali compounds (usually, calcium hydroxide in the 1st stage and sodium bicarbonate in the 2nd stage) and subsequent filtration for the capture of the solid residues produced by the reaction. However, in spite of their growing industrial importance, the experience with two-stage technologies is mostly empirical (De Greef et al., 2013) and scarce data are reported on the optimal performance of this process. In particular, the optimal integration of first and second stage to maximise efficiency and removal of acid gases still needs to be explored (Acquistapace et al., 2014), since the operational optimum depends on the concentration of acid pollutants in the flue gas and ultimately on the waste composition. The empirical model developed by Antonioni et al. (2014), which needs to be calibrated on actual plant data, as described in section 7.1 and 7.2, constitutes a first attempt to describe the acid gas removal efficiency of a two-stage system and to identify the configuration operating at the optimal economic performance, taking into account the costs for reactants and disposal of solid residues.

Aim of the case study presented here is to show the application of the operational model in a methodology for the economic assessment of a two-stage (2S) dry acid gas removal system. Goal of the analysis is to assess the cost-effectiveness of a 2S system in comparison to single stage (1S) alternative processes. Three alternative 1S configurations (with electrostatic precipitator as pre-dusting equipment, with fabric filter as pre-dusting equipment, without pre-dusting equipment) all based on the injection of NaHCO_3 , applied in several operating MSWI systems, were selected as benchmark technologies. The Na-based single stage dry alternatives may be considered as the most effective technologies currently adopted for acid gas removal in coupling emission standards compliance with low capital and operational costs (BREF WI, 2006).

Figure 7.3 shows the reference schemes defined to carry out the comparison among the two stage (2S) technology and the selected benchmark single stage technologies. The reference scheme of the 2S system shown in Figure 7.3a can be considered representative of a typical 2S dry treatment system, and is based on the design of an actual plant located in Italy, described in detail elsewhere (Antonioni et al., 2014). The untreated flue gas flows in a reactor (actually, a ductwork designed in order to assure a given residence time), where the injection of a dry powder of calcium hydroxide (Ca(OH)_2 , commercially known as hydrated lime or slaked lime) takes place. This alkaline material acts as a sorbent towards the acid pollutants, triggering the gas-solid reactions R1 to R3 reported in Table 7.2. The flue gas is then fed to a fabric filter, where the reactions continue on the filter cake of ash and powders deposited on the bags. Here, the solid products of the reactions (calcium-based

wastes, CBW) are captured and removed from the flue gas stream. Part of the solids collected by the filter can be recycled to the reactor feed, since they generally contain unreacted lime. Eventually, CBW and ash are stored in a silo and sent to appropriate disposal sites. The second stage of the process consists of another reactor (a vertical Venturi-shaped pipe section) followed by a fabric filter, and its goal is to complete the removal of acid gases by the injection of sodium bicarbonate (NaHCO_3). Non-porous bicarbonate decomposes to porous carbonate with an almost instantaneous and complete process (see reaction R4 in Table 7.2) at temperatures above 130 °C (Brivio, 2007). Then, sodium carbonate reacts with the acid gases (reactions R5–R6 in Table 7.2). No solid recirculation is carried out, since sodium bicarbonate is much more efficient than slaked lime and very few unreacted particles can be found in the sodium-based wastes (SBW) collected by the fabric filter (Bodénan and Deniard, 2003). As already mentioned in section 2.3, the collected SBW can be sent to a processing plant in order to recover a purified brine suitable as raw material in the sodium carbonate production process (Brivio, 2005; ISWA, 2008), thus reducing the mass of residues to landfill.

Table 7.2. Chemical reactions involved in acid gas removal process.

1st stage: calcium hydroxide	2nd stage: sodium bicarbonate	
$\text{Ca(OH)}_2 + 2 \text{HCl} \rightarrow \text{CaCl}_2 + 2 \text{H}_2\text{O}$	R1	$2 \text{NaHCO}_3 \rightarrow \text{Na}_2\text{CO}_3 + \text{CO}_2 + \text{H}_2\text{O}$
$\text{Ca(OH)}_2 + \text{SO}_2 + 1/2 \text{O}_2 \rightarrow \text{CaSO}_4 + \text{H}_2\text{O}$	R2	$\text{Na}_2\text{CO}_3 + 2 \text{HCl} \rightarrow 2 \text{NaCl} + \text{CO}_2 + \text{H}_2\text{O}$
$\text{Ca(OH)}_2 + \text{CO}_2 \rightarrow \text{CaCO}_3 + \text{H}_2\text{O}$	R3	$\text{Na}_2\text{CO}_3 + \text{SO}_2 + 1/2 \text{O}_2 \rightarrow \text{Na}_2\text{SO}_4 + \text{CO}_2$

With respect to benchmark technologies, the reference scheme of single stage treatment without pre-dusting (1S) consists in the injection of sodium bicarbonate through a Venturi-shaped reactor, followed by a fabric filter (Figure 7.3b). Reactions R4-6 take place in the system and the process scheme itself is actually the same as the 2nd stage of the reference 2S system. Although listed among the BAT for acid gas abatement (BREF WI, 2006), the 1S scheme has the drawback of not segregating SBW from fly ash. This prevents the possibility of recycling the SBW to produce sodium carbonate as described for the 2nd stage of the 2S system. Therefore, the 1S system is often integrated with a de-dusting stage prior to the injection of bicarbonate (pre-dusting, Figure 7.3c). The pre-dusting device can be either an electrostatic precipitator (ESP-1S) or a fabric filter (FF-1S). 1S, ESP-1S and FF-1S configurations share the same approach to acid gas removal (reactions R4-6) and differ only in the investment and operating costs related to the pre-dusting equipment and in the consequent fate of the SBW.

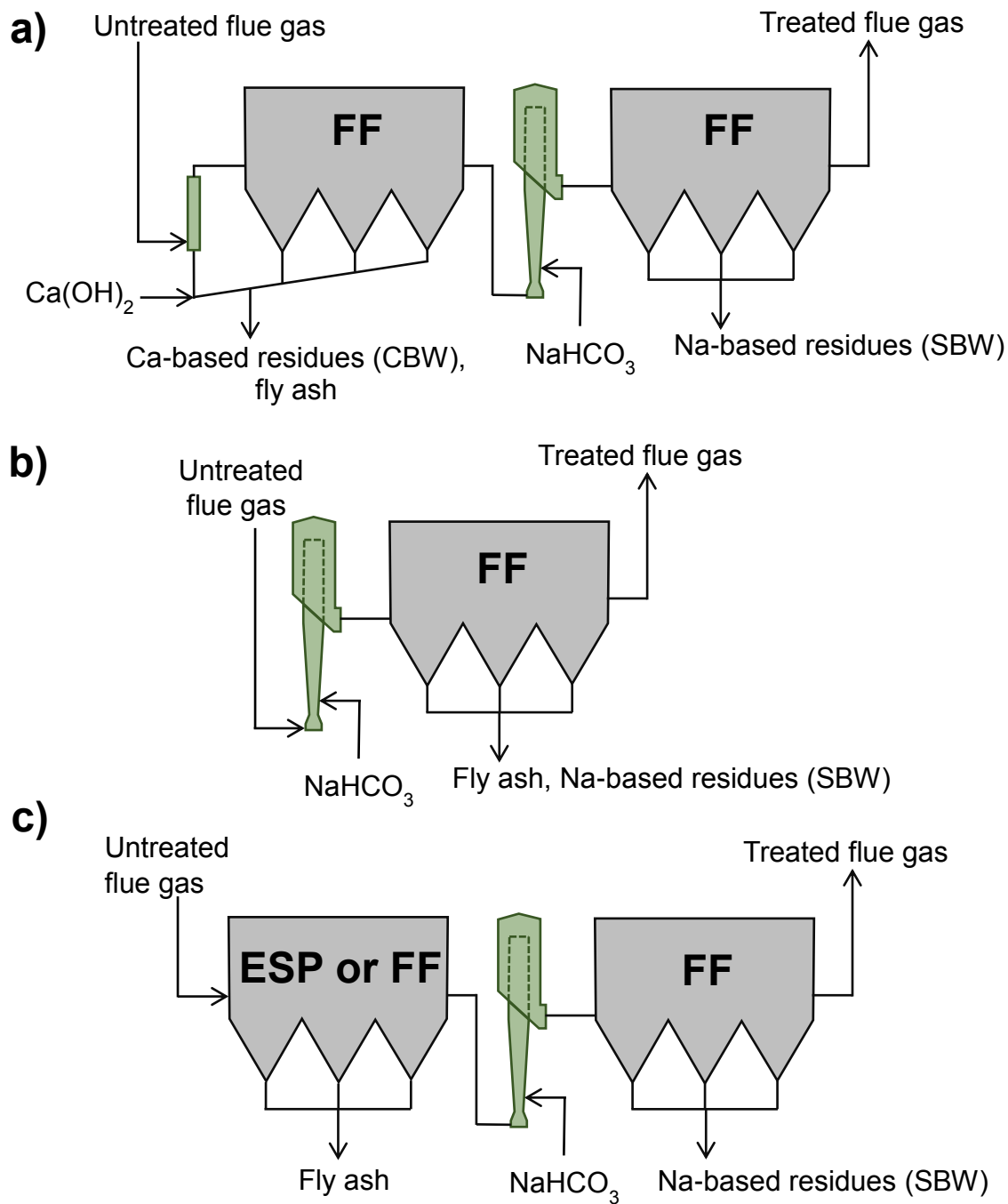


Figure 7.3. Alternative acid gas removal systems: a) two-stage (2S), b) single stage without pre-dusting (1S), c) single stage with pre-dusting device: electrostatic precipitator (ESP-1S) or fabric filter (FF-1S).

7.4 Methodology

Figure 9.3 summarises the methodology followed for carrying out the comparison of the total cost of operation of alternative dry technologies for acid gas removal from flue gas, given as input data the elemental composition of the waste feed and the required emission limits for HCl and SO_2 . The methodology is summarised in Figure 1. The composition of the flue gas leaving the combustion system, if not available from operational data, is calculated from the waste composition through a simplified mass balance approach. Given the concentration of the acid components in the flue gas and the required removal performance, the operational model of Antonioni et al. (2014) allows quantifying the associated consumption of solid reactants and the generation of solid residues that

need to be disposed. Eventually, the costs related to reactant purchase and solid residue disposal are summed to the annualised cost of equipment and to other ancillary costs (utilities, replacement parts, maintenance) to determine the total operating cost per annum of the treatment system.

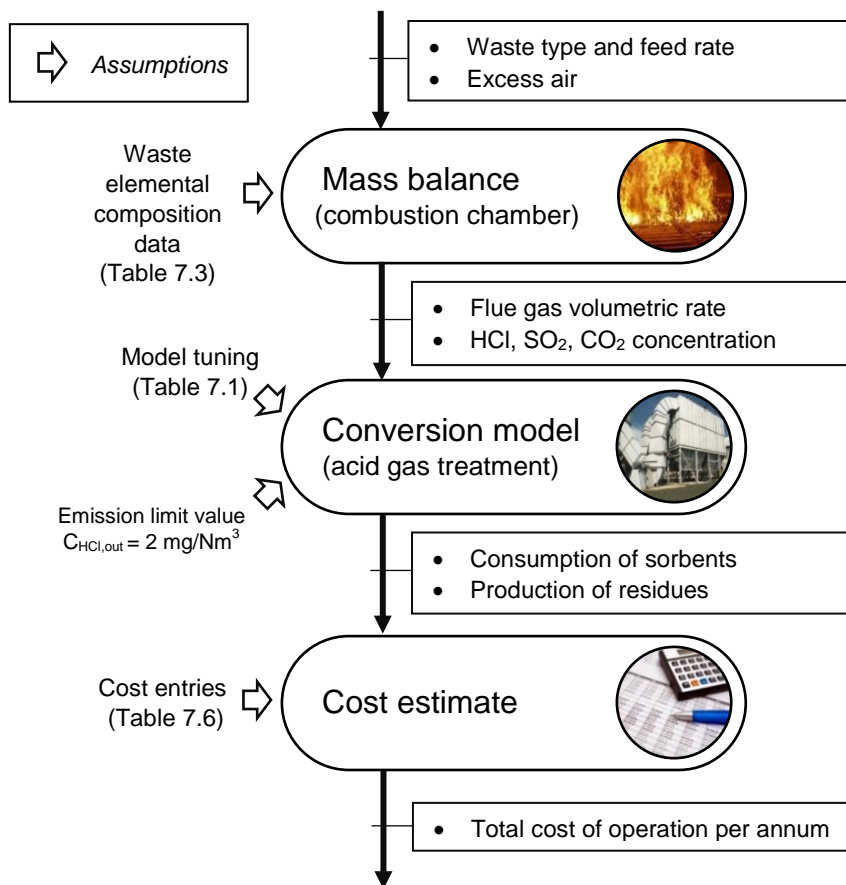


Figure 7.4. Flow chart of the modelling approach developed.

The key point of the methodology is the application of the acid gas conversion model presented in section 7.1 and tuned on actual operational data, which links the removal efficiency of the system to the actual ratio of reactant feed to acid pollutants load in the flue gas. This approach allows avoiding the use of fixed generic values of reactant feed rate per mass unit of waste, which are usually introduced in life cycle studies of air pollution control lines (Scipioni et al., 2009, Damgaard et al., 2010). Thus, the selectivity of the different solid reactants towards HCl and SO₂ is correctly taken into account.

7.5 Benchmarking data

In order to allow the benchmarking of the alternative technologies, some assumptions were introduced, and input data based on operating experience of actual facilities were defined. The same process specifications were applied to all the four alternatives considered. A medium-sized line was considered, treating an off-gas flow rate of 110,000 Nm³/h. The plant was assumed to operate 8000 h/year. The required flue gas cleaning performance was set imposing an outlet HCl concentration of 2 mg/Nm³, 5 times below the emission limit value set by Directive 2010/75/EU. This conservative choice is adopted by several plant operators, in order to guarantee a safety margin for HCl, which is the most critical pollutant in the MSWI context, and to assure at the same time that the emission concentrations of the other less abundant acid gases (SO₂, HF) under typical process conditions are as well below their emission limits.

Table 7.3. Waste composition scenarios.

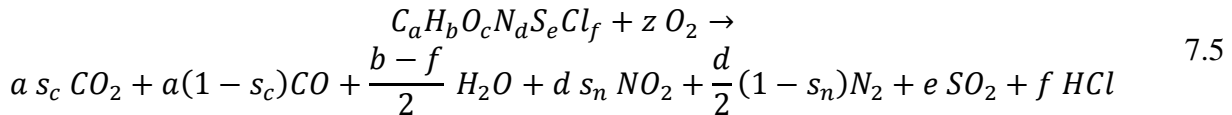
Scenario	Waste components (wt%)								S + Cl (%wt)	Cl/S ratio
	C	H	O	N	S	Cl	Moisture	Ash		
W_A	26	4	14	0.5	0.05	0.3	35	20.15	0.35	6
W_B					0.05	0.8		19.65	0.85	16
W_C					0.1	1.6		19.6	1.7	16

The concentrations of acid pollutants in the raw flue gas entering the treatment system were linked to the chemical composition of the waste fed to the furnace of the WtE plant. Clearly, the heterogeneous nature of waste makes the elemental composition of the fuel rather variable both geographically and temporally, thus influencing the emission of fuel-related pollutants as the acid gases addressed in the present study. The average composition of the municipal solid waste fed to a MSWI in Piacenza (LEAP, 2009), a town in Northern Italy, was used as a reference input data for the elemental waste composition: 35% of moisture, 20% of unburning matter (fly and bottom ash) and 45% of combustible fraction (26% C, 4% O, 14% H, 0.5% N and the remaining part made up of S and Cl). With the aim of investigating a meaningful range for the composition of acid gases generated during combustion, three different waste composition scenarios were derived from these data by slightly varying the Cl and S content and adjusting the mass fraction of inert material (ash) accordingly (see Table 7.3). The scenarios labelled W_A and W_B refer to typical municipal solid wastes, roughly corresponding respectively to the lower and upper limit of the mass fraction of Cl in urban waste, according to literature data (see Table 7.4). Scenario W_B generates HCl and SO₂ concentrations in the flue gas consistent with the operational data of the 2S reference plant on which the operational model was tuned (Antonioni et al., 2014), therefore it constitutes a case of particular importance. Finally, scenario W_C, presenting twice the Cl and S content of scenario W_B, represents a feed with a higher presence of chlorine typical of co-combustion of MSW with high fractions of industrial (Viganò et al., 2010) or biomedical wastes (Barba et al., 2015). Indeed, in order to compensate for the lack of household-generated waste or to increase the heating value of the waste feed (Petersen et al., 2005), MSW is increasingly burnt in association with wastes from commercial or industrial activities, which generally exhibit higher mass fractions of Cl and S (Biganzoli et al., 2015). Scenario W_C accounts for this significant trend, presenting a conservative upper limit for the expected Cl and S content. It should be remarked that the combustion of industrial waste “as is” falls out of the scope of the present study, since it is usually carried out in dedicated facilities that apply specific flue gas treatment strategies different from those applied in MSWI (Block et al., 2015).

Table 7.4. Chlorine content in wastes according to literature references (MSW: municipal solid waste).

Cl in waste (wt%)	Waste type	Source
0.2-0.8	MSW	Rigo et al., 1995
0.2-0.8	MSW	Randall and Shoraka-Blair, 1994
0.32-0.78	MSW	Wang et al., 2003
0.58	MSW	Themelis, 2005
0.36	MSW	Manders, 2009
0.87	Refuse-derived fuel from MSW	Patel et al., 2012
0.55-0.83	Refuse-derived fuel from plastics	Mapelli, 2014
1.1-2.1	Biomedical waste	Randall and Shoraka-Blair, 1994
2.0	Biomedical waste	Barba et al., 2015

On the basis of the assumed composition of the solid waste feed, the composition of the resulting flue gas was estimated from a mass balance approach, considering the combustion reaction of the combustible part of the waste, represented as the pseudo-component $C_aH_bO_cN_dS_eCl_f$, where the stoichiometric coefficients were calculated on the basis of waste composition data (Table 7.3). Thus, the combustion reaction can be written as follows:



The combustion of elemental carbon was assumed to give both CO_2 and CO, with the distribution between the two determined by the combustion completion grade s_c . Nitrogen contained in the waste is converted to diatomic gaseous nitrogen, with the exception of a fraction s_n converted to nitrogen oxides (reported to NO_2). The parameters s_c and s_n were set at 0.9995 and 0.0001, respectively. These values were chosen in order to obtain a concentration of CO and NO_2 in the untreated flue gas compatible with the actual data of the 2S reference plant (Antonioni et al., 2014), well within the typical range indicated by the BAT reference document for waste incineration (BREF WI, 2006). Actually, CO and NO_2 are not among the pollutants addressed in this analysis and their estimate is only intended to replicate a likely composition of a typical flue gas. For further reference, operational estimates of CO and NO_x generation in waste combustion processes are reported, for instance, by Yang et al. (2005) and Liuzzo et al. (2007).

The chlorine and sulphur contents in the waste, listed in Table 7.3, were assumed to be entirely converted to HCl and SO_2 . As a matter of fact, part of the Cl and S in the waste (e.g. inorganic chlorine from NaCl) does not burn and remains in the bottom ash, but it is already accounted for in the “ash” entry of Table 7.3.

Under the above assumptions, the moles of oxygen needed for the theoretical combustion of the waste can be calculated according to eq. 7.6.

$$z = a \left(\frac{s_c}{2} + \frac{1}{2} \right) + \frac{b - f}{4} + d s_n + e - \frac{c}{2} \quad 7.6$$

Typical excess air requirements with reference to solid waste fuels in moving grate furnaces are 80-100% of the stoichiometric demand (Petchers, 2003; Niessen, 2010). An 80% excess air was assumed. The moisture content of air was estimated with reference to mean temperature and relative humidity in Northern Italy ($T = 15^\circ C$, RH = 70%). Consequently, water content in the flue gas is the sum of waste moisture, moisture content of the air and water generated by reaction 7.5.

Concentrations of HCl and SO_2 in the flue gas generated by the combustion of the waste are listed in Table 7.5. Cases FG_A, FG_B and FG_C are those obtained directly considering the waste composition reported in Table 7.3 and will be used as base reference cases in the following.

Table 7.5. Concentration (mg/Nm³) of pollutants in untreated flue gas considered for the three waste composition scenarios and different Cl/S ratios. Cases FG_A, FG_B and FG_C are those corresponding to waste composition in Table 7.3. To generate the other cases, only the Cl/S ratio was changed as indicated in the table.

Cases	S and Cl content in input waste		Concentrations in untreated flue gas (mg/Nm ³) ^a	
	Cl + S (%wt)	Cl/S ratio	SO ₂	HCl
FG_A	0.35	6	170	525
FG_A.1		1	600	300
FG_A.2		2	400	405
FG_A.16		16	70	580
FG_A.40		40	25	600
FG_B	0.85	16	170	1400
FG_B.1		1	1440	740
FG_B.2		2	960	990
FG_B.6		6	410	1275
FG_B.40		40	70	1455
FG_C	1.7	16	340	2800
FG_C.1		1	2870	1475
FG_C.2		2	1915	1975
FG_C.6		6	825	2545
FG_C.40		40	140	2905

^a dry gas, 11 vol% O₂

Beside the reference cases used for benchmarking (based on waste composition in Table 7.3 and flue gas compositions FG_A, FG_B and FG_C in Table 7.5), a more extended set of flue gas composition cases was defined and is included in Table 7.5. The set was obtained considering the waste composition in Table 7.3, keeping constant the combined mass fraction of Cl and S with respect to that in Table 7.3, but varying the Cl/S ratio in the waste. The more extended set of flue-gas compositions thus defined in Table 7.5 is intended to explore a wider range of S and Cl content in waste, resulting in combinations of SO₂ and HCl raw flue gas concentration covering the operational experience of European MSWI (Rylander, 1997) and will be used to investigate in detail the influence of Cl/S on the flue gas treatment performance (see section 7.8).

7.6 Cost estimate

The costs related to the operation of the acid gas removal systems were assessed on the basis of the feed rate of reactants and the production of solid residues from the mass balance at each reaction stage, calculated according to the conversion model. The cost structure was assumed as the sum of the following terms:

- *Equipment costs* (or *capital costs*), related to the purchase and installation of required process equipment;
- *Reactant costs*, i.e. the purchase cost of calcium hydroxide and sodium bicarbonate required for process operation;
- *Disposal costs*, i.e. the costs connected with the landfilling (for CBW and SBW mixed with fly ash) or recycling (for SBW without fly ash) of the solid residues;
- *Other operating and maintenance (O&M) costs*, i.e. energy requirements, replacement parts, maintenance labour.

The values assumed for all the considered cost entries are summarised in Table 7.6, where the TIC entry stands for the total installed cost of the related equipment. In order to determine the capital costs, an inventory of the equipment items in the alternative acid gas removal systems was compiled. The overall investment cost ranges from 2.5 M€ for the 1S system to 4.7 M€ for the 2S system. These figures are in line with the estimates of Achternbosch and Richers (2002) and of Quicker et al. (2014) for similar air pollution control lines. Capital costs were translated in equivalent annual costs (EAC, annualised cost of equipment), considering a discount rate of 5 % and a service time of 20 years (EPA, 2002). The average values reported in Table 7.6 for operating costs were obtained from the analysis of commercial, technical and literature. Details on the estimate of capital and operating costs are reported hereafter.

Table 7.6. Cost values assumed for the cost assessment phase.

Cost entry		Value	Unit
TIC	Fabric filter	2,405,000	€
	ESP	2,040,000	€
Reactant cost	Calcium hydroxide	80	€/t
	Sodium bicarbonate	240	€/t
Cost for residue management	Disposal	200	€/t
	Brine recovery	200	€/t
Electricity		0.07	€/kWh
Compressed air		0.01	€/m ³
Replacement bags for fabric filter		Initial purchase cost: 360,000 € ^a	
Maintenance	Fabric filter	1 % of equipment cost + labour cost (20 €/h)	
	ESP	1 % of equipment cost + labour cost (20 €/h)	

^a Annualised bag cost calculated as in eq. 7.8, assuming $n = 2$ years, $i = 0.05$

Capital costs. An inventory of the equipment items in the alternative acid gas removal systems considered is presented in Table 7.7. Since the scope of the study is a comparative analysis of the four alternatives, the capital costs associated with the flue gas pipes and the fan were neglected, since such elements are common to all the benchmarking alternatives selected.

The filtration devices are the more costly equipment items. The reference baghouse considered in all the alternatives is designed to treat 110,000 Nm³/h of flue gas. Its PTFE-made bags cover a total cloth area of 3460 m², while the apparatus is made in stainless steel and thermally insulated. The basic equipment cost of a fabric filter is a function of the cloth area and it was estimated from the average between values taken from the online database *Matches' Process Equipment Cost Estimates* (Matche, 2015) and Peters and Timmerhaus (2002). The stainless steel add-on and the insulation costs were taken as 2/3 and 1/3 of the basic equipment cost respectively, according to EPA (2002). The cost for the PTFE-made bags was estimated from EPA (2002), as well.

The sum of the aforementioned costs represents the fabricated equipment cost (FEC) of the baghouse. The purchased equipment cost (PEC) is higher than the FEC because of instruments and controls, sales tax and freight. These charges can amount to 18 % of the PEC (Cooper and Alley, 1994). In addition, the installation costs (both direct and indirect) are approximately equal to the PEC: for fabric filtration systems, it is reported that the total installed cost (TIC) equals 2.17 times the PEC (Cooper and Alley, 1994).

For the reference electrostatic precipitator (ESP), assuming a design efficiency of 99% and a drift velocity of 12 m/s, a collection plate area of the equipment equal to 1150 m² was estimated by

following the simplified procedure described by EPA (2002). The basic equipment cost as a function of the collection area was estimated by following three methods (Vatavuk, 1990; EPA, 2002; Peters and Timmerhaus, 2002). Figures calculated according to the three sources differ only for the 8% and an average value was chosen. The stainless steel add-on cost was estimated as 30% of the basic equipment cost (EPA, 2002). PEC was set to 1.18 FEC and TIC to 2.22 PEC (Cooper and Alley, 1994).

Table 7.7. Equipment inventory for the considered treatment systems.

System	Elements	
Single stage without pre-dusting (1S)	Silo with hopper bottom for reactant storage (volume: 84 m ³) Silo with hopper bottom for residue storage (volume: 90 m ³) 2 x ball mill device for bicarbonate grinding 4 x feeder device (auger) for silos 2 x pneumatic conveyor (air flow rate: 2136 m ³ /h, min speed: 17 m/s) 2 x blower (operating and reserve) Vertical Venturi-shaped reactor Baghouse with PTFE-made bags, stainless steel apparatus and thermal insulation (total cloth area: 3460 m ²) Drag conveyor + dense phase pneumatic conveyor for the collection of baghouse residues	
Single stage with ESP as pre-dusting equipment (ESP-1S)	Electrostatic precipitator (collection plate area: 1150 m ²) Drag conveyor + dense phase pneumatic conveyor for the collection of ESP residues <i>1S equipment inventory</i>	
Single stage with baghouse as pre-dusting equipment (FF-1S)	Baghouse with PTFE-made bags, stainless steel apparatus and thermal insulation (total cloth area: 3460 m ²) Drag conveyor + dense phase pneumatic conveyor for the collection of baghouse residues <i>1S equipment inventory</i>	
Two-stage system (2S)	1 st stage	Silo with hopper bottom for fresh lime (volume: 84 m ³) Silo with hopper bottom for residues to recirculation (volume: 10 m ³) Silo with hopper bottom for residues to disposal (volume: 90 m ³) 6 x feeder device (auger) for silos 2 x pneumatic conveyor (air flow rate: 2136 m ³ /h, min speed: 17 m/s) 2 x blower (operating and reserve) Baghouse with PTFE-made bags, stainless steel apparatus and thermal insulation (total cloth area: 3460 m ²) Drag conveyor + dense phase pneumatic conveyor for the collection of baghouse residues
	2 nd stage	<i>1S equipment inventory</i>

The costs of other auxiliary equipment costs, among those listed in the equipment inventory, were taken from Matche (2015). Collected cost data were referenced to different years and different currencies. All values were reported to Euros, year 2015 and Italy as follows:

$$C_{\text{€},2015} = C_{\$,19xx} \cdot \frac{CEPCI_{2015}}{CEPCI_{19xx}} \cdot CPL_{IT/US} \cdot EX_{USD \rightarrow EUR} \quad 7.7$$

where $C_{\text{€},2015}$ is the present cost in Euros and $C_{\$,19xx}$ represents the cost in US Dollars referenced to the generic year 19xx. The CEPCI (Chemical Engineering Plant Cost Index) was adopted for inflation adjustment, while the difference in purchasing power across countries was taken into

account through $CPL_{IT/US}$, the comparative price level between Italy and USA (OECD, 2015). The exchange rate US Dollar to Euro ($EX_{USD \rightarrow EUR}$) as of October 2015 was considered.

The investment cost of a system was translated in an equivalent annual cost (EAC, annualised cost of equipment), which is the yearly cost of owning and operating an asset (in the present case, an air pollution control system) over its entire lifespan. It is calculated by dividing the present value of the asset (PV) by the present value of an annuity factor (AF):

$$EAC = \frac{PV}{AF} = PV \cdot \frac{i(1+i)^n}{(1+i)^n - 1} \quad 7.8$$

where i is the discount rate and n the lifetime of the project (in years). The term which multiplies the PV in the equation above is also known in engineering cost calculations as capital recovery factor (CRF). In estimating CRF for air pollution control equipment, EPA (2002) recommends to consider a lifetime of 20 years and a discount rate of 7%. The indication for the service life was applied in the present study, whereas a discount rate of 5%, more representative of the European scenario, was adopted.

Reactant costs. A list of references for bulk supply prices of the reactants used in acid gas treatment systems is reported in Table 7.8. Calcium hydroxide is an abundant and relatively inexpensive material, obtained from the calcination and subsequent slaking of limestone. Its cost can vary depending on local availability and transportation needs. Since Italy is one of the main producers of limestone (USGS, 2012), the relatively low value of 80 €/t was taken as a representative figure for the bulk supply of hydrated lime for the reference plant. Sodium bicarbonate is produced by the Solvay process. In determining its price, the processing cost is the main part, thus the price is less geographically dependent than lime. The purchase cost adopted in the present study was 240 €/t.

Table 7.8. Reactant costs.

Material	Cost	Source
Calcium hydroxide	90 \$/t	Sinnott, 2005
	45-70 \$/t (+ 10-40 \$/t due to transportation)	Sedlak, 1991
	65-74 \$/t	Chemical Market Reporter, 2006
	80 €/t	Yassin et al., 2007
	90 €/t	Quicker et al., 2014
	80 €/t	Antonioni et al., 2014
Sodium bicarbonate	289 \$/t	Solvay Chem. North America, 2015
	245 €/t	Quicker et al., 2014
	240 €/t	Antonioni et al., 2014

Disposal costs. As mentioned in chapter 4, the handling of solid by-products from flue gas cleaning processes (the so-called APC residues) is a controversial matter and no general consensus regarding residue disposal solutions has been reached even in the European Union (ISWA, 2008; Margallo et al., 2015). The management practices of APC residues are different from country to country, depending on the local regulations.

The Italian legislation (D.Lgs. 152/2006) classifies APC residues from WtE plants as a hazardous waste, due to their leaching potential. Therefore, disposal in landfill can take place only after a specific treatment, aimed to stabilise the residues by means of the addition of cement and chemicals. In Northern Italy, a diffuse alternative practice is the exportation of untreated APC residues to Germany, where they can be disposed in depleted salt mines as backfilling materials (Özarslan et al., 2001). The soundness of this alternative with respect to the stabilisation method is economically dependent on the transport cost and juridically on the respect of the closeness principle.

A third alternative is viable in the case of Na-based residues. The alkaline salts produced by dry treatment units fed with sodium bicarbonate are collected by the seller and treated in a dedicated plant (Brivio, 2005), where a brine suitable for sodium carbonate production is recovered. As already mentioned in chapter 4 and in section 7.3, this solution requires that the air pollution control system is equipped with a pre-dusting device before sodium bicarbonate injection, in order to pull apart alkaline salts from fly ash. Consequently, the recovery process can be applied to SBW generated from the 2nd stage of the 2S system or from the single stage systems with pre-duster (ESP-1S and FF-1S).

The costs associated with the management alternatives described above are listed in Table 7.9. In the light of the above, in the present study it was assumed that CBW, as well as the SBW mixed with fly ash of the 1S system, are disposed of in authorised landfill sites after stabilisation treatments or in appropriate underground storage sites. Conversely, SBW coming from the 2nd stage of the 2S system, the ESP-1S system or the FF-1S system were assumed to be sent to a processing plant for the recovery of a purified brine suitable for sodium carbonate production. The value of 200 €/t was adopted both for CBW/SBW disposal and for SBW recycling. However, it has to be noted that these costs depend on different factors, thus different ranges of variability were attributed to them in the Monte Carlo sensitivity analysis on cost data.

Table 7.9. Disposal costs.

Disposal method	Cost (€/t of residue)	Source
<i>Stabilisation and landfilling</i>	225 ^a	IEA, 2000 (<i>data about France</i>)
	200 ^a	ATOR, 2008
	200 ^a	Antonioni et al., 2014
<i>Backfilling in German salt mines</i>	100-140 ^b	Bertin Technologies, 2000
	100-125 ^b	ISWA, 2003
	100 ^b	Nethe, 2008
<i>Brine recovery from alkaline salts (only for SBW)</i>	200 ^a	ATOR, 2008
	170 ^b	Lostorto, 2009
	200 ^a	Antonioni et al., 2014
^a including transport		
^b excluding transport		

Other O&M costs. Operating an air pollution control line requires additional expenses other than the costs for reactants. In particular, the following costs were taken into account:

- **Fan operation:** power is needed in order to overcome the pressure drop given by the passages through baghouse (estimated $\Delta P = 1.5 \text{ kPa}$) and ESP (estimated $\Delta P = 0.25 \text{ kPa}$). The required power was estimated according to the following relationship (EPA, 2002):

$$Power_{fan}(kW) = \frac{\dot{V} \cdot \Delta P}{\eta_f} \quad 7.9$$

where \dot{V} is the gas flow rate, ΔP the pressure drop and η_f the combined fan-motor efficiency (assumed equal to 0.65). Energy cost was set to 0.07 €/kWh.

- **Compressed air:** compressed air is needed for the pulse-jet cleaning of the fabric filter. EPA (2002) suggests that the required air flow rate is equal to 2 % of the flue gas flow rate (i.e. 360 m³/h in the design conditions of the reference plant), while the provider of the actual baghouses installed in the plant estimates a consumption of 275 m³/h. Discounted cost estimates for compressed air range from 0.20 €/1000 ft³ (Sinnott, 2005) to 0.35 \$/1000 ft³ (EPA, 2002). The latter value was adopted.
- **Replacement bags:** the lifetime of PTFE-made bags was assumed to be 2 years. Therefore, the annualised replacement cost was estimated by evaluating a capital recovery factor for the initial purchase of bags assuming $n = 2$ years, $i = 0.05$ in equation (B.2)
- **ESP operating power:** an empirical formula for the estimate of the power consumption of an ESP device as a function of collection plate area A is provided by EPA (2002):

$$Power_{ESP}(kW) = 1.94 \times 10^{-3} \cdot A \quad 7.10$$

- **Maintenance:** general rules of thumb for estimating maintenance costs are provided by EPA (2002). For ESPs having a collection area < 50,000 ft², the average yearly labour cost associated to maintenance is around 3500 €. For fabric filters, it is estimated 1 h/day of work dedicated to maintenance (estimated cost: 20 €/h). As for the material costs due to maintenance, they are assumed as 1 % of FEC of the related equipment (EPA, 2002).

7.7 Optimal configuration of the two-stage system and benchmarking results

A first set of simulations was aimed at the determination of the optimal operating conditions of the 2S system, i.e. the best distribution of the reactant feed between the two stages considering the three different cases of composition of the input waste (see Table 7.3). The optimal operating conditions were assessed only with respect to costs, neglecting the issue of the different environmental impact of solid residues produced by the two stages but considering the different cost of residue disposal or reuse (an extension of the present methodology to environmental assessment is the scope of chapter 8). Moreover, only variable costs – costs of reactants and of waste disposal – were considered, since the limited variations considered in the required conversion of acid gases between first and second stage of the system do not affect equipment design but only operating conditions.

The feed rate of waste was set at 18 t/h, which generates the flue gas flow rate of 110,000 Nm³/h under the assumptions introduced in section 7.5. The recirculation ratio of the CBW was kept constant at a value of 0.21, which is the operating value of the reference plant considered by Antonioni et al. (2014). Simulations were carried out by varying the HCl conversion in the first stage $X_{HCl,Ca(OH)_2}$, while keeping constant the concentration of hydrogen chloride in the outflow of second stage at 2 mg/Nm³. Given the overall HCl conversion required, the second stage conversion, as well as the required feed rate of reactants in the first and in the second stage, were calculated using the equations of the operational model.

In Figure 7.5 the hourly costs due to purchase of reactants and disposal of residues are plotted as a function of 1st stage conversion for each of the three waste composition scenarios in Table 7.3. In the figure, square dots pinpoint the values of 1st stage conversions for which reactant consumption is minimum, while circle dots indicate the values of 1st stage conversions for which the economic optimum is obtained. For all the three waste composition scenarios, the optimised 1st stage

conversion value is in the range 55-60%. The plots also evidence that deviation from the optimal operating point implies steeper cost increases when the acid gas concentration in the untreated flue gas is higher (scenario W_C).

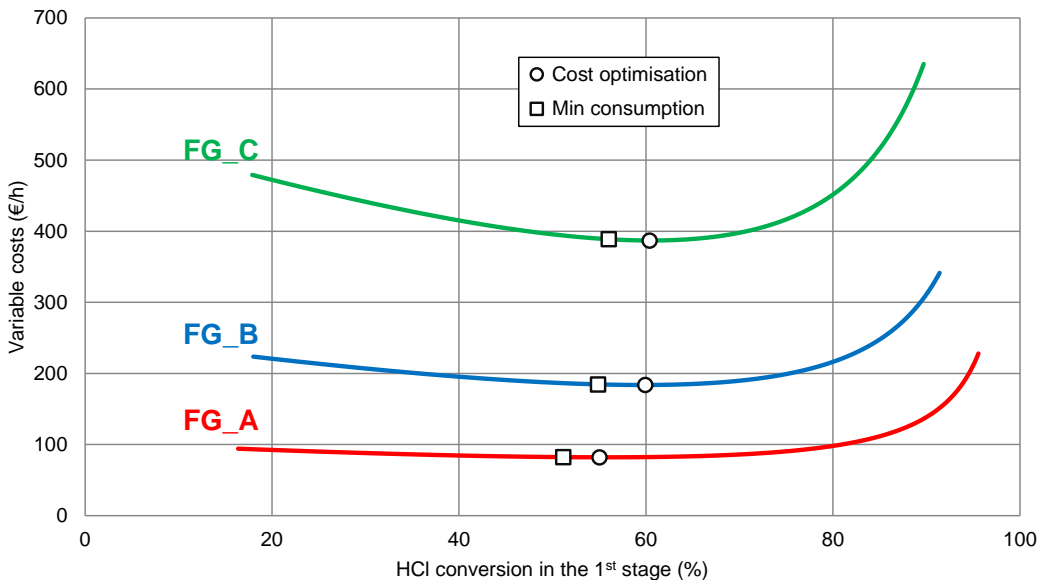


Figure 7.5. Variable costs (reactant purchase and residue disposal) of the two-stage system as a function of 1st stage HCl conversion for the three different flue gas compositions FG_A, FG_B and FG_C in Table 7.5, generated by the waste composition scenarios in Table 7.3. Square dots: minimum reactant consumption; circle dots: minimum cost.

Having identified the economic optimum of the 2S system for the different waste composition scenarios, it is possible to compare these figures with the single stage alternatives based on bicarbonate injection (with and without pre-dusting devices). As a term of comparison, the *total annual cost* of the system was assumed, which includes the annualised equipment cost, the reactant costs (purchase of reactants and disposal of residues) and the other O&M costs (energy requirements, replacement parts, maintenance).

The parameters of the conversion model for the single stage fed with sodium bicarbonate were taken equal to those assumed for the 2nd stage of the reference 2S facility (Table 7.1), which is actually identical to a single stage NaHCO₃ injection. Thus, the reactant consumption was calculated imposing the same outlet value of HCl concentration assumed for the 2S system (2 mg/Nm³). The single stage conversion required was calculated accordingly. Under these assumptions, the costs related to the operation of the single stage systems were estimated for the different waste composition scenarios.

In Figure 4, the total costs calculated on annual basis for the four plant alternatives are reported for the three waste composition scenarios in Table 7.3. The three different 1S processes use the same amount of sodium bicarbonate (i.e. have same reactant costs), while waste disposal/reuse, equipment and O&M costs are different.

In scenario W_B, representing a chlorine-rich unsorted municipal waste, the 2S system is more cost-effective than the 1S benchmarking systems considered. In particular, even if the costs related to equipment and disposal of residues are the highest, the 2S system emerges as the more economical alternative due to a 48% reduction in reactant purchase cost. The equipment cost,

depreciated over 20 years of operation, ranges from 6% of the total cost for the single stage without pre-dusting to 13% for the 2S system.

When scenario W_A is considered, in which the concentration of acid gases in the untreated flue gas is the lowest, either single stage without pre-dusting or single stage with ESP pre-dusting are more economical than the 2S solution, thanks to their lower capital and maintenance costs. However, the 2S system still outperforms the FF-1S configuration.

Conversely, for scenario W_C, which corresponds to the combustion of municipal solid waste mixed with industrial or medical waste, fixed costs become marginal and the savings granted by the 2S system over the single stage alternatives become substantial (18% cost reduction with respect to the single stage without pre-dusting). In general, the 2S system shows less cost fluctuations across scenarios than the benchmarking alternatives.

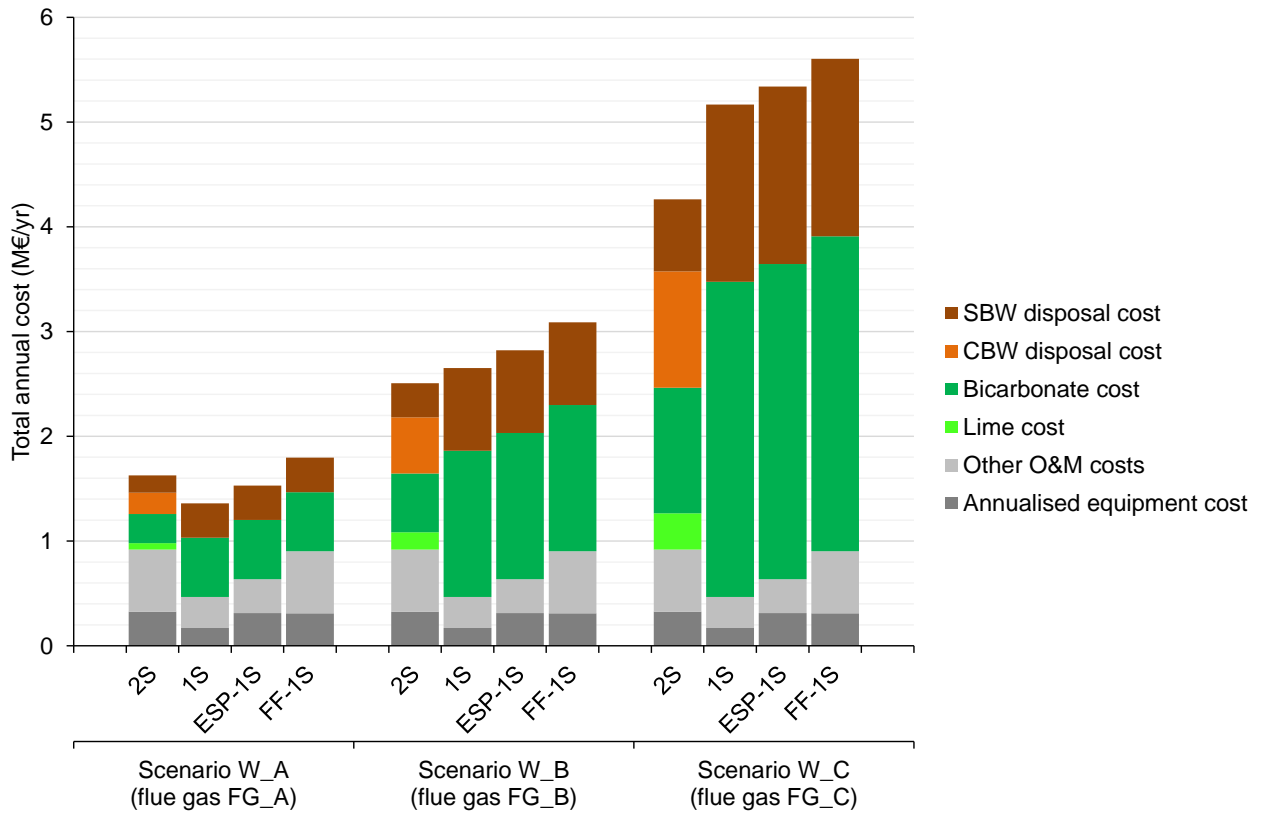


Figure 7.6. Total annual cost calculated for the four alternative dry treatment systems and waste composition scenarios W_A, W_B and W_C in Table 7.3 (flue gas composition: respectively FG_A, FG_B and FG_C in Table 7.5). A service time of 20 years was assumed.

7.8 Influence of uncertain parameters and Monte Carlo sensitivity analysis

The operating costs heavily depend also on the required performance of acid gas removal. The results discussed above all refer to a HCl outlet concentration of 2 mg/Nm³. However, depending on local regulations and requirements, systems might be operated on the basis of other emission limit values (ELVs). Thus, an assessment was carried out considering different ELVs for hydrogen chloride beside the base-case (2 mg/Nm³) considered above: 1, 5 and 10 mg/Nm³. The latter value, being the ELV prescribed by Directive 2010/75/EU, identifies the minimum performance currently allowed in the European framework.

As shown in Figure 7.7, calculated costs confirm the rankings of the alternative technologies obtained for the base-case discussed in section 7.7. A single deviation appeared: the 1S technology results more cost-effective than 2S system in scenario W_B when a HCl outlet concentration of 10 mg/Nm³ is considered.

As expected, the total costs of all technologies increase when the ELV is decreased. In this framework, the 2S configuration results more cost-effective when high performances are required. In particular, when a HCl outlet concentration of 1 mg/Nm³ is coupled to an incoming waste rich in Cl and S (scenario W_C), the 2S system provides savings as high as 1.11 M€ per annum compared to the cheapest 1S alternative for the feed rate considered (120,000 t/year waste).

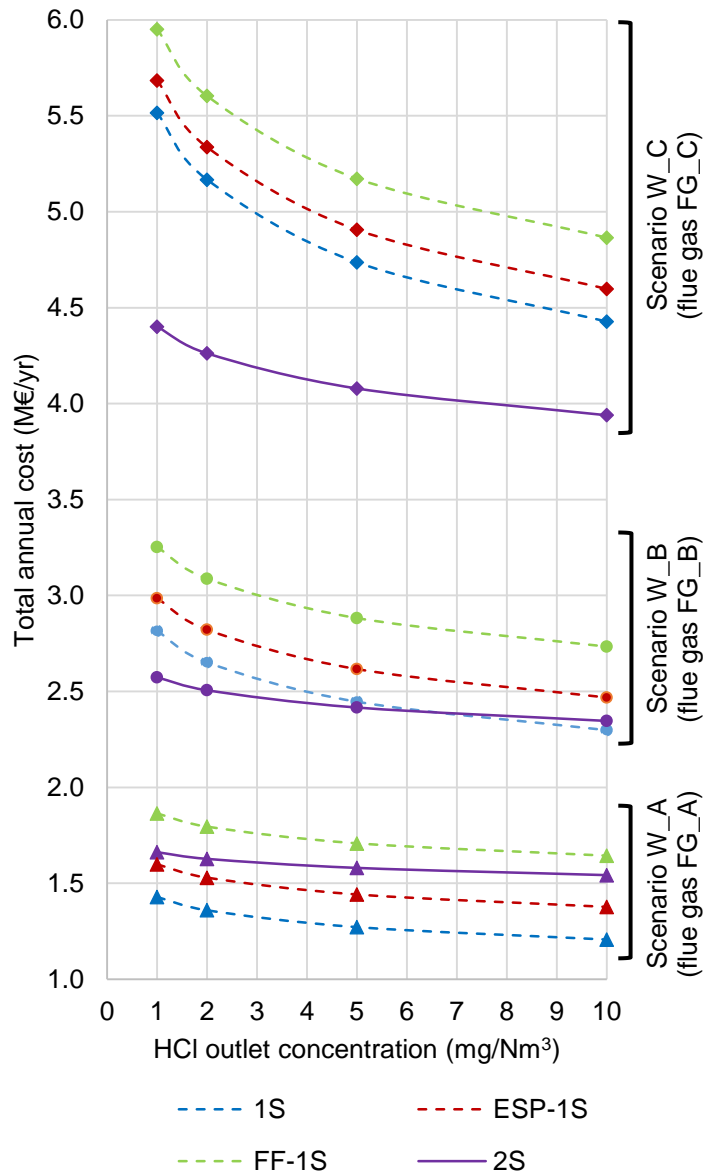


Figure 7.7. Total annual cost calculated for the four alternative dry treatment systems as a function of the required HCl outlet concentration (ELV). Scenarios W_A, W_B and W_C in Table 7.3 (flue gas composition: respectively FG_A, FG_B and FG_C in Table 7.5) were considered.

As shown in Figures Figure 7.6 and Figure 7.7, the operating costs vary widely across scenarios. In order to investigate more systematically the effect of the input waste composition on the total annual cost of operation, the complete set of flue gas compositions presented in Table 7.5 was

considered. The cases are intended to explore a reasonably broad field of variation for S and Cl content. The resulting flue gas compositions in Table 7.5 are coherent with the operational experience of European MSWI (Rylander, 1997), although cases with exceptionally high S content such as FG_B.1, FG_C.1, FG_C.2 are conservative, since even pure food waste rarely contain more than 0.5-0.6% S content on a dry basis (Komilis et al., 2012).

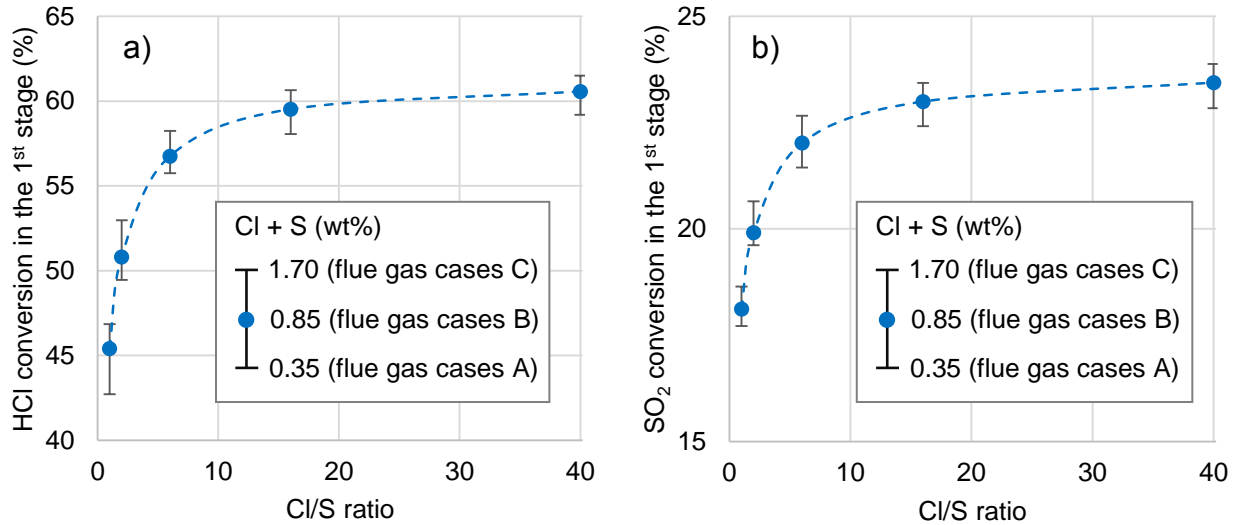


Figure 7.8. (a) HCl conversion in the 1st stage of the 2S system which optimises the operating costs expressed as a function of the Cl/S ratio in the waste feed and (b) corresponding SO₂ conversion in the 1st stage. Dots and bars cover simulation results for the different cases of flue gas composition listed in Table 7.5.

As shown in Figure 7.8, the optimal operating point of the 2S system is highly influenced by the Cl/S ratio. As the Cl/S ratio decreases, the economic optimum of the 2S system is shifted towards a lower conversion in the 1st stage and thus a higher conversion in the 2nd stage. This is caused by the lower reactivity towards SO₂ of calcium hydroxide with respect to sodium bicarbonate. When the costs of the 2S system are compared to that of the 1S alternatives, the ranking of alternatives is unchanged with respect to that reported in Figure 7.6 when the combined mass fraction of Cl and S in the input waste is 0.35 % (flue gas cases A) and 1.7 % (flue gas cases C). Differently, when the combined mass fraction of Cl and S in the waste feed is 0.85 % (flue gas cases B in Table 4) the ranking of alternatives changes at low values of the Cl/S ratio (cases FG_B.1 and FG_B.2). As shown in Figure 7.9, the total cost of each system rises, but the cost associated with the 2S system increases more rapidly due to the above mentioned low affinity of calcium hydroxide towards SO₂. Thus, the single stage system without pre-dusting becomes more cost-effective. In general, adding a lime injection line before the pre-dusting section appears to be uneconomical when the WtE plant is fed with fuels rich in sulphur and poor in chlorine (e.g. co-combustion of sewage sludge).

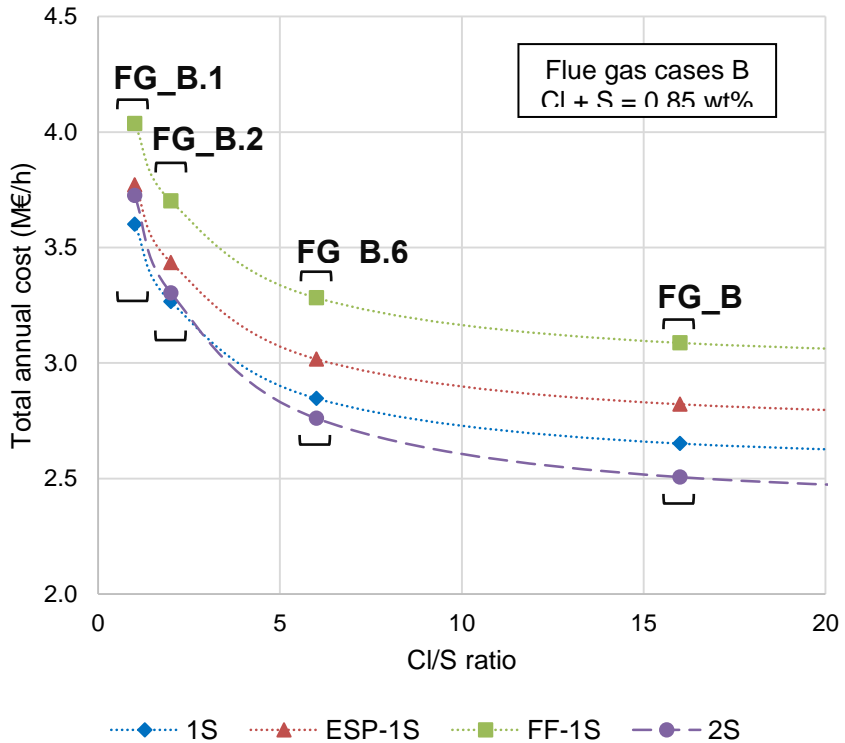


Figure 7.9. Total annual cost calculated for the four alternative dry treatment systems as a function of C/S ratio for a fixed combined amount of Cl and S in the input waste of 0.85 wt% (flue gas cases B in Table 7.5).

Eventually, it is worth considering that the cost values presented in section 7.6 are obviously dependent on the assumptions made during the cost estimate. Preliminary estimates for the equipment cost are affected by uncertainties, while the purchase cost of reactants can fluctuate both geographically and temporally. Furthermore, even the management costs for solid residues might vary with time: for instance, additional taxes on landfill disposal could be raised by policymakers in order to better compensate the externalities generated by the environmental burden of landfilling, whereas costs related to the brine recovery process might drop thanks to technological improvements.

Therefore, a sensitivity analysis was performed in order to check the robustness of the results even for widely different values of the unit cost entries. The sensitivity analysis was carried out considering the three most cost-effective alternatives in the light of Figure 7.6 and Figure 7.9: the 2S, 1S and ESP-1S systems. A Monte Carlo approach was adopted. The total annual cost was expressed as a function of 6 stochastic variables: the total installed costs of the ESP and the FF device, the purchase costs of lime and bicarbonate, the disposal cost of residues and the cost of recovering brine from SBW. A typical distribution of probability (a symmetric beta distribution with $\alpha = \beta = 2$) was associated to each variable, within the respective intervals of variation reported in Table 7.10. The mean values were set equal to the base values discussed above and used in the assessment, while ranges were selected according to the scattering of cost data discussed in section 7.6. The largest range of variability was given to the disposal cost, in order to reflect the uncertainty due to the wide variety of alternatives (stabilisation and disposal in common landfill or disposal in hazardous waste landfill or backfilling in salt mines) and the non-homogeneous regulatory framework even within the EU.

Table 7.10. Set of beta-distributed random variables considered in the Monte Carlo simulations.

Variable	Appears in...			Range (€)
	2S	1S	ESP-1S	
TIC of ESP equipment			✓	0.5 ÷ 1.5 x estimated TIC
TIC of FF equipment	✓ x2	✓	✓	0.5 ÷ 1.5 x estimated TIC
Lime cost	✓			70 ÷ 90
Bicarbonate cost	✓	✓	✓	230 ÷ 250
Residue disposal cost	✓	✓		150 ÷ 250
Brine recovery cost	✓		✓	170 ÷ 230

The results of the Monte Carlo sensitivity analysis are reported in Figure 7.10. The figure shows the cumulative probability of the overall cost difference between the 2S system and the two benchmarking alternatives for all the flue gas composition cases considered in Table 7.5. The results confirm the previous findings.

For a low content of Cl and S in the waste feed (flue gas cases A), the operation of a 2S system is not cost-effective, being the differences plotted in the corresponding panels of Figure 7.10 always higher than zero. Conversely, for medium mass fractions of Cl and S (flue gas cases B) the 2S system is usually more cost-effective than the alternative technologies. An exception can be noted in the comparison 2S versus 1S, which shows a higher cost of the 2S system for Cl/S ratios equal to 2 and 1 (with associated probabilities of 70 and 90%, respectively). This effect is much lower in the comparison of 2S versus ESP-1S, where the corresponding probabilities decrease to 5 and 25%, respectively. For a high content of Cl and S in the input waste (flue gas cases C), the 2S system performance is noticeably higher than the 1S alternatives, independently of the relative costs of reactants and waste disposal.

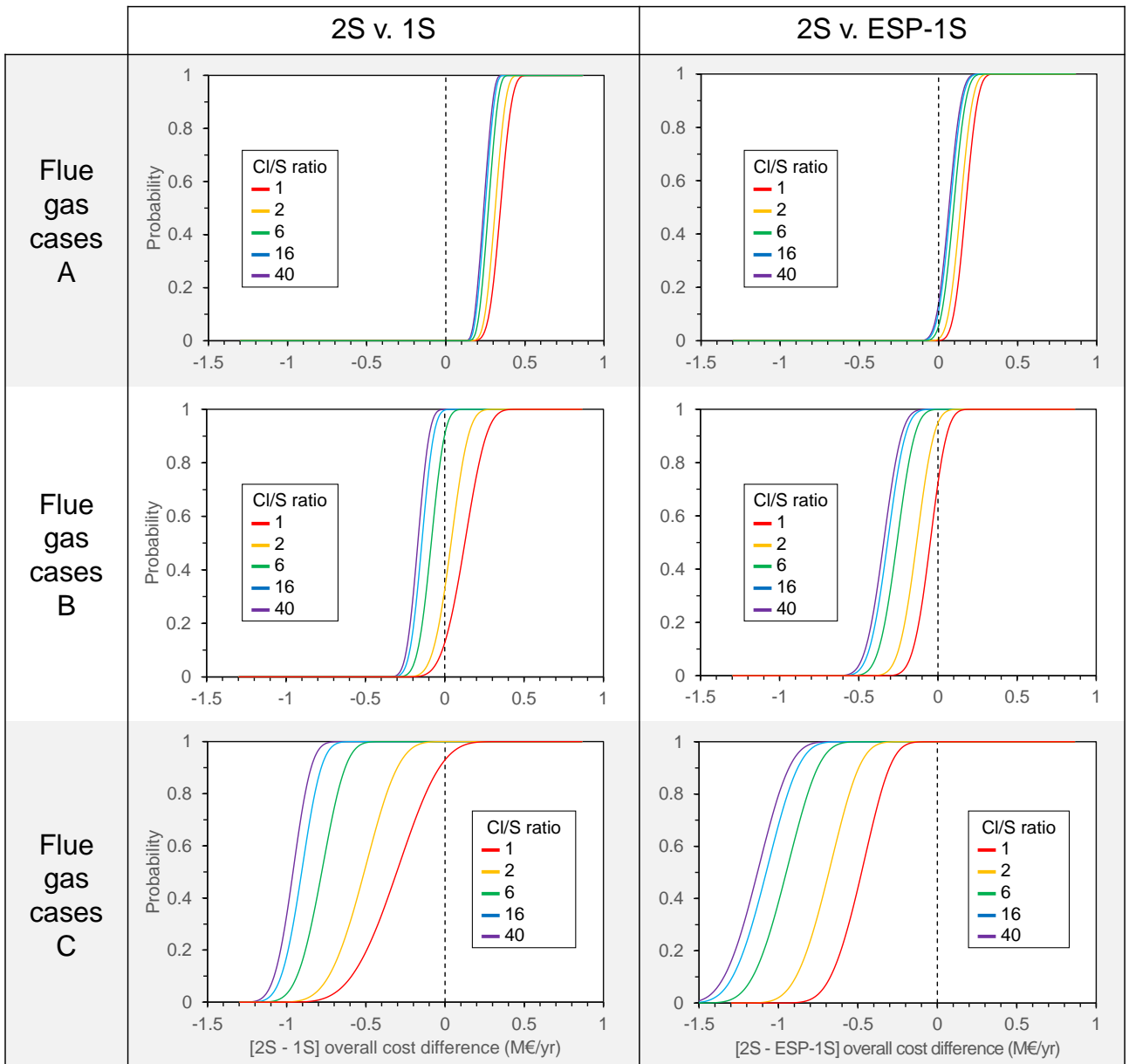


Figure 7.10. Cumulative probability of the difference in terms of total annual cost between: i) the 2S and the 1S system (left column), ii) the 2S and the ESP-1S system (right column). Flue gas composition for the cases considered is reported in Table 7.5.

8 Sustainability analysis of acid gas removal systems

8.1 A holistic approach to environmental protection

As mentioned in chapter 4, the optimisation of end-of-pipe technologies for air pollution control has to take into account not only process performance but also indirect impacts related to the production of reactants and the generation of residues. A very efficient flue gas cleaning technology might rely on the use of a particular reactant, whose supply chain gives rise to environmental impacts so high that offset the benefits obtained by flue gas cleaning and simply shift the environmental burden from the power plant to other processes. In this perspective, a thorough assessment of the life cycle impacts associated with the adoption of alternative technologies is a powerful tool for the selection of an all-round environmentally sound solution.

Recently, the life cycle thinking (LCT) approach has been extensively applied to evaluate the environmental footprint of waste incinerators as a whole. However, as stated by Astrup et al. (2015), air pollution control systems have been frequently overlooked in life cycle assessment (LCA) studies on WtE technologies. Their review of 136 papers produced in the years 1995-2013 evidenced that in more than 50% of the studies the acid gas cleaning technology was not even specified.

Only a few studies specifically focused on the environmental performance of the flue gas cleaning section of a WtE plant. Damgaard et al. (2010) analysed the historical improvement of the environmental footprint of air pollution control lines in Danish incinerators over the last 40 years. Møller et al. (2011) and Van Caneghem et al. (2016) evaluated specific flue gas cleaning steps from a life cycle perspective, namely the selective non-catalytic and catalytic reduction of NO_x. Scipioni et al. (2009) applied a comparative LCA to the selection of the best design solution between a dry and a wet acid gas removal system. Stasiulaitiene et al. (2016) proposed a LCA to explore the potential advantages of plasma-based technologies for the removal of NO_x, SO_x and volatile organic compounds in comparison with conventional end-of-pipe approaches. Margallo et al. (2014, 2015) investigated the life cycle impacts of WtE plants in Spain and Portugal, devoting particular attention to flue gas treatment and fly ash disposal processes. Biganzoli et al. (2015) assessed the environmental consequences of introducing a furnace injection of a dolomitic sorbent – the commercially known Depurcal mentioned in section 2.4 – as a preliminary acid gas removal step before sodium bicarbonate addition. The literature review also evidenced a consolidated role of the LCA technique in the analysis of the environmental performance of these systems.

In this chapter, the aim was to perform a LCA-type comparative evaluation of the two-stage dry treatment system versus two benchmarking single-stage solutions already presented in the previous chapter: sodium bicarbonate injection with (FF-1S) and without (1S) pre-dusting. The assumed system boundaries included the extraction and processing of the reactants and the disposal or reuse of the residues. A set of relevant environmental indicators (acidification, resource depletion, global warming contribution, photochemical oxidation, human toxicity, waste generation) was adopted in order to characterise the environmental profile of the alternative technologies.

Eventually, the results of the following LCA assessment and of the economic performance assessment detailed in chapter 7 were put in comparison. It is worth recalling that a cornerstone of the environmental policy of the European Union is the concept of BATNEEC: best available technique not entailing excessive costs (Sorrell, 2002). Any pollution mitigation technology which guarantees only a slight improvement of the environmental performance but entails significant cost increases might not be worth the implementation, as it would be better investing on other actions

which provide higher environmental returns (Directive 2010/75/EU, 2010). In this perspective, the joint evaluation of environmental and economic aspects was needed in order to draw a conclusion on the overall sustainability of the two-stage dry treatment systems.

8.2 Definition of the case study

The aim of the study is performing a comparative sustainability assessment of alternative dry technologies for the acid gas removal in WtE plants, integrating the economic analysis of the case study shown in section 0. Three reference technological schemes, namely single stage without pre-dusting (1S), single stage with pre-dusting (FF-1S), and two-stage (2S), are compared on the basis of the environmental and economic performances. The three schemes

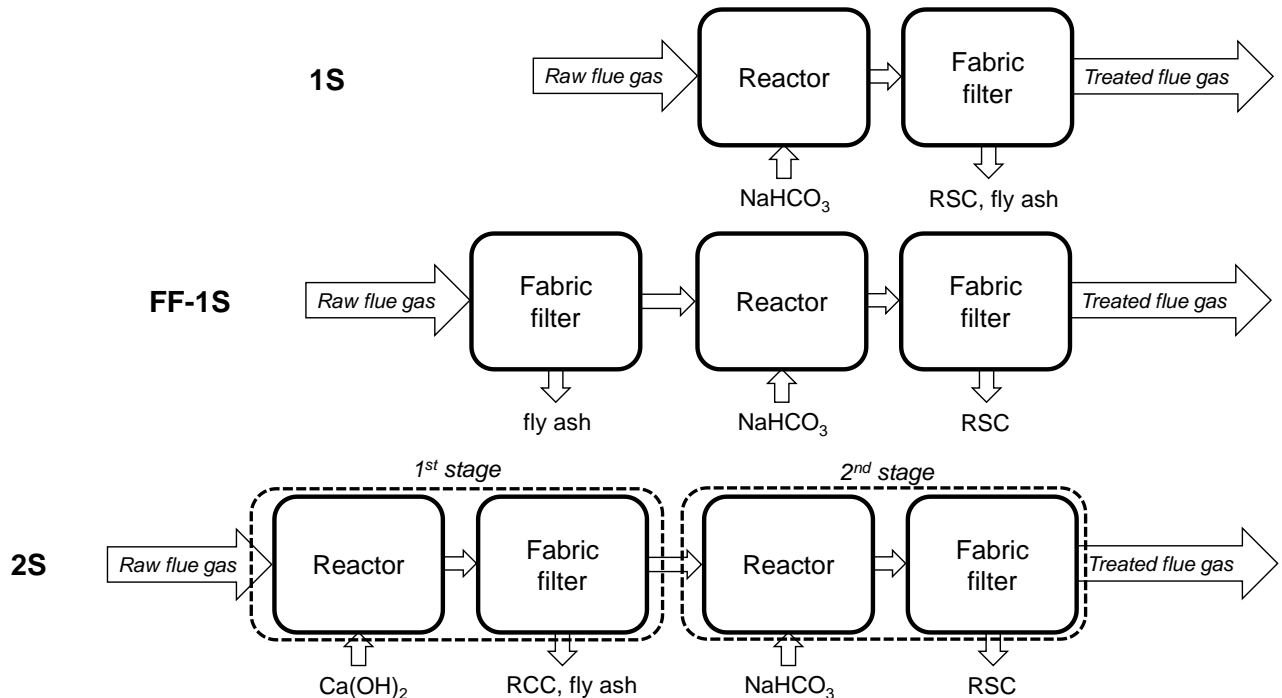


Figure 8.1. Block diagrams for the acid gas removal systems considered: single stage without pre-dusting (1S), single stage with fabric filter as a pre-dusting device (FF-1S), two-stage (2S).

The functional unit of the study is 1 hour of operation of the dry treatment system, installed on a medium-sized air pollution control line, treating a flue gas flow rate of 110,000 Nm³/h from a WtE plant. The same process specifications were assumed for the three alternatives considered. In order to realistically define the location-sensitive parameters of the system (emission limit values, transportation distances, etc.), the location of the plant was arbitrarily chosen in Northern Italy (Emilia-Romagna region). Three reference waste mixtures were considered, allowing the exploration of system performance under different acid gas concentrations: municipal solid waste (MSW), Plasmix, and sewage sludge. The elemental compositions assumed for the reference wastes are presented in Table 8.1.

The MSW composition is representative of a typical unsorted MSW as collected in the European territory (CEWEP, 2008). The Plasmix is a refuse-derived fuel (RDF), sulphur-free but rich in chlorine, obtained from the recycling of plastic packaging (Mapelli, 2014). The sewage sludge is the residual product of municipal wastewater treatment. Along with anaerobic digestion, incineration is a common practice to recover energy from this sludge. The elemental composition of sewage sludge can vary widely, but at least with reference to S and Cl content even data collected in different geographical contexts do not differ significantly (Thipkhunthod et al., 2005; UBA, 2013).

Although both Plasmix and sludge are usually burnt in co-combustion with other wastes, they are considered here as extreme cases for waste composition in terms of Cl and S content of possible wastes fed to a WtE process. Fluorine content in the considered waste mixtures is usually negligible (CEWEP, 2008; Mapelli, 2014; UBA, 2013; LEAP, 2009), resulting in insignificant concentrations of HF in the flue gases (European Commission, 2006). Therefore, in the present application, the analysis of the acid gas removal was limited to HCl and SO₂.

The concentration of acid pollutants in the flue gas was derived from the stoichiometry of the wastes, assuming that the Cl and S content in the waste is completely converted to HCl and SO₂, respectively. The Cl and S in the original waste which remains in the bottom ash (e.g. inorganic chlorine contained in NaCl) is actually already accounted for in the “ash” entry of the elemental analysis. The specifications for the off-gases leaving the plant at stack were set having in mind the current emission limit values (10 mg/Nm³ for HCl and 50 mg/Nm³ for SO₂ as for Directive 2010/75/EU): an off-gas concentration of 2 mg/Nm³ for HCl was considered as base case for all the technological options and reference wastes. This choice is in line with the common practice in actual WtE plants (Antonioni et al., 2014) and has the twofold goal of keeping a safety margin for HCl emission and ensuring complying with the emission threshold for SO₂. The effect of different specifications for the off gases was also explored, considering outflow concentrations of HCl in the range from 1 to 10 mg/Nm³.

Table 8.1. Elemental composition of the three reference wastes considered.

Components	Municipal solid waste ^a	Plasmix ^b	Sewage sludge ^c
C	25.0	60.8	36.2
H	4.0	5.6	3.5
O	18.0	19.9	15.0
N	0.8	0.3	4.0
S	0.13	0.0	1.0
Cl	0.36	0.8	0.3
Ash	17.7	7.6	5.0
Moisture	34.0	5.0	35.0
LHV (MJ/kg)	10.1	24.3	13.7

References: ^a CEWEP (2008), ^b Mapelli (2014), ^c UBA (2013)

The boundaries of the system analysed are described in Figure 8.2. For what concerns the WtE plant, the system boundaries include only the unit processes which differ between the alternative dry treatment technologies. The boundaries include the production (including the extraction of raw materials) and transportation of the solid reactants (bicarbonate and lime) necessary for the dry treatment and the fate of the solid residual products of the plant. While RCC and ashes may be considered a solid waste to be appropriately disposed, RSC can be processed to recover a brine suitable for further bicarbonate production if they are collected separately from ash and activated charcoal. Therefore, in option 1S the produced RSC is disposed, while the system boundaries for the FF-1S alternative include the recycling route of RSC. In option 2S, instead, RCC is disposed and RSC is processed in a recovery plant.

The process for recycling RSC, already mentioned in chapter 2, is described by several sources (Brivio, 2005; Ninane et al., 1995; ISWA, 2008; Solvay, 2014). The RSC are mixed with water in order to obtain a saturated brine of the soluble salts (NaCl, Na₂SO₄, Na₂CO₃), while the heavy metals and impurities precipitate. Additives such as sodium sulphide, sodium silicate and iron chloride are usually added in this phase. The brine is then filtered in a filter press, and further

purified by activated charcoal and ion exchange resins. The depurated brine is suitable for use as a raw material in the sodium carbonate production (European Commission, 2007).

The solid fraction to be disposed is generally known under the collective name of “*air pollution control (APC) residues*”. The impacts associated with the handling of APC residues considered in the present analysis are limited to the fraction constituted by the unreacted sorbents and the reaction products (i.e. RCC and RSC). The other solid components mentioned above (e.g. fly ash, activated charcoal) are not affected by the acid gas treatment and are left outside the boundaries of the study. A detailed assessment of the impacts associated with the management of these components is provided by Fruergaard et al., 2010. The disposal method considered for APC is the long term storage in depleted salt mines (ISWA, 2008; Özarslan et al., 2001). These underground sites may be considered as permanent and safe deposits, since the host rock formation (salt rock) constitutes an impermeable and stable geological barrier to groundwater infiltrations which prevents leaching (European Commission, 2003). Therefore, even hazardous wastes with high leaching potential can be stored safely. In particular, refuses such as RCC and RSC mixed with fly ash, thanks to their pozzolanic activity, are used as backfilling material to fill excavations leftover from the mining activities. This use is claimed to be classified as “recovery” and not “landfilling” by German law (ISWA, 2008). Nonetheless, since the employed residues substitute other waste materials also utilised in the mines rather than virgin materials (Fruergaard et al., 2010), here the storage of RSC and RCC in mines is conservatively categorised as landfilling (e.g. for the determination of the waste production indicator).

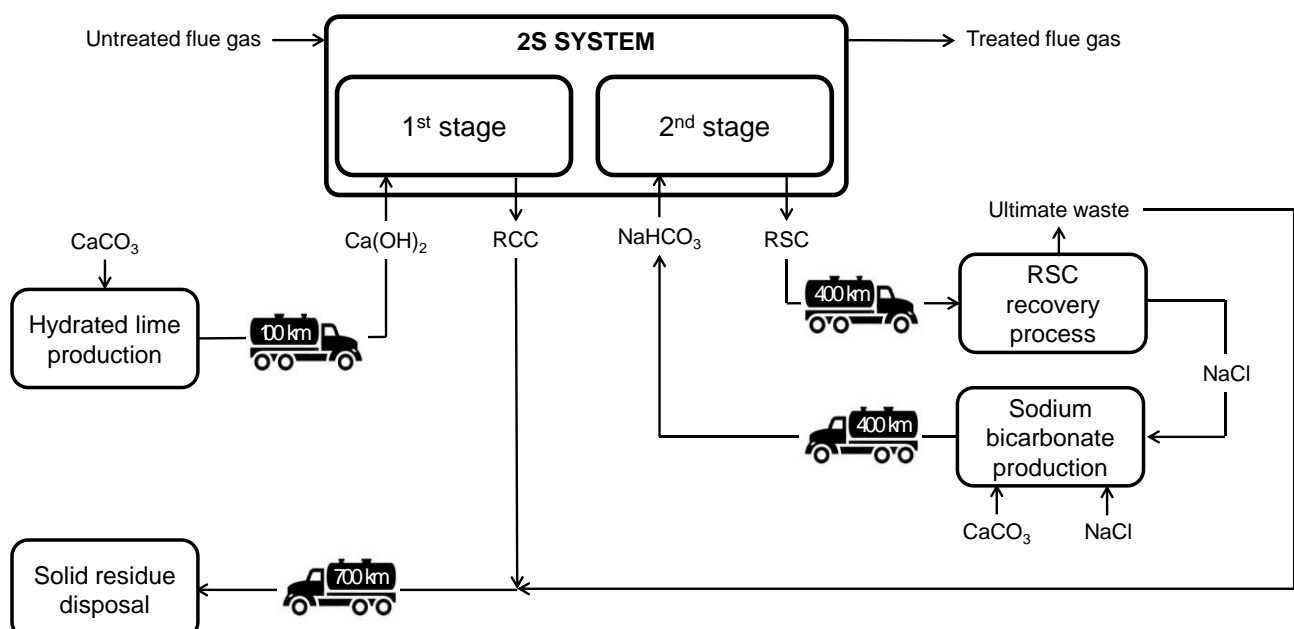
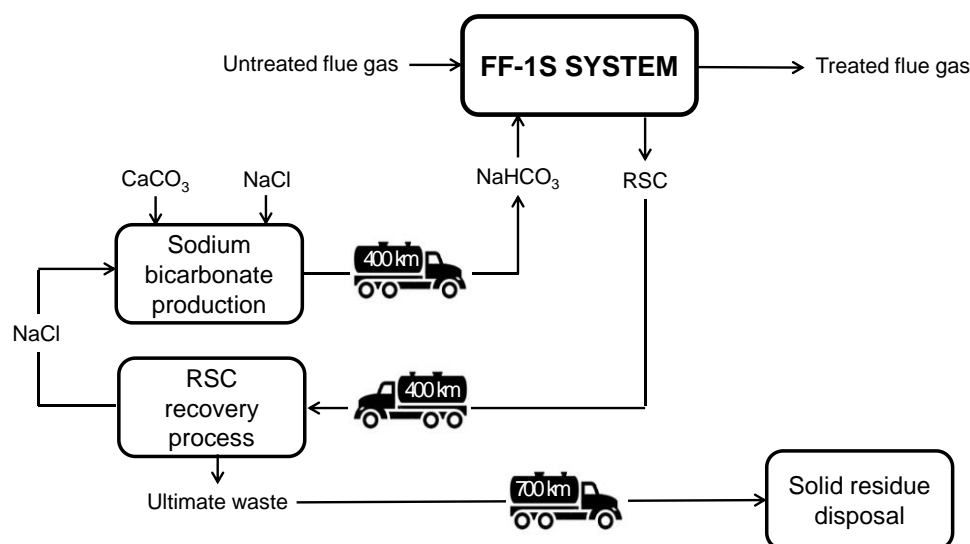
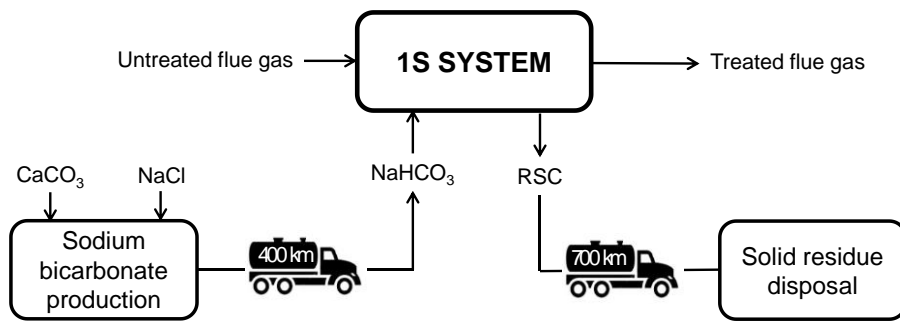


Figure 8.2. Unit processes considered in the sustainability analysis for the reference technologies.

8.3 Data inventories and associated uncertainties

Once defined the case study, data for the considered unit processes were obtained as follows.

The main foreground process, i.e. the operation of the dry treatment system, was modelled by means of the operational model for acid gas removal presented in chapter 7. It is worth recalling here that this model takes into account the non-linear relationship between the injection of the sorbent and the removal of acid gases, as well as the competing effects between HCl, SO₂ and CO₂. Hence, its adoption allowed a more precise evaluation of the acid gas removal process if compared with the over-simplified fixed generic values of sorbent feed rate per mass unit of waste usually introduced in life cycle studies (Scipioni et al., 2009, Damgaard et al., 2010).

Data for the supply chain of sorbents (bicarbonate and lime), as well as inventories for utilities and road transport, were retrieved from the European reference Life Cycle Database (ELCD, 2016) and CPM LCA Database (Swedish Life Cycle Center, 2014). The general overview of data sources is reported in Table 3. The energy consumption data for the disposal of residues in the underground sites are derived from Fruergaard et al. (2010). A pre-treatment with addition of hydrated lime and water (Rigamonti et al., 2012) is considered at WtE plant to stabilise the residues before sending them to disposal.

The burdens from the RSC recycling are mainly associated with the electrical and thermal energy inputs and the use of chemicals. These were estimated from energy and mass balances on available process data (Brivio, 2005; Biganzoli et al. 2015; Bichisecchi, 2014). Electricity was modelled according to the current Italian energy mix (ELCD, 2016). A mass cut-off criterion (ISO, 2006a) led to neglecting the production cycle of most of the additives, with exception of sodium hydroxide (NaOH), used to keep a pH value at 11.2 (basic conditions) in the vessels for RSC treatment (Bichisecchi, 2014). The availability of the recovered brine in the bicarbonate production process was taken into account in terms of avoided impacts related to the extraction and processing of sodium chloride (see e.g. ISO, 2012).

The transport distances for sorbents and residues were assessed considering the commercially available options for a WtE plant located in Northern Italy (see Figure 8.3). A distance of 100 km was assumed for the supply of hydrated lime (Nethe, 2008), given the high density of limestone quarries in Italy, which is one of the main worldwide producer of this raw material (USGS, 2012). While sodium bicarbonate production sites are quite evenly distributed across Europe, only two of them currently host a processing plant for the recycling of RSC: one of them is at a distance of about 400 km from the considered WtE plant. The nearest underground disposal site for solid waste is instead located in Germany, at a distance of about 700 km. Clearly enough, these distances can vary widely for a generic European WtE plant: this aspect is further discussed in section 8.5.

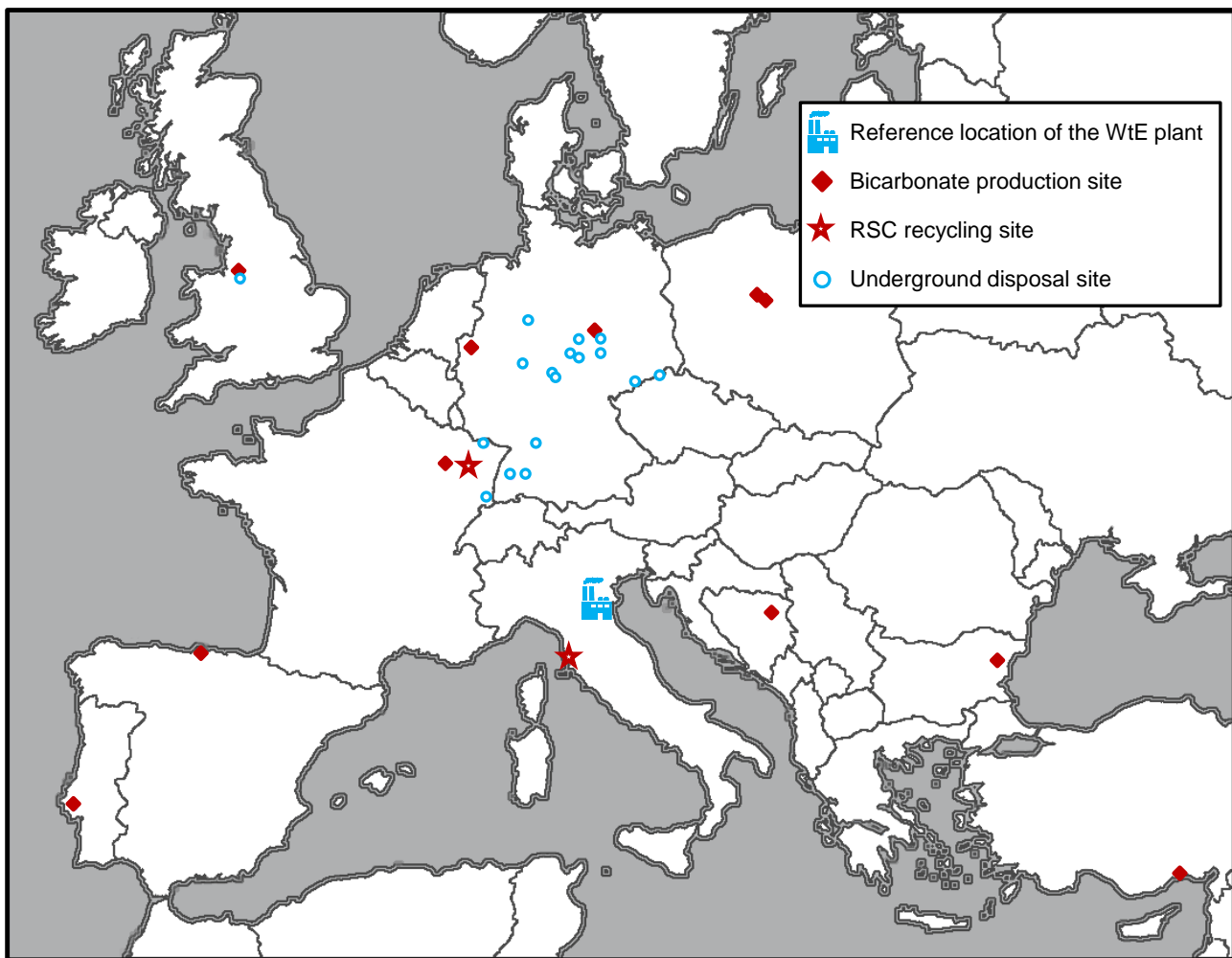


Figure 8.3. Location of bicarbonate production plants, RSC recycling plants and mines authorised for underground disposal of APC residues in Europe. The assumed location for the WtE plant is pinpointed.

Table 8.2 reports the data quality pedigree matrix (Weidema and Wesnaes, 1996) for the processes considered. Although only semi-quantitative, this approach to data quality assessment allowed identifying where the most relevant data uncertainties lie.

Table 8.2. Data quality pedigree matrix. Rating is based on a scale from 1 (high data quality) to 5 (poor data quality) according to the category specific criteria detailed by Weidema and Wesnaes (1996).

Process	Source	Reliability of source	Completeness	Temporal differences	Geographical differences	Further technological differences
Hydrated lime production	ELCD	1	1	2	2	1
Sodium bicarbonate production	Limestone extraction	ELCD	1	1	2	2
	Salt extraction	ELCD	1	1	4	2
	Bicarbonate production	CPM	1	1	3	2
	Electricity	ELCD	1	1	4	1
	Heat	ELCD	1	1	4	1
Acid gas treatment system at WtE	Modelled according to Antonioni et al. (2014)	1	1	1	1	1
Road transport of reactants and residues	ELCD	1	1	4	1	1
RSC recovery process	RSC recovery process	Brivio et al. (2005)	1	1	1	1
	Sodium hydroxide production	ELCD	1	1	4	2
	Electricity	ELCD	1	1	4	1
Solid residue disposal	Fruergaard et al. (2010)	1	1	1	1	1

In order to quantitatively study uncertainty propagation from the dataset to the results, a Monte Carlo method was adopted, by assuming a probability distribution for each uncertain parameter and then repeating the calculation for a reasonably high number of times, randomly sampling in each one the input parameters according to a specific probability distribution (Clavreul et al., 2012).

The approach is an extension of the one followed in the sensitivity analysis of the economic assessment in chapter 7. In the current application, both the main economic variables determining the cost index I_{CST} and the input/output data of the considered unit processes were taken as stochastic variables following a beta distribution. Normal distributions are a common choice when attributing uncertainty to life cycle inventories (Meier, 1997; Sonnemann et al., 2003) and symmetrical beta distributions can reproduce the shape of a Gaussian bell without having to deal with unbounded tails.

The parameters of each beta distribution were defined as follows: the mean value (μ) was based on the value used in the deterministic evaluations, while the shape parameters (α and β) were calculated on the basis of the desired standard deviation (σ) according to:

$$\alpha = \beta = \left(\frac{1 - \mu}{\sigma^2} - \frac{1}{\mu} \right) \mu^2 \quad 8.1$$

The standard deviation for each variable was calculated on the basis of a coefficient of variation CV, defined as follows:

$$CV = \frac{\sigma}{\mu} \quad 8.2$$

The values of CV were assumed on the basis of the uncertainty expected. For the input/output dataset used in the environmental assessment, the score in the pedigree matrix of Table 8.2 was used as a guideline to assign the values of CV (Table 8.3), as described in Weidema and Wesnaes, 1996.

Table 8.3. Stochastic variables considered in the Monte Carlo method.

	Variable or inventory	Source/mean value	CV
Environmental variables	Hydrated lime production	ELCD	20%
	Sodium bicarbonate production: energy, limestone and salt requirements	CPM	10%
	Limestone extraction	ELCD	20%
	Salt extraction	ELCD	20%
	Electricity	ELCD	30%
	Heat	ELCD	30%
	Road transport of reactants and residues	ELCD	20%
	RSC recovery process: energy and material requirements	Calculations based on Brivio, 2005	10%
Economic variables	Solid residue disposal: energy and material requirements	Fruergaard et al., 2010	10%
	Hydrated lime cost	80 €/t	5%
	Sodium bicarbonate cost	240 €/t	2%
	Solid residue disposal cost	200 €/t	10%
	RSC recovery cost	200 €/t	10%
	Fabric filter capital cost	Estimated TIC	25%

8.4 Characterisation approach and adopted indicators

The potential environmental impacts associated with the alternative dry acid gas removal technologies were characterised by a set of problem-oriented impact categories (resource depletion, global warming, rain acidification, photochemical oxidation, toxicity in air, waste generation). The choice was based on the review of the previous contributions analysing similar treatment systems (Damgaard et al., 2010; Møller et al., 2011; Van Caneghem et al., 2016; Scipioni et al., 2009; Stasiulaitiene et al., 2016; Biganzoli et al., 2015).

Characterisation factors for all the indicators, except waste generation, were based on the CML-IA database (CML, 2016), which is a widely adopted midpoint system (EC-JRC, 2011) and quantifies the impact category in terms of impact benchmarking (equivalent mass of a relevant reference substance). The indicator for waste generation was specifically introduced to account for the impact of RCC and RSC disposal: it simply quantifies the amount of solid residues (kg) to be disposed, evidencing therefore a lack of opportunities for material recovery in a circular economy perspective (European Commission, 2015).

An economic indicator was also used to group the overall costs associated with the operation of the alternative treatment systems, estimated according to the procedure described in chapter 7. As shown, the considered cost structure aimed to be comprehensive, including the purchase costs of the

reactants, the costs for the disposal of RCC/RSC with fly ash and for the recycling of RSC, as well as other operating & maintenance costs (electricity and compressed air for the operation of the dedusting devices, replacement parts, maintenance labour). The capital costs were taken into account in terms of an equivalent fixed hourly cost, considering 20 years of service time and 7500 h/year of operation.

Normalisation was required for a direct comparison between the environmental indicators adopted. Several criteria can be followed in defining normalisation factors (Tugnoli et al., 2008). In the present case, an external normalisation was used (Norris, 2001). The normalisation factors were calculated on the basis of average annual environmental loads in the Emilia-Romagna region (Italy), where the reference WtE plant is fictitiously located. By analogy, the economic indicator (cost index, I_{CST}) was normalised by a reference value for the same region. The values adopted for the normalisation factors and the sources and criteria used for their calculation are listed in Table 8.4.

Table 8.4. Indicators, normalisation factors and set of weights considered in the analysis.

Indicator	Normalisation factor	Unit	Value	Source	Weight in I_{ENV}
Resource depletion (RD)	Regional consumption of oil, gas and solid fuels	MJ/y	4.59×10^{11}	ENEA, 2008	0.1
Global warming (GW)	Regional CO ₂ and CH ₄ emissions	kg CO ₂ eq./y	4.74×10^{10}	ARPA, 2011	0.1
Toxicity in air (TA)	Normalisation value from CML, rescaled according to a population criterion ^a	kg 1,4-dichlorobenzene eq./y	2.93×10^{10}	CML, 2016	0.1
Rain acidification (RA)	Regional SO ₂ emissions + estimate on HCl emissions from WtE plants ^b	kg SO ₂ eq./y	2.07×10^7	ARPA, 2011	0.3
Photochemical oxidation (PO)	Regional NO _x , CO, SO ₂ , NMVOC emissions	kg ethylene eq./y	2.81×10^7	ARPA, 2011	0.1
Waste generation (WG)	Regional generation of industrial waste	kg waste/y	7.88×10^9	ARPA, 2011	0.3
Cost index I_{CST}	Regional cost for the waste management service	€/y	1.00×10^9	ISPRA, 2013	-

^a $TA_{EMR} = TA_{NED} \cdot (POP_{EMR}/POP_{NED})$
 TA_{EMR} normalisation value for TA in the region of interest (Emilia-Romagna)
 TA_{NED} normalisation value for TA in Netherlands as for CML, 2016
 POP_{EMR} population of Emilia-Romagna (ISTAT, 2016)
 POP_{NED} population of Netherlands (EUROSTAT, 2016)

^b $RA = E_{SO_2} + E_{HCl}$
 $E_{HCl} = \Sigma_{plants} (\dot{V}_{flue\ gas} \cdot C_{HCl,out})$
 E_{SO_2} regional SO₂ emissions reported by ARPA (2011)
 E_{HCl} estimate on HCl from WtE present plants
 $\dot{V}_{flue\ gas}$ flowrate of flue gas from each plant (ISPRA, 2013)
 $C_{HCl,out}$ HCl concentration in the flue gas (emission limit value of Directive 2010/75/EU)

In order to present a more concise, yet representative comparison between the environmental footprints of the process alternatives, the normalised indicators were aggregated to an overall environmental index (I_{ENV}). This was accomplished by weighted summation (ISO, 2006b)

considering the base set of weight factors presented in Table 8.4. This set acknowledges greater importance (weight factor three times greater than other categories) to rain acidification and waste generation, which are recognized a priori as the core issues for dry acid gas removal. In fact, the former represents the actual environmental problem to be controlled by the treatment processes and the latter constitutes the main environmental drawback of any dry sorbent injection system (European Commission, 2006). The same weight factor value was assigned to all the remaining environmental categories, reflecting an equal a priori importance for the acid gas treatment.

Obviously, the weighting stage implies intrinsic subjectivity and different weight sets entail different outcomes: this aspect was explored in the following by a dedicated analysis. Since a lower score in I_{CST} represents a higher economic performance and a lower score in I_{ENV} indicates a higher environmental performance, Pareto plots were used to analyse the values obtained (Paolucci et al., 2016; Azapagic et al. 1999a,b,c): this approach allows a meaningful comparison among the options, while avoiding an extra aggregation step.

8.5 Two-stage system: environmental and economic optima

In the two-stage system, as already stated in chapter 7, the required performance in terms of acid gas removal can be obtained by different combinations of removal efficiencies in the first and in the second stage. Given that two different solid reactants are used in the two stages, the choice to increase or decrease the acid gas removal in the first stage, consequently decreasing or increasing that of the second stage leads to important differences on the environmental and economic performance of the process.

Under the assumptions detailed in section 8.2, a simulation of the different operative conditions of the process was performed by the operational model: the HCl conversion in the 1st stage was changed modifying the feed rate of lime. The sodium bicarbonate feed in the second stage was modified accordingly, in order to maintain a constant specification for the hydrogen chloride concentration in the flue gas leaving to stack. Inevitably, while keeping HCl outlet concentration constant, SO₂ concentration at stack changes when varying the reactant feed rates in the two stages; in facts, hydrated lime and sodium bicarbonate have different selectivity towards the two targeted acid pollutants. However, since waste feeds with limited amounts of sulphur are considered, such changes have a very limited effect on the overall performance of the 2S system. Nevertheless, the environmental effects of the variation of SO₂ outlet concentration, which remains in any case well below the emission limits, is taken into account by the rain acidification indicator. The two sorbents considered have a different interaction with CO₂, as described in equations R3 and R4 in Table 7.2. The simulations showed that only minor changes in CO₂ concentration occur in the flue gases due to these phenomena (conversion changes less than $\pm 1.1\%$).

For the sake of clarity, the results obtained simulating the operative conditions of the process corresponding to the case of flue gases from the combustion of MSW are reported in Table 8.5. The material flows of reactants and the respective waste streams associated to different HCl conversion values in the 1st stage are listed, along with corresponding values of SO₂ concentration at the emission stack. The table also reports the total conversion of HCl, SO₂ and CO₂ in the treatment process. The conversion on a mass basis of the generic component i is defined as:

$$\chi_i = \frac{m_{i,IN} - m_{i,OUT}}{m_{i,IN}} \quad 8.3$$

where $m_{i,IN}$ is the mass flowrate of i entering the system and $m_{i,OUT}$ is the mass flowrate of i leaving the system in the off-gases. Clearly enough, the generation of a substance (e.g. CO₂ from reaction R4 in Table 7.2) yields negative values of conversion. The results of the benchmarking single stage systems are also reported for comparison: detailed comparative analysis is discussed in section **Errore. L'origine riferimento non è stata trovata..**

Table 8.5. Results of the simulations obtained in the case of flue gases from the combustion of MSW and hydrogen chloride concentration at the stack of 2 mg/m³.

System	$\chi_{HCl,1st}$ stage	$m_{Ca(OH)_2}$	m_{NaHCO_3}	RCC	RSC	$c_{SO2,out}^{(3)}$	χ_{HCl}	χ_{SO2}	χ_{CO2}
	-	kg/h	kg/h	kg/h	kg/h	mg/m ³			
IS	-	-	672.7	-	457.0	0.16	99.50%	99.90%	-1.07%
FF-IS	-	-	672.7	-	457.0	0.16	99.50%	99.90%	-1.07%
2S	10.0%	27.0	601.6	37.8	409.3	0.17	99.50%	99.89%	-0.93%
	22.5%	63.9	516.2	88.2	352.2	0.19	99.50%	99.88%	-0.76%
	35.0% ⁽¹⁾	107.6	432.6	146.0	296.2	0.22	99.50%	99.86%	-0.59%
	47.5%	163.1	350.5	216.6	241.2	0.26	99.50%	99.84%	-0.41%
	60.0% ⁽²⁾	240.6	270.0	311.3	187.1	0.34	99.50%	99.79%	-0.21%
	72.5%	366.2	191.1	458.6	134.0	0.47	99.50%	99.71%	0.03%
	85.0%	638.5	113.7	765.5	81.6	0.81	99.50%	99.49%	0.39%

Notes:

⁽¹⁾ Corresponds to “environmental optimum”

⁽²⁾ Corresponds to “economic optimum”

⁽³⁾ Concentrations are expressed at a temperature of 273.15 K and a pressure of 101.3 kPa (as for Directive 2010/75/EU)

The material flows of reactants and the associated waste streams obtained from the model were combined with the data from the relevant unit processes in the analysed system producing the overall inventory of input and outputs. This inventory was used to calculate the indicators described in section 8.4. Figure 8.4 shows the results obtained in the case of flue gases from the combustion of MSW and hydrogen chloride concentration at the stack of 2 mg/Nm³. It can be noted how the costs and the environmental indicators of the 2S system vary as a function of the repartition of HCl removal between the 1st and the 2nd stage.

The cost index I_{CST}, taking into account both equipment and operating costs (reactant procurement, waste disposal, other O&M costs), shows a minimum when 1st stage conversion is of about 60%. This operating point minimises the costs associated with acid gas removal and will be referred to as the “economic optimum” in the following. The existence of a minimum, as discussed in chapter 7, is due to the fact that the unit cost of hydrated lime (the reactant used in the 1st stage) is lower than the unit cost of sodium bicarbonate (the reactant used in the 2nd stage), but hydrated lime is less efficient in removing acid gases (i.e. a higher feed rate is needed to achieve the same acid gas removal performance).

The economic optimum does not correspond to the optimal operating point in terms of minimization of environmental impacts (“environmental optimum”). In fact, most of the impact indicators (e.g. rain acidification, resource depletion, toxicity in air) show a decreasing trend when the HCl conversion in the 1st stage rises from 0% to 70%: this can be explained considering that the production of sodium bicarbonate is more energy-consuming and emits more air pollutants than the

production of hydrated lime. Hence, a higher removal of acid gas in the 1st stage reduces environmental burdens as far as the necessary quantities of lime does not become excessive compared to bicarbonate. On the other hand, the waste generation indicator shows a minimum when no sorbent injection in the 1st stage is performed and increases monotonically with a higher acid gas removal in the 1st stage. This is due to the fact that the RCC generated by the injection of hydrated lime in the 1st stage need to be disposed, and therefore are accounted by the indicator, while the RSC produced by the injection of sodium bicarbonate in the 2nd stage are recycled to a great extent thanks to the available dedicated treatment process.

Since the waste generation indicator shows an opposite behaviour than the other environmental indicators, it is clear that the “environmental optimum” of the 2S system is a trade-off between the minimisations of solid waste and air pollutants, and depends on the relative weights attributed to the different environmental indicators. According to the weights introduced in Table 8.4, the environmental optimum for the system in Figure 8.3 is found at a 1st stage HCl conversion of 35%.

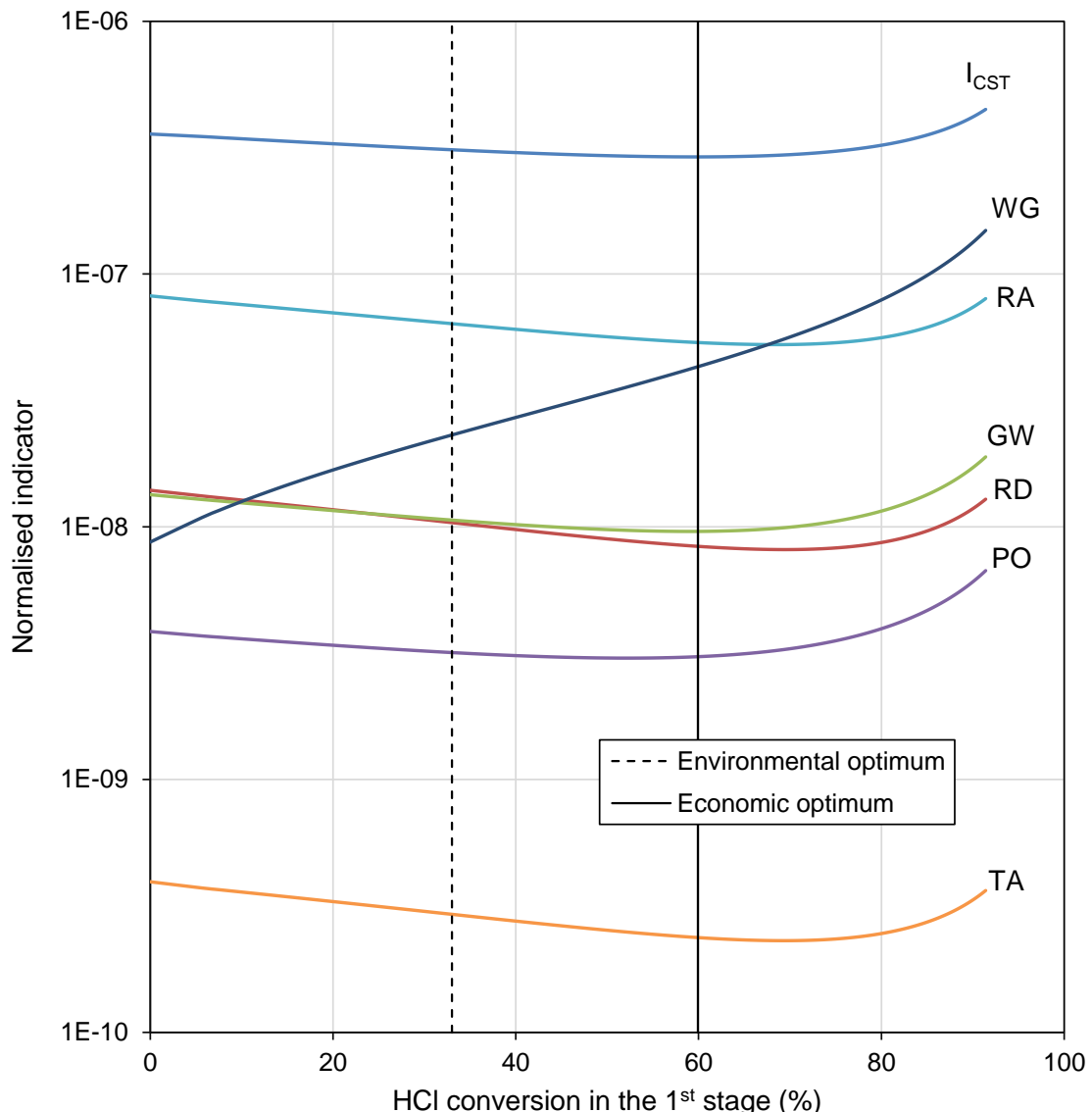


Figure 8.4. Normalised indicators evaluated for a 2S system as functions of HCl conversion in the 1st stage (reference waste: MSW; specification for HCl at stack: 2 mg/Nm³). I_{CST} : cost index; WG: waste generation; RA: rain acidification; GW: global warming; RD: resource depletion; PO: photochemical oxidation; TA: toxicity in air.

8.6 Comparison of the alternative acid gas removal systems

Having identified two 2S operative configurations corresponding to the economic optimum and the environmental optimum, it is now interesting to compare the associated normalised environmental indicators to those calculated for the alternative technologies (1S and FF-1S). The comparison is shown in Figure 8.5 and, again, it is referred to a single reference waste composition (MSW) and a single off-gas specification for HCl (2 mg/Nm³ at stack).

As evident from Figure 8.5, the impacts resulting from the 2S system are lower than the 1S system for all the impact categories considered. Also in the case of the FF-1S process the impacts of 2S technology are lower except for waste generation. The better performance of FF-1S in the waste generation indicator is due to the possibility to recycle the RSC. For the same reason, the waste generation of the 2S system, which produces both disposable RCC and recyclable RSC, is lower than that of 1S, where all the residues need to be disposed. With respect to the other impact categories, the low environmental impact of the 2S system is the result of the low consumption of solid reactants and, in particular, of bicarbonate, which has a production chain that generates higher impacts than that of hydrated lime, as discussed above. These results evidence that the development of residue management routes for RCC alternative to disposal, which is actually the target of several research projects (Quina et al., 2008; Margallo et al., 2015), would definitely allow in the future an improved performance of the 2S system, possibly reducing the current high impact from waste disposal (Vehlow et al., 2015; Stasiulaitiene et al., 2016) and allowing a better compliance to the principles of circular economy.

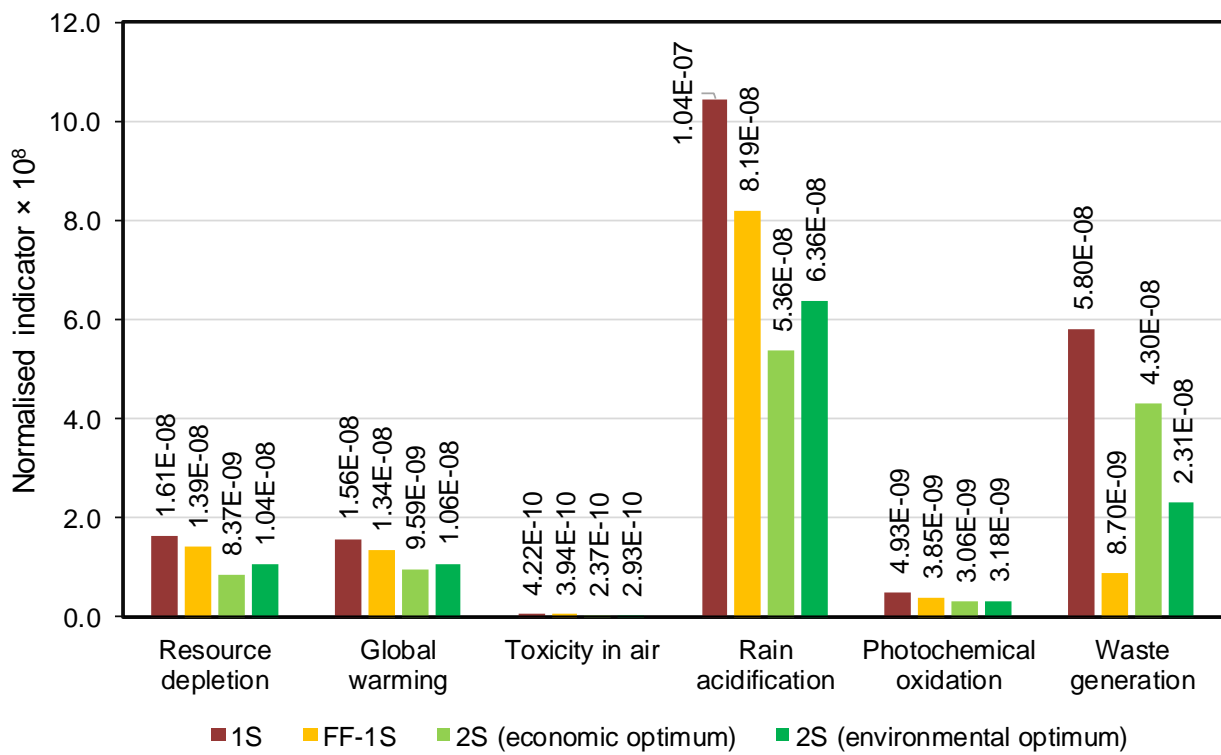


Figure 8.5. Comparison of the normalised environmental indicators for the reference technologies considered. Reference waste: MSW; specification for HCl at stack: 2 mg/Nm³.

According to the normalised indicators, rain acidification appears to be the most relevant impact category for all the technologies. Figure 8.6 shows the contributions of the different unit processes to the overall RA system indicator. The sodium bicarbonate supply chain (extraction of salt and

limestone, synthesis of sodium bicarbonate and related heat and electricity requirements) is identified as the main contributor. The transport operations generate from 8 to 12% of the total impacts, while the impact credits from recycling of RSC (i.e. avoided impacts related to salt extraction) significantly lowers the impacts of 2S and FF-1S options. The actual impact of the operation of the acid gas removal system is determined by the residual HCl and SO₂ in the stack emissions. While HCl emissions are the same in any case (2 mg/Nm³), different removal of SO₂ occurs among the technologies. In the case of 2S systems, the contribution is slightly higher than 1S and FF-1S systems because lime is slightly less efficient in removing SO₂ than bicarbonate (SO₂ outlet concentration of 0.26 mg/Nm³ instead of 0.16 mg/Nm³).

Even in the other impact categories the contributions of the different unit processes maintain similar proportions. For instance, in terms of global warming potential, the total life cycle emissions associated with the reference 2S system (environmental optimum) amount to 24.1 kg CO₂/kg waste, in line with the 23.0 kg CO₂/kg waste estimated by Biganzoli et al. (2015) for a similar kind of two-stage dry treatment system (furnace injection of dolomite + sodium-based 2nd stage), and accordingly the production of reactants is the main contributor.

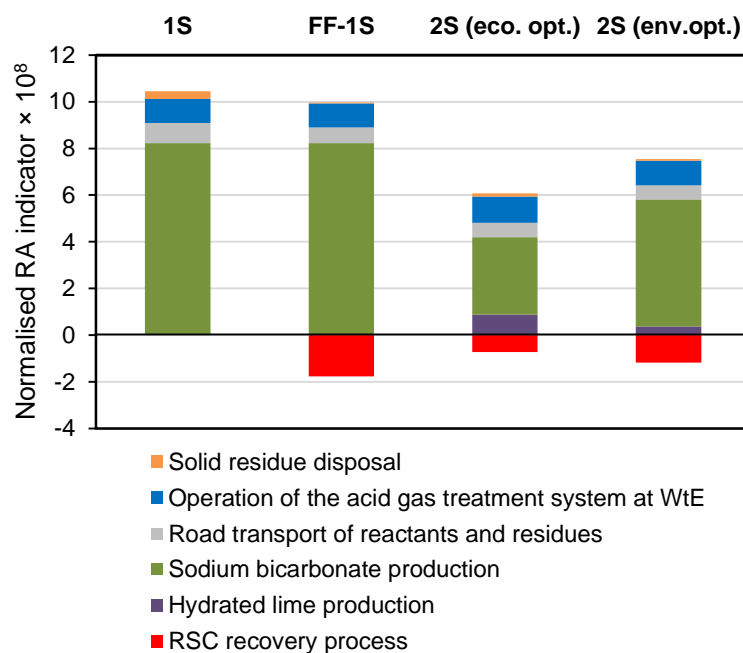


Figure 8.6. Contribution of the unit processes to the rain acidification indicator. Reference waste: MSW; specification for the HCl at stack: 2 mg/Nm³.

The overall environmental index (I_{ENV}) was obtained aggregating the environmental indicators by means of the set of weights introduced in Table 8.4. The values for the considered alternative technologies are reported in Table 8.6, along with the cost index I_{CST} . The environmental index is dominated in any case by the rain acidification and waste generation indicators, and the performance of the different technologies is thus the same discussed in the analysis of the single indicators. From the economic point of view, the 1S system without pre-dusting (1S) is clearly less expensive than the FF-1S system thanks to the lower capital cost, while the 2S system can benefit from the lower purchase cost of hydrated lime. The versatility of the two-stage configuration permits the 2S to achieve both economic performances comparable with the 1S alternative and environmental performances typical of the FF-1S alternative.

Table 8.6. Scores in I_{ENV} and I_{CST} of the alternative dry treatment systems. Reference waste: MSW; specification for the HCl at stack: 2 mg/Nm³.

Index	Acid gas dry treatment systems			
	2S (eco. opt.)	2S (env. opt.)	1S	FF-1S
Environmental index I_{ENV}	3.11×10^{-8}	2.85×10^{-8}	5.25×10^{-8}	3.03×10^{-8}
Cost index I_{CST}	2.91×10^{-7}	3.10×10^{-7}	3.07×10^{-7}	3.58×10^{-7}

Clearly enough, the score of I_{ENV} and the identified ranking between the alternative systems are dependent on the assumed set of weights. Following an approach similar to the “mixing triangle” of Hofstetter et al. (1999), the effect of different choices in the aggregation phase was explored in the ternary diagrams of Figure 8.7. Each point in the diagrams is representative of a set of weights (weight of rain acidification, waste generation and cumulative weight of all the other environmental categories). The light green shaded area in diagram (a) is the domain of weight combinations for which the 2S system (at economic optimum) has better overall environmental performance than the single stage systems. If the environmental optimum for 2S is considered, this area extends to the dark green shaded area (diagram b). On the other hand, the white area is the domain of weight sets for which the FF-1S has the lowest environmental impact. Since 1S has the highest values of the environmental indicators for each category (Figure 8.5), no weight set results in having the 1S system as the best option.

Figure 8.7 shows that the FF-1S system presents a lower I_{ENV} score than 2S when the weight set attributes greater importance to waste generation than to rain acidification. As sensitivity analysis, Figure 8.7 also compares the results of the weight set described in Table 8.4 with alternative weight sets (see Table 8.7). The ‘egalitarian set’ assigns equal weights to all the impact categories considering equal importance for all of them (PRé Consultants, 2000). The ‘normative-driven set’ attributes weights only to the impact categories for which the WtE plant is subject to environmental regulation (i.e. management motivated only by legal compliance). The set presented by Tugnoli et al. (2011) referred to process plants located in the geographical context of the current study. The set of Huppé et al. (2012) is the result of a meta-method for combining weight factors from different midpoint indicator systems. Finally, the Environmental Profiles Methodology (BRE, 2008) indicated a set of weights for the evaluation of the environmental footprint of building materials. The figure shows that the 2S system, if operated at the environmental optimum, is stably the preferable option for most of the weight sets considered; the only exception being BRE, which was however developed for the construction sector, where acidification is not considered a relevant concern.

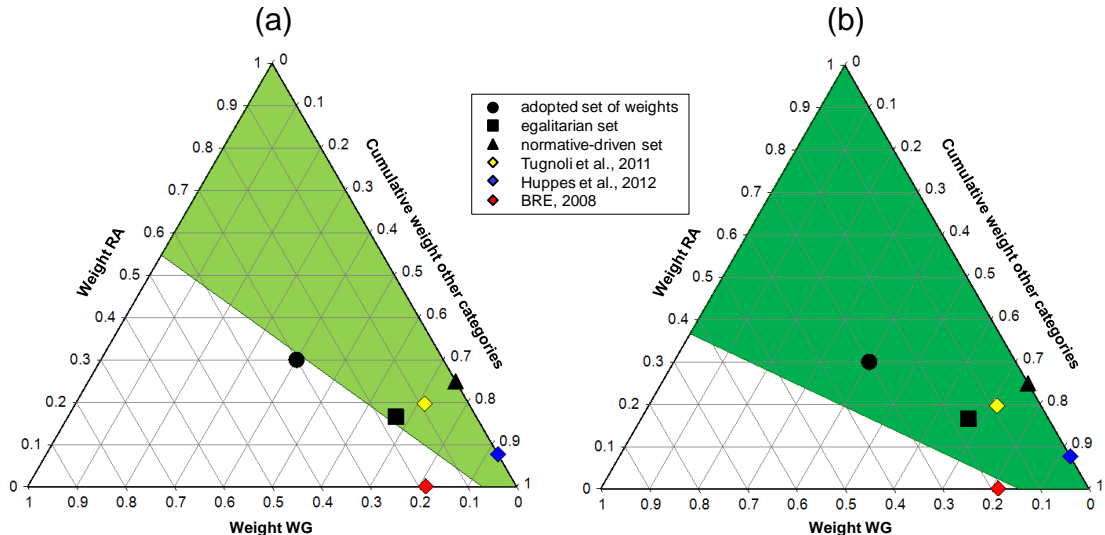


Figure 8.7. Comparison of the environmental preference of 2S system and FF-1S system as function of the weight set. In panel (a), light green shaded area identifies the sets of weights for which the 2S system, operated at its economic optimum, exhibits a I_{ENV} score lower than FF-1S. In panel (b), dark green shaded area identifies the sets of weights for which the 2S system, operated at its environmental optimum, exhibits a I_{ENV} score lower than FF-1S. Reference waste: MSW; specification for the HCl at stack: 2 mg/Nm³; ●: weight set in the present study.

Table 8.7. Alternative sets of weights used for the analysis in Figure 8.7.

Indicator	Egalitarian set	Normative-driven set	Tugnoli et al. (2011)	Huppkes et al. (2012)	BRE (2008)
Resource depletion (RD)	0.166	0.000	0.131	0.135	0.080
Global warming (GW)	0.166	0.250	0.152	0.442	0.521
Toxicity in air (TA)	0.166	0.250	0.284	0.250	0.207
Rain acidification (RA)	0.166	0.250	0.197	0.077	0.001
Photochemical oxidation (PO)	0.166	0.250	0.146	0.096	0.005
Waste generation (WG)	0.166	0.000	0.090	0.000	0.186

The stability of the results with respect to uncertainty in the input data sets was analysed by a dedicated Monte Carlo approach, as described in section 8.3. The results of the analysis are presented in Figure 8.8 as distribution of differences between selected couples of alternative options (discernibility analysis; Heijungs and Kleijn, 2001). The figure reports the cumulative probability of the overall difference in both I_{ENV} and I_{CST} indices between the 2S system, taken at the operating point of economic optimum, and the two single-stage alternatives for the case of MSW as input waste.

The 1S alternative is invariably outperformed by 2S and FF-1S on the environmental point of view and, with the assumed uncertainty ranges of the inputs, has only a 1% probability of being the most cost-effective solution. Instead, 2S and FF-1S have very similar environmental impacts and the ranking between them is affected by the input data variability. However, when economic aspects are

considered, the 2S system appears to be almost always the best option among the three. Since the sustainability profile of a technology must account for both environmental and economic aspects, the results of the sensitivity analysis confirm that the overall higher performance of 2S over the other alternatives is not affected by data uncertainty.

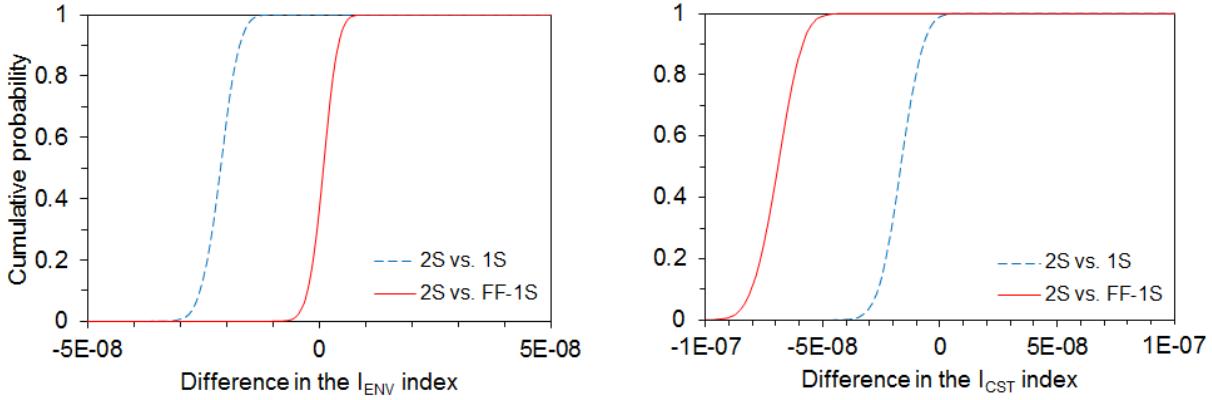


Figure 8.8. Cumulative probability of the difference in I_{ENV} (left panel) and I_{CST} (right panel) between the 2S system (economic optimum) vs. 1S (dashed blue line) and vs. FF-1S (red line). Reference waste: MSW; specification for the HCl at stack: 2 mg/Nm^3 .

The results presented so far assumed a HCl outlet concentration of 2 mg/Nm^3 . However, the specification on HCl at stack might vary. Given the location of the reference plant, the emission limit value (ELV) is set by the Directive 2010/75/EU to 10 mg/Nm^3 for HCl and 50 mg/Nm^3 for SO_2 . Internal decisions of the WtE plant management (e.g. safety margins) or local environmental authorisation agreements (e.g. presence of sensitive areas) may impose stricter ELVs for the stack emissions. The environmental index I_{ENV} and the cost index I_{CST} were calculated for HCl outlet concentrations of 1 mg/Nm^3 , 2 mg/Nm^3 , 5 mg/Nm^3 and 10 mg/Nm^3 . Given the low concentration of sulphur in the reference MSW, the current ELV for SO_2 (50 mg/Nm^3) was largely satisfied by the proposed technologies for all the specifications considered for the removal of HCl, thus is not considered as a constraint. Nonetheless, the different SO_2 emissions are accounted in environmental indicators.

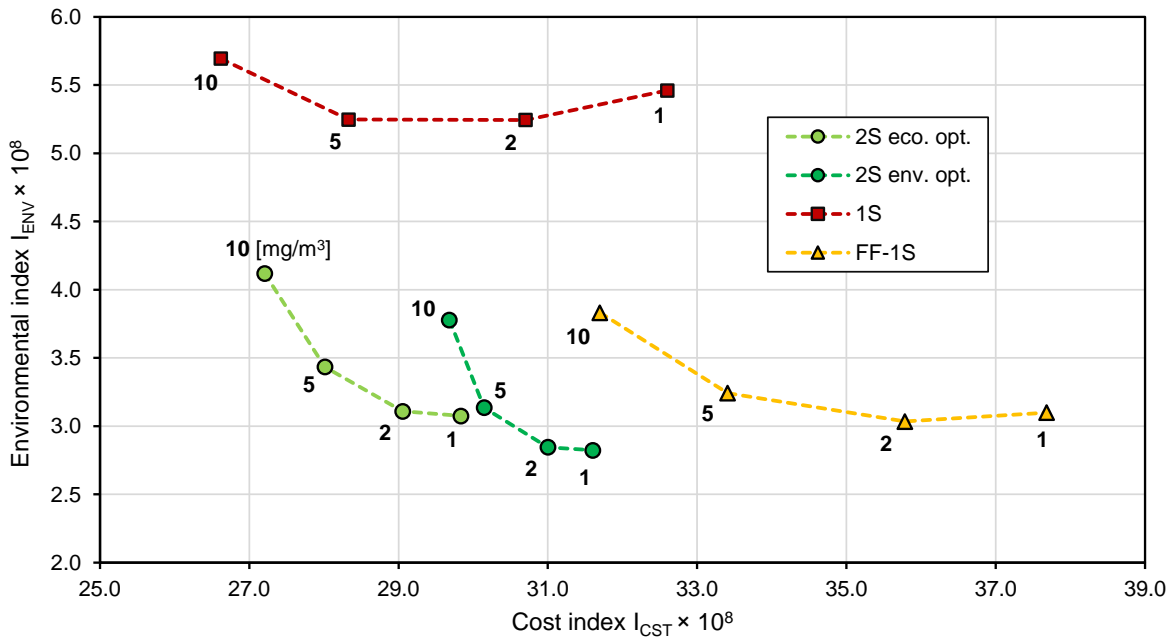


Figure 8.9. Environmental and economic performance indices of the alternative dry treatment systems for different HCl concentrations at stack (in mg/Nm^3). Reference waste: MSW.

In Figure 8.9 the environmental index I_{ENV} is plotted against the cost index I_{CST} for the considered treatment system alternatives at different HCl outlet specifications. A lower score in I_{ENV} indicates lower environmental impacts, while a lower score in I_{CST} means lower costs. Obviously, lower outlet concentrations imply higher expenditures for all the systems, but generally leads to better environmental performances (more acid gases are removed, lowering the RA indicator). In the case of very low specifications for the outlet concentration in single stage systems, the I_{ENV} rises its value because lower emissions of acid pollutants at the stack are compensated by the higher environmental impacts associated with the increased demand of reactants and generation of solid residues.

The plot extends the conclusions of the previous section to all the HCl outlet concentrations considered: 2S technology, operated either at the economic or environmental optimum, has clearly better cost performances than FF-1S, although it allows achieving very similar profiles of environmental performance. On the other hand, 1S may result in interesting values of cost index for larger ELV (even 2% better than 2S economic optimum for $10 \text{ mg}/\text{Nm}^3$) but the overall environmental performance is at least 38% worse than any other option.

Figure 8.9 also shows as the 2S system limits the cost increases related to the shift toward stricter ELVs, thus demonstrating higher flexibility of operation. From the point of view of overall sustainability, it can be noted that the choice to operate a 2S acid gas removal system with a HCl outlet concentration of $2 \text{ mg}/\text{Nm}^3$ appears a reasonable compromise for the management of a WtE plant, at least according to the adopted set of weights. In fact, lowering the outlet specification to $1 \text{ mg}/\text{Nm}^3$ of HCl produces, on the one hand, a significant cost increase and, on the other hand, only a slight improvement in I_{ENV} for the system. Generally speaking, such results highlight the importance of a life cycle perspective in correctly evaluating the sustainability of a process and call for due consideration of indirect environmental aspects in the field of air pollution control policies.

Lastly, also the composition of the waste fed to the WtE plant constitutes a significant factor in determining the overall environmental footprint of the acid gas removal process (Astrup et al.,

2011). Figure 8.10 reports the environmental and economic indices as calculated for the different technologies considering the three reference waste mixtures introduced in section 8.2. In each case the outlet concentration of HCl was specified to 2 mg/Nm³, which resulted in a SO₂ concentration always largely below the ELV of 50 mg/Nm³. For each waste mixture, the options shifted towards the bottom left-hand corner of the graph are both more cost-effective and more environmental-friendly.

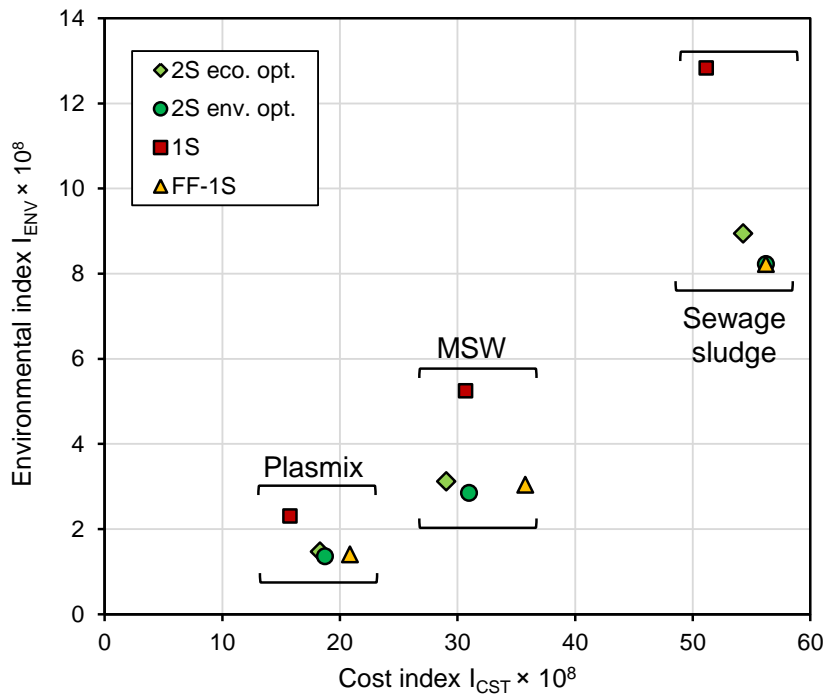


Figure 8.10. Environmental and economic indices of the alternative dry treatment systems for different waste mixture composition. Specification for the HCl at stack: 2 mg/Nm³.

When composition of Plasmix is considered as WtE plant feed, both I_{CST} and I_{ENV} exhibit lower values than in the MSW case. This is due to the absence of sulphur in the waste feed, which prevents the formation of SO₂, the acid pollutant to which both lime and bicarbonate have the lower affinity (Chin et al., 2005). In the case of Plasmix, the 2S system still outperforms the environmental performance of the 1S alternative, and the economic performance of the FF-1S alternative. Moreover, the difference in the environmental indicator between 2S and FF-1S is extremely low, ruling out FF-1S as an optimal solution for this case. On the other hand, the preference between 2S and 1S depends on the relative importance given to the environmental and economic aspect (both options are Pareto optimal alternatives).

In the case of sewage sludge, both I_{CST} and I_{ENV} soar, because of the exceptionally high sulphur content of the waste mixture. As mentioned, dry sorbents are generally less reactive towards SO₂ than HCl, resulting in both higher consumption of reactants and generation of residues. In particular, while sodium bicarbonate still retains good performance when dealing with high SO₂ loads, the conversion of calcium hydroxide particles is significantly limited by pore plugging phenomena (Chisholm and Rochelle, 1999) and diffusional resistance (Duo et al., 2004). Therefore, the advantages of the Ca(OH)₂-based 1st stage of the reference 2S system are greatly reduced for high SO₂ loads. In fact, the environmental optimum for 2S is achieved, in this case, by completely switching off the Ca(OH)₂ injection: this actually converts 2S in the FF-1S configuration. The economic optimum for 2S is achieved with a low utilisation of the 1st stage (approximately 30% of

HCl conversion in the 1st stage) and it is only slightly cheaper (-3.5%) than FF-1S solution, causing a slightly higher burden on the environmental aspects (+8.7%). The 1S options is actually slightly cheaper than the 2S (-9.0%), but significantly more problematic for the environment.

Though, while all the options belong to the Pareto frontier for sewage sludge treatment, it would be reasonable to discard this option as a best available technology for this waste mixture. It is worth remarking that the sewage sludge scenario has to be taken as a boundary case for waste composition, since the feed of sewage sludge to WtE furnaces is typically performed only in co-combustion with other wastes. Nonetheless, the results show that the addition of sulphur-rich wastes to a WtE process feed can negatively affect the performance of the hydrated lime-based acid gas removal stage. It can be concluded that, while for the MSW the 2S option was clearly superior to the other alternatives, for waste compositions with extreme concentrations of Cl or S the preference of 2S is the result of a compromise between environmental and economic priorities of the plant management. In fact, the 2S system shows a significant flexibility of operative conditions that may strongly reduce the practical differences with other techniques when appropriate optimisation strategies are adopted.

8.7 Closing remarks on single stage vs. multistage dry treatment systems

In chapter 7, the state-of-the-art single stage technologies were found to be less cost-effective than the 2S system for most of the waste and flue gas compositions considered. The 2S system resulted highly cost-effective in particular when the Cl content in the waste feed is above 1 %, which is an operating condition that is common to several WtE facilities dealing with mixed MSW and industrial waste. Therefore, for plants operating single stage technologies with high chlorine-content waste, the implementation of a lime injection line before the pre-dusting section is a retrofit that should be considered. The results of the sensitivity analysis evidenced that the 2S system assures a higher flexibility and total costs show a lower fluctuation when dealing with widely varying inlet waste compositions.

In the present chapter, a sustainability assessment was carried out to integrate the information from the economic evaluation with a representation of the environmental profile of the alternative dry treatment systems for acid gas removal. The analysis evidenced that the operating versatility of the 2S system can couple the cost-effectiveness of a 1S system with the lower environmental footprint of a FF-1S configuration. The results proved themselves stable to the uncertainties of the data sets used in the assessment. Moreover, the 2S option retained a good performance on both domains for any reasonable variation of the composition of the waste mixture fed to the WtE plant and the emission specifications set at plant stack. The retrofit of a FF-1S system to 2S in order to achieve cheaper operation, as proposed above, would not entail noteworthy environmental drawbacks. The main disadvantage of 2S operation is the high production of RCC and the lack of residue management routes alternative to disposal. The development of recycling solutions for RCC, in the light of the principles of circular economy, is therefore identified as a key issue for further improving the 2S option. Section 9.2 in Part III of the thesis exploratively proposes a possible valorisation route for RCC.

References (Part II)

- Abraham, F., 1974. *Homogeneous Nucleation Theory*. Academic Press, Cambridge, MS (USA).
- Achternbosch, M., Richers, U., 2002. *Material flows and investment costs of flue gas cleaning systems of municipal solid waste incinerators*. Technical report, Forschungszentrum Karlsruhe.
- Acquistapace, C., Marini, A., Corrente, D., 2014. *Double filtration: a new design to get outstanding performances (in Italian)*. La Termotecnica LXVIII (2), 57-60.
- Allal, K.M., Dolignier, J.C., Martin, G., 1998. *Reaction Mechanism of Calcium Hydroxide with Gaseous Hydrogen Chloride*. Oil & Gas Science and Technology 53, 871-880.
- Antonioni, G., Sarno, F., Guglielmi, D., Morra, P., Cozzani, V., 2011. *Simulation of a two-stage dry process for the removal of acid gases in a MSWI*. Chemical Engineering Transactions 24, 1063-1068.
- Antonioni, G., Guglielmi, D., Stramigioli, C., Cozzani, V., 2012. *MSWI flue gas two-stage dry treatment: modeling and simulation*. Chemical Engineering Transactions 26, pp. 213-218.
- Antonioni, G., Guglielmi, D., Cozzani, V., Stramigioli, C., Corrente, D., 2014. *Modelling and simulation of an existing MSWI flue gas two-stage dry treatment*. Process Safety and Environmental Protection 92, 242-250.
- Arena, U., 2015. *From waste-to-energy to waste-to-resources: The new role of thermal treatments of solid waste in the Recycling Society*. Waste Management 37, 1-2.
- ARPA, 2011. *Environmental data yearbook – Emilia Romagna* (in Italian). Available at: www.arpa.emr.it/dettaglio_documento.asp?id=4638&idlivello=1528 (last accessed: 14/03/2016)
- Astrup, T.F., Riber, C., Pedersen, A.J., 2011. *Incinerator performance: effects of changes in waste input and furnace operation on air emissions and residues*. Waste Management and Research 29 (10), 57-68.
- Astrup, T.F., Tonini, D., Turconi, R., Boldrin, A., 2015. *Life cycle assessment of thermal waste-to-energy technologies: review and recommendations*. Waste Management 37, 104-115.
- ATOR, 2008. *Studio di localizzazione del termovalorizzatore della zona Nord della provincia di Torino* (in Italian), Chapter 3. Available at: http://www.atorifiutitorinese.it/index.php?option=com_content&task=view&id=81&Itemid=95 (last accessed: 8/07/2015)
- Azapagic, A., Clift, R., 1999a. *The application of life cycle assessment to process optimisation*. Computer and Chemical Engineering 23 (10), 1509-1526.
- Azapagic, A., Clift, R., 1999b. *Life cycle assessment and multiobjective optimisation*. Journal of Cleaner Production 7 (2), 135-143.
- Azapagic, A., 1999c. *Life cycle assessment and its application to process selection, design and optimisation*. Chemical Engineering Journal 73 (1), 1-21.
- Bak., J., Larsen, A., 1995. *Quantitative gas analysis with FT-IR: a method for CO calibration using partial least-squares with linearized data*. Applied Spectroscopy 49, 437-443.
- Barba, D., Brandani, F., Capocelli, M., Luberti, M., Zizza, A., 2015. *Process analysis of an industrial waste-to-energy plant: theory and experiments*. Process Safety and Environmental Protection 96, 61-73.
- Bausach, M., Pera-Titus, M., Fite, C., Cunill, F., Izquierdo, J.F., Tejero, J., Iborra, M., 2006. *Water-induced rearrangement of Ca(OH)₂ (0001) surfaces reacted with SO₂*. AIChE Journal 52, 2876-2886.
- Bertin Technologies, 2000. *Feasibility study of the salt mines storage route. Step 1 Report – Appraisal of the salt mines storage route for residues from incineration*. Available at: http://www.pvc.org/upload/.../Salt_Mines_Step_1.pdf (last accessed: 8/07/2015)

- Bhatia, S.K., Perlmutter, D.D., 1982. *The Effect of Pore Structure on Fluid-Solid Reactions: Application to the SO₂-Lime Reaction*. AIChE Journal 27, 226-234.
- Bichisecchi, M., 2014. *Design of a treatment plant for residue salt solutions from ENEL power plants* (in Italian). Thesis dissertation. University of Pisa, Italy.
- Biganzoli, L., Racanella, G., Rigamonti, L., Marras, R., Grossi, M., 2015. *High temperature abatement of acid gases from waste incineration. Part I: Experimental tests in full scale plants*. Waste Management 36, 98-105.
- Biganzoli, L., Racanella, G., Marras, R., Rigamonti, L., 2015. *High temperature abatement of acid gases from waste incineration. Part II: Comparative life cycle assessment study*. Waste Management 35, 127-134.
- Block, C., Van Caneghem, J., Van Brecht, A., Wauters, G., Vandecasteele, C., 2015. *Incineration of Hazardous Waste: A Sustainable Process?* Waste and Biomass Valorization 6, 137-145.
- Bodéan, F., Deniard, P., 2003. *Characterization of flue gas cleaning residues from European solid waste incinerators: Assessment of various Ca-based sorbent processes*. Chemosphere 51, 335-347.
- Bogush, A., Stegemann, J.A., Wood, I., Roy, A., 2015. *Element composition and mineralogical characterisation of air pollution control residue from UK energy-from-waste facilities*. Waste Management 36, 119-129.
- Borgwardt, R.H., 1989. *Sintering of nascent calcium oxide*. Chemical Engineering Science 44, 53-60.
- Borgwardt, R.H., Bruce, K.R., Blake, J., 1987. *An Investigation of Product-Layer Diffusivity for CaO Sulfation*. Industrial and Engineering Chemistry Research 26, 1993-1998.
- BRE, 2008. *Environmental Profiles Methodology*. Building Research Establishment. Available at: www.bre.co.uk/greenguide/page.jsp?id=2106 (last accessed: 14/03/2016)
- Brivio, S., 2005. *The SOLVAL platform: a sodium sludges valorization, an industrial reality for the environment* (in Italian). L'Ambiente 3, 48-49. Available at: www.ranierieditore.it/pdf/solval.pdf (last accessed: 14/03/2016)
- Brivio, S., 2007. *Flue gas cleaning and by-products valorisation* (in Italian). Power Technology, 4, pp. 42-44.
- Carberry, J.J., 1976. Chemical and catalytic reaction engineering. McGraw-Hill, New York (USA).
- CEWEP, 2008. Life Cycle Assessment of the treatment of MSW in the average European Waste-to-Energy plant. Available at: www.cewep.eu/media/www.cewep.eu/org/med_529/372_LCA_Jan_Manders.pdf (last accessed: 14/03/2016)
- Chemical Market Reporter, 2006. *Indicative Chemical Prices A-Z*. Available at: <http://www.icis.com/chemicals/channel-info-chemicals-a-z/> (last accessed: 8/07/2015)
- Chin, T., Yan, R., Liang, D.T., 2005a. *Study of the Reaction of Lime with HCl under Simulated Flue Gas Conditions Using X-ray Diffraction Characterization and Thermodynamic Prediction*. Industrial and Engineering Chemistry Research 44, 8730-8738.
- Chin, T., Yan, R., Liang, D.T., Tay, J.H., 2005. *Hydrated lime reaction with HCl under simulated flue gas conditions*. Industrial and Engineering Chemistry Research 44, 3742-3748.
- Chisholm, P.N., Rochelle, G.T., 1999. *Dry absorption of HCl and SO₂ with hydrated lime from humidified flue gas*. Industrial and Engineering Chemistry Research 38, 4068-4080.
- CML, 2016. *CML-IA Characterisation Factors*. Institute of Environmental Sciences (CML), Universiteit Leiden. Available at: www.universiteitleiden.nl/en/research/research-output/science/cml-ia-characterisation-factors (last accessed: 14/03/2016)

- Cooper, C.D., Alley, F.C., 2010. *Air Pollution Control: A Design Approach*. 4th edition, Waveland Press Inc., Long Grove, IL (USA).
- Dal Pozzo, A., Antonioni, G., Guglielmi, D., Stramigioli, C., Cozzani, V., 2016. *Comparison of alternative flue gas dry treatment technologies in waste-to-energy processes*. Waste Management 51, 81-90.
- Damgaard, A., Riber, C., Fruergaard, T., Hulgaard, T., Christensen, T.H., 2010. *Life-cycle-assessment of the historical development of air pollution control and energy recovery in waste incineration*. Waste Management 30, 1244-1250.
- Daoudi, M., Walters, J.K., 1991. *The reaction of HCl gas with calcined commercial limestone particles: The effect of particle size*. The Chemical Engineering Journal 47, 11–16.
- De Greef, J., Villani, K., Goethals, J., Van Belle, H., Van Caneghem, J., Vandecasteele, C., 2013. *Optimising energy recovery and use of chemicals, resources and materials in modern waste-to-energy plants*. Waste Management 33, 2416–2424.
- Dennis, J.S., Pacciani, R., 2009. *The rate and extent of uptake of CO₂ by a synthetic, CaO-containing sorbent*. Chemical Engineering Science 64, 2147–2157.
- Directive, 2010/75/UE of the European Parliament and of the Council of 24 November 2010 on industrial emissions (Integrated Pollution Prevention and Control). Available at: eur-lex.europa.eu/legal-content/EN/TXT/PDF/?uri=CELEX:32010L0075&from=EN (last accessed: 14/03/2016)
- D.Lgs. 152/2006. *Norme in materia ambientale* (in Italian). Gazz. Uff. 88, 14 aprile 2006, n. 96, S.O. Available at: <http://www.camera.it/parlam/leggi/delegehe/06152dl.htm> (last accessed: 8/07/2015)
- Duo, W., Seville, J.P.K., Kirkby, N.F., Clift, R., 1993. *Prediction of Dry Scrubbing Process Performance*. in: Clift, R., Seville, J.P.K. (Ed.). *Gas Cleaning at High Temperatures*. Springer (The Netherlands), pp. 644-662.
- Duo, W., Seville, J.P.K., Kirkby, N.F., Clift, R., 1994. *Formation of product layers in solid-gas reactions for removal of acid gases*. Chemical Engineering Science 49, 4429–4442.
- Duo, W., Kirkby, N.F., Seville, J.P.K., Clift, R., 1995. *Alteration with reaction progress of the rate limiting step for solid-gas reactions of Ca-compounds with HCl*. Chemical Engineering Science 50, 2017–2027.
- Duo, W., Kirkby, N.F., Seville, J.P.K., Kiel, J.H.A., Bos, A., Den Uil, H., 1996. *Kinetics of HCl reactions with calcium and sodium sorbents for IGCC fuel gas cleaning*. Chemical Engineering Science 51 (11), 2541-2546.
- Duo, W., Laursen, K., Lim, J., Grace, J., 2000. *Crystallization and fracture: formation of product layers in sulfation of calcined limestone*. Powder Technology 111, 154–167.
- Duo, W., Laursen, K., Lim, J., Grace, J., 2004. *Crystallization and Fracture: Product Layer Diffusion in Sulfation of Calcined Limestone*. Industrial and Engineering Chemistry Research 43 (18), 5653-5662.
- EC-JRC, 2011. *International Reference Life Cycle Data System (ILCD) Handbook Recommendations for Life Cycle Impact Assessment in the European Context*. European Commission and Joint Research Center. 1st edition. Available at: eplca.jrc.ec.europa.eu/?page_id=86 (last accessed: 14/03/2016)
- ELCD, 2016. *European reference Life Cycle Database*. Available at: eplca.jrc.ec.europa.eu/ELCD3/index.xhtml (last accessed: 14/03/2016)
- ENEA, 2008. *Energy balance report – Emilia Romagna* (in Italian). Available at: www.enea.it/it/pubblicazioni/rapporto-energia-e-ambiente-1/rapporto-energia-e-ambiente-2009-2010/i-dati-2009-2010/statistiche-regionali (last accessed: 14/03/2016)
- EPA, 2002. *Air Pollution Control Cost Manual*. 6th edition, Environmental Protection Agency (USA).

European Commission, 2003. *Council decision of 19 December 2002 establishing criteria and procedures for acceptance of waste at landfills pursuant to Article 16 and Annex II to Directive 1999/31/EC*. Available at: eur-lex.europa.eu/legal-content/EN/TXT/?uri=CELEX%3A32003D0033 (last accessed: 14/03/2016)

European Commission, 2006. *BREF on Waste Incineration (WI)*. Available at: eippcb.jrc.ec.europa.eu/reference/BREF/wi_bref_0806.pdf (last accessed: 14/03/2016)

European Commission, 2007. *BREF on Large Volume Inorganic Chemicals - Solids and Others industry (LVIC-S)*. Available at: eippcb.jrc.ec.europa.eu/reference/BREF/lvic-s_bref_0907.pdf (last accessed: 14/03/2016)

European Commission, 2015. *Closing the loop - An EU action plan for the Circular Economy*. Available at: eur-lex.europa.eu/legal-content/EN/TXT/?uri=CELEX:52015DC0614 (last accessed: 14/03/2016)

EUROSTAT, 2016. *Statistics illustrated*. Available at: www.ec.europa.eu/eurostat/web/population-demography-migration-projections/statistics-illustrated (last accessed: 04/09/2016)

Ferguson, A., 1928. *Surface tensions of fused salts above 200 °C and liquids above 360 °C*. in: Washburn, E.W. (Ed.). *International Critical Tables of Numerical Data, Physics, Chemistry and Technology*. McGraw-Hill, New York, NY (USA).

Fletcher, N.H., 1958. *Size Effect in Heterogeneous Nucleation*. Journal of Chemical Physics 29, 572-576.

Fogler, H.S., 2005. *Elements of chemical reaction engineering*, 4th edition, Prentice Hall (USA).

Fonseca, A.M., Orfao, J.J., Salcedo, R.L., 1998. *Kinetic modeling of the reaction of HCl and solid lime at low temperatures*. Industrial and Engineering Chemistry Research 37, 4570-4576.

Fonseca, A.M., Orfao, J.J., Salcedo, R.L., 2001. *Dry Scrubbing of Gaseous HCl with Solid Lime in a Cyclone Reactor at Low Temperatures*. Industrial and Engineering Chemistry Research 40, 304-313.

Fruergaard, T., Hyks, J., Astrup, T., 2010. *Life-cycle assessment of selected management options for air pollution control residues from waste incineration*. Science of the Total Environment 408 (20), 4672-4680.

Gbor, P.K., Jia, C.Q., 2004. *Critical evaluation of coupling particle size distribution with the shrinking core model*. Chemical Engineering Science 59, 1979-1987.

Gilman, J.J., 1960. *Direct Measurements of the Surface Energies of Crystals*. Journal of Applied Physics 31, 2208-2218.

Green, D., Perry, R., 2007. *Perry's Chemical Engineers' Handbook*, 8th edition, McGraw-Hill (USA).

Guglielmi, D., 2014. *Analysis and modelling of the performance of technologies for flue gas treatment in Waste-to-Energy processes*. PhD dissertation, DICAM, University of Bologna.

Guglielmi, D., Antonioni, G., Stramigioli, C., Cozzani, V., 2014. *Investigation of performance of different sorbents in a two-stage flue gas dry treatment of a MSWI*. Chemical Engineering Transactions 36, 187-192.

Gullett, B.K., Jozewicz, W., Stefanski, L.A., 1992. *Reaction Kinetics of Ca-Based Sorbents with HCl*. Industrial and Engineering Chemistry Research 31, 2437-2446.

Gutiérrez Ortiz, F.J., Ollero, P., 2008. *Modeling of the in-duct sorbent injection process for flue gas desulfurization*. Separation and Purification Technology 62, 571-581.

Harker, J.H., Backhurst, J.R., Richardson, J.F., 2002. *Coulson and Richardson's Chemical Engineering Volume 2 - Particle Technology and Separation Processes*, 5th edition, Butterworth-Heinemann (USA).

Hartman, M., Coughlin, R.W., 1976. *Reaction of Sulfur Dioxide with Limestone and the Grain Model*. AIChE Journal 22, 490-498.

Hartman, M., Svoboda, K., Pohorely, M., Syc, M., 2013. *Thermal Decomposition of Sodium Hydrogen Carbonate and Textural Features of Its Calcines*. Industrial and Engineering Chemistry Research 52, 10619-10626.

- Heesink, A. B. M., Prins, W., van Swaaij, W. P. M., 1993. *A grain size distribution model for non-catalytic gas-solid reactions*. The Chemical Engineering Journal 53, 25-37.
- Heijungs, R., Kleijn, R., 2011. *Numerical Approaches Towards Life Cycle Interpretation – Five Examples*. International Journal of Life Cycle Assessment 6 (3), 141-148.
- Hofstetter, P., Braunschweig, A., Mettier, T., Muller-Wenk, R., Tietje, O., 1999. *The Mixing Triangle: Correlation and Graphical Decision Support for LCA-based Comparisons*. Journal of Industrial Ecology 3 (4), 97-115.
- Hu, G., Dam-Johansen, K., Wedel, S., 2008. *Oriented Nucleation and Growth of Anhydrite during Direct Sulfation of Limestone*. Crystal Growth & Design 8.
- Huppkes, G., van Oers, L., Pretato, U., Pennington, D.W., 2012. *Weighting environmental effects: Analytic survey with operational evaluation methods and a meta-method*. International Journal of Life Cycle Assessment 17, 876-891.
- IEA, 2000. *The management of residues from thermal processes*. Bioenergy Task 36 report. Available at: http://www.ieabioenergytask36.org/publications_1998_2000.htm (last accessed: 8/07/2015)
- ISO, 2006a. *ISO 14044: Environmental Management – Life Cycle Assessment – Requirements and Guidelines*. International Organization for Standardization.
- ISO, 2006b. *ISO 14040: Environmental Management – Life Cycle Assessment – Principles and Framework*. International Organization for Standardization.
- ISO, 2012. *ISO/TR 14047: Environmental management -- Life cycle assessment -- Illustrative examples on how to apply ISO 14044 to impact assessment situations*. International Organization for Standardization.
- ISPRA, 2013. *Urban waste report - edition 2013* (in Italian). Available at: www.isprambiente.gov.it/it/pubblicazioni/rapporti/rapporto-rifiuti-urbani-edizione-2013 (last accessed: 14/03/2016)
- ISTAT, 2016. *Demography in Figures*. Available at: www.demo.istat.it/index_e.html (last accessed: 04/09/2016)
- ISWA, 2003. *Position Paper on handling of APC residues*. Available at: http://www.iswa.org/index.php?eID=tx_iswaknowledgebase_download&documentUid=102 (last accessed: 8/07/2015)
- ISWA, 2008. *Management of APC residues from WtE plants – an overview of management options and treatment methods*. International Solid Waste Association. Available at: www.iswa.org/uploads/tx_iswaknowledgebase/Management_of_APC_residues_from_WtE_Plants_2008_01.pdf (last accessed: 14/03/2016)
- ISWA, 2012. *Waste-to-Energy – State-of-the-art report*. 6th edition, International Solid Waste Association.
- John, V., Angelov, I., Oncul, A.A., Thévenin, D., 2007. *Techniques for the reconstruction of a distribution from a finite number of its moments*. Chemical Engineering Science 62, 2890-2904.
- Jozewicz, W., Gullett, B.K., 1995. *Reaction Mechanisms of Dry Ca-Based Sorbents with Gaseous HCl*. Industrial and Engineering Chemistry Research 34, 607-612.
- Kaiser, S., Weigl, K., Spiess-Knafl, K., Aichernig, C., Friedl, A., 2000. *Modeling a dry-scrubbing flue gas cleaning process*. Chemical Engineering and Processing: Process Intensification 39, 425-432.
- Karlsson, H.T., Klingspor, J., Bjerle, I., 1981. *Adsorption of Hydrochloric Acid on Solid Slaked Lime for Flue Gas Clean Up*. Journal of the Air Pollution Control Association 31, 1177-1180.
- Kavouras, A., Breitschaedel, B., Krammer, G., Garea, A., Marques, J.A., Irabien, A., 2002. *SO₂ Removal in the Filter Cake of a Jet-Pulsed Filter: A Combined Filter and Fixed-Bed Reaction Model*. Industrial and Engineering Chemistry Research 41, 5459-5469.

- Kendall, K., Alford, N.M., Birchall, J.D., 1987. *A new method for measuring the surface energy of solids*. Nature 325, 794-796.
- Kierzkowska, A.M., Pacciani, R., Müller, C.R., 2013. *CaO-Based CO₂ Sorbents: From Fundamentals to the Development of New, Highly Effective Materials*. ChemSusChem 6, 1130-1148.
- Koch, M., Zhang, X., Deng, J., Kavouras, A., Krammer, G., Ge, L., 2005. *Reaction mechanism of a single calcium hydroxide particle with humidified HCl*. Chemical Engineering Science 60, 5819–5829.
- Komilis, D., Evangelou, A., Giannakis, G., Lympertis, C., 2012. *Revisiting the elemental composition and the calorific value of the organic fraction of municipal solid wastes*. Waste Management 32, 372-381.
- Land, N.S., 1972. *A Compilation of Nondimensional Numbers*. Scientific and Technical Information Office, National Aeronautics and Space Administration, Washington, DC, USA.
- LEAP, 2009. *Energy and environmental analysis of the solid waste management system in the province of Piacenza* (in Italian). Available at: www.tecnoborgo.com/docs/LEAP_Analisi_energetica_ambientale_rifiuti_solidi_161209.pdf (last accessed: 14/03/2016)
- Levenspiel, O., 1998. *Chemical Reaction Engineering*. 3rd edition, John Wiley & Sons (USA).
- Li, M., Shaw, H., Yang, C.-L., 2000. *Reaction Kinetics of Hydrogen Chloride with Calcium Oxide by Fourier Transform Infrared Spectroscopy*. Industrial and Engineering Chemistry Research 39, 1898-1902.
- Li, S., Bie, R., 2006. *Modeling the reaction of gaseous HCl with CaO in fluidized bed*. Chemical Engineering Science 61, 5468–5475.
- Liuzzo, G., Verdone, N., Bravi, M., 2007. *The benefits of flue gas recirculation in waste incineration*. Waste Management 27, 06-116.
- Lostorto, M., 2009. *Ottimizzazione pool combustibili per consumi interni di una raffineria, in relazione agli aspetti economici ed ambientali* (in Italian). Thesis dissertation, University of Bologna.
- Manders, J., 2009. *Life cycle assessment of the treatment of MSW in “the average” European Waste-to-Energy plant*. 6th Beacon Conf. on Waste-to-Energy, Malmoe, 24/11/2009. Available at: http://www.beacon-wte.net/fileadmin/avfallsverige/Documentation_2009/J._Manders.pdf (last accessed: 8/07/2015)
- Mapelli, A., 2014. *The Plasmix gasification process* (in Italian). 5th National Conference on Chemistry and Energy, Milano, 28/10/2014. Available at: www.federchimica.it/docs/default-source/eventi-102014-5conferenzachimicaenergia/Alessandro_Mapelli_Corepla.pdf (last accessed: 14/03/2016)
- Margallo, M., Aldaco, R., Irabien, A., Carrillo, V., Fischer, M., Bala, A., Fullana, P., 2014. *Life cycle assessment modelling of waste-to-energy incineration in Spain and Portugal*, Waste Management and Research 32, 492-499.
- Margallo, M., Taddei, M.B.M., Hernández-Pellón, A., Aldaco, R., Irabien, A., 2015. *Environmental sustainability assessment of the management of municipal solid waste incineration residues: A review of the current situation*. Clean Technology and Environmental Policy 17, 1333-1353.
- Marocco, L., Mora, A., 2013. *CFD modeling of the Dry-Sorbent-Injection process for flue gas desulfurization using hydrated lime*. Separation and Purification Technology 108, 205-214.
- Matches, 2015. *Matches’ Process Equipment Cost Estimates*. Available at: <http://www.matche.com> (last accessed: 8/07/2015)
- Maya, J.C., Chejne, F., 2014. *Modeling of Oxidation and Reduction of a Copper-Based Oxygen Carrier*. Energy & Fuels 28, 5434-5444.
- Maya, J.C., Chejne Janna, F., 2016. *Novel model for non catalytic solid-gas reactions with structural changes by chemical reaction and sintering*. Chemical Engineering Science 142, 258-268.

Møller, J., Munk, B., Crillesen, K., Christensen, T.H., 2011. *Life cycle assessment of selective non-catalytic reduction (SNCR) of nitrous oxides in a full-scale municipal solid waste incinerator*. Waste Management 31 (6), 1184-1193.

Mura, G., Lallai, A., 1994. *Reaction kinetics of gas hydrogen chloride and limestone*. Chemical Engineering Science 49, 4491-4500.

Nethe, L.P., 2008. *Hydrated lime vs. sodium bicarbonate (in German)*. Vortrag auf der 4. Fachtagung Trockene Abgasreinigung, Haus der Technik, Essen 13-14 Nov 2008.

Niessen, W.R., 2010. *Combustion and Incineration Processes: Applications in Environmental Engineering*. 4th edition, CRC Press, Boca Raton, FL (USA).

Ninane, L., Adam, J.F., Humblot, C., 1995. *Method for producing an aqueous industrial sodium chloride solution*. U.S. Patent 5478447A.

NIST, JANAF Thermochemical Tables.

NIST, NIST Chemistry WebBook.

Nizami A.S., Shahzad, K., Rehan, M., Ouda, O.K.M., Khan, M.Z., Ismail, I.M.I., Almeelbi, T., Basahi, J.M., Demirbas, A., 2016. *Developing waste biorefinery in Makkah: a way forward to convert urban waste into renewable energy*. Applied Energy 61, 328-340.

Norris, G.A., 2001. *The requirement for congruence in normalization*. International Journal of Life Cycle Assessment 6 (2), 85-88.

OECD, 2015. *Monthly comparative price levels*. Available at: <http://stats.oecd.org/Index.aspx?DataSetCode=CPL> (last accessed: 8/07/2015)

Ouda, O.K.M., Raza, S.A., Nizami, A.S., Rehan, M., Al-Waked, R., Korres, N.E., 2016. *Waste to energy potential: a case study of Saudi Arabia*. Renewable and Sustainable Energy Reviews 61, 328-340.

Özarslan, A., Martens, P.N., Olbrich, T., Röhrlich, M., 2001. *Underground disposal of hazardous wastes in German mines*. 17th International Mining Congress and Exhibition of Turkey- IMCET2001.

Paolucci, N., Bezzo, F., Tugnoli, A., 2016. *A two-tier approach to the optimization of a biomass supply chain for pyrolysis processes*. Biomass and Bioenergy 84, 87-97.

Partanen, J., Backman, P., Backman, R., Hupa, M., 2005. *Absorption of HCl by limestone in hot flue gases. Part II: importance of calcium hydroxychloride*. Fuel 84, 1674-1684.

Patek, J., Klomfar, J., Souckova, M., 2008. *Solid-Liquid Equilibrium in the System of CaCl₂-H₂O with Special Regard to the Transition Points*. Journal of Chemical Engineering Data 53, 2260-2271.

Patel, C., Lettieri, P., Germanà, A., 2012. *Techno-economic performance analysis and environmental impact assessment of small to medium scale SRF combustion plants for energy production in the UK*. Process Safety and Environmental Protection 90, 255-262.

Petchers, N., 2003. *Combined Heating, Cooling & Power Handbook: Technologies & Applications – an Integrated Approach to Energy Resource Optimization*. The Fairmont Press Inc. (USA).

Peters, M.S., Timmerhaus, K.D., 2002. *Plant Design and Economics for Chemical Engineers*. 5th edition, McGraw-Hill, New York, NY (USA).

Petersen, C.M., Berg, P.E.O., Ronnegard, L., 2005. *Quality control of waste to incineration – waste composition analysis in Lidköping, Sweden*. Waste Management and Research 23, 527-533.

PRé Consultants, 2000. *The Eco-indicator 99, a damage oriented method for Life Cycle Impact Assessment – Methodology Report*. 2nd edition. Available at: www.pre-sustainability.com/download/EI99_annexe_v3.pdf (last accessed: 14/03/2016)

- Prigiobbe, V., A. Polettini, Baciocchi, R., 2009. *Gas-solid carbonation kinetics of Air Pollution Control residues for CO₂ storage*. Chemical Engineering Journal 148, 270-278.
- Quicker, P., Rotheut, M., Noël, Y., Schulten, M., Athmann, U., 2014. *Treating WTE Flue Gases with Sodium Bicarbonate*. Power Magazine 158 (8), 59-63.
- Quina, M.J., Bordado, J.C., Quinta-Ferreira, R.M., 2008. *Treatment and use of air pollution control residues from MSW incineration: an overview*. Waste Management 28 (11), 2097-2121.
- Randall, D., Shoraka-Blair, S., 1994. An evaluation of the cost of incinerating wastes containing PVC. ASME Research Report, CRTD 31.
- Rigamonti, L., Grossi, M., Biganzoli, L., 2012. *Environmental Assessment of Refuse-Derived Fuel Co-Combustion in a Coal-Fired Power Plant*. Journal of Industrial Ecology 16 (5), 748-760.
- Rigo, H.G., Chandler, A.J., Lanier, W.S., 1995. *The relationship between chlorine in waste stream and dioxin emissions from waste combustor stacks*. ASME Research Report, CRTD 36.
- Ruthven, D.M., 1984. *Principles of adsorption and adsorption processes*. Wiley, New York, NY (USA).
- Rylander, H., 1997. *The evolution of WtE utilization – the European perspective*. Proceedings of the 5th Annual North American Waste-to-Energy Conference, Research Triangle Park 22-25 Apr 1997.
- Scipioni, A., Mazzi, A., Niero, M., Boatto, T., 2009. *LCA to choose among alternative design solutions: the case study of a new Italian incineration line*. Waste Management 29, 2462-2474.
- Sedlak, R., 1991. *Phosphorus and nitrogen removal from municipal wastewater: principles and practice*. CRC Press (USA).
- Shemwell, B., Levendis, Y.A., Simons, G.A., 2001. *Laboratory study on the high-temperature capture of HCl gas by dry-injection of calcium-based sorbents*. Chemosphere 42, 785-796.
- Simons, G.A., Garman, A.R., 1986. *Small pore closure and the deactivation of the limestone sulfation reaction*. AIChE Journal 32, 1491-1499.
- Sinnott, R., 2005. *Coulson & Richardson's Chemical Engineering Design* (vol. 6). 4th edition, Butterworth-Heinemann (USA).
- Smith, J.M., 1981. *Chemical Engineering Kinetics*. 3rd edition, McGraw-Hill, New York, NY (USA).
- Solvay, 2014. *SOLVAir Solutions - Clean Air Sustainable Recycling*. Available at: www.solvairsolutions.com/fr/binaries/brochure_solvair-en-2014-222496.pdf (last accessed: 01/09/2016)
- Solvay Chemicals North America, 2015. *Soda Ash*. Available at: <http://www.solvaychemicals.us/EN/Products/sodiumproducts/sodaash.aspx> (last accessed: 8/07/2015)
- Sorrell, S., 2002. *The meaning of BATNEEC: interpreting excessive costs in UK industrial pollution regulation*. Journal of Environmental Policy and Planning 4 (1), 23-40.
- Stasiulaitiene, I., Martuzevicius, D., Abromaitis, V., Tichonovas, M., Baltrusaitis, J., Brandenburg, R., Pawelec, A., Schwock, A., 2016. *Comparative life cycle assessment of plasma-based and traditional exhaust gas treatment technologies*. Journal of Cleaner Production 112 (2), 1804-1812.
- Stendardo, S., Di Felice, L., Gallucci, K., Foscolo, P.U., 2011. *CO₂ capture with calcined dolomite: the effect of sorbent particle size*. Biomass Conversion and Biorefinery 1, 149-161.
- Stendardo, S., Foscolo, P.U., 2010. *Carbon dioxide capture with dolomite: A model for gas-solid reaction within the grains of a particulate sorbent*. Chemical Engineering Science 64, 2343-2352.
- Swedish Life Cycle Center, 2014. *CPM LCA Database*. Available at: cpmdatabase.cpm.chalmers.se (last accessed: 14/03/2016)
- Szekely, J., Evans, J.W., Sohn, H.Y., 1976. *Gas-Solid Reactions*. Academic Press, London (UK).

- Themelis, N.J., 2005. *Chloride Balance in a Waste to Energy Facility*. Technical report, WTERT.
- Thipkhunthod, P., Meeyoo, V., Rangsuvigit, P., Kitiyanan, B., Siemanond, K., Rirksomboon, T., 2005. *Predicting the heating value of sewage sludges in Thailand from proximate and ultimate analyses*. Fuel 84, 849-857. DOI: 10.1016/j.fuel.2005.01.003
- Tipler, P. A., Llewellyn, R.A., 2012. *Modern Physics*. W.H. Freeman & Co., New York, NY (USA).
- Tugnoli, A., Santarelli, F., Cozzani, V., 2008. *An Approach to Quantitative Sustainability Assessment in the Early Stages of Process Design*. Environmental Science and Technology 42, 4555-4562.
- Tugnoli, A., Santarelli, F., Cozzani, V., 2011. *Implementation of Sustainability Drivers in the Design of Industrial Chemical Processes*. AIChE Journal 57 (11), 3063-3084. DOI: 10.1002/aic.12497
- UBA, 2013. *Sewage sludge management in Germany*. Umwelt Bundesamt. Available at: www.umweltbundesamt.de/en/publikationen/sewage-sludge-management-in-germany (last accessed: 14/03/2016)
- USGS, 2012. *Minerals Yearbook 2012 – lime*. United States Geological Survey. Available at: minerals.usgs.gov/minerals/pubs/commodity/lime/ (last accessed: 14/03/2016)
- Valverde, J.M., 2013. *Ca-based synthetic materials with enhanced CO₂ capture efficiency*. Journal of Materials Chemistry A 1, 447-468.
- Van Caneghem, J., De Greef, J., Block, C., Vandecasteele, C., 2016. *NO_x reduction in waste incinerators by selective catalytic reduction (SCR) instead of selective non catalytic reduction (SNCR) compared from a life cycle perspective: a case study*. Journal of Cleaner Production 112 (5), 4452-4460.
- Vatavuk, W.M., 1990. *Estimating costs of air pollution control*. CRC Press (USA).
- Vehlow, J., 2015. *Air pollution control systems in WtE units: an overview*. Waste Management 37, 58-74.
- Verdone, N., De Filippis, P., 2004. *Thermodynamic behaviour of sodium and calcium based sorbents in the emission control of waste incinerators*. Chemosphere 54, 975-985.
- Verdone, N., De Filippis, P., 2006. *Reaction kinetics of hydrogen chloride with sodium carbonate*. Chemical Engineering Science 61, 7487-7496.
- Viganò, F., Consonni, S., Grosso, M., Rigamonti, L., 2010. *Material and energy recovery from Automotive Shredded Residues (ASR) via sequential gasification and combustion*. Waste Management 30, 145–153.
- Wachtman, J.B., Tefft, W.E., Lam, D.G., Apstein, C.S., 1961. *Exponential Temperature Dependence of Young's Modulus for Several Oxides*. Physical Review 122, 1754-1759.
- Wang, L.C., Lee, W.J., Lee, W.S., Chang-Chien G.P., Tsai, P.J., 2003. *Effect of chlorine content in feeding wastes of incineration on the emission of polychlorinated dibenzo-p-dioxins/dibenzofurans*. Science of the Total Environment 302, 185-198.
- Wang, N., Teng, B., 2009. *Modeling of SO₂ removal in fabric filter*. Fuel Processing Technology 90, 636-642.
- Wang, W., Li, Y., Xie, X., Sun, R., 2014. *Effect of the presence of HCl on cyclic CO₂ capture of calcium-based sorbent in calcium looping process*. Applied Energy 125, 246-253.
- Weidema, B.P., Wesnæs, M.S., 1996. *Data quality management for life cycle inventories — an example of using data quality indicators*. Journal of Cleaner Production 4, 167–174.
- Weinell, C.E., Jensen, P.I., Dam-Johansen, K., Livbjerg, H., 1992. *Hydrogen chloride reaction with lime and limestone: kinetics and sorption capacity*. Industrial and Engineering Chemistry Research 31, 164-171.
- Wojdyga, K., Chorzelski, M., Rozycza-Wronska, E., 2014. *Emission of pollutants in flue gases from Polish district heating sources*. Journal of Cleaner Production 75, 157-165.

- Wolberg, J., 2006. *Data Analysis Using the Method of Least Squares*. Springer, Berlin (Germany).
- Yan, R., Chin, T., Liang, D.T., Laursen, K., Ong, W.Y., Yao, K., Tay, J.H., 2003. *Kinetic study of hydrated lime reaction with HCl*. Environmental Science and Technology 37, 2556-2562.
- Yang, Y.B., Ryu, C.K., Khor, A., Yates, N.E., Sharifi, V.N., Swithenbank, J., 2005. *Effect of fuel properties on biomass combustion, Part II. Modelling approach—identification of the controlling factors*. Fuel 84, 1039–1046.
- Yassin, L., Lettieri, P., Simons, S.J.R., Germana, A., 2007. *Study of the process design and flue gas treatment of an industrial-scale energy-from-waste combustion plant*. Industrial and Engineering Chemistry Research 46, 2648-2656.

Part III

Application to CO₂ capture by MgO-based sorbents

Sections 9.3 to 9.5 and chapter 10 report the research activity carried out during a 6-month stay at the Laboratory of Energy Science and Engineering, ETH Zürich (Switzerland), under the supervision of Prof. C.R. Müller.

9 Development of MgO-based sorbents

9.1 Alternatives to limestone in carbonate looping technologies

As introduced in section 3.3, carbonate looping is a potentially cost-effective solution to CO₂ capture, thanks to the lower energy penalty compared to amine scrubbing and the use of an inexpensive and widely available natural sorbent such as limestone (i.e. the calcium oxide, CaO, obtainable from limestone calcination). However, as mentioned in section 4.1, the extent of CaO carbonation suffers a relatively fast decline, resulting in a molar conversion of CaO to CaCO₃ of 8–10% after 20 or 30 cycles of carbonation/regeneration, due to sintering during high-temperature calcination (Blamey et al., 2010). Different limestones show qualitatively the same decay over a number of cycles (Grasa and Abanades, 2006), with the high temperature and high CO₂ partial pressure encountered in the calcination step as the main causes determining the loss of performance (Manovic et al., 2009). Therefore, increasing the CO₂ uptake and reducing the deactivation rate of CaO are the main targets in order to increase the economic attractiveness of carbonate looping systems (MacKenzie et al., 2007). Two main lines of research, summarised hereunder, stem from these considerations.

Modified Ca-based sorbents. Methods such as hydration (Manovic and Anthony, 2007) or thermal treatment (Manovic and Anthony, 2008) can promote the carbonation of limestone, but superior performance for Ca-based sorbents can be mainly achieved by sorbent modification. First, there are natural alternatives to limestone. The CO₂ uptake of the material can be promoted by synthesising Ca-based sorbents with high surface area and pore volume via approaches such as calcination of complex CaO precursors (Lu et al., 2006), sol-gel techniques (Broda et al., 2012), sacrificial templating (Naeem et al., 2016). The reduction of performance decay over cycling can be attained by introducing resistance to sintering, stabilising CaO by means of a support exhibiting high Tammann temperature (T_T, the onset of sintering in ceramic materials). This area of research was inspired by the promising carbonation behaviour of natural dolomite, which is an equimolar mixture of CaCO₃ and MgCO₃. Although, after calcination, only the CaO part of dolomite can be carbonated in the typical Calcium looping conditions, the sintering-resistant MgO fraction (T_T = 1276 °C) acts as a structural agent, preventing the collapse of the pore structure of the sorbent (as already illustrated for the application of calcined dolomite in acid gas removal system; see section 2.4) and producing a remarkably stable CO₂ uptake upon cycling. The drawback of dolomite is that the MgO fraction, inactive for CO₂ capture, amounts to approximately 45 wt. % of the material. The synthesis of supported Ca-based sorbents aims at coupling the effect of stabilisation with the minimisation of the quantity of support added. Hence, several investigators explored the incorporation of support materials like the oxides of Al (Broda and Müller, 2012), Mg (Filitz et al., 2012), Zr (Broda and Müller, 2014) or Y (Naeem et al., 2016) in Ca-based sorbents: a recent review (Kierzkowska et al., 2013) illustrates the most interesting results in the field, but points out the lack of techno-economic assessment demonstrating the feasibility of scaling up the presented synthesis protocols. Routes employing waste materials could help improving the economics of modified Ca-based sorbents while not dramatically depressing performance. Work in section 9.2 aims at speculatively suggesting a possible integration route with the dry acid gas removal process.

Sorbents operating in different carbonation/calcination temperature windows. CaO, the active CO₂ sorbent compound in both limestone and dolomite, shows high carbonation kinetics in the interval 600–700 °C and can be regenerated by calcination at T > 800 °C (Liu et al., 2012). It is of industrial interest to identify alternative sorbents with promising carbonation performance at different temperatures. For example, at temperatures below 100 °C sodium carbonate (Na₂CO₃)

captures CO₂ in the presence of water to form sodium bicarbonate (Nelson et al., 2009), which in turn can be decomposed back to sodium carbonate with a moderate heating up to 130 °C, as discussed in section 2.3 with reference to its application in acid gas removal. Conversely, strontium oxide (SrO) can be carbonated at temperatures higher than 1000 °C and regeneration in pure CO₂ stream requires at least 1200 °C, making it potentially useful for direct furnace sorbent injection applications (Miccio et al., 2016). Magnesium oxide (MgO) represents the solution of choice for the intermediate temperature range (200-300 °C), with regeneration possible at T > 400 °C (Zarghami et al., 2015). Active research efforts in the synthesis and/or modification of CO₂ solid sorbents face different challenges, functions of the inherent sorbent nature: for high-temperature sorbents, fast kinetics is ensured but sintering constitutes a major problem; viceversa, low-to-intermediate temperature sorbents face mild conditions in terms of sintering but generally exhibits a slower kinetics, which has to be somehow “promoted”. The latter case is the rationale behind the investigation of MgO-based CO₂ sorbents which will be explored in sections 9.3-9.5 and chapter 10.

9.2 Use of residues from dry acid gas removal as CO₂ sorbents

As introduced in section 9.1, several investigators focused on the modification of Ca-based sorbents in order to obtain a noteworthy enhancement of CO₂ uptake upon cycling (Kierzkowska et al., 2013), but most complex methods of sorbent modification appear to be prohibitively expensive for scale-up (Erans et al., 2016). Some authors suggested that the use of waste materials – otherwise to be sent to disposal – as sorbents or precursors for modified sorbents could be a potential route for achieving cost-effective improvement of performance. For example, Tian et al. (2015) demonstrated that Fe-functionalised sorbents synthesised starting from slag from the steelmaking process can sustain efficient, autothermal CO₂ capture process.

Taking into account the dry acid gas removal systems studied in Part II of the thesis and, in particular, the Ca(OH)₂-based sorbent injection, it has been shown that the sorbent conversion in the process is far from complete, due to the product layer-related limitations described in sections 6.1 and 6.2. Thus, the Ca-based waste discharged by the process and generally sent to disposal, as described in chapter 8, contains a large amount of unreacted Ca(OH)₂, as well as CaCO₃ generated by the undesired reaction with CO₂ facilitated by the high relative humidity in the flue gas from waste combustion (as recalled in section 7.1). The chemical composition of a typical Ca-based waste (from now on called RCC, in agreement with chapter 8) generated by the Ca-based stage of a two-stage dry acid gas treatment system was analysed by means of thermogravimetric analysis, in analogy to the experiments performed in section 5.5 for the characterisation of the laboratory solid residues of the reaction between Ca(OH)₂ and HCl. The analysed sample was dried at 105 °C under a dry nitrogen flow rate of 60 mL/min for 10 min and then heated up to 900 °C under the same nitrogen purge gas flux at a heating ramp of 10 °C/min. As shown in Figure 9.1, the derivative weight loss curve allows to identify the main components according to their decomposition temperature: unreacted Ca(OH)₂ calcines to CaO in the interval 350-400 °C, CaOHCl decomposes to CaCl₂ at 450 °C (as illustrated in section 5.5), CaCO₃ calcines to CaO at 600 °C and the sulphate phases (CaSO₃ and CaSO₄) show slow decomposition at temperatures higher than 800 °C, in agreement with Bogush et al. (2015). Other weight loss events can be ascribed to degradation of the activated charcoal which is injected in the flue gas system together with Ca(OH)₂. Another relevant fraction of the sample, the fly ash originated from waste combustion (with its potential content of hazardous trace metals), which are inevitably mixed with RCC as a consequence of the typical layout of the flue gas cleaning system in WtE plants, does not undergo thermal degradation.

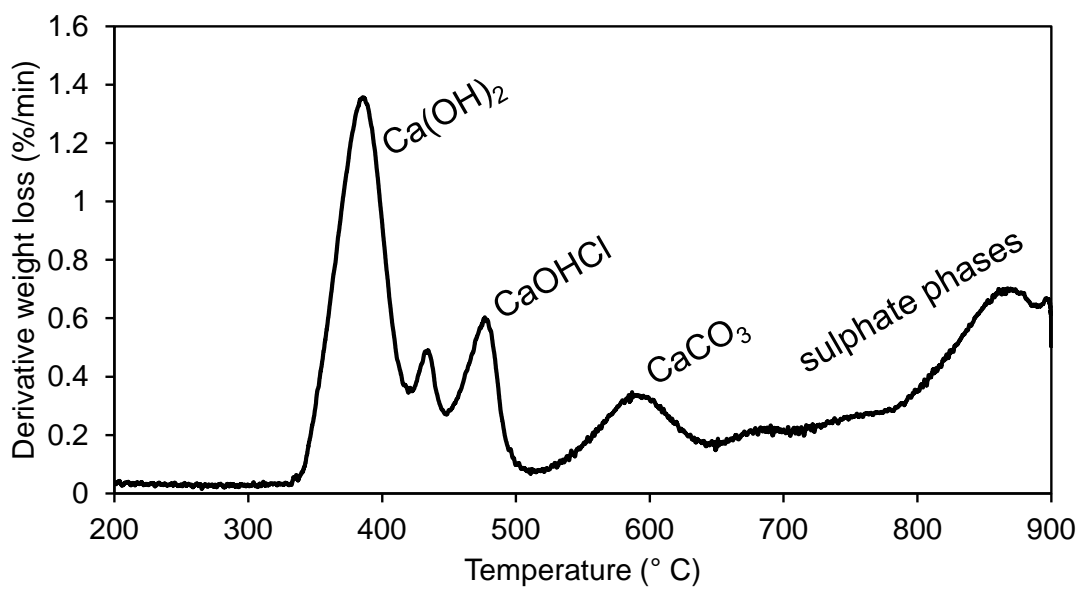


Figure 9.1. Derivative weight loss curve for a RCC sample from the Ca-based stage of a two-stage dry acid gas removal system. Heating up rate: 10 °C/min.

Recently, accelerated carbonation has been considered as a management route for RCC. Instead of sending the residues to disposal “as is”, in this approach the RCC are contacted with a gas stream containing CO₂ at high temperature, triggering the carbonation of the Ca(OH)₂ fraction of the residues. Carbonation significantly decreases the mobility of some of the trace metals contained in the fly ash fraction (Pb, Zn and Cu, in particular) and reduces the solubility of the residues, thus effectively producing a residue that is less prone to leaching (Baciocchi et al., 2009). This effect improves the environmental behaviour of RCC, guaranteeing safer disposal, yet it appears not to be a sufficient driver to persuade WtE operators to invest on the accelerated carbonation process.

Here, the carbonation behaviour of RCC was compared to the one of a reference limestone in order to understand the potential for the use of RCC in carbonate looping applications. If carbonation of RCC could be effectively performed upon multiple cycles, the accelerated carbonation approach would become not just a pre-treatment before disposal but an actual valorisation route, increasing its potential attractiveness.

Figure 9.2a reports the CO₂ uptake of both RCC and reference limestone (20 mg powdered samples) in TGA at different temperatures under a gas flow rate of 100 mL/min (60% CO₂ in N₂). At 600 and 700 °C, natural limestone exhibits a very fast initial reaction rate, thus achieving CO₂ uptake higher than 50 wt. % within a couple of minutes. Conversely, at 500 °C the fast reaction stage is abruptly interrupted at a CO₂ uptake lower than 5 wt. % and replaced by a very slow reaction regime. The marked difference in performance with temperature could be explained by a change in the gas diffusion mechanism with temperature: Bhatia and Perlmutter (1983) suggest that at T < 515 °C diffusion is a solid-state process, while at higher temperature is gas diffusion. In contrast, RCC exhibits similar CO₂ uptake both at the end of the fast initial reaction stage and after 1 h carbonation for all the three operating temperatures. This is in agreement with similar findings by Prigobbe et al. (2009) and Tian and Jiang (2012). Clearly enough, the total CO₂ uptake capacity (\approx 30 wt. %) is lower than that of limestone at 600 and 700 °C due to the presence of the chlorinated and sulphated phases, which are inactive towards carbonation. More interestingly, at 500 °C RCC

outperforms limestone even if its Ca content available to carbonation is lower. This could be the consequence of a possible promoting effect produced by the chlorinated phase ($\text{CaOHCl}/\text{CaCl}_2$). As a matter of fact, it has been observed in acid gas removal systems that CO_2 sorption by $\text{Ca}(\text{OH})_2$ is enhanced in presence of HCl (Chin et al., 2005) and, in addition, both hydrogen halides and their salts have been found to act as dopants for limestone in calcium looping applications (Al-Jeboori et al., 2013). The observed phenomenon requires further investigation, but, for the scope of the present exploratory screening of RCC potentialities as CO_2 sorbent, the following testing of cyclic CO_2 capture was performed at 700 °C, under the typical calcium looping conditions adopted for limestone.

The cyclic performance of RCC and limestone was tested over 10 cycles of 20 min carbonation at 700 °C under a gas flow rate of 100 mL/min (60% CO_2 in N_2) and 10 min calcination at 800 °C in N_2 . The results are reported in Figure 9.2b, along with the performance of “commercial lime” (the same $\text{Ca}(\text{OH})_2$ used in the WtE plant where the RCC was collected) and Depurcal, the commercial calcined dolomite used in acid gas removal by furnace sorbent injection as described in section 2.4.

The reference limestone follows the characteristic decay over cycling mentioned in section 9.1. Commercial lime (i.e., calcium hydroxide) shows higher stability than limestone. Morphologically speaking, the improved performance could be ascribed to the formation of cracks during the hydration of the raw material (Wu et al., 2007), resulting in a higher pore surface area which is retained even when $\text{Ca}(\text{OH})_2$, at the temperatures tested in the TGA runs, is converted to CaO and cycled in that form. RCC, which is actually commercial lime after reaction with acid gases mixed with fly ash and charcoal, shows an abrupt decline in performance at the 2nd cycle and a slow decay over the following cycles. Here, two counteracting effects could be at play:

- 1) the CaCl_2 fraction in the RCC has its melting point at 772 °C, thus it changes phase between the carbonation and the calcination steps. Although the presence of the chlorinated phase could entail a slight promoting effect on carbonation, as discussed with reference to Figure 9.2a, the repeated phase change should have detrimental effect on the morphology of the sorbent, actually favouring sintering.
- 2) the fly ash included in the RCC are mainly Al_2O_3 and SiO_2 . These compounds, exhibiting high T_T , could act as sintering-resistant support for the reactive Ca content of the RCC.

Clearly enough, RCC performs poorly compared to natural limestone in the 10-cycle comparison. However, it is worth remarking that at the moment RCC is an unrecyclable waste, which can only be sent to disposal paying 150-250 €/t (as described in chapter 7). A residual CO_2 uptake performance of 10 wt. % over multiple cycles, obtained with a waste material, could still be useful, if e.g. RCC were to be used as co-feeding to a carbonate looping vessel mainly fed with limestone. A thorough techno-economic assessment is required to evaluate the viability of this option.

Eventually, Figure 9.2b shows also the cyclic CO_2 uptake performance of the calcined dolomite commercially known as Depurcal (chemically, $\text{MgO}\cdot\text{Ca}(\text{OH})_2$). MgO does not undergo carbonation at these temperatures (as detailed in section 9.3 and the following) and, therefore, the stoichiometric capture capacity of calcined dolomite is just 0.46 g CO_2 / g sorbent compared to 0.79 g CO_2 / g sorbent for CaO . However, the lower CO_2 uptake obtained in the first cycles is compensated by a remarkable stability in performance: no significant decay in reactivity is observed in a 10 cycles interval. This behaviour is a consequence of the preservation of the porous structure of the sorbent upon cycling (Valverde et al., 2015). The MgO fraction, although unreactive towards CO_2 , exhibits

a high Tamman temperature (Kierzkowska et al., 2013) and less sintering occurs. Its intrinsic resistance to sintering makes calcined dolomite an ideal sorbent for acid gas removal in combustion chamber in the first place (as presented in section 2.4) and a potential CO₂ sorbent. In the present study, it has not been possible to collect solid residues derived from the reaction between Depurcal and acid gases in WtE plants employing the furnace sorbent injection of this material. Speculatively speaking, RCC derived from Depurcal could offer quite different characteristics than the RCC derived from commercial lime tested in Figure 9.2b: namely, a lower CO₂ uptake capacity and a higher cyclic stability. Depending on the convenience of the trade-off, Depurcal-derived RCC could be more promising sorbents than lime-derived RCC.

This very preliminary screening of the CO₂ capture potential of Ca-based sorbents and residues related to acid gas treatment had the objective to highlight the possible integration between the acid gas removal and the carbonate looping processes. Similarly to cement plants where limestone could be used first as CO₂ sorbent and then as feedstock (Dean et al., 2011), medium-to-large waste-to-energy plants, emitting up to 10³ t CO₂/day (ISWA, 2012), could host a dual use of Ca-based sorbents: the residues of acid gas removal could be fed to a carbonate looping system, as exploratively proposed in this section, or, viceversa, the limestone particles elutriated from the carbonate looping unit after some cycling could be fed to the acid gas removal system to use their residual sorption capacity to bind HCl and SO₂.

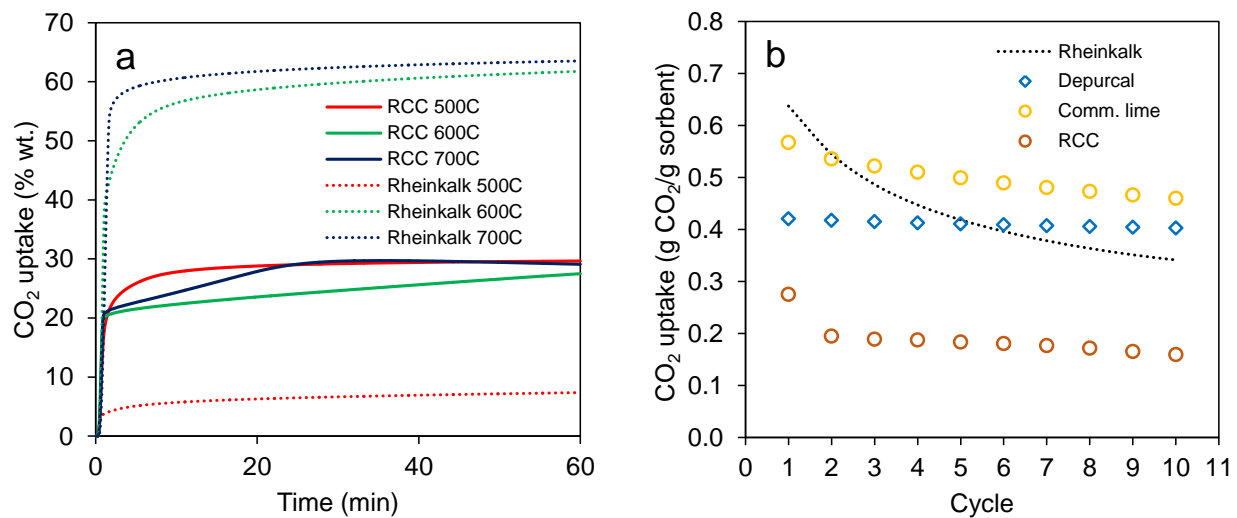
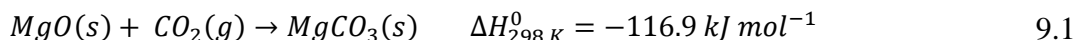


Figure 9.2. a) Carbonation behaviour of RCC versus a reference natural limestone (Rheinkalk) in 60% CO₂ atmosphere at different temperatures; b) CO₂ uptake by RCC compared to their fresh counterpart (commercial lime), a dolomitic sorbent (Depurcal) and reference limestone over 10 cycles. Carbonation at 700 °C in 60% CO₂(20 min), calcination at 800 °C in N₂(10 min). Data are average of 3 runs.

9.3 Potentiality of MgO as a CO₂ sorbent

Recently, there has been a resurgence of research into magnesium oxide (MgO) as an alternative CO₂ sorbent. When compared to other solid sorbents (Dunstan et al., 2016a), MgO offers a number of promising characteristics such as (i) a high theoretical CO₂ uptake capacity of ~1.09 g CO₂/ g MgO, (ii) low- to moderate-temperature operating conditions and, thus, energy savings for sorbent regeneration with respect to competitive metal oxide-based CO₂ sorbents, like the aforementioned CaO, Li₂ZrO₃ (Ida and Jin, 2003) or Li₄SiO₄ (Qi et al., 2013), (iii) low purchase cost due to natural abundance, and (iv) inherently safe and environmentally benign nature.

MgO captures CO₂ via the formation of magnesium carbonate:



Regeneration (i.e. the release of a pure stream of CO₂) can be performed through the reverse (calcination) reaction, possible in pure CO₂ atmosphere for temperatures > 400°C (Zarghami et al., 2015). Figure 9.3 puts the equilibrium of reaction 9.1 in comparison to that of CaO carbonation.

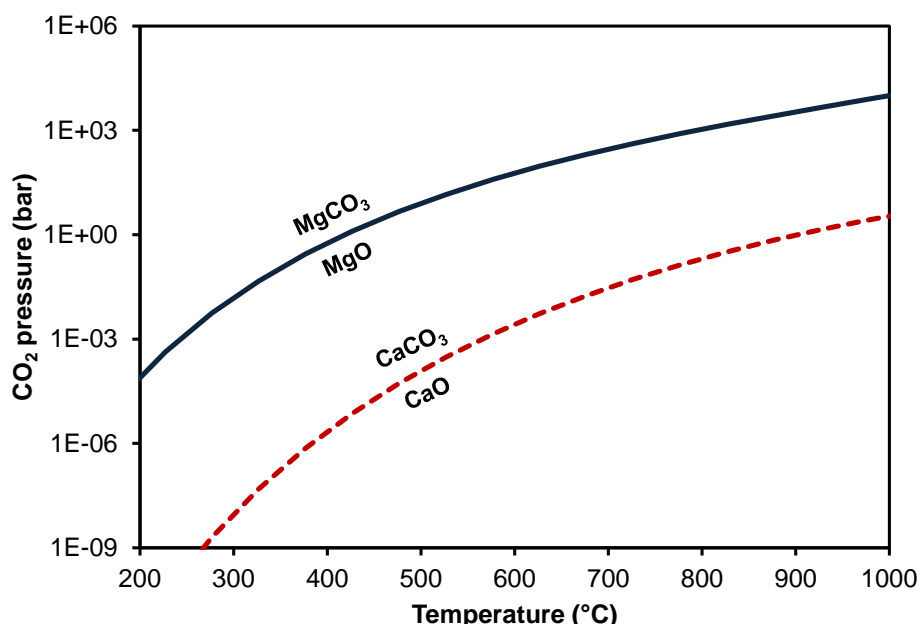


Figure 9.3. Equilibrium for the reactions between CaO and CO₂ and between MgO and CO₂. Thermodynamic data of compounds from JANAF Thermochemical Tables (NIST, 2016).

However, in spite of its high theoretical capture capacity, the actual uptake of CO₂ by pure MgO is remarkably lower, viz. < 4 wt.%. This has been attributed to the formation of a dense MgCO₃ layer on the surface of the material, severely hindering further carbonation through mass transfer limitations (Gregg and Ramsay, 1970; Fagerlund et al., 2012). Therefore, research efforts have been aimed at overcoming this issue. Zarghami et al. (2015) found that increasing the system pressure to 20 bar and adding 30 vol. % water vapor improved the apparent rate of carbonation, leading in turn to the almost complete conversion of the solid sorbent, while Ding et al. (2016) showed that even at atmospheric pressure MgO in presence of 70% relative humidity can reach CO₂ uptakes four times higher than for the reference dry gas. The improved kinetics in presence of steam was explained by the formation of an adsorbed water vapor layer, partially dissolving magnesium and carbonate ions, and, thus, promoting access to MgO unreacted surface (Fagerlund et al., 2012).

9.4 Enhancement of MgO reactivity with molten salt promotion

More recently, the promotion of MgO reactivity with alkali metal salts has been found to increase appreciably the CO₂ uptake of MgO. Double salts synthesized by mixing MgO and an alkali metal carbonate (e.g., K₂CO₃ or Na₂CO₃) via precipitation or simple wet mixing methods showed a significantly higher sorption capacity than pure MgO, namely up to 8 wt.% for K-promoted MgO (Singh et al., 2009; Xiao et al., 2011) and 15 wt.% for N-promoted MgO (Zhang et al., 2013) over 1 h carbonation at intermediate temperature. This was associated with the fact that the double salt carbonate, K₂Mg(CO₃)₂ or Na₂Mg(CO₃)₂, formed during exposure to CO₂ has a lower free energy of formation than that of MgCO₃, according to density functional theory calculations (Duan et al., 2014).

Similarly, the addition of alkali metal nitrates (e.g., LiNO₃, NaNO₃, KNO₃) to MgO in order to form nitrate-coated sorbents via wet mixing or ball milling was shown to produce an even higher promoting effect on MgO reactivity. Vu et al. (2014) reported that MgO·KNO₃ composites synthesised via an aerogel method exhibited 13.9 wt. % CO₂ uptake after 2 h carbonation at 325 °C. Zhang et al. (2014) and Prashar et al. (2016) produced NaNO₃-promoted MgO respectively via ball milling and impregnation and stated up to 75% conversion of MgO at 330 °C. Harada et al. (2015) showed that MgO coated with a ternary mixture of Li, Na, K nitrates presented 43.6 wt. % CO₂ uptake after 4 h carbonation at 300 °C, satisfactory regenerability and faster kinetics than MgO coated with single nitrates. The promoting effect of NaNO₃ was also reported for dolomite (Yang et al., 2013a), Na-Mg double salts (Zhang et al., 2016) and synthetic hydrotalcite (Kim et al., 2016).

The enhancement of MgO carbonation in presence of alkali metal nitrates has been attributed to a facilitation in the contact between the solid and gaseous reactants. In the intermediate temperature regime (250-350 °C) adopted for the carbonation of nitrate-coated MgO sorbents, the alkali metal nitrates melt, forming a molten layer around MgO particles. It is speculated that either MgO (Zhang et al., 2014) or CO₂ (Harada et al., 2015) might dissolve in the liquid, reacting to form [Mg²⁺ ... CO₃²⁻] ionic pairs which subsequently form solid MgCO₃ upon saturation. This reaction mechanism might overcome the aforementioned constraints of the unpromoted gas-solid reaction, preventing the deposition of the rigid surface layers of unidentate carbonates typically formed when CO₂ adsorbs on pure MgO (Leon et al., 2010). A possible reaction scheme is sketched in Figure 1.

However, the formulated hypotheses still fall short of experimental verifications and the exact mechanism behind the improved MgO carbonation in the presence of molten salts is yet to be elucidated. In addition, there is still lack of understanding regarding the marked differences in performance between various nitrate coating mixtures, even if all are in molten state at the tested operating conditions. The latest studies that couple the coating of MgO with alkali metal salts with synthesis techniques (e.g. sol-gel) yielding highly-porous MgO, are demonstrating CO₂ uptakes as high as 0.69 g CO₂/g sorbent (Harada and Hatton, 2015; Vu et al., 2016). Addressing the still obscure theoretical aspects governing the alkali metal salt promotion could help identifying viable routes to improve the already promising performance of MgO-based CO₂ sorbents.

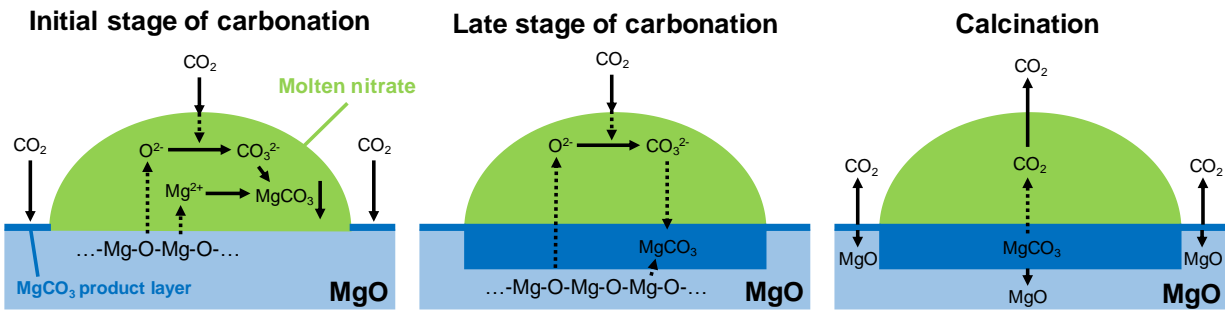


Figure 9.4. Proposed reaction scheme for MgO carbonation promoted by alkali metal nitrates. Redrawn from Harada et al. (2015).

9.5 Synthesis protocol for alkali metal nitrate-coated MgO-based CO₂ sorbents

In order to produce alkali metal nitrate-coated MgO-based CO₂ sorbents, a synthesis approach similar to the one described in Harada et al. (2015) was adopted. Samples of alkali metal nitrate-coated MgO were prepared by calcination of a suspension of a MgO precursor after impregnation with different compositions of alkali metal salts via wet mixing. The following MgO precursor were tested: commercial basic magnesium carbonate ($Mg_5(CO_3)_4(OH)_2 \cdot 4H_2O$, Acros Organics), commercial magnesium hydroxide ($Mg(OH)_2$, Sigma-Aldrich) and laboratory-synthesised magnesium carbonate ($MgCO_3$). The latter was prepared by precipitation of a 1 M solution of magnesium nitrate ($Mg(NO_3)_2$, Sigma-Aldrich) in a 2 M solution of sodium carbonate (Na_2CO_3 , Sigma-Aldrich), keeping a constant pH of 11 by dropwise addition of a 3 M solution of sodium hydroxide ($NaOH$, Fisher Chemicals). Alkali metal nitrates ($LiNO_3$, $NaNO_3$, KNO_3) were purchased from Sigma-Aldrich.

Typically, 6 g of magnesium carbonate (corresponding to ~0.015 mol of Mg) and appropriate amounts of salts in order to reach a 10% molar ratio with respect to Mg were mixed in 15 mL of water and stirred magnetically for 1 h at room temperature. Table 9.1 reports the synthesised samples sorted by composition of the alkali metal salt coating mixture. Samples coated with molar ratios of salts ranging from 5 to 25% mol. were also prepared in order to assess the effect of a varying quantity of coant, while calcium oxide (CaO) and aluminum oxide (Al_2O_3) were used as alternative supports. The obtained aqueous slurries were oven dried at 120 °C overnight, ground in a crucible and put in a muffle furnace for calcination in air (450 °C, 4 h, heating rate 3 °C/ min). The selected temperature allowed the calcination of both magnesium carbonate and hydroxide without triggering the decomposition of alkali metal nitrates, which is significant above 550 °C (Stern, 2000). Furthermore, lower calcination temperatures generate MgO with higher reactivity (Liu et al., 2007).

Table 9.1. Different mixtures of alkali metal nitrates used to coat the synthesised MgO-based sorbents.

Coating mixture	Composition (mol. fraction in the mixture)			Melting point of the mixture (°C) ^a
	LiNO ₃	NaNO ₃	KNO ₃	
LiNO ₃	1	-	-	255
NaNO ₃	-	1	-	308
KNO ₃	-	-	1	334
(Li-K)NO ₃	0.9	-	0.1	240
	0.7	-	0.7	200
	0.45	-	0.55	130 ^b
	0.3	-	0.7	200
	0.1	-	0.9	300
(Na-K)NO ₃	-	0.9	0.1	290
	-	0.8	0.2	270
	-	0.6	0.4	230
	-	0.46	0.54	221 ^b
	-	0.4	0.6	230
	-	0.25	0.75	270
(Li-Na)NO ₃	0.8	0.2	-	230
	0.6	0.4	-	200
	0.5	0.5	-	200 ^b
	0.4	0.6	-	220
	0.2	0.8	-	270
(Li-Na-K)NO ₃	0.30	0.18	0.52	120 ^b

a experimental m.p. of the mixture of pure alkali metal nitrates, according to Coscia et al. (2013)

b eutectic point of the listed binary or ternary mixture (Janz et al., 1978; Bradshaw and Meeker, 1990)

Before proceeding with a systematic investigation of alkali metal nitrate promotion, nitrate-coated MgO samples were prepared starting from different Mg precursors in order to identify the most suitable synthesis route to allow a facile preparation of performing sorbents.

CO₂ uptake of the synthesised sorbents was measured by means of a thermogravimetric analyser (TGA, Mettler Toledo TGA/DSC 3+). A small amount (~ 10 mg) of sorbent was placed in an alumina crucible and precalcined at 450°C under a N₂ flow of 80 mL/min for 30 min to evaporate adsorbed water and ensure all magnesium to be in the oxide state. Then, the sample was cooled down at the desired reaction temperature and the gas flow was switched to pure CO₂. Repeated cycles of carbonation and regeneration were tested in the same way, performing CO₂ adsorption at the desired reaction temperature for 1 h and desorption at 450 °C for 15 min.

As shown in Figure 9.5 for samples coated with 10% mol. (Li-Na-K)NO₃ eutectic mixture, the sorbent prepared by using basic magnesium carbonate as MgO precursor showed higher CO₂ uptake than the one prepared from magnesium hydroxide. Accordingly, BET measurements stated a surface area of 25.3 m²/g for the sample prepared from basic magnesium carbonate and of 3.3 m²/g for the sample prepared from Mg(OH)₂. This result confirms for MgO the observations of Borgwardt (1989) for CaO: carbonate precursors generate more porous and more performing oxide sorbents than hydroxide precursors. Conversely, the performance of sorbents prepared from commercial basic magnesium carbonate and from precipitated magnesium carbonate were comparable.

Presenting higher reactivity than samples prepared from $Mg(OH)_2$ and a quicker synthesis protocol than samples prepared from precipitated $MgCO_3$, samples synthesised from commercial basic magnesium carbonate were selected for the following analyses. Nonetheless, it is worth remarking that precipitated magnesium carbonates or hydroxy-carbonates could constitute a promising precursor for industrial MgO -based sorbents. Ongoing research (Glasser et al., 2016) is focusing on CO_2 mineralization by means of accelerated carbonation in Mg -containing solutions, resulting in the precipitation of different carbonated Mg -based species (hydromagnesite, dypingite, nesquehonite). The possible utilization of the product of CO_2 mineralization for further CO_2 abatement in CCS systems could be a viable process integration.

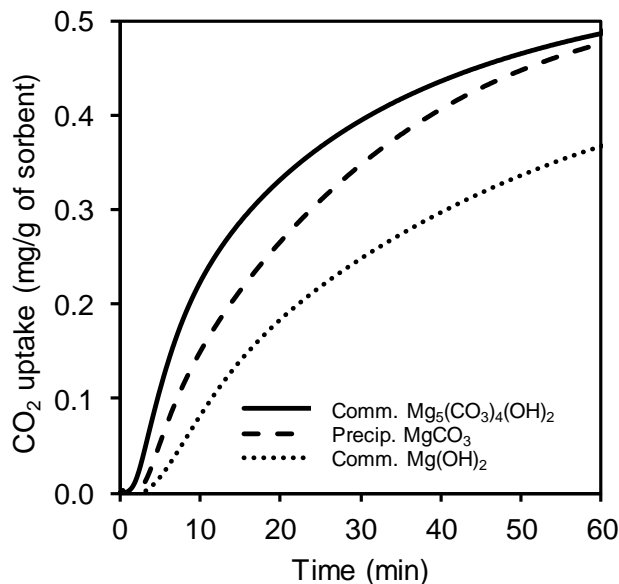


Figure 9.5. CO_2 uptake at 300 °C in pure CO_2 atmosphere for $(Li,Na,K)NO_3$ -coated MgO samples synthesised from different Mg precursors: commercial basic magnesium carbonate, magnesium carbonate prepared via precipitation and commercial magnesium hydroxide.

The crystallinity and composition of the synthesised sorbents were investigated using powder X-ray diffraction (Bruker, AXS D8 Advance). The X-ray diffractometer was operated at 40 mA and 40 kV. Each sample was scanned within the 2θ range of 10–90°. The step size was 0.025° with a time duration per step of 0.8 s.

Figure 9.6 shows the XRD patterns and the SEM images of a representative MgO sample coated with 10% mol. $NaNO_3$ synthesised and tested according to the protocol. The as-prepared sample, dried after wet mixing of basic magnesium carbonate and sodium nitrate, exhibited the typical plate-like aspect of hydromagnesite (Hänen et al., 2008), as confirmed by XRD identification. Upon calcination, the Mg phase was converted to MgO , in the form of porous particles composed by grains of diameter < 100 nm. The sample after reaction with CO_2 at 300 °C, whose performance will be discussed in section 10.1, maintained the grain-like geometry and XRD analysis stated that carbonation resulted in the formation of $MgCO_3$. After repeated carbonation and calcination cycles (see section 10.4), the sample in carbonated form maintained the XRD speciation, with less intense $MgCO_3$ peaks due to loss of carbonation performance over cycling.

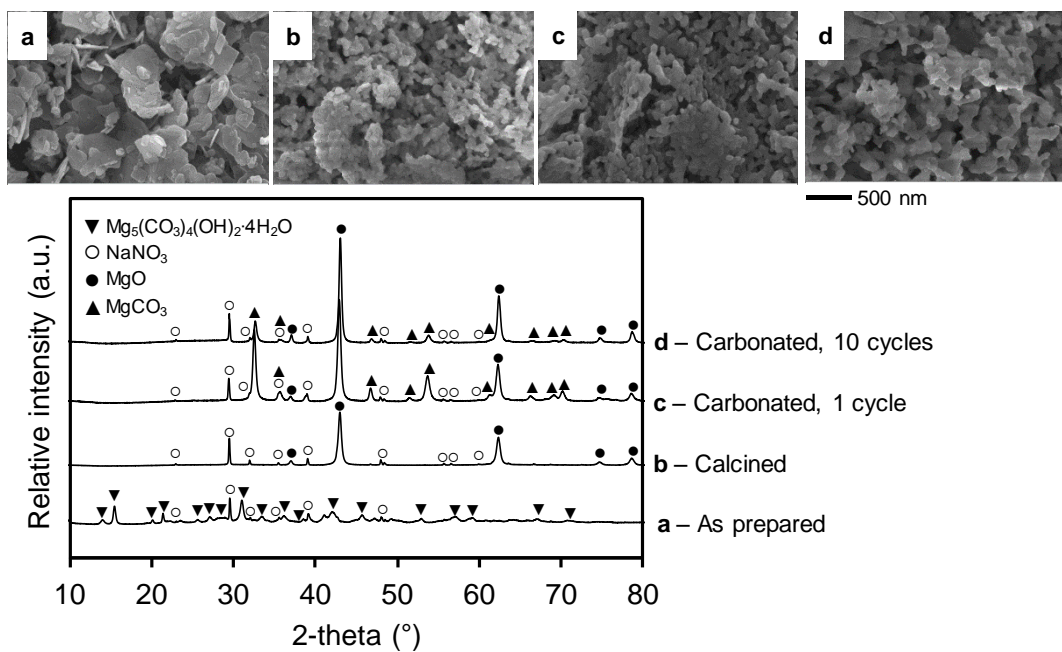


Figure 9.6. SEM images and XRD spectra of MgO coated with 10% mol. NaNO_3 : a) after wet mixing and drying (as prepared); b) after calcination at 450°C (calcined); c) after 1 h carbonation at 300°C in pure CO_2 (carbonated, 1 cycle); d) after 10 cycles of 1 h carbonation at 300°C and regeneration at 450°C (carbonated, 10 cycles).

10 Analysis of the carbonation of MgO-based sorbents

10.1 CO₂ uptake

The CO₂ uptake of MgO samples coated with a 10% mol. amount of different alkali metal nitrates after 1 h carbonation in pure CO₂ atmosphere at 300 °C – tested in TGA as reported in section 9.5 – is presented in Figure 10.1. While uncoated MgO mainly reacted in the first minutes quickly reaching a limit loading of 19 mg CO₂/g sorbent due to diffusional limitations, the carbonation of MgO samples coated with nitrates was initially slower, presenting an induction time of ~2 min before a substantial acceleration, which allowed significantly higher CO₂ uptakes. Among the sorbents coated with single nitrates, MgO-LiNO₃ and MgO-NaNO₃ captured 196 and 432 mg CO₂/g sorbent respectively and only MgO-KNO₃ did not show the onset of any accelerating carbonation regime, resulting in an uptake of 8 mg CO₂/g sorbent after 1 h reaction. The effect of binary and ternary mixtures of nitrates at their eutectic composition on MgO carbonation is also reported in Figure 10.1. MgO incorporating the eutectic mixture of (Na,K)NO₃ exhibited a slower kinetics than MgO-NaNO₃, in agreement with the results of Harada et al. (2015), while the not previously tested eutectic mixtures of (Li,Na)NO₃ and (Li,K)NO₃ promoted the uptake of their respective sorbents up to 433 and 470 mg CO₂/g sorbent. The eutectic ternary mixture of (Li,Na,K)NO₃ obtained the highest CO₂ uptake of 474 mg CO₂/g sorbent.

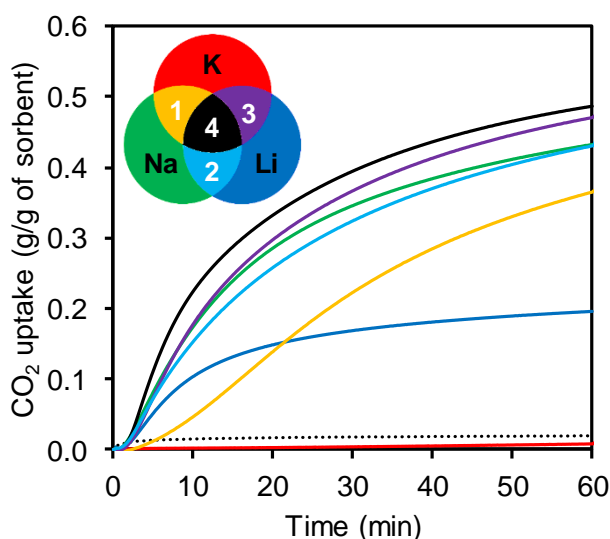


Figure 10.1. CO₂ uptake at 300 °C, in pure CO₂ atmosphere, by MgO sorbents coated with different alkali metal nitrates (LiNO₃, NaNO₃, KNO₃) and their eutectic mixtures: 1) (Na,K)NO₃; 2) (Li,Na)NO₃; 3) (Li,K)NO₃; 4) (Li,Na,K)NO₃.

Figure 10.2 depicts the effect of different nitrate-to-Mg ratios on the CO₂ uptake of LiNO₃- and NaNO₃-coated MgO. For the former, the conversion of MgO to MgCO₃ monotonically increased when the molar ratio of LiNO₃ to Mg increased from 5 to 25%. For the latter, the optimal ratio resulted to be 10% mol., with MgO conversion slightly decreasing for higher ratios.

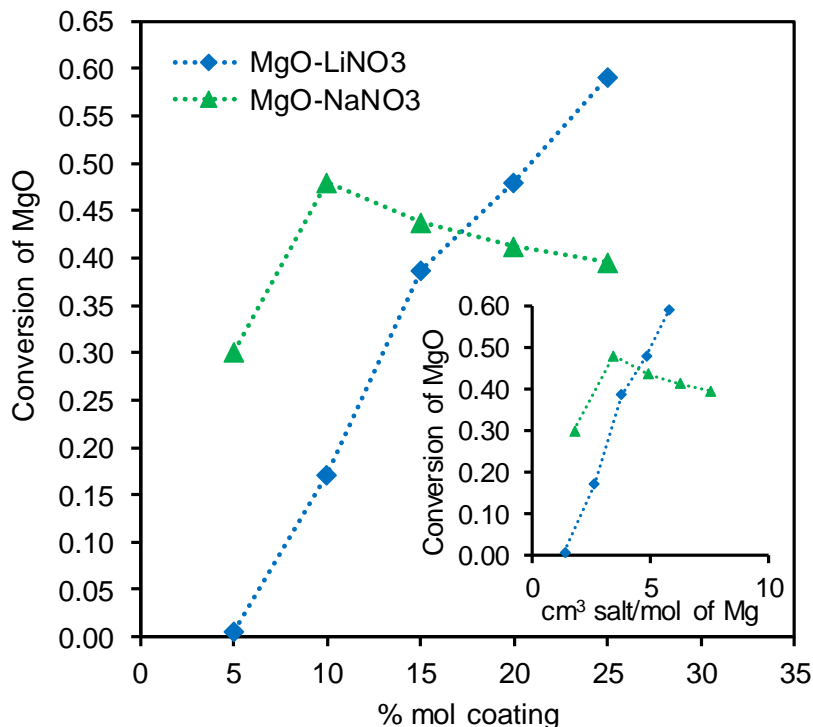


Figure 10.2. *MgO conversion to $MgCO_3$ after 1 h carbonation at 300 °C, in pure CO_2 atmosphere, for samples coated with different amount of $LiNO_3$ or $NaNO_3$. Inset: results reported as function of volume of coantant per mole of Mg.*

Figure 10.3 reports the temperature-programmed carbonation of different nitrate-promoted MgO sorbents. The samples were exposed to a pure CO_2 gas flow during heating up to 500 °C. Uncoated MgO started reacting immediately at the onset of the experiment (50 °C), reaching its maximum CO_2 uptake at 150 °C and then slowly releasing the adsorbed CO_2 . The gradual slope of the CO_2 release profile can be attributed to the variety of species formed during carbonation of pure MgO, *viz.* from weakly physisorbed CO_2 to chemisorbed monodentate carbonates and bulk $MgCO_3$ (Hu et al., 2007; Downing et al., 2014).

Conversely, for the MgO samples coated with alkali metal nitrates, carbonation was negligible at low temperature and accelerated abruptly only after a sort of threshold temperature, different from sample to sample, was reached. The behaviour appears to be consistently linked to the physical state of the coating: while at low temperature the nitrates are in the solid state, hindering carbonation by covering active MgO surface, their phase change upon approaching melting point allows a sudden acceleration in the kinetics of CO_2 sorption.

For $MgO-LiNO_3$ ($m.p.-LiNO_3 = 255$ °C), the acceleration took place at 230 °C. For $MgO-NaNO_3$ ($m.p.-NaNO_3 = 308$ °C), the acceleration occurred at 275 °C. The fact that enhanced CO_2 sorption started at temperatures below the bulk melting temperature of the coantant could be attributed to “premelting” phenomena, *i.e.* the gradual disordering of the surface of the compound with the formation of liquid films at solid interfaces (Yang et al., 2013a), as suggested by Zhang et al. (2016). For instance, $NaNO_3$ is known to undergo a solid-state transition at 275 °C before melting (Janz et al., 1964), causing a structural rearrangement that could be related to the observed simultaneous acceleration of CO_2 uptake.

Lee et al. (2014) postulated that eutectic mixtures of nitrates could lower the effective carbonation temperature. Indeed, Figure 10.3 shows that, by lowering the melting point of the coating by

adopting a (Na,K)NO₃ mixture (60% NaNO₃, 40% KNO₃, m.p. 230 °C), the onset of significant carbonation was moved down to 250 °C. With a ternary eutectic mixture of (Li,Na,K)NO₃ (m.p. 120 °C), the onset of carbonation was further shifted down to 180 °C.

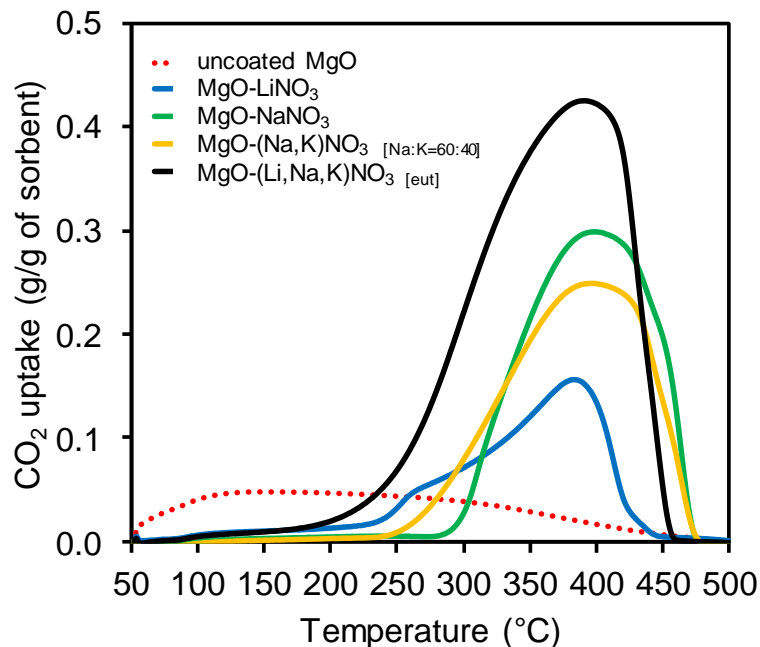


Figure 10.3. CO₂ uptake of different 10% mol. alkali metal nitrate-coated MgO samples during heating in pure CO₂ atmosphere at a ramp rate of 10 °C/min.

In order to get a broader picture of molten salt-promoted CO₂ capture, LiNO₃ was used to coat different supports: an inert material (aluminum oxide, Al₂O₃) and another alkaline earth metal oxide (calcium oxide, CaO). Figure 10.4 reports the outcome of their exposure to pure CO₂ at 300 °C for 1 h. LiNO₃-coated Al₂O₃ showed no CO₂ uptake, demonstrating that the alkali metal nitrate coating mixture cannot undergo carbonation *per se*. In contrast, LiNO₃-coated CaO captured significantly more CO₂ than its uncoated counterpart. Indeed, pure CaO showed a limited CO₂ uptake which quickly plateaued to a maximum value of 40 mg CO₂/g sorbent, as a consequence of the transition from a kinetic-controlled to a product layer diffusion-controlled regime (Li et al., 2012), while LiNO₃-coated CaO presented enhanced performance in both the kinetic and diffusion-controlled stages, resulting in a final CO₂ uptake of 160 mg CO₂/g sorbent. The LiNO₃ coating greatly extended the CO₂ uptake achieved in the kinetic stage and allowed significant residual reactivity in the diffusion-limited stage. The promotion could be linked with the dissolution of CO₂ in the nitrates and related enhanced mobility of carbonate ions, since for T < 500 °C the carbonation of CaO is supposed to be governed by solid-state diffusion of CO₃²⁻ (Bhatia and Perlmutter, 1983). Since the temperature needed to regenerate CaO (> 800 °C; Liu et al., 2012) is far higher than the decomposition temperature of LiNO₃ and the other alkali metal nitrates, this finding has no implications for carbonate looping applications, but it is nonetheless a clear confirmation that the molten salt promotion is a general mechanism catalyzing the carbonation of alkaline earth metal oxides.

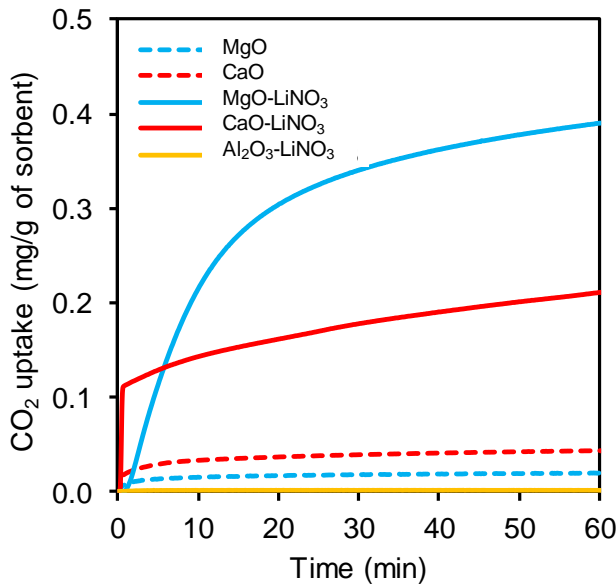


Figure 10.4. CO_2 uptake at 300 °C, in pure CO_2 atmosphere, by different supports (MgO , CaO , Al_2O_3) coated with 20% mol. $LiNO_3$.

Although all nitrates appears to promote reactivity thanks to their molten state, there is a wide variation of performance between different nitrates and nitrate mixtures. In order to explore more systematically the effect of coating mixture composition, MgO samples coated with 10% mol. binary mixtures of nitrates of different composition were tested at 300 °C in pure CO_2 . Figure 10.5 reports the CO_2 uptake for MgO incorporating $(Na,K)NO_3$, $(Li,Na)NO_3$ and $(Li,K)NO_3$ mixtures along with their respective melting point as a function of mixture composition. Raman spectra of selected samples before and after carbonation are presented in Figure 10.6 in order to show their different composition. Raman scattering was analysed by means of a Raman spectrometer (Thermo Scientific, DXR) equipped with a Olympus confocal microscope. The excitation wavelength was 455 nm and the laser power was set at 3 mW, collecting each spectra with 3 exposures of 5 s each.

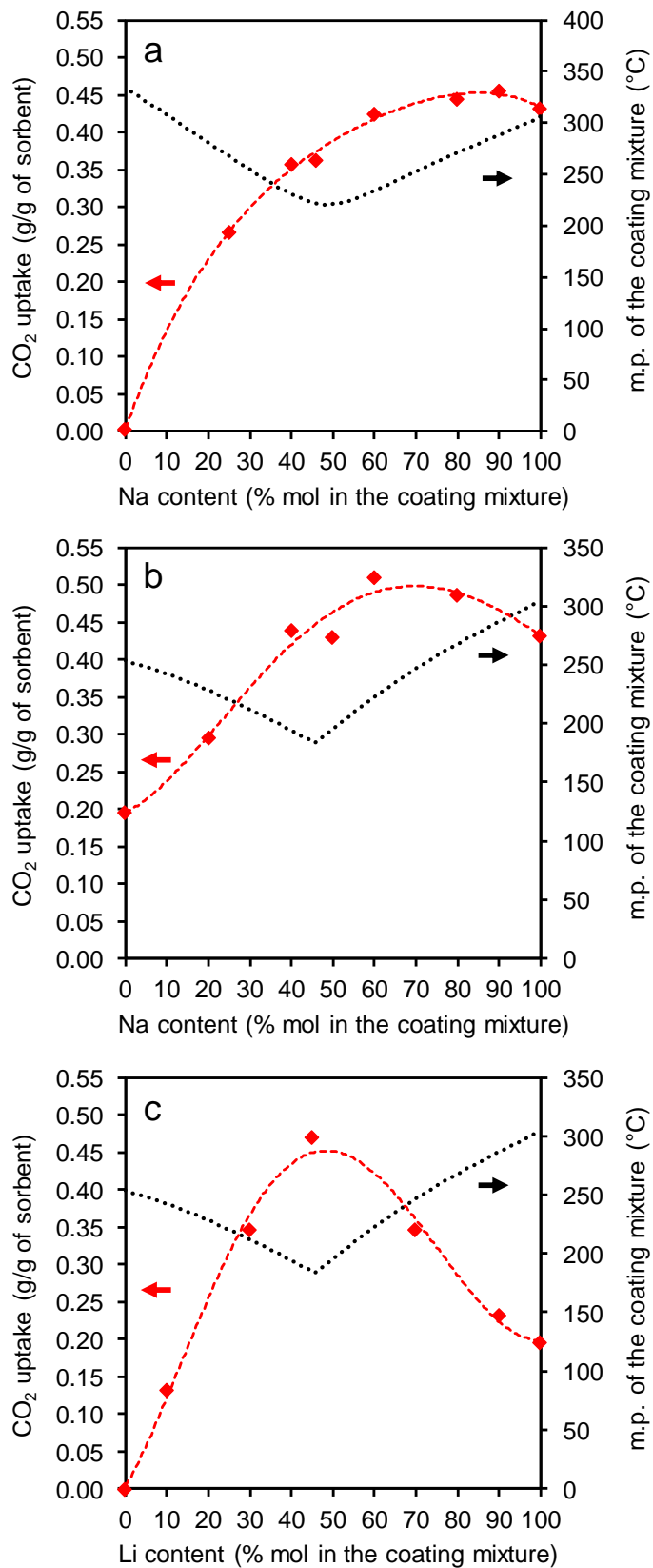


Figure 10.5. CO_2 uptake at 300°C , in pure CO_2 atmosphere, by MgO sorbents coated with 10% mol. binary mixtures of alkali metal nitrates as a function of composition of the coating mixture: a) $(\text{Na},\text{K})\text{NO}_3$, b) $(\text{Li},\text{Na})\text{NO}_3$, c) $(\text{Li},\text{K})\text{NO}_3$. Source for the melting points of the mixtures: Coscia et al. (2013).

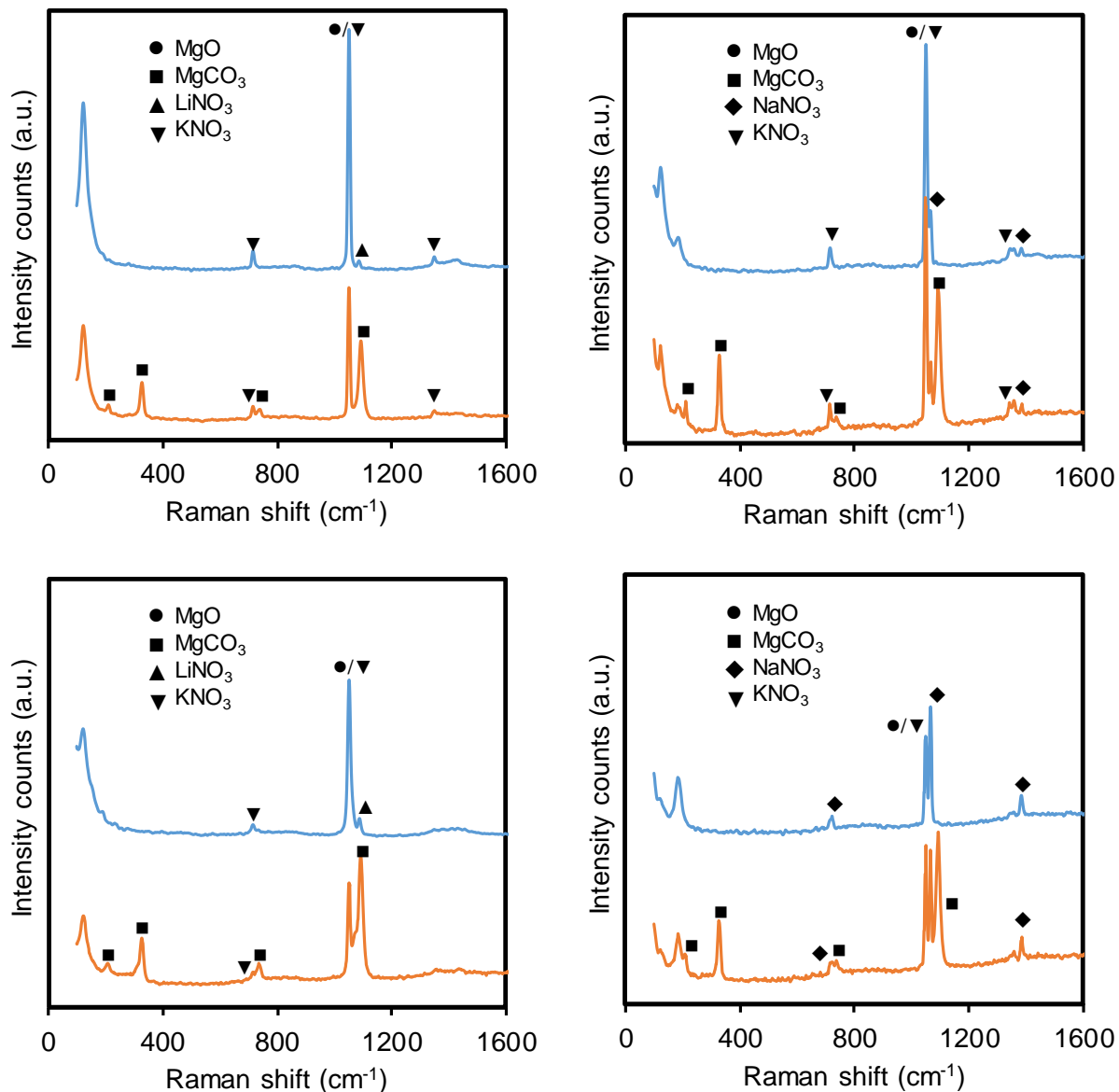


Figure 10.6. *Ex situ Raman spectra of sorbents before (blue line) and after (orange line) carbonation at 300 °C. MgO coated with: a) $(\text{Li},\text{K})\text{NO}_3$, Li:K ratio = 30:70; b) $(\text{Li},\text{K})\text{NO}_3$, Li:K ratio = 70:30; c) $(\text{Na},\text{K})\text{NO}_3$, Na:K ratio = 25:75; d) $(\text{Na},\text{K})\text{NO}_3$, Na:K ratio = 60:40. See Table 10.1 for attribution of vibrational modes to nitrates.*

Table 10.1. *Vibrational frequencies of alkali metal nitrates in solid state (Ref: Janz and James, 1961).*

Salt (solid state)	Raman frequencies (cm^{-1})		
	ν_1	ν_3	ν_4
LiNO_3	1086	1391	728
NaNO_3	1069	1387	728
KNO_3	1050	1343/1361	714

For $\text{MgO-(Li,K)}\text{NO}_3$ there was a notable alignment between CO_2 uptake and m.p. of the coating mixture. For $\text{MgO-(Na,K)}\text{NO}_3$ and $\text{MgO-(Li,Na)}\text{NO}_3$, CO_2 uptake and m.p. were misaligned, with higher uptakes shifted towards higher Na content in the mixture. The fact that, at the same carbonation temperature of 300 °C, mixtures with lower melting point generate a stronger promoting effect on MgO reactivity could be attributed to enhanced CO_2 diffusion in the molten salt

layer, thanks to either higher solubility of CO₂ or lower viscosity of the nitrates. As a matter of fact, for pure nitrates it is known that CO₂ solubility (see Figure 10.7) increases with temperature (Novozhilov et al., 2007) and it is expected that nitrate mixtures that are further from their m.p. better dissolve carbon dioxide. Consolidated data about viscosity of nitrate mixtures are lacking (see Figure 10.8), but a similar trend with m.p. is expected.

For mixtures containing NaNO₃, melting point appears not to be the only predictor of performance. Since the best performing (Na,K)NO₃- and (Li,Na)NO₃-coated samples have a higher Na content than the eutectic composition, their marked CO₂ uptake might result from a superimposition of effects between a physical promotion which is higher for a lower m.p. of the coating mixtures and an “affinity” promotion which is exclusive of NaNO₃.

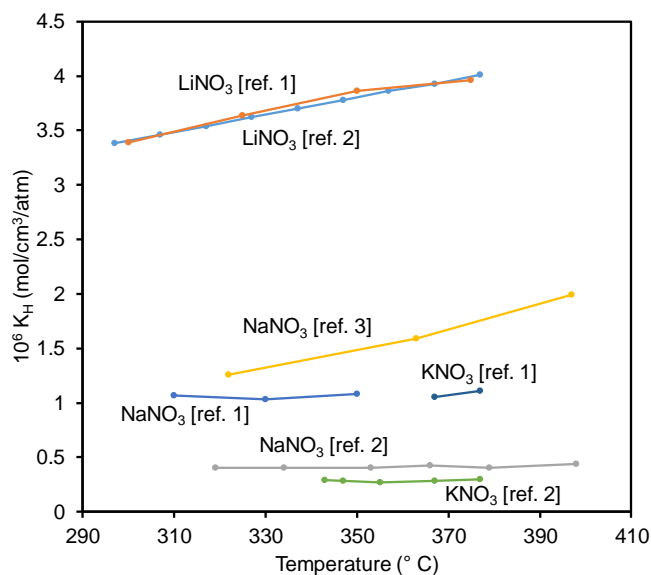


Figure 10.7. Henry's law constant for CO₂ solubility in different nitrates as a function of temperature. References: 1) Paniccia and Zambonin (1973); 2) Sada et al. (1981); 3) Bratland and Krohn (1969).

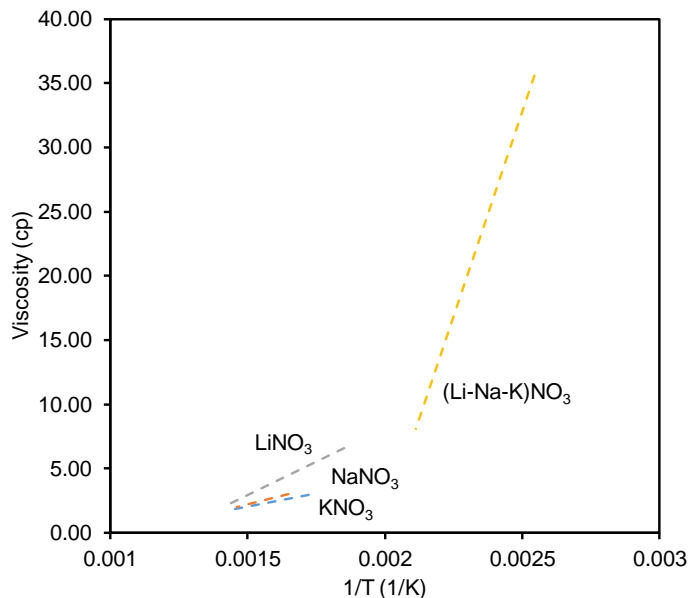


Figure 10.8. Viscosity of nitrates as a function of the inverse of temperature. References: Janz (1967) for the single nitrates and Bradshaw (2010) for the ternary mixture.

10.2 In situ analysis of carbonation: DRIFTS spectroscopy

A series of *in situ* analyses were performed in order to get further insights on the mechanism of MgO carbonation promoted by alkali metal nitrates. Diffuse reflectance infrared spectroscopy (Nicolet, 6700 FT-IR) was employed to characterize the speciation of carbonates adsorbed on the MgO sorbents. *In situ* DRIFTS data were collected by placing the sample to be tested in a Harrick Praying Mantis cell. After heating up to 450 °C in N₂ to guarantee the desorption of CO₂ and H₂O adsorbed at room temperature, the sample was exposed to a CO₂ flow of 30 mL/min at different temperatures (100, 150, 200, 250, 275, 300, 350, 400 °C).

Firstly, the carbonation of nitrate-coated MgO was examined by DRIFTS in order to detail the chemical speciation of the adsorbed CO₂. Figure 10.9 presents the variations occurring in the DRIFTS spectra of MgO coated with 10% mol. NaNO₃ after carbonation at 300 °C in CO₂ and subsequent regeneration at 450 °C in N₂. The spectrum before reaction was clearly populated by peaks ascribed to the nitrate ion (see for comparison the spectrum of inert Al₂O₃ coated with NaNO₃ in Figure 10.11), like the out-of-plane bending at 836 cm⁻¹, the antisymmetric stretch at 1380 cm⁻¹ and the $\nu_1 + \nu_4$ mode at 1780 cm⁻¹ (Beleke et al., 2003), slightly shifted and broadened by the deformation of molten NaNO₃ compared to its low-temperature structure (Harris et al., 1990). After carbonation, the sample exhibited a broad adsorption band in the range 1400-1600 cm⁻¹, attributable to the reflectance of carbonate ions (Genge et al., 1995), and the characteristic peaks of out-of-plane and in-plane bending of the carbonate ion at 879 cm⁻¹ and 749 cm⁻¹ (Du et al., 2010), which disappeared after calcination at 450 °C. The speciation of carbonate species can be compared to the one exhibited on a pure, uncoated MgO sample exposed to CO₂ at the same temperature (Figure 10.10): in this case, the bending modes of the carbonate ion were not observable, while adsorption peaks typical of monodentate carbonates (Phillips and Fujimoto, 1992) emerged at 1526 and 1420 cm⁻¹.

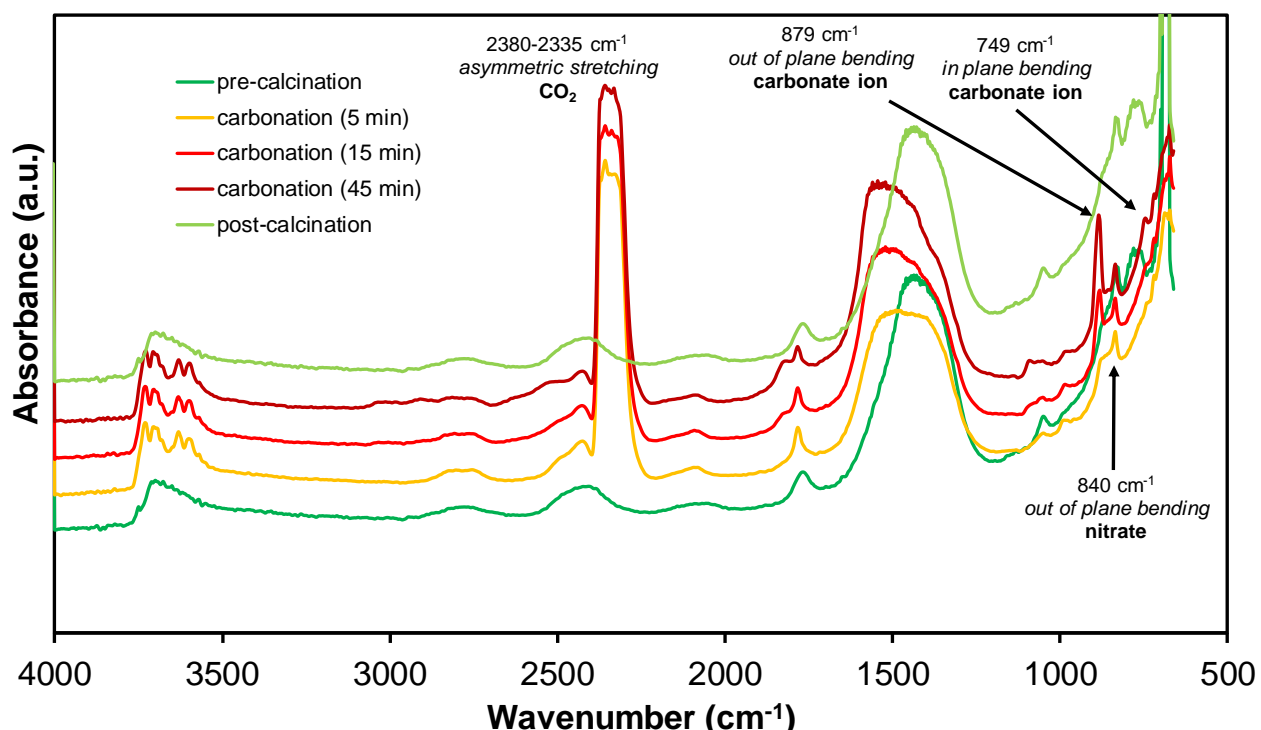


Figure 10.9. *In situ* DRIFTS spectra of MgO coated with 10% mol. NaNO₃ before, during and after carbonation in pure CO₂ atmosphere at 300 °C.

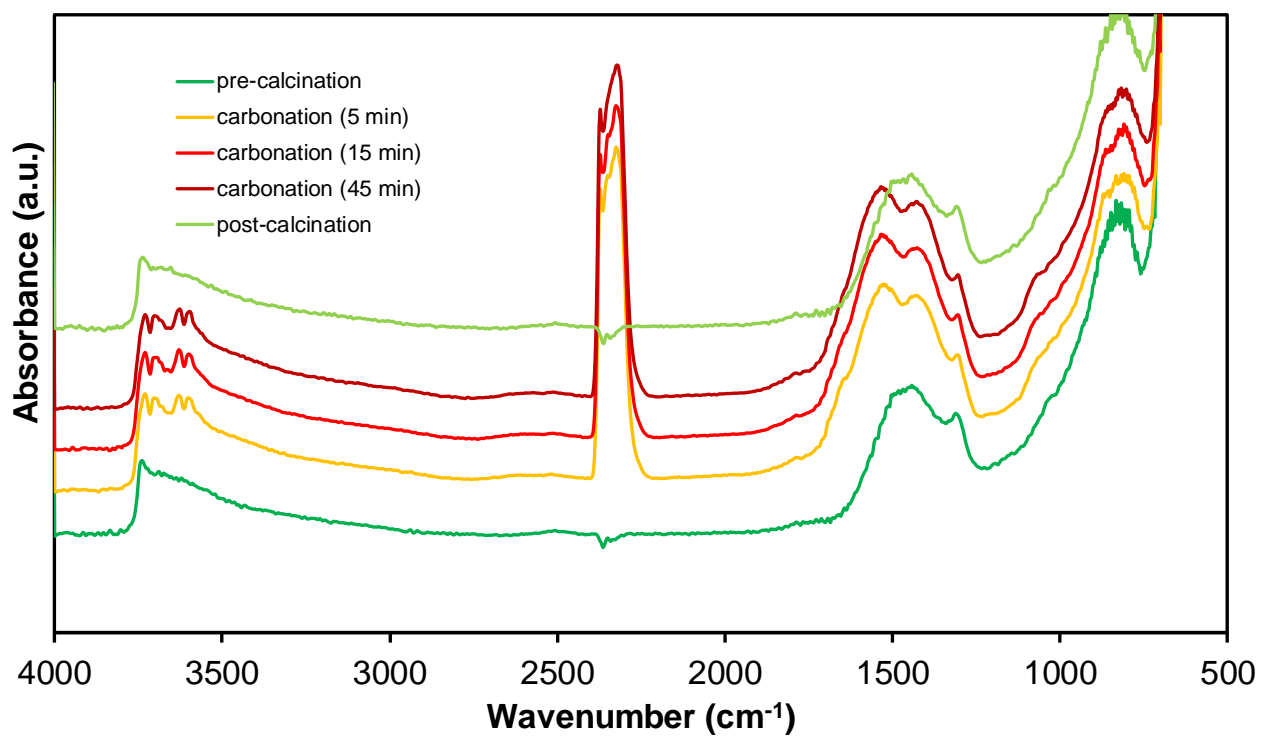


Figure 10.10. *In situ* DRIFTS spectra of pure, uncoated MgO before, during and after carbonation in pure CO₂ atmosphere at 300 °C.

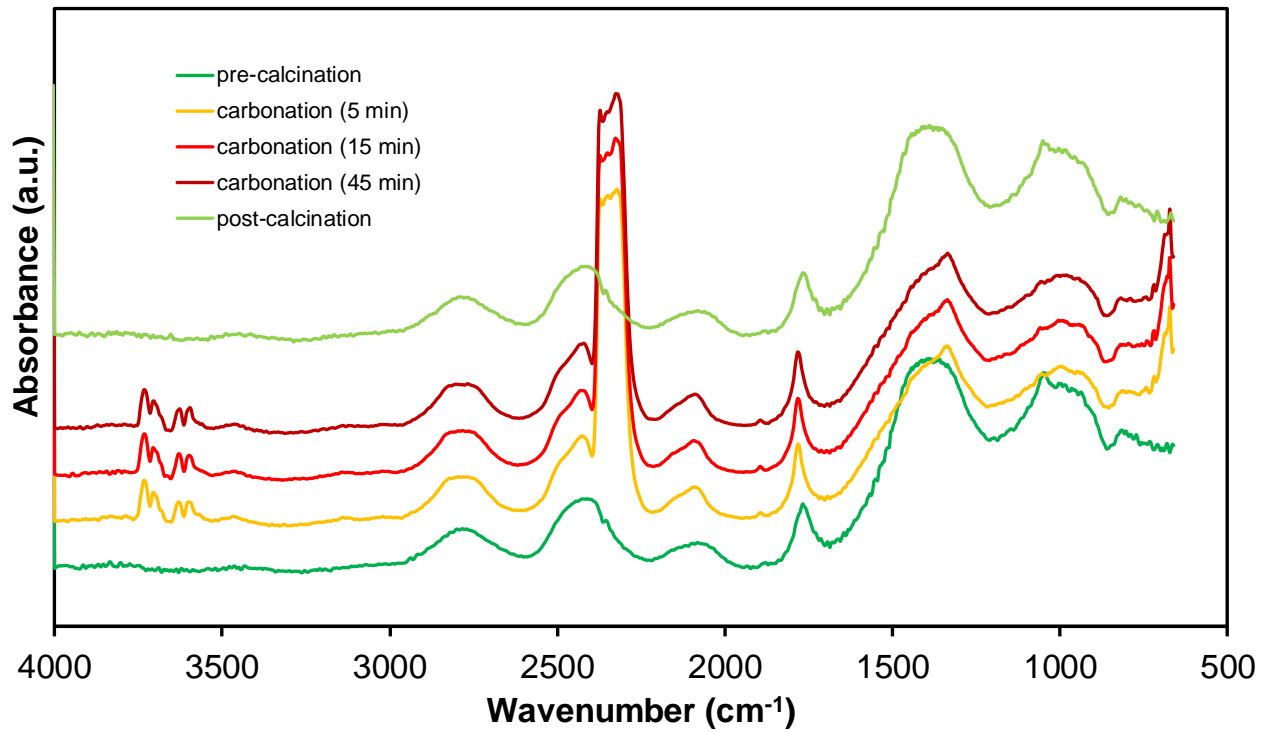


Figure 10.11. *In situ* DRIFTS spectra of Al₂O₃ coated with 20% mol. NaNO₃ before, during and after carbonation in pure CO₂ atmosphere at 300 °C.

Samples coated with mixtures of nitrates (*viz.* the $(\text{Na},\text{K})\text{NO}_3$ - and $(\text{Li},\text{Na},\text{K})\text{NO}_3$ -coated MgO sorbents in Figure 10.3) were also analyzed *in situ*, by collecting their DRIFTS spectra during heating up in CO_2 atmosphere in order to reproduce the conditions of TGA runs in Figure 10.3. As shown in Figure 10.12, the temperature at which peaks related to the carbonate ion emerged were in agreement with the thermogravimetric data.

A close-up on the low frequency region of the infrared spectra allowed pinpointing a subtle change in a peak ascribed to the nitrate ion. At temperatures higher than 275°C , for both the tested samples, the frequency at 836 cm^{-1} , attributable to the out-of-plane bending of the nitrate ion (Stein, 2016), was gradually shifted to 825 cm^{-1} . This variation is characteristic of the phase transition of NaNO_3 from ordered to disordered calcite (Harris et al., 1990). The presence of a feature typical of NaNO_3 in the spectra of both $(\text{Li},\text{Na},\text{K})\text{NO}_3$ -MgO and $(\text{Na},\text{K})\text{NO}_3$ -MgO might reveal that the $(\text{Na},\text{K})\text{NO}_3$ coating still retains modes related to pure NaNO_3 . Actually, even a pure $(\text{Na},\text{K})\text{NO}_3$ melt can exhibit vibrational bands proper of Na-rich or K-rich regions slightly beyond the melting point of the mixture (Berg and Kerridge, 2004) and similar inhomogeneities are reasonably expected to be more persistent in the complex environment of a $(\text{Na},\text{K})\text{NO}_3$ mixture permeating voids and interstitial spaces of porous MgO particles. In terms of CO_2 uptake performance, this might translate in the superimposition of promoting effects deriving from the mixture and from NaNO_3 , as postulated in section 10.1 as a possible explanation for the trends in Figure 10.5a and Figure 10.5b.

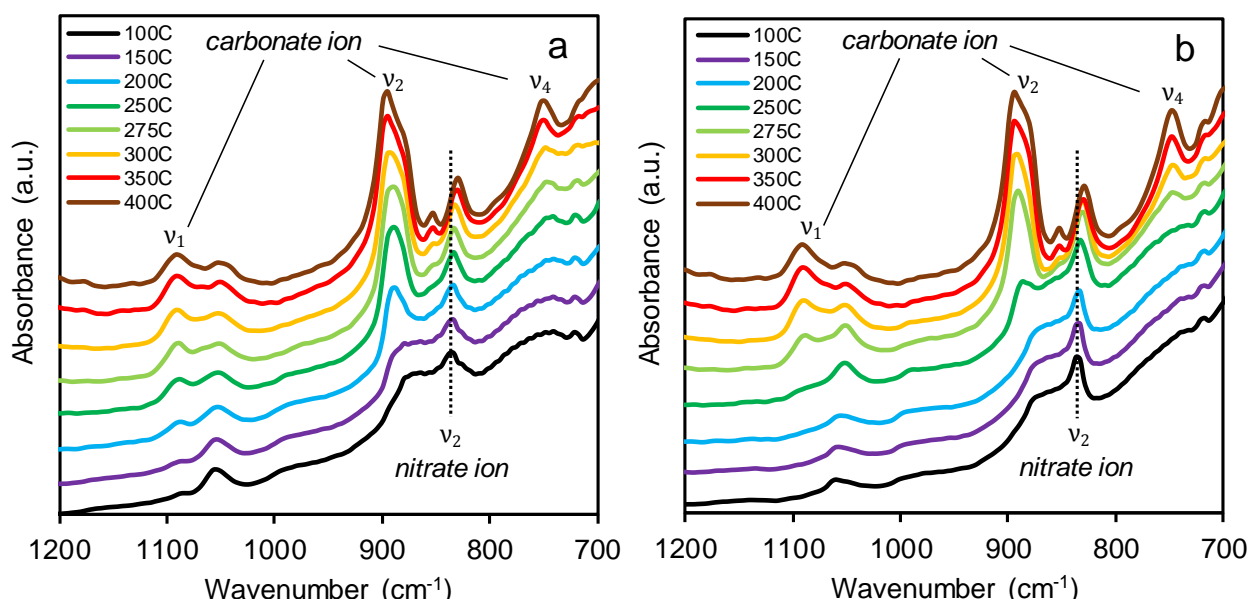


Figure 10.12. *In situ* DRIFTS spectra of MgO coated with a) 10% mol. $(\text{Na},\text{K})\text{NO}_3$ ($\text{Na}:\text{K}$ ratio = 60:40), b) 10% mol. $(\text{Li},\text{Na},\text{K})\text{NO}_3$ (eutectic composition) during heating in pure CO_2 atmosphere at a ramp rate of $10^\circ\text{C}/\text{min}$.

10.3 *In situ* analysis of carbonation: synchrotron-based XRD/PDF analysis

In order to clarify if the reaction mechanism involved in molten salt promotion implies the formation of different intermediate species depending on the salt used in the coating, two MgO samples coated respectively with 20% mol. LiNO_3 and NaNO_3 were also analyzed in synchrotron-based total scattering *in situ* experiments. *In situ* total scattering experiments aimed at characterizing the local structure of sorbents during CO_2 sorption were performed at the ID31 beamline of the European Synchrotron Radiation Facility (ESRF) in Grenoble (France). The synthesised nitrate-coated MgO sorbents were placed in a capillary quartz reactor heated up to the

required temperature by hot-air blowing. Samples were heated up to 450 °C under a N₂ flow of 5 mL/min to desorb H₂O and CO₂ possibly adsorbed at room temperature and then brought to the reaction temperature of 300 °C and kept for 60 min under a CO₂ flow of 5 mL/min. In addition to Bragg scattering (required for XRD analysis), diffuse scattering was also collected, in order to examine the local, short-range structure of samples. Diffraction data were converted to radial atomic pair distribution function (PDF) by means of the PDFgetX3 software (Juhás et al., 2013).

XRD patterns (Figure 10.13) were collected for the samples at room temperature, after heating up to 450 °C in N₂ and during carbonation at 300 °C in CO₂. At room temperature, the MgO-LiNO₃ sample showed also peaks related to Mg(OH)₂, since LiNO₃ is a highly deliquescent salt (Albayrak et al., 2014) and tends to attract moisture triggering hydration of the underlying MgO. Upon heating, peaks related to the nitrates disappeared because of melting and during carbonation MgCO₃ peaks emerged, while the intensity of MgO peaks diminished.

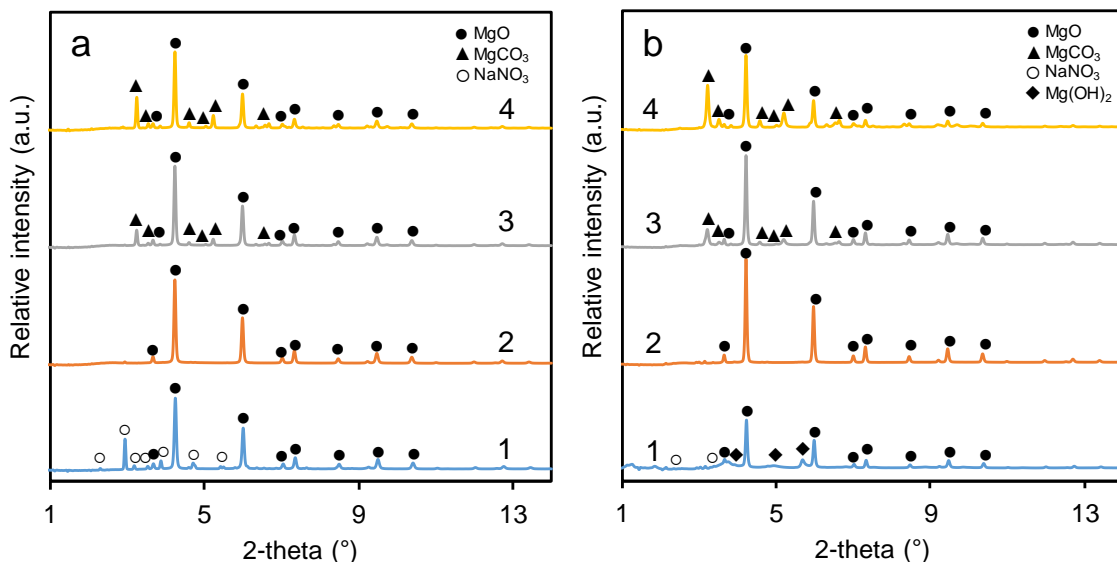


Figure 10.13. XRD spectra of MgO coated with a) 20% mol. NaNO₃, b) 20% mol. LiNO₃ collected: 1) at room temperature, 2) after heating up to 450 °C in N₂, 3) after 5 min carbonation at 300 °C in CO₂, 4) after 60 min carbonation at 300 °C in CO₂.

PDFs for the same samples before and during carbonation were generated from the X-ray total scattering data and put in comparison with theoretical PDFs for the MgO and MgCO₃ phases in Figure 10.14.

Focusing of the shorter radial range, the main peaks for both MgO-LiNO₃ and MgO-NaNO₃ before reaction were related to the interatomic distances of 2.1 Å, ascribed to the Mg-O bond, and 3.0 Å, attributable to the (100)-inclined edge of the octahedral MgO geometry (Effenberger et al., 1981). During carbonation, the peaks attributable to MgO shranked, while concurrently the signal increased for distances related to the theoretical PDF of MgCO₃ (e.g., 4.0 Å and 5.6 Å). This behaviour is similar to the results observed by Dunstan et al. (2016b) in their pioneering PDF analysis of CaO carbonation.

MgO-LiNO₃ and MgO-NaNO₃ showed similar matches to the theoretical PDFs of MgO and MgCO₃, differing only for the extent of carbonation (higher for the LiNO₃-coated sample, in agreement with Figure 10.2). No differing intermediate species were identified, thus suggesting that the reaction proceeds with the same mechanism when different nitrates are involved.

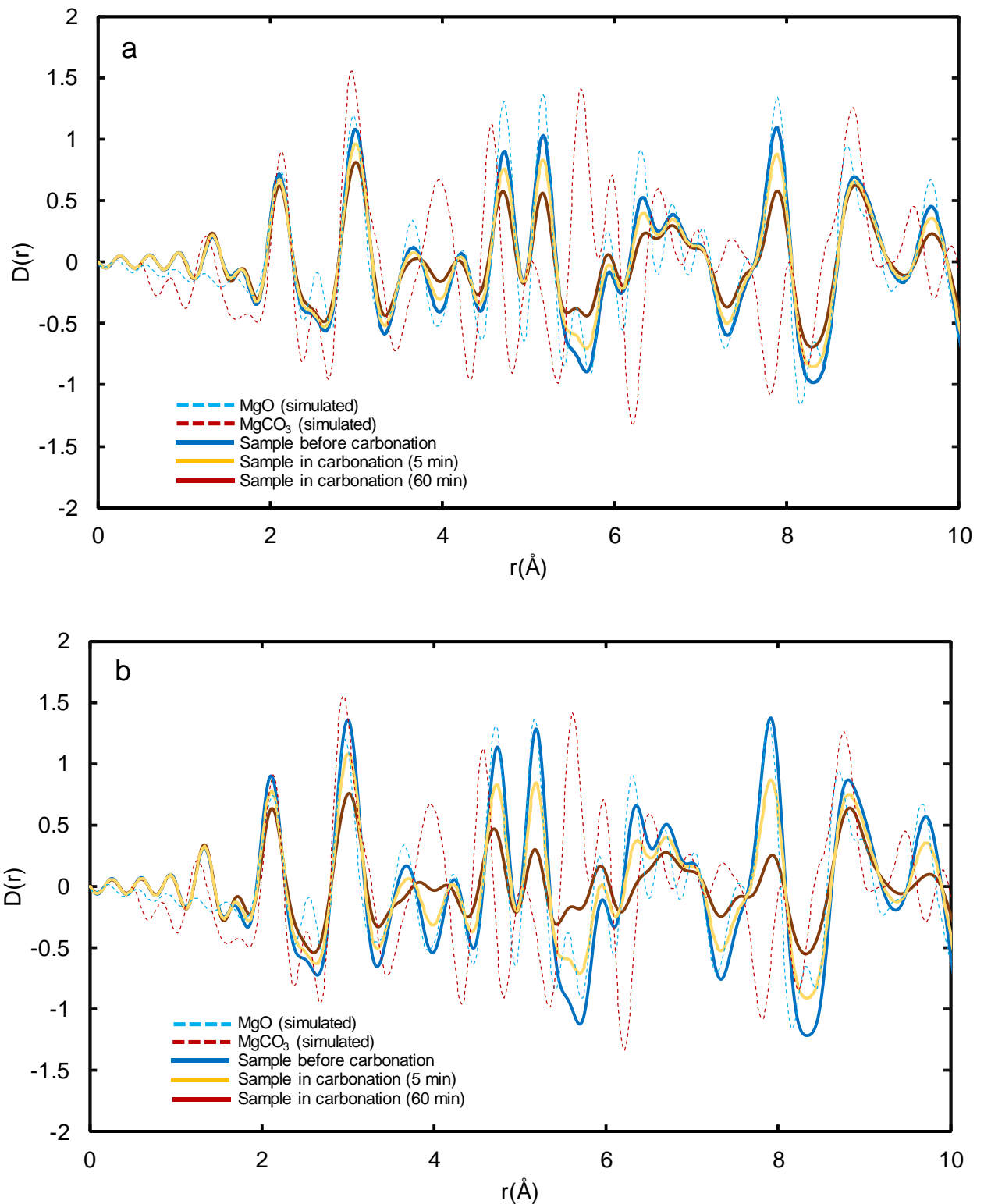


Figure 10.14. Comparison of the experimental X-ray PDFs for MgO coated with a) 20% mol. NaNO_3 , b) 20% mol. LiNO_3 with the calculated PDFs of MgO and MgCO_3 . Experimental data were collected before and during carbonation at 300 °C in CO_2 .

10.4 Performance of MgO-based sorbents over repeated carbonation/calcination cycles

The stability of the CO₂ uptake of nitrate-coated MgO samples was tested over 10 cycles of carbonation at 300 °C in CO₂ and subsequent regeneration at 450 °C in N₂, as reported in Figure 10.15. NaNO₃-coated MgO showed a marked deterioration of performance in the first 3 cycles, in agreement with the findings of Zhang et al. (2014) and Prashar et al. (2016). In contrast, the CO₂ uptake of samples coated with (Li,Na,K)NO₃ and LiNO₃ exhibited a constant decline over cycles, resulting in the respective values of 353 and 73 mg CO₂/g sorbent at the 10th carbonation. The marked difference in cyclic stability among sorbents could be due to the fact that, while LiNO₃ and (Li,Na,K)NO₃ were in molten state during the entire experiment, NaNO₃ during carbonation at 300 °C was at a temperature slightly lower than its bulk melting point (308 °C).

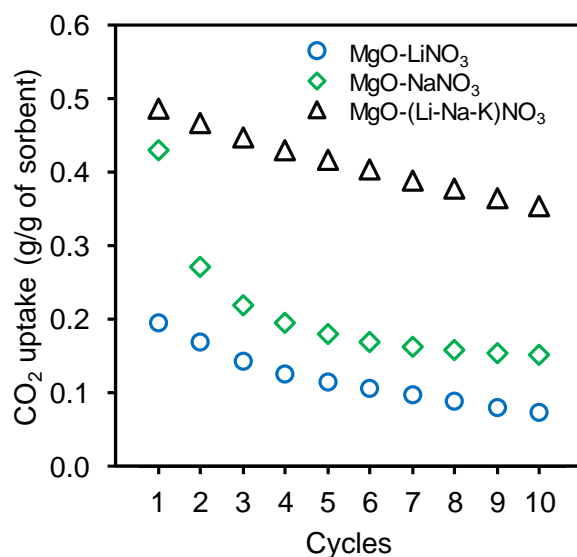


Figure 10.15. CO₂ uptake by different 10% mol. alkali metal nitrate-coated MgO sorbents over 10 cycles of carbonation (300 °C, 100% CO₂) and calcination (450 °C, 100% N₂).

The best performing sample, coated with (Li,Na,K)NO₃, was also tested under lower partial pressures of CO₂ (Figure 10.16a). Although the performance for 50 vol. % CO₂ in the gas stream was comparable to the uptake obtained in pure CO₂, further lowering CO₂ volumetric fraction to 20% resulted in a sharp decrease in performance (average CO₂ uptake over 10 cycles of 101 mg CO₂/g sorbent). The uptake in 20% CO₂ gas stream was additionally tested by varying the operating conditions, as shown in Figure 10.16b: the studied variations were a slightly lower temperature and the presence of steam provided by a water bubbler at room temperature installed before the inlet of the TGA. By lowering the reaction temperature to 275 °C, the average CO₂ uptake more than doubled, setting at 243 mg CO₂/g sorbent. This phenomenon, reported also by Harada and Hatton (2015) for a sol-gel prepared metal nitrate/nitrite coated MgO sorbent, was probably due to a thermodynamic effect: distancing from the turnover temperature for MgO carbonation (i.e. the temperature at which the equilibrium of the reaction in presence of 100% CO₂ at 1 bar shifts towards calcination) resulted in an increased driving force for reaction.

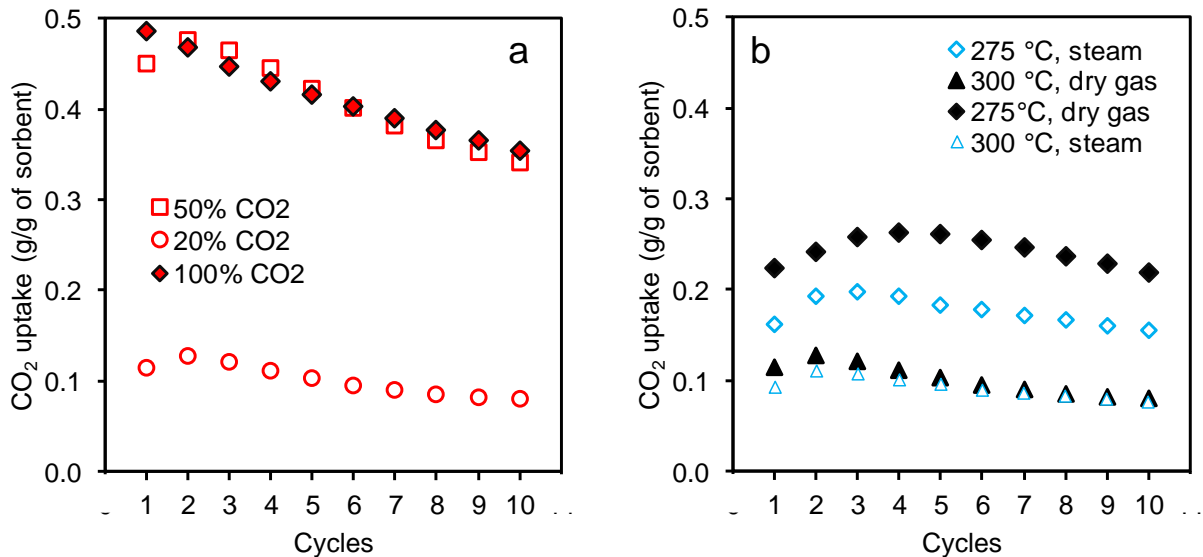


Figure 10.16. CO_2 uptake by 10% mol. $(\text{Li},\text{Na},\text{K})\text{NO}_3$ -coated over 10 cycles of carbonation and calcination: a) varying CO_2 concentration during carbonation at 300 °C; b) varying temperature and steam presence during carbonation in 20% CO_2 atmosphere. Calcination at 450 °C in N_2 .

10.5 Indications for further research in MgO-based sorbents

The investigation of the carbonation performance of the different nitrate-promoted MgO sorbents allowed to draw some preliminary considerations for the potential full-scale use of these materials in CCS systems. First, TGA runs in realistic gas conditions (Figure 10.16) highlighted the steep dependency of CO_2 uptake by MgO on CO_2 partial pressure in the gas. This implies that MgO-based sorbents could perform better in pre-combustion (e.g., syngas upgrading) than in post-combustion environments. While CO_2 concentration in a typical flue gas exiting from a combustion chamber ranges from 8 vol. % for waste-to-energy plants (BREF WI, 2006) to 15 vol. % for coal-fired power plants (Dieter et al., 2014), the syngas produced in coal gasification can contain up to 35 vol. % CO_2 (Boon et al., 2016). Furthermore, syngas is conventionally fed to water gas shift (WGS) reactors in which H_2O and CO are catalytically converted to H_2 and CO_2 . Coupling WGS with CO_2 capture allows the purification of the generated H_2 stream while shifting reaction equilibrium on the product side, by continuously removing CO_2 . This sorption-enhanced WGS process, firstly proposed by Hufton et al. (1999) with the use of K-promoted hydrotalcites as CO_2 sorbents, could effectively make use of nitrate-promoted MgO sorbents, since 250-400°C is an operating range compatible with both WGS and MgO carbonation (Abbasi et al., 2014).

Secondly, the analysis of MgO sorbents coated with different alkali metal nitrate formulations evidenced that eutectic mixtures of nitrates can produce higher CO_2 uptakes (Figure 10.3) and improved regenerability (Figure 10.15) than coatings with a single nitrate, NaNO_3 or LiNO_3 . In addition, the lower melting point of eutectic mixtures enables a wider operability range in terms of carbonation temperatures: while NaNO_3 -coated MgO starts showing significant carbonation only for $T > 275^\circ\text{C}$, MgO coated with an eutectic $(\text{Na}-\text{K})\text{NO}_3$ can be carbonated at T as low as 240 °C. This is noteworthy for industrial application for at least two reasons:

- i) while coated MgO sorbents show their highest CO_2 uptake in pure CO_2 atmosphere at $T > 300$ °C, when CO_2 partial pressure is lowered to 15 vol. % CO_2 uptake increases as

temperature decreases (Figure 13), actually favouring sorbents active at lower temperatures (i.e., coatings having lower melting points).

- ii) a wider operating temperature window guarantees against loss in performance due to the inhomogeneous temperature distribution it can be expected in a carbonator vessel (Dieter et al., 2015).

References (Part III)

- Abbasi, E., Hassanzadeh, A., Zarghami, S., Arastoopour, H., Abbasian, J., 2014. *Regenerable MgO-based sorbent for high temperature CO₂ removal from syngas: 3. CO₂ capture and sorbent enhanced water gas shift reaction*. Fuel 137, 260-268.
- Albayrak, C., Barim, G., Dag, O., 2014. *Effect of hygroscopicity of the metal salt on the formation and air stability of lyotropic liquid crystalline mesophases in hydrated salt-surfactant systems*. Journal of Colloid and Interface Science 433, 26-33.
- Baciocchi, R., Costa, G., Di Bartolomeo, E., Polettini, A., Pomi, R., 2009. *The effects of accelerated carbonation on CO₂ uptake and metal release from incineration APC residues*. Waste Management 29, 2994-3003.
- Beleke, A.B., Mizuhata, M., Deki, S., 2003. *Diffuse reflectance FT-IR spectroscopic study of interactions of α-Al₂O₃/molten NaNO₃ coexisting systems*. Physical Chemistry Chemical Physics 5, 2089-2095.
- Berg, R.W., Kerridge, D.H., 2004. *The NaNO₃/KNO₃ system: the position of the solidus and subsolidus*. Dalton Transactions 15, 2224-2229.
- Bhatia, S.K., Perlmutter, D.D., 1983. *Effect of the product layer on the kinetics of the CO₂-lime reaction*. AIChE Journal 29 (1), 79-86.
- Blamey, J., Anthony, E.J., Wang, J., Fennell, P.S., 2010. *The calcium looping cycle for large-scale CO₂ capture*. Progress in Energy and Combustion Science 36 (2), 260-279.
- Bogush, A., Stegemann, J.A., Wood, I., Roy, A., 2015. *Element composition and mineralogical characterisation of air pollution control residue from UK energy-from-waste facilities*. Waste Management 36, 119-129.
- Borgwardt, R.H., 1989. *Sintering of nascent calcium oxide*. Chemical Engineering Science 44, 53-60.
- Bradshaw, R.W., Meeker, D.E., 1990. *High-temperature stability of ternary nitrate molten salts for solar thermal energy systems*. Solar Energy Materials 21, 51-60.
- BREF WI, 2006. *Reference Document on the Best Available Techniques for Waste Incineration*. <
- Broda, M., Müller, C.R., 2012. *Synthesis of highly efficient, Ca-based, Al₂O₃-stabilized, carbon gel-templated CO₂ sorbents*. Advanced Materials 24 (22), 3059-3064.
- Broda, M., Müller, C.R., 2014. *Sol-gel-derived, CaO-based, ZrO₂-stabilized CO₂ sorbents*. Fuel 127, 94-100.
- Chin, T., Yan, R., Liang, D.T., Tay, J.H., 2005. *Hydrated lime reaction with HCl under simulated flue gas conditions*. Industrial and Engineering Chemistry Research 44, 3742-3748.
- Choi, S., Drese, J.H., Jones, C.W., 2009. *Adsorbent Materials for Carbon Dioxide Capture from Large Anthropogenic Point Sources*. ChemSusChem 2 (9), 796-854.
- Coscia, K., Elliott, T., Mohapatra, S., Oztekin, A., Neti, S., 2013. *Binary and Ternary Nitrate Solar Heat Transfer Fluids*. Journal of Solar Energy Engineering - Transactions of the ASME 135 (2), 021011.
- Dean, C.C., Blamey, J., Florin, N.H., Al-Jeboori, M.J., Fennell, P.S., 2011. *The calcium looping cycle for CO₂ capture from power generation, cement manufacture and hydrogen production*. Chemical Engineering Research and Design 89, 836-855.
- Dieter, H., Bidwe, A.R., Varela-Duelli, G., Charitos, A., Hawthorne, C., Scheffknecht, G., 2014. *Development of the calcium looping CO₂ capture technology from lab to pilot scale at IFK, University of Stuttgart*. Fuel 127, 23-37.

- Dieter, H., Bidwe, A.R., Scheffknecht, G., 2015. *Pilot plant experience with calcium looping*. In: *Calcium and Chemical Looping Technology for Power Generation and Carbon Dioxide (CO₂) Capture*, Eds. Fennell, P., Anthony, E., Woodhead Publishing, Cambridge (UK), 171-194.
- Ding, Y.-D., Song, G., Liao, Q., Zhu, X., Chen, R., 2016. *Bench scale study of CO₂ adsorption performance of MgO in the presence of water vapor*. Energy 112, 101-110.
- Downing, C.A., Sokol, A.A., Catlow, C.R.A., 2014. *The reactivity of CO₂ on the MgO(100) surface*. Physical Chemistry Chemical Physics 16, 184-195.
- Du, H., Williams, C.T., Ebner, A.D., Ritter, J.A., 2010. *In Situ FTIR Spectroscopic Analysis of Carbonate Transformations during Adsorption and Desorption of CO₂ in K-Promoted HTlc*. Chemistry of Materials 22, 3519-3526.
- Duan, Y., Zhang, K., Li, X.S., King, D.L., Li, B., Zhao, L., Xiao, Y., 2014. *ab initio Thermodynamic Study of the CO₂ Capture Properties of M₂CO₃ (M =Na, K)- and CaCO₃-Promoted MgO Sorbents Towards Forming Double Salts*. Aerosol and Air Quality Research 14, 470-479.
- Dunstan, M.T., Jain, A., Liu, W., Ong, S.P., Liu, T., Lee, J., Persson, K.A., Scott, S.A., Dennis, J.S., Grey, C.P., 2016a. *Large scale computational screening and experimental discovery of novel materials for high temperature CO₂ capture*. Energy & Environmental Science 9, 1346-1360.
- Dunstan, M.T., Maugeri, S.A., Liu, W., Tucker, M.H., Taiwo, O.O., Gonzalez, B., Allan, P.K., Gaulois, M.W., Shearing, P.R., Keen, D.A., Phillips, A.E., Dove, M.T., Scott, S.A., Dennis, J.S., Grey, C.P., 2016b. *In situ studies of materials for high temperature CO₂ capture and storage*. Faraday Discussions 192, 217-240.
- Effenberger, H., Mereiter, K., Zemann, J., 1981. *Crystal structure refinements of magnesite, calcite, rhodochrosite, siderite, smithonite, and dolomite, with discussion of some aspects of the stereochemistry of calcite type carbonates*. Zeitschrift für Kristallographie 156, 233-243.
- Erans, M., Manovic, V., Anthony, E.J., 2016. *Calcium looping sorbents for CO₂ capture*. Applied Energy 180, 722-742.
- Fagerlund, J., Highfield, J., Zevenhoven, R., 2012. *Kinetics studies on wet and dry gas–solid carbonation of MgO and Mg(OH)₂ for CO₂ sequestration*. RSC Advances 2 (27), 10380-10393.
- Filitz, R., Kierzkowska, A.M., Broda, M., Müller, C.R., 2012. *Highly efficient CO₂ sorbents: Development of synthetic, calcium-rich dolomites*. Environmental Science and Technology 46 (1), 559-565.
- Genge, M.J., Jones, A.P., Price, G.D., 1995. *An infrared and Raman study of carbonate glasses: Implications for the structure of carbonatite magmas*. Geochimica et Cosmochimica Acta 59 (5), 927-937.
- Glasser, F.P., Jauffret, G., Morrison, J., Galvez-Martos, J.-L., Patterson, N., Imbabí, M.S., 2016. *Sequestering CO₂ by Mineralization into Useful Nesquehonite-Based Products*. Frontiers in Energy Research 4 (3), 1-7.
- Grasa, G.S., Abanades, J.C., 2006. *CO₂ capture capacity of CaO in long series of carbonation/calcination cycles*. Industrial and Engineering Chemistry Research 45, 8846-8851.
- Gregg, S., Ramsay, J., 1970. *Adsorption of carbon dioxide by magnesia studied by use of infrared and isotherm measurements*. Journal of the Chemical Society A: Inorganic, Physical, Theoretical, 2784-2787.
- Hänenchen, M., Prigobbe, V., Baciocchi, R., Mazzotti, M., 2008. *Precipitation in the Mg-carbonate system—effects of temperature and CO₂ pressure*. Chemical Engineering Science 63, 1012-1028.

Harada, T., Simeon, F., Hamad, E.Z., Hatton, T.A., 2015. *Alkali Metal Nitrate-Promoted High-Capacity MgO Adsorbents for Regenerable CO₂ Capture at Moderate Temperatures*. Chemistry of Materials 27, 1943-1949.

Harada, T., Hatton, T.A., 2015. *Colloidal Nanoclusters of MgO Coated with Alkali Metal Nitrates/Nitrites for Rapid, High Capacity CO₂ Capture at Moderate Temperature*. Chemistry of Materials 27, 8153-8161.

Harris, M.J., Salje, E.K.H., Gütler, B.K., 1990. *An infrared spectroscopic study of the internal modes of sodium nitrate: implications for the structural phase transition*. Journal of Physics: Condensed Matter 2, 5517-5527.

Hu, J., Zhu, K., Chen, L., Kübel, C., Richards, R., 2007. *MgO(111) Nanosheets with Unusual Surface Activity*. Journal of Physical Chemistry C 111 (32), 12038-12044.

Hufton, J.R., Mayorga, S., Sircar, S., 1999. *Sorption-enhanced reaction process for hydrogen production*. AIChE Journal 45 (2), 248-256.

Ida, J.-I., Lin, Y.S., 2003. *Mechanism of high-temperature CO₂ sorption on lithium zirconate*. Environmental Science and Technology 37 (9), 1999-2004.

IEA, 2016. *Key World Energy Statistics*. International Energy Agency. <<http://www.iea.org/publications/freepublications/publication/key-world-energy-statistics.html>> (accessed: 12/12/2016)

IPCC, 2014. *Fifth Assessment Report (AR5)*. Intergovernmental Panel on Climate Change. <<http://www.ipcc.ch/report/ar5/>> (accessed: 12/12/2016)

ISWA, 2012. *Waste-to-Energy – State-of-the-art report*. 6th edition, International Solid Waste Association.

Janz, G.J., Allen, C.B., Downey, J.R., Tomkins, R.P.T., 1978. *Physical Properties Data Compilations Relevant to Energy Storage – I. Molten Salts: Eutectic Data*. Technical report, National Standard Reference Data System, USA. <http://www.nist.gov/sites/default/files/documents/srd/NSRDS-61_Part-1.pdf> (accessed: 12/12/2016)

Janz, G.J., James, D.W., 1961. *Raman Spectra and Ionic Interactions in Molten Nitrates*. The Journal of Chemical Physics 35, 739-744.

Janz, G.J., Kelly, F.J., Perano, J.L., 1964. *Melting and Pre-Melting Phenomena in Alkali Metal Nitrates*. Journal of Chemical and Engineering Data 9, 133-136.

Juhás, P., Davis, T., Farrow, C.L., Billinge, S.J.L., 2013. *PDFgetX3: A rapid and highly automatable program for processing powder diffraction data into total scattering pair distribution functions*. Journal of Applied Crystallography 46, 560-566.

Kierzkowska, A.M., Pacciani, R., Müller, C.R., 2013. *CaO-Based CO₂ Sorbents: From Fundamentals to the Development of New, Highly Effective Materials*. ChemSusChem 6 (7), 1130-1148.

Kim, S., Jeon, S.G., Lee, K.B., 2016. *High-Temperature CO₂ Sorption on Hydrotalcite Having a High Mg/Al Molar Ratio*. ACS Applied Materials & Interfaces 8, 5763-5767.

Lafuente, B., Downs, R.T., Yang, H., Stone, N., 2015. *The power of databases: the RRUFF project*. In: *Highlights in Mineralogical Crystallography*, Eds. Armbruster, T., Danisi, R.M., De Gruyter, Berlin (Germany), 1-30.

Lee, H.J., Kim, J.H., Kim, J.W., Cho, S.J., 2014. *Structure Transformation of Na-Mg Based Salts for CO₂ Capture and Storage at High Temperature Probed with Variable Temperature X-ray Powder Diffraction*. Energy Procedia 63, 253-265.

- Leon, M., Diaz, E., Bennici, S., Vega, A., Ordonez, S., Auroux, A., 2010. *Adsorption of CO₂ on Hydrotalcite-Derived Mixed Oxides: Sorption Mechanisms and Consequences for Adsorption Irreversibility*. Industrial & Engineering Chemistry Research 49 (8), 3663-3671.
- Li, Z.S., Fang, F., Tang, X., Cai, N., 2012. *Effect of Temperature on the Carbonation Reaction of CaO with CO₂*. Energy & Fuels 26, 2473-2482.
- Liu, B., Thomas, P.S., Ray, A.S., Guerbois, J.P., 2007. *A TG analysis of the effect of calcination conditions on the properties of reactive magnesia*. Journal of Thermal Analysis and Calorimetry 88 (1), 145-149.
- Liu, W., An, H., Qin, C., Yin, J., Wang, G., Feng, B., Xu, M., 2012. *Performance Enhancement of Calcium Oxide Sorbents for Cyclic CO₂ Capture—A Review*. Energy & Fuels 26, 2751-2767.
- Lu, H., Reddy, E.P., Smirniotis, P.G., 2006. *Calcium Oxide Based Sorbents for Capture of Carbon Dioxide at High Temperatures*. Industrial and Engineering Chemistry Research 45 (11), 3944-3949.
- MacDowall, N., Florin, N., Buchard, A., Hallett, J., Galindo, A., Jackson, G., Adjiman, C.S., Williams, C.K., Shah, N., Fennell, P., 2010. *An overview of CO₂ capture technologies*. Energy & Environmental Science 3, 1645-1669.
- Manovic, V., Anthony, E.J., 2007. *Steam Reactivation of Spent CaO-Based Sorbent for Multiple CO₂ Capture Cycles*. Environmental Science and Technology 41 (4), 1420-1425.
- Manovic, V., Anthony, E.J., 2008. *Thermal Activation of CaO-Based Sorbent and Self-Reactivation during CO₂ Capture Looping Cycles*. Environmental Science and Technology 42 (11), 4170-4174.
- Manovic, V., Charland, J.P., Blamey, J., Fennell, P.S., Lu, D.Y., Anthony, E.J., 2009. *Influence of calcination conditions on carrying capacity of CaO-based sorbent in CO₂ looping cycles*. Fuel 88, 1893-1900.
- Martinez, A., Lara, Y., Lisbona, P., Romeo, L.M., 2012. *Energy penalty reduction in the calcium looping cycle*. International Journal of Greenhouse Gas Control 7, 74-81.
- McKinsey & Company, 2008. *Carbon Capture & Storage: Assessing the Economics*. Technical report. <<http://assets.wwf.ch/downloads/mckinsey2008.pdf>> (accessed: 12/12/2016)
- Naeem, M.A., Armutlulu, A., Broda, M., Lebedev, D., Müller, C.R., 2016. *The development of effective CaO-based CO₂ sorbents via a sacrificial templating technique*. Faraday Discussions 192, 85-95.
- Nelson, T.O., Coleman, L.J.I., Green, D.A., Gupta, R.P., 2009. *The Dry Carbonate Process: Carbon dioxide recovery from power plant flue gas*. Energy Procedia 1, 1305-1311.
- Novozhilov, A.L., Bamburov, V.G., Fedotova, N.N., 2007. *Solubility of Carbon Dioxide in Molten Alkali-Metal Nitrates*. Russian Journal of Inorganic Chemistry 52 (11), 1679-1681.
- Philipp, R., Fujimoto, K., 1992. *FTIR Spectroscopic Study of CO₂ Adsorption/Desorption on MgO/CaO Catalysts*. Journal of Physical Chemistry 96 (22), 9035-9038.
- Prashar, A.K., Seo, H., Choi, W.C., Kang, N.Y., Park, S., Kim, K., Min, D.Y., Kim, H.M., Park, Y.K., 2016. *Factors Affecting the Rate of CO₂ Absorption after Partial Desorption in NaNO₃-Promoted MgO*. Energy & Fuels 30, 3298-3305.
- Prigiobbe, V., Polettini, A., Baciocchi, R., 2009. *Gas-solid carbonation kinetics of Air Pollution Control residues for CO₂ storage*. Chemical Engineering Journal 148, 270-278.
- Qi, Z., Daying, H., Yang, L., Qian, Y., Zibin, Z., 2013. *Analysis of CO₂ sorption/desorption kinetic behaviors and reaction mechanisms on Li₄SiO₄*. AIChE Journal 59 (3), 901-911.

Scripps Institution of Oceanography, 2016. *The Keeling Curve*. <
<http://scripps.ucsd.edu/programs/keelingcurve/>> (accessed: 12/12/2016)

Singh, R., Ram Reddy, M.K., Wilson, S., Joshi, K., Diniz da Costa, J.C., Webley, P., 2009. *High temperature materials for CO₂ capture*. Energy Procedia 1, 623-630.

Stern, K.H., 2000. *High Temperature Properties and Thermal Decomposition of Inorganic Salts with Oxyanions*. CRC Press, Boca Raton, FL (USA).

Stein, S.E., 2016. *IR and Mass Spectra*. In: *NIST Chemistry WebBook, NIST Standard Reference Database Number 69*, Eds. P. J. Linstrom and W. G. Mallard, National Institute of Standards and Technology, Gaithersburg, MD (USA). <http://webbook.nist.gov> (accessed: 12/12/2016).

Tian, S., Jiang, J., 2012. *Sequestration of flue gas CO₂ by direct gas-solid carbonation of air pollution control system residues*. Environmental Science and Technology 46 (24), 13545-13551.

Tian, S., Jiang, J., Hosseini, D., Kierzkowska, A.M., Imtiaz, Q., Broda, M., Müller, C.R., 2015. *Development of a Steel-Slag-Based, Iron-Functionalized Sorbent for an Autothermal Carbon Dioxide Capture Process*. ChemSusChem 8 (22), 3839-3846.

Valverde, J.M., Sanchez-Jimenez, P.E., Perez-Maqueda, L.A., 2015. *Ca-looping for postcombustion CO₂ capture: a comparative analysis on the performances of dolomite and limestone*. Applied Energy 138, 202-215.

Vu, A.-T., Park, Y., Jeon, P.R., Lee, C.-H., 2014. *Mesoporous MgO sorbent promoted with KNO₃ for CO₂ capture at intermediate temperatures*. Chemical Engineering Journal 258, 254-264.

Vu, A.-T., Ho, K., Jin, S., Lee, C.-H., 2016. *Double sodium salt-promoted mesoporous MgO sorbent with high CO₂ sorption capacity at intermediate temperatures under dry and wet conditions*. Chemical Engineering Journal 291, 161-173.

Wang, J., Huang, L., Yang, R., Zhang, Z., Wu, J., Gao, Y., Wang, Q., O'Hare, D., Zhong, Z., 2014. *Recent advances in solid sorbents for CO₂ capture and new development trends*. Energy & Environmental Science 7, 3478-3518.

Wu, S.F., Beum, T.H., Yang, J.I., Kim, J.N., 2007. *Properties of Ca-based CO₂ sorbent using Ca(OH)₂ as precursor*. Industrial and Engineering Chemistry Research 46, 7896-7899.

Xiao, G., Singh, R., Chaffee, A., Webley, P., 2011. *Advanced adsorbents based on MgO and K₂CO₃ for capture of CO₂ at elevated temperatures*. International Journal of Greenhouse Gas Control 5, 634-639.

Xu, K., 1999. *Raman evidence for the congruently melting compound KLi(NO₃)₂ in the LiNO₃-KNO₃ system*. Journal of Physics and Chemistry of Solids 60, 5-11.

Yang, X., Zhao, L., Xiao, Y., 2013a. *Effect of NaNO₃ on MgO-CaCO₃ Absorbent for CO₂ Capture at Warm Temperature*. Energy & Fuels 27, 7645-7653.

Yang, Y., Asta, M., Laird, B.B., 2013b. *Solid-Liquid Interfacial Premelting*. Physical Review Letters 110, 96-102.

Zarghami, S., Hassanzadeh, A., Arastoopour, H., Abbasian, J., 2015. *Effect of Steam on the Reactivity of MgO-Based Sorbents in Precombustion CO₂ Capture Processes*. Industrial & Engineering Chemistry Research 54 (36), 8860-8866.

Zhang, K., Li, X.S., Duan, Y., King, D.L., Singh, P., Li, L., 2013. *Roles of double salt formation and NaNO₃ in Na₂CO₃-promoted MgO absorbent for intermediate temperature CO₂ removal*. International Journal of Greenhouse Gas Control 12, 351-358.

Zhang, K., Li, X.S., Li, W.-Z., Rohatgi, A., Duan, Y., Singh, P., Li, L., King, D.L., 2014. *Phase Transfer-Catalyzed Fast CO₂ Absorption by MgO-Based Absorbents with High Cycling Capacity*. Advanced Materials Interfaces 1, 140030.

Zhang, K., Li, X.S., Chen, H., Singh, P., King, D.L., 2016. *Molten Salt Promoting Effect in Double Salt CO₂ Absorbents*. The Journal of Physical Chemistry C 120, 1089-1096.

Conclusions

The comprehensive investigation of dry processes for acid gas removal and CO₂ capture performed in the present PhD study addressed both fundamental and operating aspects and contributed to cast light on issues ranging from gas-solid reaction mechanism to techno-economic comparison of full-scale system configurations.

The thorough analysis of the state-of-the-art on end-of-pipe technologies for HCl, SO₂ and CO₂ sequestration presented in Part I allowed to identify a handful of key issues which are common to both the industry-ready acid gas removal systems and the developing sorbent-based CO₂ capture technologies: namely, the intrinsic limitations of gas-solid reactions such as incomplete conversion and vulnerability to sintering of the sorbent.

With reference to acid gas removal in the waste-to-energy industry, Part II proposed different approaches to the modelling of gas-solid reactions between solid sorbents (calcium hydroxide and sodium bicarbonate), which can constitute the theoretical basis for process optimisation, a way to overcome – or, at least, mitigate – the inherent shortcomings of solid sorbents for flue gas cleaning. A fundamental model, based on the integration of a conventional grain model with a crystallisation and fracture model to take into account the inhibition of the reaction caused by the product layer, was developed for the description of the reaction process between HCl and solid sorbent particles of Ca(OH)₂, which accomplishes for a saturation effect that leads to a temperature-dependent ultimate conversion yield much lower than the equilibrium conversion. The model, validated against literature and experimental data, represents a step forward to interpret and predict the overall rate of gas-solid reactions in dry acid gas removal processes, laying the foundations for a broader modelling approach which should also take into account competitive reactions and promoting effect of humidity. In parallel, analysis of full-scale dry treatment systems was conducted by means of economic and environmental assessment relying on an empirical operational model for process simulation. The adopted methodology allowed to identify the optimal operating configuration of two-stage dry acid gas removal systems and to compare the performance of single stage and two-stage systems in a wide range of process specifications (inlet waste composition, emission limit value at stack, varying unit costs for reactant purchase and residue disposal, varying indirect environmental impacts), thus resulting in a robust demonstration of the advantages associated with multistage acid gas treatment, if properly operated.

With reference to the reaction between MgO and CO₂, a promising route for carbon capture processes, Part III explored the possibility to overcome the inherent limitation of the gas-solid reaction by synthesis approach. Carbonation of pure MgO is severely hindered by mass transfer limitations, since the growth of a carbonate shell covering the unreacted MgO particles prevents molar conversions higher than 3-4%. Incorporating alkali metal nitrates in the sorbent was found to dramatically increase the total CO₂ uptake up to values of 40-50 wt. % by altering the way the product layer grows. Different alkali metal nitrates and their mixtures were systematically tested as coating for MgO-based sorbents, identifying a relationship between carbonation performance of nitrate-coated MgO-based sorbents and melting point of the coating mixture. *In situ* analyses such as diffuse reflectance IR spectroscopy and X-ray total scattering provided a first attempt at observing the mechanisms of molten salt-mediated carbonation.

Generally speaking, the study of gas-solid reactions in two different, albeit comparable flue gas cleaning contexts suggests that the practical knowledge and operational experience historically

developed in the acid gas removal sector can be usefully exported to the developing CO₂ capture sector, whereas new ideas coming out in the latter could be adapted and experimented in the former.

Suggestions for future work

The work carried out in the present PhD project opens clear pathways for follow-up studies.

As for the modelling of dry acid gas treatment in WtE plants, the phenomenological model of chapter 6 is a significant step towards a physically-based description of the acid gas removal process. A follow-up of the experimental campaign presented in chapter 5, exploring competitive sorption of HCl and SO₂ in both dry and wet atmosphere, could provide the necessary basis for model validation in a wider framework, which would be preparatory for the modelling of full-scale systems. The simplified operational model presented in chapter 7 proved to be a useful tool for process optimisation, but requires plant-specific calibration to give reliable results. Training the operational model on the results of the phenomenological model could lead to linking its empirical parameters to the actual physical and chemical variables involved in the process, eventually emancipating the operational model from the need of site-specific tuning.

The enhancement of MgO reactivity towards CO₂ as mediated by molten salts was found to be promising, but the promising results obtained in TGA environment need to be verified in more realistic gas conditions (lower CO₂ inlet concentration and presence of steam) and configuration (fluidised bed operation). Then, the best formulation for the alkali metal coating should be selected on the basis of a complete techno-economic assessment. Furthermore, since the promoting effect provided by molten salt resulted active also for Ca-based sorbent, it would be interesting to test the performance of nitrate-coated CaO in HCl/SO₂ removal and assess if sorbent modification could mitigate the incomplete sorbent conversion issue also in this context.

Lastly, section 9.2 in the thesis proposed, although only preliminarily, a possible route for valorising the solid residues from acid gas removal as CO₂ sorbents. The integration between the acid gas removal process and the carbonate looping scheme for CO₂ capture could be explored in both directions, testing both the use of acid gas treatment residues in CO₂ capture and exhaust CO₂ sorbents in acid gas removal.

List of publications

Peer-reviewed journals

Published:

Dal Pozzo, A., Antonioni, A., Guglielmi, D., Stramigioli, C., Cozzani, V. (2016). *Cost comparison of different alternatives for the dry treatment of flue gas in WtE plants.* Waste Management 51, 81-90.

Antonioni, G., Dal Pozzo, A., Guglielmi, D., Tugnoli, A., Cozzani, V. (2016). *Enhanced modelling of heterogeneous gas-solid reactions in acid gas removal dry processes.* Chemical Engineering Science 148, 140-154.

In progress:

Dal Pozzo, A., Guglielmi, D., Antonioni, G., Tugnoli, A. (2017). *Sustainability analysis of dry treatment technologies for acid gas removal in Waste-to-Energy plants.* Under review for publication in Journal of Cleaner Production.

Dal Pozzo, A., Guglielmi, D., Moricone, R., Antonioni, G., Tugnoli, A., Cozzani, V. (2017). *Experimental investigation of the low-temperature reaction process of HCl with Ca(OH)₂.* In preparation for publication in Fuel.

Peer-reviewed conference contributions

Dal Pozzo, A., Guglielmi, D., Antonioni, G., Tugnoli, A., Cozzani, V. (2017). *Environmental assessment of combined acid gas emission control with alternative dry sorbent injection systems.* Accepted for ICheaP-13, 28-31 May 2017, Milano.

Dal Pozzo, A., Guglielmi, D., Antonioni, G., Tugnoli, A. (2017). *Two-stage vs. single stage acid gas treatment systems: a performance assessment based on economic and environmental indices.* Submitted for ICEEM-09, 6-9 September 2017, Bologna.

Dal Pozzo, A., Guglielmi, D., Antonioni, G., Tugnoli, A. (2017). *Accounting for the indirect environmental burdens in Waste-to-Energy flue gas cleaning: a sustainability assessment of dry acid gas removal systems.* Submitted for ICOSSE '17, 2-4 October 2017, Barcelona.

Non peer-reviewed technical journals

Dal Pozzo, A., Guglielmi, D., Antonioni, G., Cozzani, V., Calvani, S., Bonanini, G. (2016). *Trattamento a secco dei fumi di combustione prodotti nella termovalorizzazione di RSU.* La Termotecnica 70 (3), 53-57.

Ringraziamenti / Acknowledgments

Desidero ringraziare il Prof. Valerio Cozzani per avermi supportato nella decisione di intraprendere il dottorato su un argomento relativamente nuovo per il gruppo di ricerca e per avervi investito tempo e fondi anche in momenti in cui i risultati tardavano a palesarsi. Grazie ai correlatori Giacomo Antonioni e Alessandro Tognoli, per i consigli e gli insegnamenti.

Il mio grazie più sentito va a Daniele Guglielmi, per svariati motivi. Il suo dottorato ha aperto la strada a questo filone di attività, nato dal nulla e ora in grado di attrarre l'interesse di diversi partner industriali. La sua meticolosità e preparazione sono stati per me esempio di come vada impostata la ricerca. La sua scrupolosa supervisione ha migliorato ampiamente la qualità del mio lavoro. Un grande grazie anche a Raffaella Moricone per il decisivo supporto nel portare avanti l'attività di laboratorio e nell'affrontare le non poche magagne tecniche e burocratiche che si sono succedute in questi anni.

Ringrazio il Prof. Francesco Santarelli, per avermi indirizzato verso quest'ambito di ricerca fin da quando mi rivolsi a lui per la tesi magistrale nell'ormai lontano 2012, e la Prof.ssa Gigliola Spadoni, per avermi affidato i cicli di lezioni che mi hanno permesso di integrare nel dottorato l'istruttiva esperienza come "teaching assistant". Ringrazio Nicoletta, amica e prima coinquilina d'ufficio, per avermi incoraggiato a scegliere la strada del dottorato.

Grazie ai miei genitori, Mara e Antonio, per la pazienza dimostrata nel sopportare un figlio ancora alle prese con lo studio e ben lontano anche solo dall'immaginare l'agognato "posto fisso", e a tutti i miei amici e amiche, che hanno imparato a loro spese che a ogni innocua domanda su "come va in università?" può seguire un excusus torrenziale sui vantaggi del trattamento a doppio stadio per la rimozione dei gas acidi e sull'assurdità della programmazione annuale dell'acquisto dei reagenti.

I wish to thank Prof. Christoph Müller for having hosted me at the Laboratory of Energy Science and Engineering. The 6 months spent in Zürich have been an open-minding experience both professionally and personally. The opportunity to study the enhancement of MgO-based CO₂ sorbents helped me broaden the scope of my PhD towards an innovative topic and learn a remarkable amount of new skills and concepts, which I look forward to applying in future research, if I have the chance to continue my adventure in academia. My gratitude goes to the post-docs which advised me directly: Andaç Armutlulu, who followed and documented via SEM my fortunate and unfortunate outcomes with sorbent synthesis, and Paula Abdala, who introduced me to the world of synchrotron-based experiments. Thanks to all the ESE team for the warm reception and the helpfulness in providing me training in synthesis techniques and use of instrumentation.